Scientific Drilling

Reports on Deep Earth Sampling and Monitoring

Editorial Preface

Dear Reader:

We are happy to report that scientific ocean drilling will continue beyond the current Integrated Ocean Drilling Program (IODP), which ends September 2013. A new program, the International Ocean Discovery Program is planned to replace IODP by October 2013 without interruption of operations. What is more, the International Scientific Continental Drilling Program (ICDP) is advancing towards renewal in fall of 2013 (p. 77).

On the backdrop of this exciting news, this issue brings reports that illuminate the incompletely understood workings of the interior of our planet, the mechanisms of subduction-related earthquakes, and the exploration of the distribution of subsurface microbial life below one of the most nutrient-starved ocean basins on Earth. Drilling into the Louisville Seamount chain in the Pacific Ocean (p. 11) in a comparison to previous studies of the Hawaii-Emperor Seamount chain suggests that the mantle roots ("plumes") of these linear chains of volcanic hot-spot activity move relative to each other, and it is speculated that subduction of oceanic lithosphere can induce a complex mantle flow causing hotspots to move differently. The relationship between plate subduction and major earthquakes is the topic of a drilling project off Costa Rica (p. 23). In this location, the downgoing plate is believed to erode the basis of the overriding plate, unlike other subduction zones in which material is scraped off the downgoing plate and accumulated as an accretionary prism overlying the seismogenic zone.

Like chains of seamounts, the Yellowstone Hotspot spur in the Snake River Plain of Idaho suggests a deep mantle root of this hotspot below the North American plate. A drilling project (p.36) addresses the deep nature of this fascinating super-volcano, as well as explores whether its track through Idaho created geothermal energy sources. Another ambitious project will investigate in detail how Earth's crust below the oceans is forming. The Semail Ophiolite of Oman is proposed to ICDP (p. 64) as the place to examine the detailed 3-D nature of the crust-mantle transition, how melt is transferred from the mantle into the crust, and how it is distributed within the crust. IODP drilling results on this same general topic—and recovered from a so-called tectonic window in the Atlantic Ocean into the deeper ocean crust—are reported (p. 31).
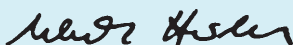
Each new step of exploration of subsurface microbial life provides novel data from this vast and largely unknown habitat for life. IODP recovered cores from below the nutrient-starved South Pacific Gyre (p. 4). Extremely low microbial activity is indicated within the marine sediments of this vast area, suggesting that previous estimates of total subsurface biomass beneath the oceans may need a downward revision.

Engineering developments play a crucial role in scientific drilling. Consequently, we offer reports on real-time natural gamma-ray spectrometry (p. 57), a new heave compensation system for wireline borehole instruments (p. 46), and a wireline downhole penetrometer to record formation pressure and temperature (p. 51).

We wish readers some relaxing time in their armchairs reading about the diverse topics covered by this issue of *Scientific Drilling*!

Hans Christian Larsen
Editor-in-Chief

Ulrich Harms
Editor

Jamus Collier
Managing Editor

Front cover: The most sampled core from Exp.330 with many stickers used to mark requested samples. (Photo Credit: Takeshi Hanyu & IODP)
Left inset: Scientists taking part in a hard rock sampling party (Photo Credit: Exp. 334, John Beck, IODP/TAMU)

Contents

Science Reports

Progress Reports

Technical Developments

Workshop Reports

Program Development

News and Views

Schedules

IODP Expedition 329: Life and Habitability Beneath the Seafloor of the South Pacific Gyre

by Steven D'Hondt, Fumio Inagaki, Carlos Alvarez Zarikian, and
the IODP Expedition 329 Scientific Party

Abstract

Integrated Ocean Drilling Program (IODP) Expedition 329 made major strides toward fulfilling its objectives. Shipboard studies documented (1) fundamental aspects of habitability and life in this very low activity subseafloor sedimentary ecosystem and (2) first-order patterns of habitability within the igneous basement. A broad range of post-expedition studies will complete the expedition objectives.

Throughout the South Pacific Gyre (SPG; Sites U1365–U1370), dissolved oxygen and nitrate are present throughout the entire sediment sequence, and sedimentary microbial cell counts are lower than at all previously drilled IODP/Ocean Drilling Program (ODP)/Deep Sea Drilling Program (DSDP) sites. In contrast, at Site U1371 in the upwelling zone just south of the gyre, detectable oxygen and nitrate are limited to the top and bottom of the sediment column, manganese reduction is a prominent electron-accepting process, and cell concentrations are higher than at the same depths in the SPG sites throughout the sediment column.

Geographic variation in subseafloor profiles of dissolved and solid-phase chemicals are consistent with the magnitude

of organic-fueled subseafloor respiration declining from outside the gyre to the gyre center.

Chemical profiles in the sedimentary pore water and secondary mineral distributions in the basaltic basement indicate that basement alteration continues on the timescale of formation fluid replacement, even at the sites with the oldest basement (84–120 Ma at Sites U1365 and U1366).

Introduction

The nature of life in the sediment beneath mid-ocean gyres is poorly known. Almost all sites where subseafloor sedimentary life has been studied are on ocean margins (ODP Legs 112, 180, 201, and 204 and IODP Expeditions 301, 307, and 323) or in the equatorial ocean (ODP Legs 138 and 201). Despite those studies, the extent and character of subseafloor life throughout most of the ocean remains unknown (National Research Council of the National Academies, 2003). This absence of knowledge is largely due to ignorance of subseafloor life in the major ocean gyres, which collectively cover most of the area of the open ocean.

The SPG is the ideal region for exploring the nature of subseafloor sedimentary communities and habitats in the low-activity heart of an open-ocean gyre. It is the largest of the ocean gyres, and its center is farther from continents than the center of any other gyre. Surface chlorophyll concentrations and primary photosynthetic productivity in the seawater are lower in this gyre than in other regions of the world ocean (Fig. 1; Behrenfeld and Falkowski, 1997). Its surface water is the clearest in the world (Morel et al., 2007). The sediment of this region has some of the lowest organic burial rates in the ocean (Jahnke, 1996). Sediment of this region contains the lowest cell concentrations and lowest rates of microbial activity ever encountered in shallow marine sediment (D'Hondt et al., 2009).

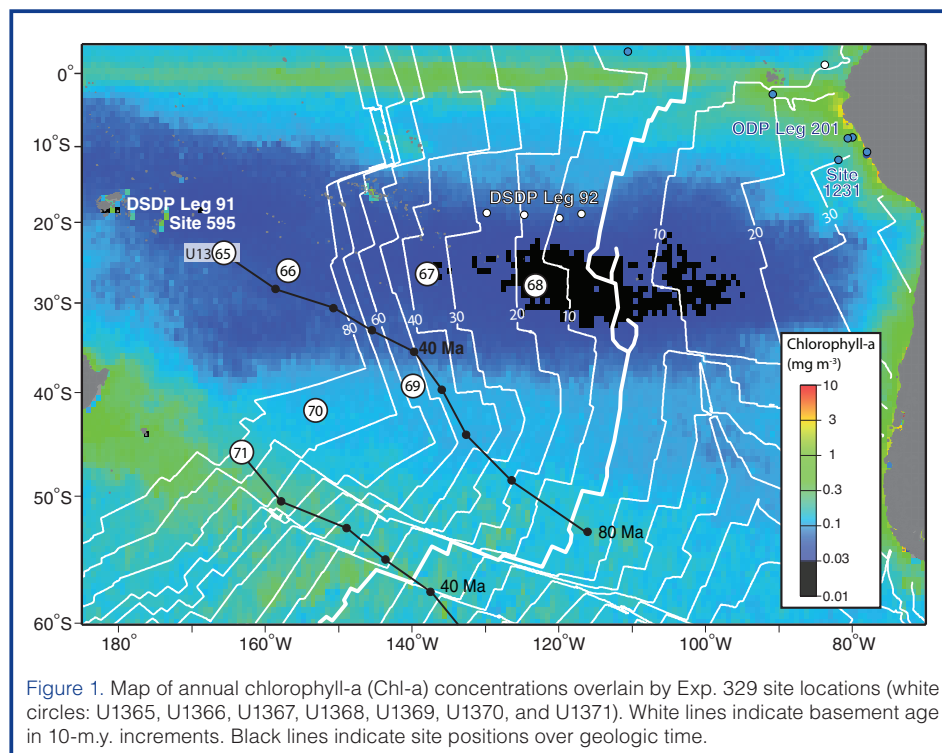The SPG contains a continuous sweep of oceanic crust with thin

Figure 1. Map of annual chlorophyll-a (Chl-a) concentrations overlain by Exp. 329 site locations (white circles: U1365, U1366, U1367, U1368, U1369, U1370, and U1371). White lines indicate basement age in 10-m.y. increments. Black lines indicate site positions over geologic time.

(1–100 m) sedimentary cover that spans thousands of kilometers and >100 m.y. of seafloor age. It is therefore ideal for testing hypotheses of the factors that limit hydrothermal circulation and chemical habitability in aging oceanic crust (sedimentary overburden, basement permeability, and decreasing basal heat flow).

The SPG contains the largest portion of the seafloor that has never been explored with scientific ocean drilling. Consequently, Exp. 329 will advance scientific understanding across a broad front, will help to constrain the nature of crustal inputs to the subduction factory, and will constrain the origin of the Cretaceous Normal Superchron (CNS) and tectonic history of a region as large as Australia. Recovery of sedimentary interstitial waters at several of the proposed sites will provide novel constraints on glacial-interglacial pCO_2 models.

Geological Setting

Exp. 329 drill sites span nearly the entire width of the Pacific plate in the Southern Hemisphere between 20°S and 45°S (Fig. 1; D'Hondt et al., 2011a). This oceanic crust was accreted along at least four different plate boundaries (Pacific/Phoenix, Pacific/Antarctic, Pacific/Farallon, and Pacific/Nazca). Crustal ages range from ~100 Ma (Chron 34n) at Site U1365 to ~13 Ma (Chron 5ABn) at Site U1368 (Gradstein et al., 2004). Based on crust age and regional tectonic histories (Larson et al., 2002; Tebbens and Cande, 1997), spreading rates range from slow-intermediate (<20 km m.y.$^{-1}$, half-rate) to ultrafast (>80 km m.y.$^{-1}$, half-rate).

The site locations cover a relatively wide range of crustal ages, spreading rates, and tectonic/volcanic environments. The depth and crustal age of each site correlates well with the predicted depth versus age curve (Stein and Stein, 1994), which suggests the sites are located on representative ocean crust. Calculated spreading rates at each site are somewhat biased toward fast and ultrafast spreading rates (28–95 km m.y.$^{-1}$, half-rate). Surprisingly, the 95 km m.y.$^{-1}$ value is one of the fastest spreading half-rates measured globally. The abyssal hill fabric is relatively well defined for most coring sites. However, off-axis volcanism at Site U1368 masked the original seafloor fabric. Sediment thickness ranges from <3 m to 122–130 m and generally increases west and south of our survey area. This sediment thickness trend is consistent with greater sediment cover on older crust and on crust located farther away from the center of the gyre. Sediment at each of the Exp. 329 sites generally appears as pelagic drape, with some localized mass wasting deposits.

Microbiological Setting

The sedimentary communities and activities of shallow (0–8 meters below seafloor [mbsf]) SPG sediment are unlike those in any sediment of equal depth previously explored by scientific ocean drilling (D'Hondt et al., 2009). A shallow coring survey prior to IODP drilling demonstrated that cell concentrations and organic-fueled respiration in the shallow sediment of Sites U1365–U1370 are orders of magnitude lower than concentrations in previously examined sediment of equivalent depth (D'Hondt et al., 2009). Dissolved oxygen penetrates extremely deeply (D'Hondt et al., 2009; Fischer et al., 2009).

These pilot results demonstrated that, at least in the shallow sediment, (1) net metabolic activities are low and oxygen is the principal net terminal electron acceptor and (2) biomass is substantially different than in any previously examined deep-sea sediment. In contrast, on the southern edge of the gyre, where sea-surface chlorophyll content is much higher, cell concentrations and dissolved chemical concentrations in the shallow (0–4 mbsf) sediment (D'Hondt et al., 2009) resemble those of ODP Site 1231 (on the northeastern edge of the gyre), where most of the subseafloor interstitial water is anoxic. At these sites the microbial community may be principally supported by oxidation of organic matter coupled to reduction of Mn(IV), Fe(II), and NO_3^- migrating up from the underlying basaltic aquifer (D'Hondt et al., 2004; Shipboard Scientific Party, 2003). These results suggested that biomass and microbial activity in subseafloor sediment may vary predictably with sea-surface chlorophyll content.

Scientific Objectives

The fundamental objectives of Exp. 329 are

- To document the habitats, metabolic activities, genetic composition, and biomass of microbial communities in subseafloor sediment with very low total activity;
- To test how oceanographic factors (such as surface ocean productivity) control variation in sedimentary habitats, activities, and communities from gyre center to gyre margin;
- To quantify the extent to which subseafloor microbial communities of this region may be supplied with electron donors by water radiolysis, a process independent of the surface photosynthetic world; and
- To determine how basaltic basement habitats, potential activities and, if measurable, microbial communities vary with crust age and hydrologic regime (from ridge crest to abyssal plain).

Exp. 329 provided key data and the samples necessary to meet these objectives (D'Hondt et al., 2011a). However, fully meeting these objectives requires post-expedition studies across a very broad front, including but not limited to studies that rely on environmental nucleic acids, microbial cultivations, biogeochemistry, and mineralogy. In combination, the shipboard and post-expedition studies will address several significant questions. Are communities in mid-gyre subseafloor sediment uniquely structured? Do they contain previously unknown organisms? What are their principal sources of metabolic energy? Do their principal metabolic activities and composition vary with properties of the surface world, such as sea-surface chlorophyll concentrations or

organic flux to the seafloor? Is microbial activity sustainable in subseafloor basalt by mineral oxidation (e.g., oxidation of iron and sulfur species in the basaltic minerals) for tens of millions of years after basalt formation? Post-expedition studies are building on expedition results to definitively answer these questions (D'Hondt et al., 2011b; Reese et al., 2012; Sauvage et al., 2012; Steele et al., 2012; Ziebis et al., 2012).

The results of Exp. 329 and subsequent shore-based studies are also testing (i) the factors that control evolution of geothermal circulation and chemical alteration in oceanic crust, (ii) models of regional tectonic history (Zhang et al., 2012), (iii) South Pacific paleoceanographic history (Alvarez Zarikian et al., 2012; Amaya et al., 2012; Berger et al., 2012; Dubois et al., 2012; Dunlea et al., 2012; Huang et al., 2012), and (iv) models of glacial-interglacial ocean-climate change (Lado Insua et al., 2011).
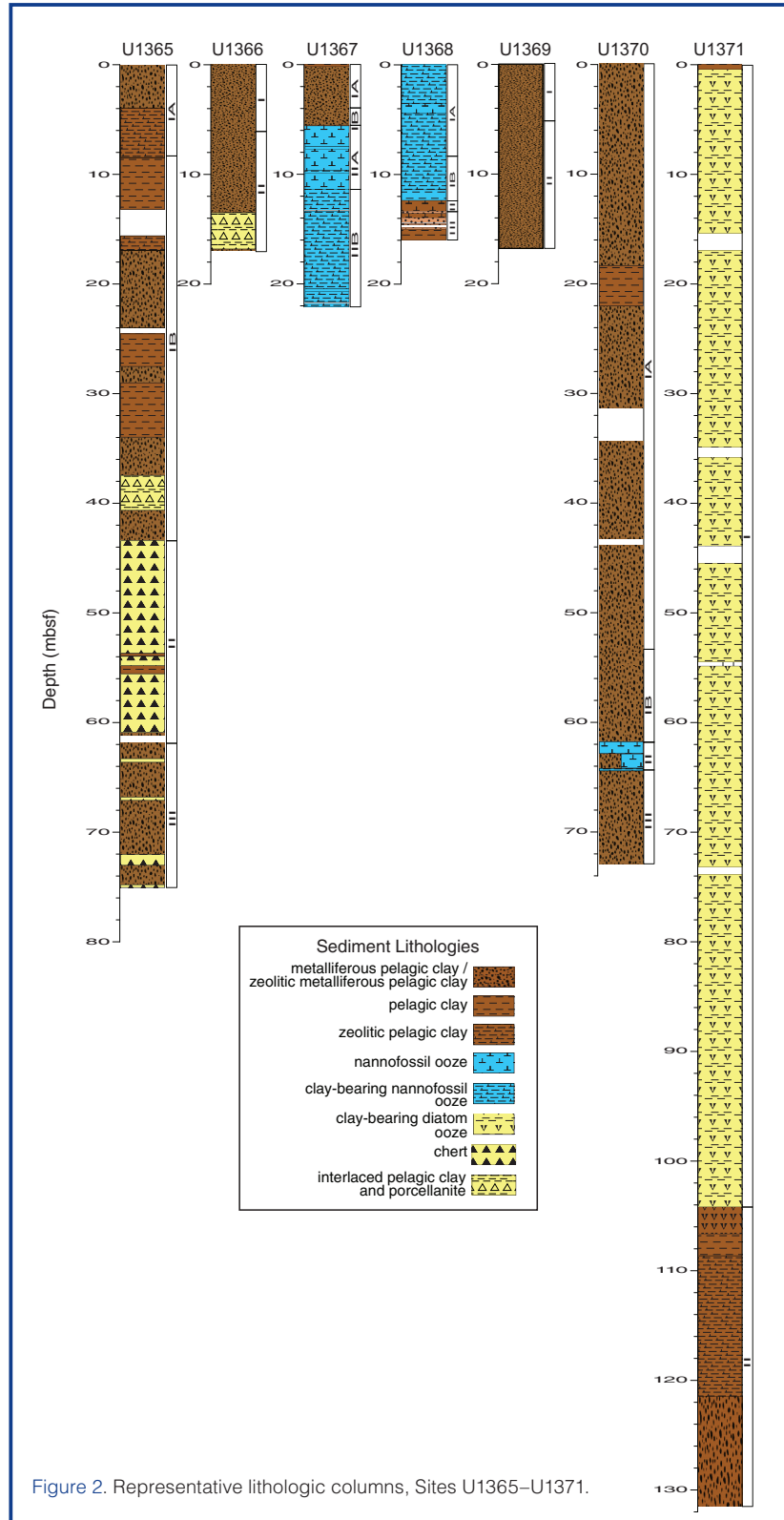
Coring-Drilling Strategy

The general coring strategy was to sample the entire sediment column multiple times at seven sites and to core the upper basement at three sites. The sites (Fig. 1) collectively underlie the full range of surface-ocean productivity conditions present in the SPG, ranging from the extremely low productivity conditions of the gyre center (Site U1368) to the moderately high (for open ocean) productivity at the southern edge of the gyre (Site U1371, at the northern edge of the Antarctic Convergence). This series of sites is composed of two transects, with the first transect centered at ~26°S, beneath the heart of the SPG, and the second transect centered at ~42°S in the southern portion of the gyre (Fig. 1).

The sites in the northern sequence have been continuously far from shore and beneath the low-productivity gyre waters for many tens of millions of years. They provide an ideal opportunity to document the nature of life in subseafloor sediment with very low biomass and very low rates of activity. In combination with the southern transect, the northern transect also will allow us to determine how subseafloor sedimentary microbial activities and communities vary from gyre center to gyre margin.

The sites in the second transect have been in the southern portion of the present gyre (Sites U1369 and U1370) or south of the gyre (Site U1371) for tens of millions of years. Particularly at Site U1371, chlorophyll-a concentrations and primary productivity are much higher than at all of the sites in the northern transect (Fig. 1). This transect helps document how subseafloor sedimentary microbial activities and communities vary from gyre center to gyre margin. Because Site U1371 provides an anoxic standard of comparison for the other sites, it is also crucial for documenting the potential uniqueness (or ubiquity) of the microbial communities and activities that persist in the low-activity, low-biomass sediment beneath the gyre center.

Figure 2. Representative lithologic columns, Sites U1365–U1371.

The northern sequence of sites (U1365–U1368) is placed on basaltic basement of steadily increasing age from east to west (Fig. 1). Basaltic basement ranges in age from 7 Ma to as much as 125 Ma (Site U1365). Basement age of the southern sites ranges from 39 Ma to 73 Ma. Their water depths generally follow the classic curve (Parsons and Sclater, 1977) of increasing water depth with increasing basement age. These sites allow the Exp. 329 science party to document the mineralogic and hydrologic evolution of the basement and its implications for metabolic habitability and microbial communities in ocean crust under very thin sediment cover.

Expedition Synthesis

Sediment

The dominant lithology is zeolitic metalliferous clay at the deeper water sites on older basement (58 Ma to ≤120 Ma) within the gyre (Sites U1365, U1366, U1369, and U1370; Figs. 1, 2). Manganese nodules occur at the seafloor and intermittently within the upper sediment column at these sites. Chert and porcellanite layers are pronounced in the lower half of the sediment column at Sites U1365 and U1366. The dominant lithology is carbonate ooze at Site U1368, the site on youngest basement (13.5 Ma) and, consequently, in the shallowest water. At Site U1371, which lies on relatively old basaltic basement (71.5–73 Ma) just south of the gyre, the dominant lithology is siliceous ooze, although metalliferous zeolitic clay dominates the lowest portion of this sediment column.

The dominant lithology shifts from clay to carbonate ooze at depth in two of the sites (Fig. 2). At Site U1367, the transition from clay to carbonate at 6–7 mbsf marks the time that the site subsided beneath the carbonate compensation depth (CCD) as the underlying basement cooled with age. At Site U1370, carbonate ooze is the dominant lithology for a short interval deposited during planktonic foraminiferal Zone P1. This foraminifer-bearing interval is most simply interpreted as resulting from the CCD diving to greater water depth than the water depth of this site during the early Paleocene interval of low planktonic carbonate production and low organic flux to the seafloor.
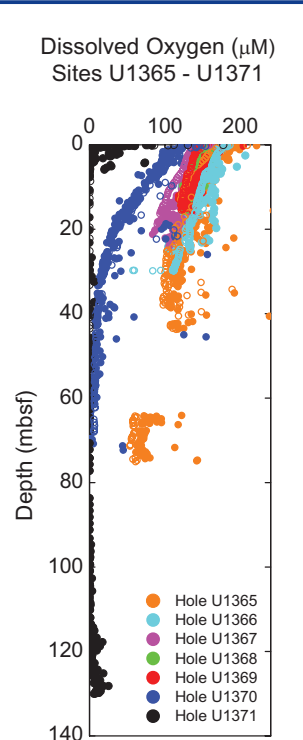
Figure 3. Dissolved oxygen (μM) vs. depth, Sites U1365–U1371.
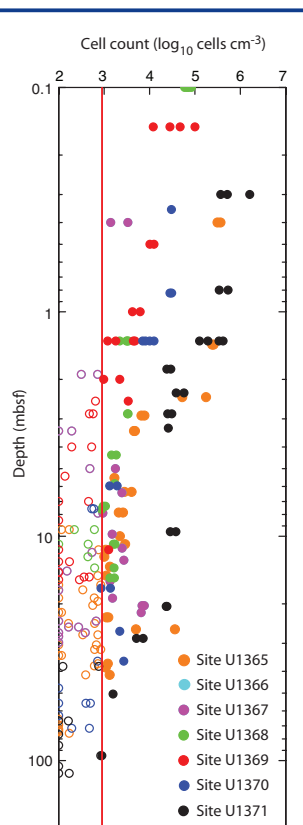
Figure 4. Cell counts vs. depth, Sites U1365–U1371, data from D'Hondt et al., 2011a. The vertical red line is the minimum detection limit (MDL). The filled symbols represent counts above the MDL and the open symbols represent counts below the MDL.

Sediment thickness is generally very low throughout the gyre (Fig. 2). When sites of broadly similar age are compared (Site U1366, 84–120 Ma; Site U1369, 58 Ma; Site U1370, 74–80 Ma; and Site U1371, 71.5–73 Ma), thickness of the sediment column generally increases with increasing distance from the gyre center (Figs. 1, 2).

Sedimentary Microbial Communities and Habitability

Throughout the SPG (Sites U1365–U1370), dissolved oxygen and dissolved nitrate are present throughout the entire sediment column (Fig. 3), indicating that microbial respiration is oxic throughout the column, as predicted by D'Hondt et al. (2009) and Fischer et al. (2009). The concentration profiles indicate that the subseafloor rate of microbial respiration is generally extremely low.

In contrast, at Site U1371 in the upwelling zone just south of the gyre (Fig. 1), detectable dissolved oxygen and dissolved nitrate are limited to just below the sediment/water interface and just above the sediment/basalt interface. Between these interfaces, the sediment is anoxic. Very high concentrations of dissolved (presumably reduced) manganese indicate that manganese reduction is a prominent electron-accepting process throughout most of this sediment column, with very short intervals of iron reduction suggested by minor peaks in dissolved iron concentration associated with local minima in dissolved manganese concentration. The rapid drop of dissolved oxygen and nitrate below their detection limits at the upper and lower edges of this sediment column and the relatively high concentrations of dissolved phosphate within this column indicate that the subseafloor rate of microbial respiration is much higher at this site than at the sites located in the gyre.

At the sites located within the gyre (Sites U1365–U1370), microbial cell counts are below ~10^6 cells cm^{-3} near the seafloor and decrease rapidly with depth (Fig. 4). These concentrations are three or more orders of magnitude lower than at the same sediment depths in all sites previously cored by scientific ocean drilling (Kallmeyer et al., 2012). Microbial cell counts are generally higher at Site U1371 than at the sites within the gyre

(Sites U1365–U1370), but are lower than at all other sites previously drilled.

At the sites in the gyre, total organic carbon (TOC) and total nitrogen decline rapidly with depth in the upper sediment column and are generally constant at greater depth. In contrast, at Site U1371, TOC and total nitrogen are generally much higher than at the other sites at all depths.

The presence of dissolved oxygen, dissolved nitrate, dissolved phosphate, and dissolved inorganic carbon throughout the entire sediment column at all sites in the gyre (Sites U1365–U1370; Fig.3), indicates that microbial life is not limited by availability of electron acceptors or major nutrients (carbon, nitrogen, and phosphorus) in this sedimentary environment. Although dissolved oxygen is absent from most of the sediment column at Site U1371, the presence of dissolved sulfate, dissolved phosphate, and dissolved inorganic carbon throughout its entire sediment column indicates that microbial life is not limited by availability of electron acceptors or major nutrients in this sedimentary environment either.

Basalt and Basalt Alteration

The uppermost basaltic basement at Site U1365 is composed of lava flows, whereas the uppermost basement at Sites U1367 and U1368 is primarily composed of pillow basalt. Some flows at U1365 are only decimeters thick, whereas other flows are tens of meters thick.

Alteration in lava flow units, as evident at Site U1365, appears to be strongly controlled by lithologic structure, with most alteration focused at the flow boundaries (Fig. 5). In contrast, alteration in pillow lava units (the dominant igneous lithologies at Sites U1367 and U1368) appears to be more evenly distributed.

At all sites, the presence of dissolved oxygen in the lowermost sediment at below-deepwater concentrations (Fig. 3) suggests that either (1) basement oxidation has occurred since seawater migrated into the formation or (2) oxygen has been lost to the overlying sediment along the flow path.

At the sites with oldest basement, alteration of the basement basalt continues on the timescale of formation fluid replacement. Natural gamma radiation (NGR) core logs, downhole NGR logs (Site U1368), and chemical analyses of the rock demonstrate that potassium has been consistently taken up during basalt alteration at all three sites where the basaltic basement was drilled (Sites U1365, U1367, and U1368). At the sites with deepest sediment (Site U1365, where basalt was drilled, plus Sites U1370 and U1371, where basalt was not drilled), dissolved potassium concentrations are noticeably lower in the deepest sediment than in the shallow sediment, indicating that (1) dissolved potassium fluxes into the underlying basalt and (2) basalt alteration continues despite the great age of basement at all three sites (84–120 Ma, 74–79.5 Ma, and 71.5–73 Ma, respectively).

At all three sites where basement was cored by rotary core barrel (RCB; Sites U1365, U1367, and U1368), secondary minerals provide evidence of both oxidative alteration (iron oxyhydroxide and celadonite) and oxygen-poor alteration (saponite and secondary sulfides). Some samples have undergone multiple stages of alteration. Late vein infills suggest that alteration may be continuous, or at least occurs intermittently throughout the life of the ocean crust. At Site U1365, the presence in the lowermost sediment of dissolved Mg at below-deepwater concentrations and dissolved Ca at above-deepwater concentrations indicates that basalt-water interaction in the form of Mg exchange for Ca has occurred since seawater migrated into the formation. This exchange may continue to drive late-stage calcite precipitation, despite the great age of basement at this site (80–120 Ma).

Habitability of Basaltic Basement

Profiles of dissolved oxygen, dissolved inorganic carbon, dissolved nitrate, and dissolved phosphate in the lowermost sediment at each site indicate that if microbial life is present in the uppermost basalt (Fig. 4), it is not limited by access to electron acceptors (oxygen and nitrate) or major nutrients (carbon, nitrogen, and phosphorus).

Hole U1365E Igneous Lithologic Summary

Figure 5. Relationship between igneous units, visually observed alteration intensity, and potassium content (determined by NGR core logging), Hole U1365E.

Igneous lithologies
- aphyric basalt (<1% phenocrysts)
- phyric basalt
- sparsely phyric basalt (1-5% phenocrysts)
- moderately phyric basalt (5-10% phenocrysts)
- highly phyric basalt (>10% phenocrysts)
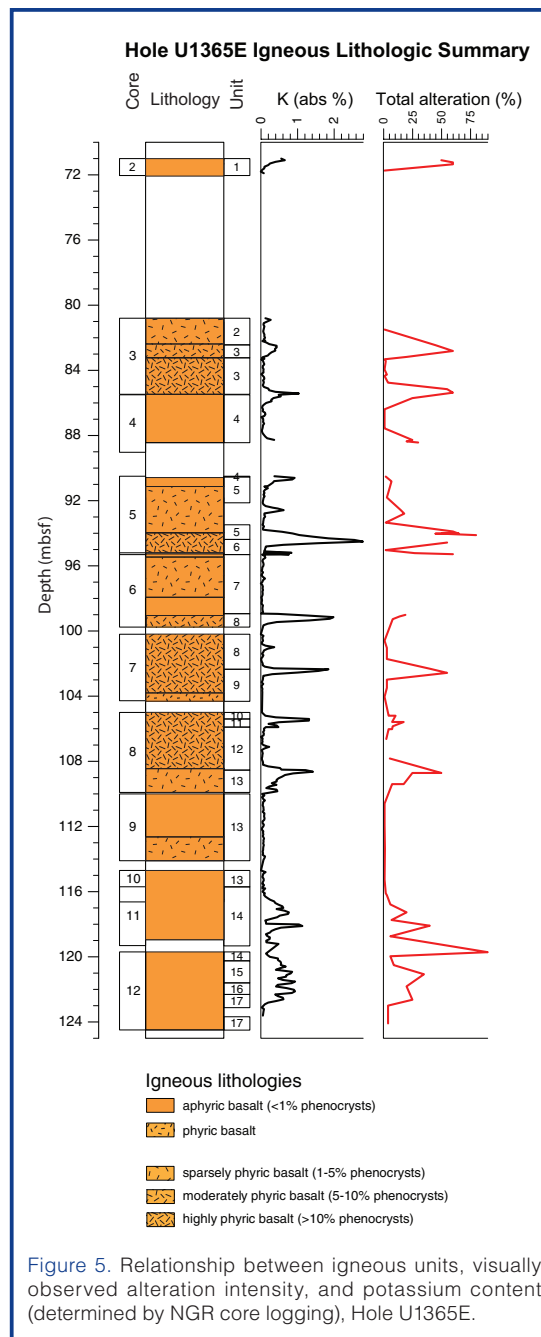
Past Microbial Activity?

Tube-like micro-scale weathering features occur in altered glass from Site U1365. They are arranged in discrete clusters or in masses adjacent to or near fractures and iron oxyhydroxide within the glass. Similar features have been observed in marine basaltic glass elsewhere and attributed to microbial origin (Fisk et al., 1998).

Technical Advances

Exp. 329 used a wide range of instruments and techni-ques that have not been used often on scientific ocean drilling expeditions. Details of their application are provided in the "Methods" chapter of the IODP Proceedings (Exp. 329 Scientists, 2011), particularly in the sections on biogeochemistry, microbiology, and physical properties.

Two new technical approaches were used by the Exp. 329 Scientific Party on an experimental basis, with the intention of refining them for future application. The first of these techniques was a new method of cell counting using flow cytometry (Morono et al., 2011). The second was use of NGR core logging for shipboard quantification of absolute concentrations of ^{238}U-series elements, ^{232}Th-series elements, and potassium (Dunlea et al., 2013).

The IODP Expedition 329 Scientific Party

Nathalie Dubois, Tim Engelhardt, Helen Evans, Timothy Ferdelman, Britta Gribsholt, Robert N. Harris, Bryce W. Hoppie, Jung-Ho Hyun, Jens Kallmeyer, Jinwook Kim, Jill E. Lynch, Satoshi Mitsunobu, Yuki Morono, Richard W. Murray, Takaya Shimono, Fumito Shiraishi, David C. Smith, Christopher E. Smith-Duque, Arthur J. Spivack, Bjorn Olav Steinsbu, Yohey Suzuki, Michal Szpak, Laurent Toffin, Goichiro Uramoto, Yasuhiko T. Yamaguchi, Guo-liang Zhang, Xiao-Hua Zhang, Wiebke Ziebis.

Acknowledgments

References

Alvarez Zarikian, C. A., Wade, B. S., Villarejo, J., and Firth, J. V., 2012. Oligocene to mid-Pliocene deep sea Ostracoda from the South Pacific Gyre and their paleoceanographic significance [paper presented at the 2012 American Geophysical Union Fall Meeting, San Francisco, CA, 3–7 December 2012]. Abstract PP31B-2029. http://fallmeeting.agu.org/2012/eposters/eposter/pp31b-2029/

Amaya, D., Thomas, D. J., Marcantonio, F., Korty, R., Huber, M., Winckler, G., and Alvarez Zarikian, C. A., 2012. Reconstruction of South Pacific dust accumulation during the Early Paleogene Greenhouse [paper presented at the 2012 American Geophysical Union Fall Meeting, San Francisco, CA, 3–7 December 2012]. Abstract PP13A-2063. http://fallmeeting.agu.org/2012/eposters/eposter/pp13a-2063/

Behrenfeld, M. J., and Falkowski, P. G., 1997. Photosynthetic rates derived from satellite-based chlorophyll concentration. *Limnol. Oceanogr.*, 42(1):1–20. doi:10.4319/lo.1997.42.1.0001

Berger, A. C., Thomas, D. J., and Alvarez Zarikian, C. A., 2012. The Paleogene record of South Pacific deep water – Nd isotopes from IODP Site U1370 [Paper presented at the 2012 American Geophysical Union Fall Meeting, San Francisco, CA, 3–7 December 2012]. Abstract PP31A-2006. http://fall-meeting.agu.org/2012/eposters/eposter/pp31a-2006/

D'Hondt, S., Inagaki, F., Alvarez Zarikian, C. A., Dubois, N., Engelhardt, T., Evans, H., Ferdelman, T., et al., 2011a. *Proc. IODP*, 329: Washington, DC (Integrated Ocean Drilling Program Management International, Inc.). doi:10.2204/iodp.proc.329.2011.

D'Hondt, S., Jørgensen, B. B., Miller, D. J., Batzke, A., Blake, R., Cragg, B. A., Cypionka, H., et al., 2004. Distributions of microbial activities in deep subseafloor sediments. *Science*, 306(5705):2216–2221. doi:10.1126/science.1101155

D'Hondt, S., Spivack, A. J., Pockalny, R., Ferdelman, T. G., Fischer, J. P., Kallmeyer, J., Abrams, L. J., et al., 2009. Subseafloor sedimentary life in the South Pacific Gyre. Proc. Natl. Acad. Sci. U.S.A., 106(28):11651–11656. doi:10.1073/pnas.0811793106

D'Hondt, S. L., Inagaki, F., Alvarez Zarikian, C. A., and the Integrated Ocean Drilling Program Expedition 329 Shipboard Scientific Party, 2011b. A deep oxic ecosystem in the subseafloor South Pacific Gyre [Paper presented at the 2011 American Geophysical Union Fall Meeting, San Francisco, CA, 5–9 December 2011]. Abstract B44B-03. http://adsabs.harvard.edu/abs/2011AGUFM.B44B..03D

Dubois, N., Mitchell, N. C., and Hall, I. R., 2012. Sedimentation in an oceanic desert: The South Pacific Gyre [Paper presented at the 2012 American Geophysical Union Fall Meeting, San Francisco, CA, 3–7 December 2012]. Abstract PP13A-2062.

Dunlea, A. G., Murray, R. W., Sauvage, J., Spivack, A. J., Harris, R. N., and D'Hondt, S. L., 2012. Geochemically tracking provenance changes in marine sediment from the South Pacific Gyre throughout the Cenozoic [Paper presented at the 2012 American Geophysical Union Fall Meeting, San Francisco, CA, 3–7 December 2012]. Abstract PP21C-06.

Dunlea, A. G., Murray, R. W., Harris, R. N., Vasiliev, M. A., Evans, H., Spivack, A. J., and D'Hondt, S., 2013. Assessment and use of NGR instrumentation on the *JOIDES Resolution* to quantify U, Th, and K concentrations in marine sediment. *Sci. Drill*, 15:57–63. doi:10.2204/iodp.sd15.05.2013.

Expedition 329 Scientists, 2011. Expedition 329 methods. *In* D'Hondt, S., Inagaki, F., Alvarez Zarikian, C. A., and the Expedition

329 Scientists, *Proc. IODP*, 329: Washington, DC (Integrated Ocean Drilling Program Management International, Inc.). doi:10.2204/iodp.proc.329.102.2011

Fischer, J. P., Ferdelman, T. G., D'Hondt, S., Røy, H., and Wenzhöfer, F., 2009. Oxygen penetration deep into the sediment of the South Pacific gyre. *Biogeosciences*, 6:1467–1478. http://www.biogeosciences.net/6/1467/2009/bg-6-1467-2009.pdf

Fisk, M. R., Giovannoni, S. J., and Thorseth, I. H., 1998. Alteration of oceanic volcanic glass: Textural evidence of microbial activity. *Science,* 281(5379):978–980. doi:10.1126/science.281.5379.978

Gradstein, F. M., Ogg, J. G., and Smith, A. G., 2004. *A Geologic Time Scale 2004:* Cambridge (Cambridge University Press). http://cambridge.org/uk/catalogue/catalogue.asp?isbn=9780521781428

Huang, Y., Spivack, A. J., Røy, H., Gribsholt, B., Ziebis, W., Murray, R. W., Hyun, J- H., and D'Hondt, S., 2012. The Redfield ratio over the past 70 million years [Paper presented at the 2012 American Geophysical Union Fall Meeting, San Francisco, CA, 3–7 December 2012]. Abstract PP23F-03.

Jahnke, R. A., 1996. The global ocean flux of particulate organic carbon: Areal distribution and magnitude. *Global Biogeochem. Cycles*, 10(1):71–88. doi:10.1029/95GB03525.

Kallmeyer, J., Pockalny, R., Adhikari, R., Smith, D. C., and D'Hondt, S., 2012. Global distribution of subseafloor sedimentary biomass. *Proc. Natl. Acad. Sci. U.S.A.*, 109(40):16213–16216.

Lado Insua, T., Spivack, A. J., D'Hondt, S. L., Graham, D., Moran, K., the Expedition Knorr 195 (III) Shipboard Scientific Party, and the Integrated Ocean Drilling Program Expedition 329 Shipboard Scientific Party, 2011. Reconstruction of Pacific bottom water salinity during the Last Glacial Maximum [Paper presented at the 2011 American Geophysical Union Fall Meeting, San Francisco, CA, 5–9 December 2011]. Abstract PP11B-1791.

Larson, R. L., Pockalny, R. A., Viso, R. F., Erba, E., Abrams, L. J., Luyendyk, B. P., Stock, J. M., and Clayton, R. W., 2002. Mid-Cretaceous tectonic evolution of the Tongareva triple junction in the southwestern Pacific Basin. *Geology*, 30(1):67–70. doi:10.1130/0091-7613(2002)030<0067:MCTEOT>2.0.CO;2

Morel, A., Gentili, B., Claustre, H., Babin, M., Bricaud, A., Ras, J., and Tiéche, F., 2007. Optical properties of the "clearest" natural waters. *Limnol. Oceanogr.,* 52(1):217–229. doi:10.4319/lo.2007.52.1.0217

Morono, U., Kallmeyer, J., Inagaki, F., and the Expedition 329 Scientists, 2011. Preliminary experiment for cell count using flow cytometry. *In* D'Hondt, S., Inagaki, F., Alvarez Zarikian, C. A., and the Expedition 329 Scientists, *Proc. IODP,* 329: Washington, DC (Integrated Ocean Drilling Program Management International, Inc.). doi:10.2204/iodp.proc.329.110.2011

National Research Council of the National Academies (U.S.), 2003. *Enabling Ocean Research in the 21st Century: Implementation of a Network of Ocean Observatories:* Washington, DC (National Academies Press). http://www.nap.edu/openbook.php?isbn=0309089905

Parsons, B., and Sclater, J. G., 1977. An analysis of the variation of ocean floor bathymetry and heat flow with age. *J. Geophys. Res.*, 2(5):803–827. doi:10.1029/JB082i005p00803

Reese, B. K., Ariza, M., St. Peter, C., Hoffman, C., Edwards, K. J., and Mills, H. J., 2012. Re-defining the subsurface biosphere: Characterization of fungal populations from energy limited deep marine subsurface sediments [Paper presented at the 2012 American Geophysical Union Fall Meeting, San Francisco, CA, 3–7 December 2012]. Abstract B43G-0490. http://fallmeeting.agu.org/2012/eposters/eposter/b43g-0490/

Sauvage, J., Spivack, A. J., Dunlea, A. G., Murray, R. W., Smith, D. C., and D'Hondt, S. L., 2012. Radiolysis and life in deep subseafloor sediment of the South Pacific Gyre [Paper presented at the 2012 American Geophysical Union Fall Meeting, San Francisco, CA, 3–7 December 2012] Abstract B43G-0488. http://fallmeeting.agu.org/2012/eposters/eposter/b43g-0488/

Shipboard Scientific Party, 2003. Explanatory notes. *In* D'Hondt, S. L., Jørgensen, B. B., Miller, D. J., et al., *Proc. ODP, Init. Repts.,* 201: College Station, TX (Ocean Drilling Program), 1–103. doi:10.2973/odp.proc.ir.201.105.2003

Steele, J. A., Dekas, A. E., Harrison, B. K., Morono, Y., Inagaki, F., Ziebis, W., and Orphan, V. J., 2012. Mineral-association and activity of bacteria and Archaea in the deep subsurface South Pacific Gyre sediment [paper presented at the 2012 American Geophysical Union Fall Meeting, San Francisco, CA, 3–7 December 2012]. Abstract B43G-0492. http://fallmeeting.agu.org/2012/eposters/eposter/b43g-0492/

Stein, C. A., and Stein, S., 1994. Constraints on hydrothermal heat flux through the oceanic lithosphere from global heat flow. *J. Geophys. Res.*, 99(B2):3081–3095. doi:10.1029/93JB02222

Tebbens, S. F., and Cande, S. C., 1997. Southeast Pacific tectonic evolution from Early Oligocene to Present. *J. Geophys. Res.*, 102(B6):12061–12084. doi:10.1029/96JB02582.

Zhang, G., Smith-Duque, C., Tang, S., Li, H., Zarikian, C., D'Hondt, S., Inagaki, F., and IODP Expedition 329 Scientists, 2012. Geochemistry of basalts from IODP site U1365: Implications for magmatism and mantle source signatures of the mid-Cretaceous Osbourn Trough. *Lithos*, 144:73–87. doi:10.1016/j.lithos.2012.04.014

Ziebis, W., Patel, A., Krupke A., and Ferdelman, T. G., 2012. Exploring metabolic activities of deeply buried microbial communities in oxic sediments underlying oligotrophic open ocean gyres [Paper presented at the 2012 American Geophysical Union Fall Meeting, San Francisco, CA, 3–7 December 2012]. Abstract B42C-02.

Authors

Steven D'Hondt, Graduate School of Oceanography, University of Rhode Island, 100A, Horn Building, 215 South Ferry Road, Narragansett, RI 02882, U.S.A., e-mail: dhondt@gso.uri.edu

Fumio Inagaki, Kochi Institute for Core Sample Research, Japan Agency for Marine-Earth Science and Technology (JAMSTEC), 200 Monobe Otsu, Nankoku City, Kochi, 783-8502 Japan

Carlos Alvarez Zarikian, Integrated Ocean Drilling Program, Texas A&M University, 1000 Discovery Drive, College Station, TX 77845-9547, U.S.A.

and the IODP Expedition 329 Scientific Party

IODP Expedition 330: Drilling the Louisville Seamount Trail in the SW Pacific

by Anthony A.P. Koppers, Toshitsugu Yamazaki, Jörg Geldmacher, and the IODP Expedition 330 Scientific Party

Abstract

Deep-Earth convection can be understood by studying hotspot volcanoes that form where mantle plumes rise up and intersect the lithosphere, the Earth's rigid outer layer. Hotspots characteristically leave age-progressive trails of volcanoes and seamounts on top of oceanic lithosphere, which in turn allow us to decipher the motion of these plates relative to "fixed" deep-mantle plumes, and their (isotope) geochemistry provides insights into the long-term evolution of mantle source regions. However, it is strongly suggested that the Hawaiian mantle plume moved ~15° south between 80 and 50 million years ago. This raises a fundamental question about other hotspot systems in the Pacific, whether or not their mantle plumes experienced a similar amount and direction of motion. Integrated Ocean Drilling Program (IODP) Expedition 330 to the Louisville Seamounts showed that the Louisville hotspot in the South Pacific behaved in a different manner, as its mantle plume remained more or less fixed around 48°S latitude during that same time period. Our findings demonstrate that the Pacific hotspots move independently and that their trajectories may be controlled by differences in subduction zone geometry. Additionally, shipboard geochemistry data shows that, in contrast to Hawaiian volcanoes, the construction of the Louisville Seamounts doesn't involve a shield-building phase dominated by tholeiitic lavas, and trace elements confirm the rather homogenous nature of the Louisville mantle source. Both observations set Louisville apart from the Hawaiian-Emperor seamount trail, whereby the latter has been erupting abundant tholeiites (characteristically up to 95% in volume) and which exhibit a large variability in (isotope) geochemistry and their mantle source components.

Introduction and Objectives

Linear trails of volcanic islands and seamounts are a striking and abundant feature in the Pacific Ocean basin. They are believed to form as oceanic crust moves over a relatively stationary magma source or hotspot, which in turn may be caused by a narrow zone of mantle upwelling that results in the partial melting of the ascending mantle plume material (Morgan, 1971; Wilson, 1963). Consequently, the individual volcanoes in these trails grow older in the direction of plate motion. The 6000-km-long Hawaiian-Emperor seamount trail represents the most famous example, and it is used in many textbooks to explain the hotspot model. Because of its linear morphology, its lack of interfering seamount trails, and its long-lived age-progressive volcanism, the Louisville seamount trail (Fig. 1) is the South Pacific counterpart of the much better studied Hawaiian-Emperor seamount trail (Koppers et al., 2004; Lonsdale, 1988). Both the Hawaiian and Louisville hotspots are considered *primary* hotspots because of characteristics indicating a deep mantle origin (Courtillot et al., 2003), and since they are located on the same plate, the spatial and age patterns of their volcanoes and seamounts should match the same plate motion parameters (Duncan and Clague, 1985; Koppers et al., 2001; Wessel and Kroenke, 2008; Wessel et al., 2006), assuming that these hotspots remained fixed in the mantle. For example, the distinctive ~47-Myr-old
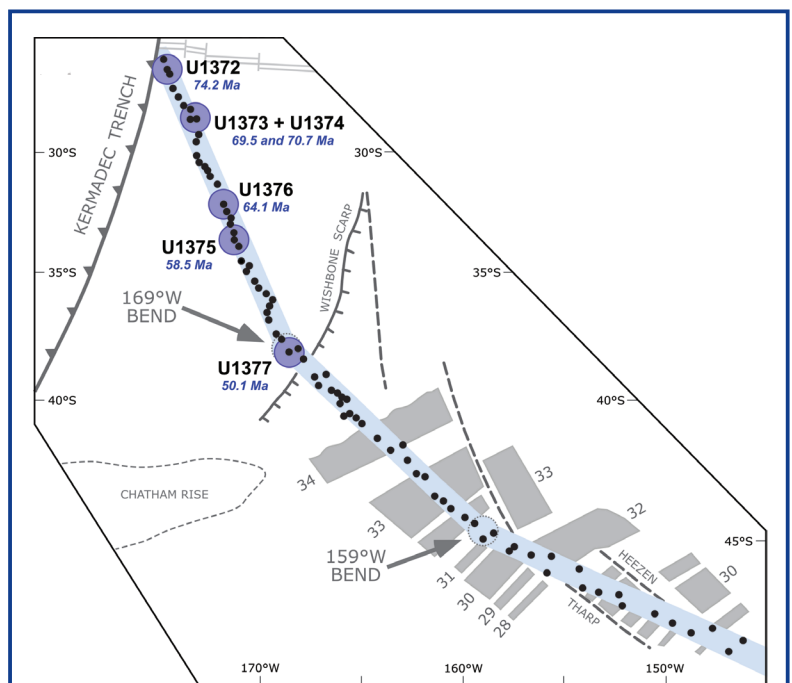
Figure 1. The Louisville seamount trail is defined by a narrow 75-km-wide chain of guyots and seamounts. The five guyots drilled during IODP Exp. 330 are indicated by purple circles. Also indicated are the Wishbone Scarp, which marks the easternmost boundary of the Exp. 330 drill sites and a likely sudden transition in age and thickness of the Pacific ocean crust, and the 169°W bend, which is equivalent (but less pronounced and slightly older in age; Koppers et al., 2011) to the distinctive 120° bend in the Hawaiian-Emperor seamount trail. Figure after Koppers et al. (2012a).

bend observed in the Hawaiian-Emperor seamount trail is generally thought to reflect a drastic change in the direction of Pacific plate motion at this time. However, drilling in the Emperor seamounts during Deep Sea Drilling Project Leg 55 and Ocean Drilling Program (ODP) Legs 145 and 197 documented a ~15° southward shift of the Hawaiian hotspot (relative to the geomagnetic field) between 80 Ma and 50 Ma (Kono, 1980; Tarduno, 2007; Tarduno and Cottrell, 1997; Tarduno et al., 2003, 2009). This large amount of plume motion alone could explain the 120° bend in the Hawaiian-Emperor seamount trail. In addition, numerical models of mantle-convection confirm that plume conduits may become tilted in response to large-scale horizontal mantle flow, in turn resulting in an absolute motion of hotspots along the Earth's surface (Steinberger and O'Connell, 1998). These models reproduce the observed latitudinal motion of the Hawaiian hotspot but predict essentially no latitudinal but rather a west-to-east longitudinal shift for Louisville models (Steinberger and Antretter, 2006; Steinberger and Calderwood, 2006; Steinberger et al., 2004).

IODP Exp. 330 to the Louisville seamount trail was designed to determine how much the Louisville hotspot moved (if at all) during the 80 Ma to 50 Ma time interval, and if it required a significant plume motion, to determine whether it moved independently from Hawaii (as predicted from the mantle flow models) or in concert (Koppers et al., 2010). To test these end-member geodynamic models was the primary goal of Exp. 330. This required detailed measurements of paleomagnetic inclination onboard the D/V *JOIDES Resolution* to determine the paleolatitude of the Louisville hotspot at the time of seamount formation, but also the sampling of unaltered basalt flows for onshore $^{40}Ar/^{39}Ar$ geochronology to establish the time frame for potential changes in the Louisville hotspot paleolatitude.

Other objectives of Exp. 330 centered around why existing geochemical data from dredged lavas (Beier et al., 2011; Cheng et al., 1987; Hawkins et al., 1987) indicate that the mantle plume source of the Louisville hotspot has been remarkably homogeneous for as long as 80 Myr, and why those lavas are predominantly alkali basalts. So far, no evidence has been found that show Louisville seamounts follow a geochemical evolution, such as that observed at the Hawaiian Islands, which comprises a voluminous, tholeiitic shield stage followed by an alkali basalt post-shield or rejuvenated stage. Shipboard geochemistry and planned onshore isotopic analyses of recovered lava flows (and melt inclusions) will provide important insights into the following: (1) origin and magmatic evolution of the Louisville volcanoes and hotspot source, (2) possible plume-lithosphere interaction, and (3) validity of the old hypothesis that the Ontong Java Plateau formed from the initial activity of the Louisville mantle plume around 120 Ma.

Finally, during Exp. 330 we also sampled a wide range of lithologies for geomicrobiological studies. Microbiologists accompanying earlier ODP and IODP expeditions documented the presence of microbial life in deeply buried sediments and basaltic basement, but most work to date concentrated on sediments or ocean crust younger than 3.5 Ma (Cowen et al., 2003; Mason et al., 2010). Stable isotope evidence (Rouxel et al., 2008) and microbial fossils (Fisk, et al., 1998; Parkes et al., 1994) indicate that there is a subsurface biosphere in older volcanic basement rocks as well. Exp. 330 provided an excellent opportunity to study living and extant microbial resi-dents within 80–50 Myr old seamount basalt flows as well as volcaniclastics that make up the Louisville seamounts. In total, more than sixty microbiology samples were collected from four seamounts up to a maximum depth of 516 meters below seafloor (mbsf).

Geologic Setting

The 4300-km-long Louisville seamount trail (Fig. 1) is a linear age-progressive chain of at least sixty-five major volcanic seamounts (Koppers et al., 2011; Lonsdale, 1988) and is considered a classical example of a hotspot track. The seamounts of the Louisville seamount trail range in age from ~80 Ma at its northwestern end (Koppers et al., 2004) to pro-

Table 1. IODP Exp. 330 drilling statistics and paleomagnetic sampling of basalts.

		IODP Expedition 330			In Situ Confidence Index (ISCI)					Total Number
Drill Site	Seamount Name	Penetration Depth (m)	Basement Cored (m)	Recovery Rate (%)	**3**	**2**	**1**	**0**	**N/A**	Discrete Samples
					(*in situ* basalt units)				(volc sed)	
U1372	Canopus Guyot	232.9	187.3	55.8	**19/8** (22)	**2/1** (4)	8	2	10	100
U1373	Rigil Guyot	65.7	31.8	90.6	**10/9** (10)	**0/0** (0)	--	--	14	34
U1374	Rigil Guyot	522.0	505.3	87.8	**12/14** (18)	**6/5** (7)	18	8	47	243
U1375	Achernar Guyot	20.0	--	--	--	--	--	--	--	--
U1376	Burton Guyot	182.8	140.9	75.6	**6/7** (8)	**2/1** (3)	6	0	10	99
U1377	Hadar Guyot	90.3	66.1	36.5	**12/2** (15)	**0/1** (1)	0	0	2	17
				TOTALS	**59/40** (73)	**10/8** (15)	32	10	79	493

On the left-hand side drilling statistics include depth of penetration, total thickness of igneous basement drilled and core recovery. On the right-hand side sample statistics list number of inclination averages that are available for individual lithological units from 2-cm archive half measurements (first number in bold) and from discrete samples (second number in bold). These numbers are expressed as a function of the *In Situ* Confidence Index (ISCI) that ranges from ISCI=3 for units that are definitely *in situ* to ISCI=0 for those that are likely not. Most volcaniclastic units were assigned an ISCI value of "not applicable" as it is unclear whether clasts in these volcanic sediments retained their orientation since eruption and emplacement. For the paleolatitude estimates we use results only from the most reliable units (ISCI=3 or 2) although it is significant that many volcaniclastic units yield inclinations consistent with intercalated *in situ* flows (cf. Figs. 7 and 8). Table from Koppers et al. (2012b).

bably recent times at its southeastern end. The exact location of the present-day hotspot is difficult to determine; it lies somewhere near the Eltanin Fracture Zone and the SW Pacific-Antarctic Ridge (Koppers et al., 2011; Watts et al., 1988). At the northern end of the trail, Osbourn Guyot (79 Ma; Koppers et al., 2004) is being subducted into the Tonga-Kermadec trench at 25.8°S. The oceanic crust beneath the northern part of the trail was formed at Osbourn Trough, a fossil spreading center that was active before 87 Ma or 93 Ma (Downey et al., 2007; Worthington et al., 2006) or 115 Ma (Mortimer et al., 2006), depending on the plate reconstruction models used. At ~38°S, the Louisville seamount trail crosses the western branch of the Wishbone Scarp that separates older oceanic crust formed at the Osbourn Trough to the west from younger crust created at the Pacific-Antarctic Ridge (Watts et al., 1988). It is expected that the presence of the fracture zone and the associated step in lithosphere thickness influences the mantle melting zone and hence the geochemical compositions of the lavas from Hadar Guyot, the youngest seamount drilled during Exp. 330. Dredged samples from Louisville seamounts located between the two branches of the Wishbone Scarp confirm this view by being more variable in composition compared to the general quite uniform geochemical composition of the Louisville seamounts (Beier et al., 2011).

Figure 2. Stratigraphic summary of the four deepest IODP Exp. 330 drill sites. The drilled sequences of Sites U1372 (Canopus Guyot), U1373 and U1374 (Rigil Guyot), and U1376 (Burton Guyot) are displayed in a simplified fashion to emphasize the overall lithological construction of the Louisville seamounts. Four lithology groups are recognized, from young to old: (i) recent pelagic ooze; (ii) an older seamount sedimentary cover; (iii) an upper volcanic sequence dominated by massive lava flows and interlayered with volcaniclastics; and (iv) a lower volcanic sequence characterized principally by volcaniclastics and hyaloclastites, but interspersed with lava flows and subvertical dike intrusions. The large fraction of volcaniclastics in these sequences sets the Louisville seamount trail apart from the lava-flow-dominated Emperor seamounts (Duncan et al., 2006). Downhole data plots for Sites U1375 and U1377 are omitted because of the shallow penetration depths. Figure after Koppers et al. (2012a).

Summary of Drilling Results

Exp. 330 replicated as closely as possible the drilling strategy of ODP Leg 197, which provided compelling evidence for mantle plume motion of the Hawaiian hotspot between ~80 Ma and 50 Ma. The seamounts drilled in the Louisville seamount trail were of similar ages with respect to Detroit, Suiko, Nintoku, and Koko seamounts in the Hawaiian-Emperor seamount trail. In total, six sites were drilled during Exp. 330 along the old end of the Louisville seamount trail on the summit plains of Canopus (U1372), Rigil (U1373, U1374), Burton (U1367), Achernar (U1375),

and Hadar (U1377) Guyots. In two cases larger seamount structures were targeted and drilled near their flanks; in the other three cases smaller edifices were drilled closer to their centers. Drilling and logging plans for each of these sites were similar, with coring reaching maximum depth of 522.0 mbsf for Site U1374 and 232.9, 65.7, 11.5, 182.8 and 53.3 mbsf for Sites U1372, U1373, U1375, U1376 and U1377, respectively (Table 1). The pelagic ooze cover was cored using a gravity-push approach with little or no rotation of the rotary core barrel assembly to maximize recovery; when no pelagic ooze was present, the holes were started directly into (often) cobble-rich hardgrounds. Volcanic basement was reached at four of the drilling targets, and downhole logging was successfully carried out for Sites U1374 and U1376.

From top to bottom the drilled sequences are generally characterized by (i) an absent or thin (<13.5-m-thick) layer of recent pelagic ooze; (ii) an older seamount sedimentary cover (0.3–41.9 m thick) of volcanic breccias, conglomerates and sandstones, and condensed limestones; (iii) an upper volcanic sequence (23.0–99.8 m thick) dominated by massive lava flows inter-layered with volcaniclastic sediments; and (iv) a lower volcanic sequence (70.2–405.5 m thick) characterized principally by volcaniclastics and hyaloclastites, but interspersed with *in situ* massive lava flows, smaller lava pods, pillow lavas, and subvertical dike intrusions (Fig. 2). At all sites the older sedimentary cover comprised sequences of volcanic sandstone (Fig. 3a) and various kinds of breccia (Fig. 3c) or conglomerate (Fig. 3d) that in some cases were interlayered with the spatter/tephra products of submarine eruptions (Fig. 3f) or (autobrecciated) basaltic lava flows with peperite flow tops (Fig. 3g). In this cover several (thin) intervals of carbonate were cored, with an occurrence of a ~15-m-thick algal limestone reef (Fig. 3b) at Site U1376 on Burton Guyot. At Sites U1372 through U1375 the underlying volcanic seamount sequences all were comprised of a high fraction of volcaniclastics (Figs. 3e, 3h) interspersed by *in situ* lava flows and a few dike intrusions (Fig. 3h). All lava flows and dikes drilled are alkali (or transitional) basalts (Fig. 4) that progressed from submarine (deeper in the sequences) to subaerial eruptive environments at the top of the volcanic basement (Fig. 5). However, at Sites U1376 and U1377 the igneous basements comprised submarine volcanic sequences only.
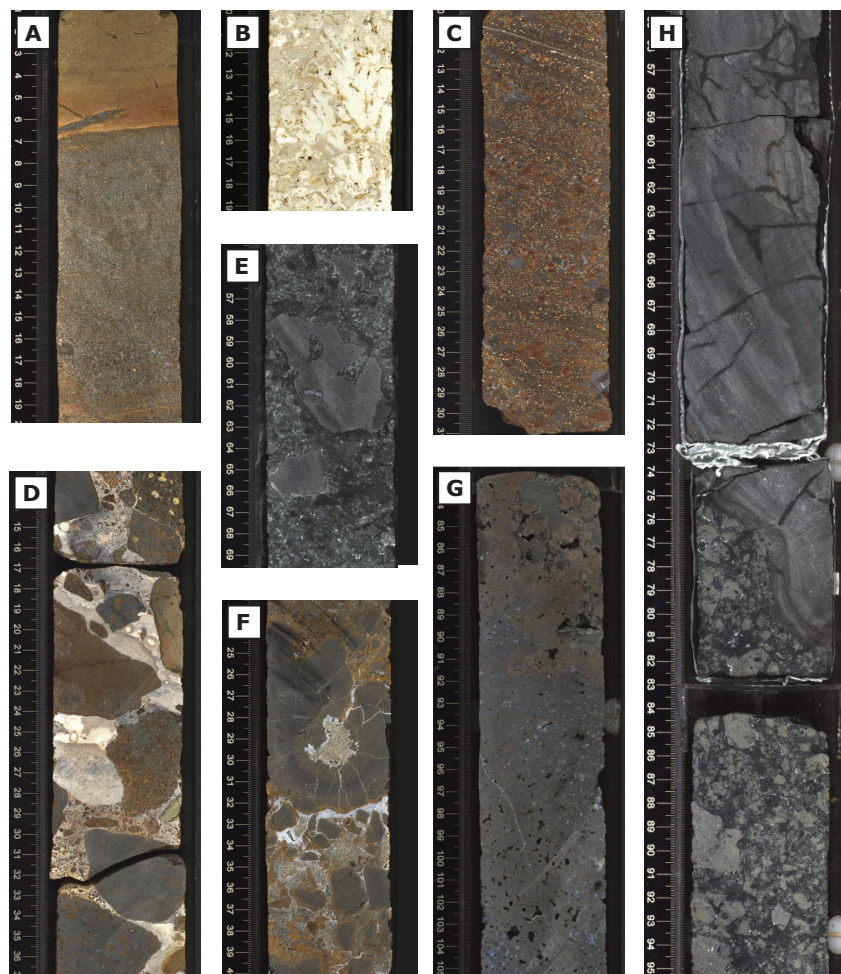
Figure 3. Lithological variation displayed in core images. [A] Monolithic bioturbated brown coarse tuff (top) and heterolithic multicolor volcanic sandstone (bottom) from Site U1376 (interval 330-U1376A-3R-4, 1–41 cm) deposited as turbidites in a hemipelagic or pelagic environment. [B] Algal boundstone with a branching growth form of algae from Site U1376 (interval 330-U1376A-3R-5, 10–29 cm) interpreted as a reef. [C] Multicolor coarse (layered) volcanic sandstone/breccia at Site U1374 (interval 330-U1374A-8R-1, 10–50 cm) interpreted to have been emplaced on a shallow-marine slope as a hyperconcentrated flow. [D] Multicolor basalt conglomerate emplaced under hemipelagic conditions at Site U1375 (interval 330-U1375A-2R-1, 1–41 cm) with inter-pebble spaces composed of foraminiferal limestone, finer-grained volcaniclastic sediment and carbonate cement. [E] Angular aphyric basalt clasts in hyaloclastite matrix at Site U1374 (interval 330-U1374A-66R-6, 55–69 cm). [F] Example of magma-sediment (peperitic) interaction observed at Site U1374 (interval 330-U1374A-17R-3, 20–40 cm). [G] Flow top at the upper (peperitic) boundary of a massive (~23-m-thick) aphyric basalt flow at Site U1373 (interval 330-U1373A-9R-2, 83–105 cm). [H] Aphyric subvertical dike intrusion (top) into hyaloclastite breccia sequence (bottom) at Site U1376 (interval 330-U1376A-15R-2A, 22–95 cm). Figure after Koppers et al. (2012a).

The average coring recovery rate was high at 72.4%, and in the case of Site U1374 on Rigil Guyot, a total of 522 meters was drilled at a record-breaking 87.8% (Table 1; Expedition 330 Scientists, 2011). The high recovery rates provide a high level of confidence in our understanding of the volcanic history at each drill site and seamount. Although the flat guyot tops indicate that these Louisville volcanoes formerly had subaerial summits, there is no evidence for extensive subaerial eruptions, and most recovered material represents (shallow) submarine volcanism during the main constructional phase of each volcano. The ^{40}Ar/^{39}Ar age dating, paleomagnetic measurements, and (isotope) geochemistry studies are focusing primarily on the *in situ* lava flows, pillow units, and subvertical dike intrusions from this submarine constructional phase, all of which will allow direct comparison of the paleolatitude estimates and geochemical signatures of the two longest-lived hotspot systems in the Pacific Ocean.

Site U1372 on Canopus Guyot

At Hole U1372A ~46 meters of sedimentary deposits and ~187 meters of igneous basement were drilled (Fig. 2). The hole was abandoned at 232.9 mbsf, and no downhole logging was carried out, because the drill string became irretrievably stuck in rubbly volcaniclastic breccia. The sedimentary units consist of ~14 meters of unconsolidated sandy foraminiferal ooze of late Miocene or younger in age, overlying ~32 meters of basaltic breccia and conglomerate with a minor interval of foraminiferal limestone of Cretaceous to early Paleogene age, which is interpreted to have been formed under neritic to hemipelagic water conditions.

The igneous basement section of the hole can be divided broadly into an upper (83-m-thick) part consisting of lava flows and a lower (104-m-thick) part composed mostly of volcaniclastics. The lava flows likely erupted subaerially or in very shallow marine conditions, because peperitic or scoriaceous, oxidized flow tops were observed. The igneous rocks typically have phenocryst assemblages of olivine only, olivine + plagioclase (+ augite) (Fig. 4a) or plagioclase + augite. Pyroxene phenocrysts and microphenocrysts are always titaniferous. Olivine is present in the groundmass in several of the upper series of lava flows but not in those from the lower part of the succession, implying an increase in alkalinity upward through the basement section. The presence of titanaugite indicates that these rocks are not tholeiitic. Geopetal structures in the upper part of the sequence are all horizontal, indicating that the drilled succession has not been tilted since its formation. Similar horizontal geopetal structures were observed also at all succeeding sites drilled during Exp. 330.

The entire igneous section has undergone various degrees of secondary alteration by low-temperature water-rock interaction and weathering. Down to ~90 mbsf the volcanic basement has a dominantly reddish alteration color, indicating an oxidizing environment under likely subaerial or shallow submarine conditions, but below ~90 mbsf the alteration becomes more greenish, pointing toward more reducing conditions related to a deeper submarine environment (Fig. 5). Typically, these basaltic lava flow units are fresher than volcaniclastic units and are only moderately altered. Relatively unaltered olivine phenocrysts were found throughout all basement units, as were zones with fresh volcanic glass, particularly in hyaloclastites (Fig. 4a). Shipboard major and trace element data indicate that the majority of the igneous rocks are alkali basalt, but several are transitional (Fig. 6a). Using shipboard geochemistry alone, no distinction between shield and post-shield stages of volcanism can be made (Fig. 6b).

The natural remanent magnetization (NRM) was measured on archive halves at 2-cm intervals (Fig. 7) as well as on discrete samples. Most of the lava flows and a few volcaniclastic sequences also have relatively high magnetic coercivities, whereas drilling-induced magnetic overprinting was negligible. In intervals that can be most confidently identified as *in situ* lava flows, inclinations are generally steep and negative (normal polarity). The flow-unit mean
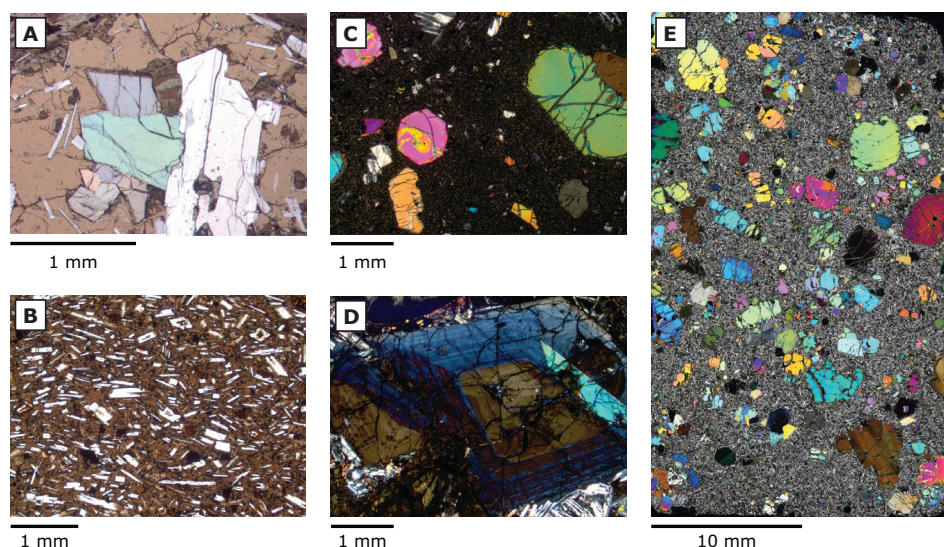
Figure 4. Petrographic variation in alkali basalt lava flows displayed in photomicrographs. [A] Olivine and plagioclase phenocrysts in a glass matrix with smaller plagioclase microcrysts at Site U1372 (sample 330-U1372A-18R-3, 14–16 cm; cross-polarized light). [B] Aphyric basalt showing glassy groundmass, small unaltered groundmass olivine, and flow-aligned plagioclase laths at Site U1374 (sample 330-U1374A-19R-1, 50–53 cm; plane-polarized light). [C] Highly olivine-titanaugite-plagioclase-phyric basalt from a clast in a conglomerate of the sediment cover at Site U1373 (sample 330-U1373A-1R-2, 123–125 cm; cross-polarized light). [D] Ti-augite phenocryst in highly olivine-augite-phyric basalt at Site U1373 (sample 330-U1373A-7R-1, 84–86 cm; cross-polarized light). [E] Highly olivine-augite-phyric basalt at Site U1376 (sample 330-U1376A-8R-6, 136–140cm; cross-polarized light). Figure after Koppers et al. (2012a).

inclination determined shipboard from discrete samples on nine *in situ* flow units (Fig. 8a) is -61.7° ± 7.2° / 8.8° (2σ) after applying bootstrapping techniques and inclination-only statistics (Koppers et al., 2012a).

Sites U1373 and U1374 on Rigil Guyot

Site U1373

At Hole U1373A ~31.8 meters of igneous basement was drilled beneath a ~34-m-thick sediment cover of consolidated sediments of latest Cretaceous to Miocene age that also includes three intercalated autobrecciated basaltic lava flows (Fig. 2). Because reentry using a free-fall funnel failed, this hole had to be abandoned at 65.7 mbsf. The sequence of volcanic and sedimentary rocks recovered is part of the subaerial phase of Rigil Guyot construction. Volcanological features of the igneous sequence suggest lava flowing into an area where water or water-saturated sediment is present but not fully submarine. Above ~45 mbsf the sequence has a dominantly reddish alteration color, pointing toward an oxidizing environment under likely subaerial conditions, but below ~45 mbsf nearly fresh basalt is faintly greenish, pointing to more reducing conditions related to the submarine environment of lava flow emplacement (Fig. 5).

The igneous basement consists of highly olivine-titanaugite-phyric basalt with well-preserved olivine phenocrysts and aphyric basalt (Fig. 3g). The presence of titanaugite and olivine-titanaugite phenocryst assemblages is characteristic of alkalic basalt (Figs. 4c, 4d). Shipboard chemical analyses showed that igneous samples from Site U1373

are closely similar in major and trace element composition to basalt from Site U1372 (Fig. 6b). Total alkali ($Na_2O + K_2O$) and SiO_2 concentrations indicate that all Site U1373 samples are alkali basalt, except one sample classified as a transitional basalt (Fig. 6a).

Paleomagnetic measurements showed mostly negative (normal polarity) inclinations, but positive (reversed polarity) inclinations were recorded in the uppermost units, which comprise sediments and volcanic breccia (Figs. 7, 8b). The mean inclination of nine *in situ* flow units is -55.2° ± 10.6 (2σ) as determined from discrete samples using inclination-only statistics (Koppers et al., 2012b).

Site U1374

The drilled sequence of Hole U1374A constitutes 6.6 m of Pleistocene-Holocene sandy foraminiferal ooze, a 10.1-m-thick sediment layer of Cretaceous age consisting of consolidated volcanic sandstone, a thin layer of limestone and basalt conglomerate, and 505.3 m of igneous basement (Fig. 2). The igneous sequence, from the bottom up, starts with submarine volcanism, producing a series of volcanic breccia units with an increasing number of *in situ* lava lobes and more massive flows upward in the sequence. In the bottom 186 m, the breccia units are frequently interrupted by a series of intrusive sheets or dikes of mainly aphyric basalt. The sequence above ~291 mbsf is occasionally interrupted by sedimentary intervals. Magmatism progressed to a shallow-marine and then subaerial environment. This progression is particularly evident in the various breccia types (Figs. 3c, 3e, 3f) recovered at this site that range from green hyaloclastite breccia with frothy basaltic clasts (marine) through blocky breccia (shallower marine) to scoriaceous (near sea level or subaerial). Changes in alteration color are consistent with this progression (Fig. 5).

The phenocryst assemblage in the breccia and lava flows changed from plagioclase-dominated in the lower part of the succession to olivine-dominated in the upper part, suggesting that the magmas became generally more alkaline with time (Fig. 4b). Major and trace element data for igneous samples from Site U1374 overlap considerably with data for Sites U1372 and U1373, but are slightly more alkalic as a group (Fig. 6b). Most Site U1374 samples are classified as alkali basalt, but nearly one-third of the samples are basanite or tephrite (Fig. 6a). No transitional compositions were found. Despite the compositional overlap and close proximity of Sites U1373 and U1374, the rocks from the two sites cannot be correlated, and they probably represent distinct eruptive events. Likewise, the intrusive sheets at Site U1374
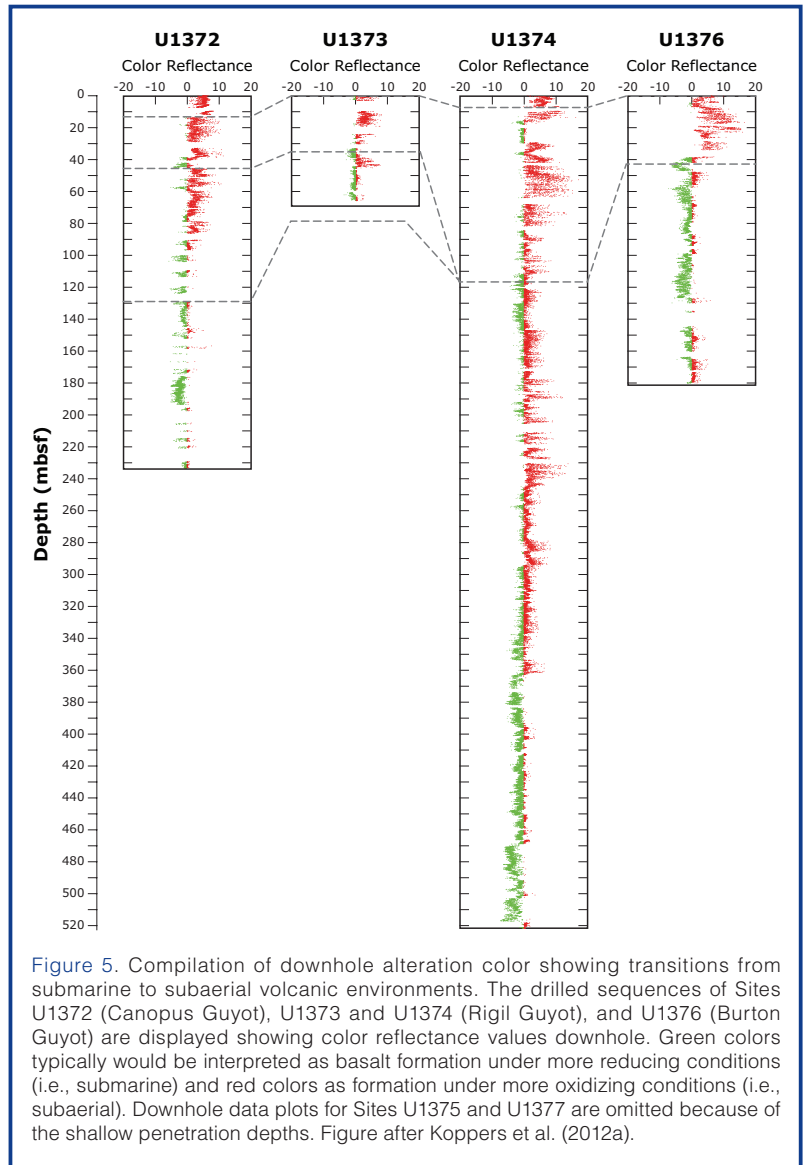
Figure 5. Compilation of downhole alteration color showing transitions from submarine to subaerial volcanic environments. The drilled sequences of Sites U1372 (Canopus Guyot), U1373 and U1374 (Rigil Guyot), and U1376 (Burton Guyot) are displayed showing color reflectance values downhole. Green colors typically would be interpreted as basalt formation under more reducing conditions (i.e., submarine) and red colors as formation under more oxidizing conditions (i.e., subaerial). Downhole data plots for Sites U1375 and U1377 are omitted because of the shallow penetration depths. Figure after Koppers et al. (2012a).

cannot be correlated with any specific lava flow or eruption package higher up in the drilled sequence.

The entire lower sequence has a normal magnetic polarity, which above ~45 mbsf is overlain by a package of reversely magnetized lava flows and volcaniclastics (Figs. 7, 8c). The mean inclination of the nineteen *in situ* flow units determined from discrete samples is -68.7° ± 8.4° (2σ) after correction for deviation of the borehole from vertical and using inclination-only statistics (Koppers et al., 2012b). It is notable that volcaniclastic units, especially in the lower half of the cored igneous basement, provided inclination values similar to intercalated lava flows or lobes. In addition, many of the intrusive sheets intruding these volcaniclastic units also have comparable negative inclinations. The most reliable inclination estimate for Rigil Guyot can be obtained by combining these results with the nine *in situ* lava flows recovered at Site U1373, which are younger by only ~1 Myr (Koppers et al., 2012b). This results in a combined bootstrap mean inclination of -65.0° ± 4.6° / 7.3°(2σ) using inclination-only averaging that is within error (on 1σ and 2σ uncertainty levels) of

the geocentric axial dipole inclination (±68°) for the present-day Louisville hotspot location at ~51°S (Koppers et al., 2012b).

Site U1375 on Archernar Guyot

Hole U1375A was drilled to only 11.5 mbsf. Latest Miocene and younger foraminiferal ooze were recovered, underlain by Paleocene basalt conglomerate (Fig. 3d) and breccia, which represent a pelagic cap and the older sedimentary cover of Achernar Guyot. Hole U1375B was drilled to 8.5 mbsf, and it recovered 57 cm of igneous rock only, which likely is from a large boulder in the sediment cover. Severe hole instabilities were encountered at both holes, and this site had to be abandoned.

The igneous rock from Hole U1375B is composed of moderately olivine-augite-phyric microgabbro (dolerite) with olivine and augite phenocrysts larger than 10 mm. This unit is moderately altered and highly evolved (Fig. 6b). It represents one of the most alkalic rocks recovered during Exp. 330 as it lies in the field of basanite and tephrite in a classification diagram of total alkali ($Na_2O + K_2O$ vs. SiO_2) (Fig. 6a).

Site U1376 on Burton Guyot

At Hole U1376A a ~42-m-thick Cretaceous to Miocene consolidated sediment cover and a ~141-m-thick igneous basement sequence were drilled (Fig. 2). At the top, the sediment cover comprises mainly volcanic sandstones (Fig. 3a) and breccias that overlie a remarkable ~15-m-thick white algal limestone (Fig. 3b). At its base, the sedimentary cover is composed of basalt conglom-erate uncon-formably overlying the igneous basement. Record of a post-erosional or rejuvenation phase of mag-matism at this site is provided by the volcanic sand and breccia. Some of the sand layers contain frag-ments of hornblende and biotite, implying the eruption of magma more evolved than that repre-sented by the more basic basement succession. The sequence contains olivine-pyroxene aggrega-tes that may be mantle xenoliths. This is support-ed by the occurrence of partly resorbed ortho-pyroxene xenocrysts in basalt clasts with clear reaction coronas, suggesting that the rejuvenated stage magmas were strongly alkaline.

The igneous basement is composed of a sequence of submarine pillow basalts, hyaloclas-tites, and autobrecciated lava flows. No subaerial eruptive products were encountered. The domi-nance of submarine eruption is also indicated by alteration type. Two stratigraphic units were de-fined for the igneous basement: the lower unit con-tains mostly olivine phenocrysts, overlain by the upper unit containing olivine and augite pheno-crysts. The lower unit is cut by dikes, and it has an erosional surface at its top (Fig. 3h). The presence of olivine and augite phenocrysts in this basalt (Fig. 4e) and the complete absence of plagioclase phenocrysts suggest that the seamount magma was alkaline and more basic than that at Sites U1372, U1373, and U1374. Geochemical analyses show that the basalt at Site U1376 is slightly less alkaline, although it is still classified as transi-tional basalt rather than tholeiitic (Fig. 6).

Inclination data from paleomagnetic measure-ments on archive halves and discrete samples pro-vide a remarkably consistent picture of moderate to steep reversed polarity magnetization (Figs. 7, 8d). Very similar inclinations were measured for
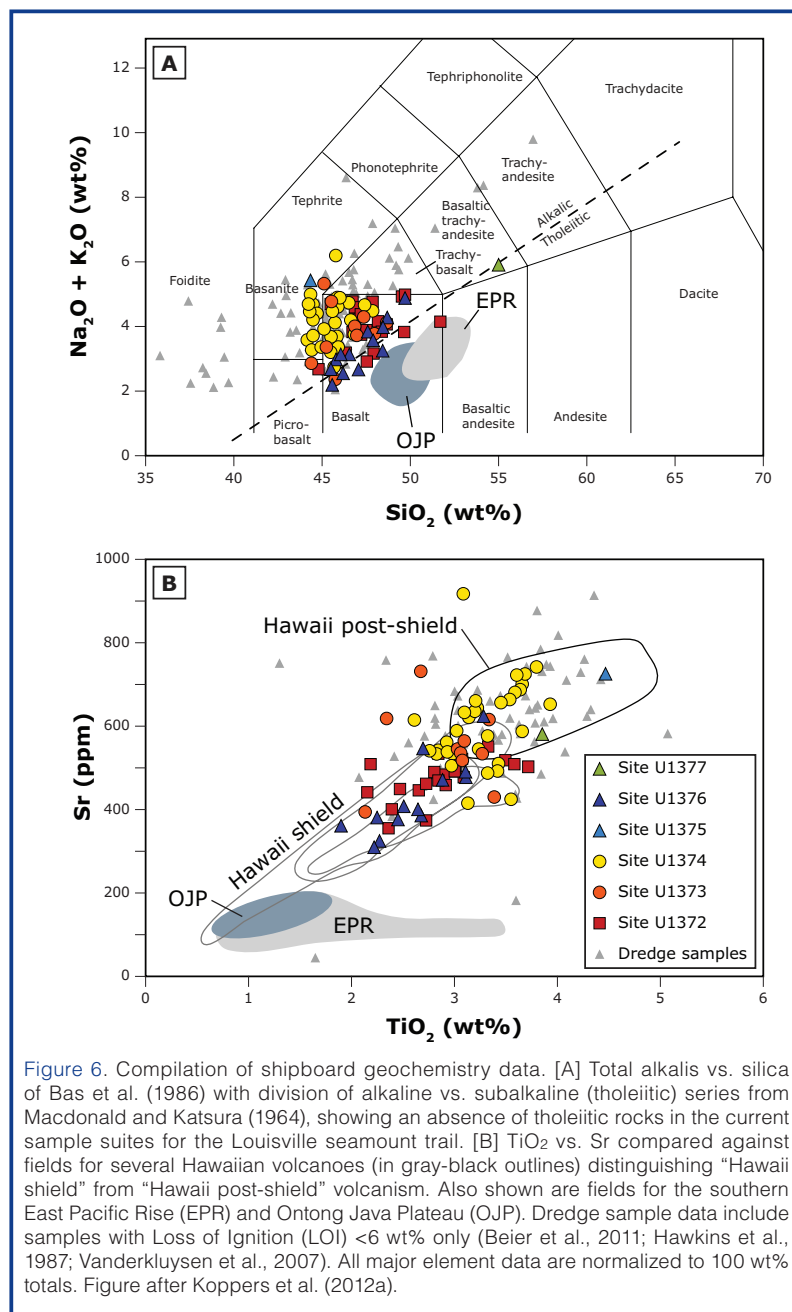
Figure 6. Compilation of shipboard geochemistry data. [A] Total alkalis vs. silica of Bas et al. (1986) with division of alkaline vs. subalkaline (tholeiitic) series from Macdonald and Katsura (1964), showing an absence of tholeiitic rocks in the current sample suites for the Louisville seamount trail. [B] TiO_2 vs. Sr compared against fields for several Hawaiian volcanoes (in gray-black outlines) distinguishing "Hawaii shield" from "Hawaii post-shield" volcanism. Also shown are fields for the southern East Pacific Rise (EPR) and Ontong Java Plateau (OJP). Dredge sample data include samples with Loss of Ignition (LOI) <6 wt% only (Beier et al., 2011; Hawkins et al., 1987; Vanderkluysen et al., 2007). All major element data are normalized to 100 wt% totals. Figure after Koppers et al. (2012a).

volcaniclastic and sedimentary units, as well as for two intrusive dikes, which suggests it is possible to obtain a reliable paleolatitude for this site. The bootstrap mean inclination of eight *in situ* flow units determined from discrete samples is -67.1° ± 3.5° / 3.5° (2σ) after correction for deviation of the borehole from vertical (Koppers et al., 2012a).

Site U1377 on Hadar Guyot

Two holes were drilled at Hadar Guyot, but drilling reached only 53.3 mbsf in Hole U1377A and 37 mbsf in Hole U1377B due to hole instabilities. Both holes started out with nannofossil foraminiferal ooze, followed by an older sedimentary cover including middle-late Eocene pelagic limestone and late Paleocene to early Eocene volcanic breccia and conglomerate.

The igneous basement at Site U1377 consists of trachybasalt, which is a more evolved lithology than the alkali basalt drilled at the other Exp. 330 sites, but similar to lithologies drilled during prior dredging expeditions (Fig. 6). These trachybasalts exhibit intervals of pronounced flow banding, suggesting they formed as massive lava or smaller lobate flows, although lower in Hole U1377B smaller cooling units with well-preserved curved glassy margins were encountered. These margins are diagnostic of lobate flows or pillows and emplacement in a submarine environment. Brown to reddish-brown alteration indicates the prevalence of oxidizing conditions in both holes. Paleomagnetic measurements revealed that samples of three *in situ* flow units have positive inclinations (reversed polarity) resulting in a bootstrap mean inclination of -68.9° ± 14.6° / 13.6° (2σ) (Koppers et al., 2012b).

Discussion

Limited Louisville Mantle Plume Motion

In a scenario with all Pacific mantle plumes sustaining similar large motions as the Hawaiian hotspot, mantle convection is likely to sustain only a few global-scale cells and to create a prevailing "mantle wind" in the Pacific that advects mantle plumes into parallel directions with equal speeds. Hotspots still would provide a valuable reference frame against which plate motions can be measured, as this network of mantle plumes would move consistently over geological time. However, in an alternate scenario, with each hotspot experiencing its own amount and a unique direction of mantle plume motion, inter-hotspot motion would be substantial resulting from plume motions that are regionally controlled (for example, by different configurations of
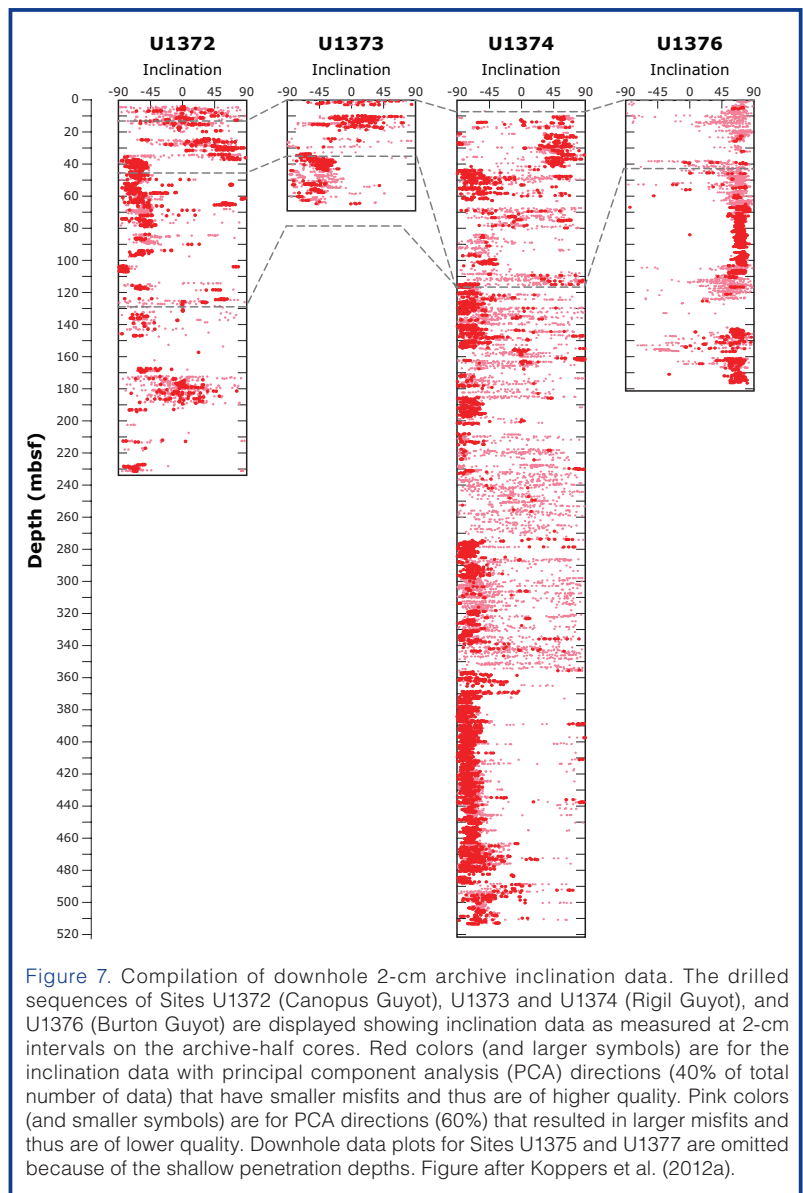
Figure 7. Compilation of downhole 2-cm archive inclination data. The drilled sequences of Sites U1372 (Canopus Guyot), U1373 and U1374 (Rigil Guyot), and U1376 (Burton Guyot) are displayed showing inclination data as measured at 2-cm intervals on the archive-half cores. Red colors (and larger symbols) are for the inclination data with principal component analysis (PCA) directions (40% of total number of data) that have smaller misfits and thus are of higher quality. Pink colors (and smaller symbols) are for PCA directions (60%) that resulted in larger misfits and thus are of lower quality. Downhole data plots for Sites U1375 and U1377 are omitted because of the shallow penetration depths. Figure after Koppers et al. (2012a).

large-scale deep mantle upwellings (such as superplumes) and downwellings (such as subduction zones)). Using shipboard paleomagnetic data, we could show (Koppers et al., 2012b) that the latter scenario is the more likely. Between 70 Ma and 50 Ma, the Louisville hotspot paleolatitude varied only 3°–5° north of its present-day 51°S latitude. These observations match predictions from whole Earth mantle flow modeling, which amount to a maximum of 2°–2.5° of southward motion (Koppers et al., 2004; Steinberger et al., 2004), even though these models do allow for a significant amount of longitudinal motion that paleomagnetic measurements cannot detect. Nevertheless, the observed limited latitudinal motion for the Louisville hotspot (Koppers et al., 2012b) suggests that the Hawaiian and Louisville mantle plumes have been moving independently and that the motion of the Louisville hotspot is likely governed by the subduction of the Pacific plate in the Tonga-Kermadec subduction zone to the west, causing a pronounced return flow in the mantle toward the east and in the direction of the Pacific-Antarctic mid-ocean ridge. The large difference in mantle plume motions also has consequences for interpreting the morpholo-

gies of seamount trails. It now becomes more likely that the Hawaiian-Emperor bend is caused by the strong independent motion of the Hawaiian plume (Tarduno, 2007) and that the shape and age progression of the Louisville seamount trail is providing a better indication of Pacific plate motion. However, an alternate option (which cannot be disproven with paleomagnetic data) could be that a strong eastward motion of the Louisville plume is masking the true motion of the Pacific plate as those two motion vectors would be anti-parallel in direction.

Louisville Seamounts Construction and the Mantle Source

The composition of the drilled rock samples overlaps those analyzed from the dredged rocks but covers a smaller range of variation. All dredged and drilled samples from the Louisville seamount trail are alkali and transitional basalts or basanites and tephrites containing normative nepheline (Fig. 6a). Drilling of up to 505 m into the igneous basement of Rigil Guyot and into the submarine-erupted parts of (in total) four Louisville seamounts did not reveal any tholeiitic basalts and, therefore, did not yield any evidence that Louisville volcanoes evolve through compositionally different stages, such as observed for Hawaii and most intra-plate (hotspot) islands/seamounts. Together with the remarkably homogeneous trace element (Fig. 6b) and isotopic composition of all Louisville lavas, this indicates a homogeneous mantle source that is not significantly affected by variable degrees of melting and/or source fertility (Chen and Frey, 1985; Geldmacher et al., 2006; Phipps Morgan, 1999). Alternatively, only limited variation in lithospheric thickness (along the seamount trail) could be responsible for uniform melting conditions (Beier et al., 2011), but this would not explain the compositional homogeneity observed for each individual seamount (e.g., the lack of tholeiitic shield stages) unless different melting processes (compared to Hawaii) are considered. Further detailed post-cruise studies including Sr, Nd, Pb and Hf isotope ratios on whole rocks, volcanic glass and melt inclusions are underway to investigate these questions.

Major element and Sc variations in the Exp. 330 lava flows indicate that olivine and clinopyroxene are the main fractionating mineral phases controlling the magmatic differen-
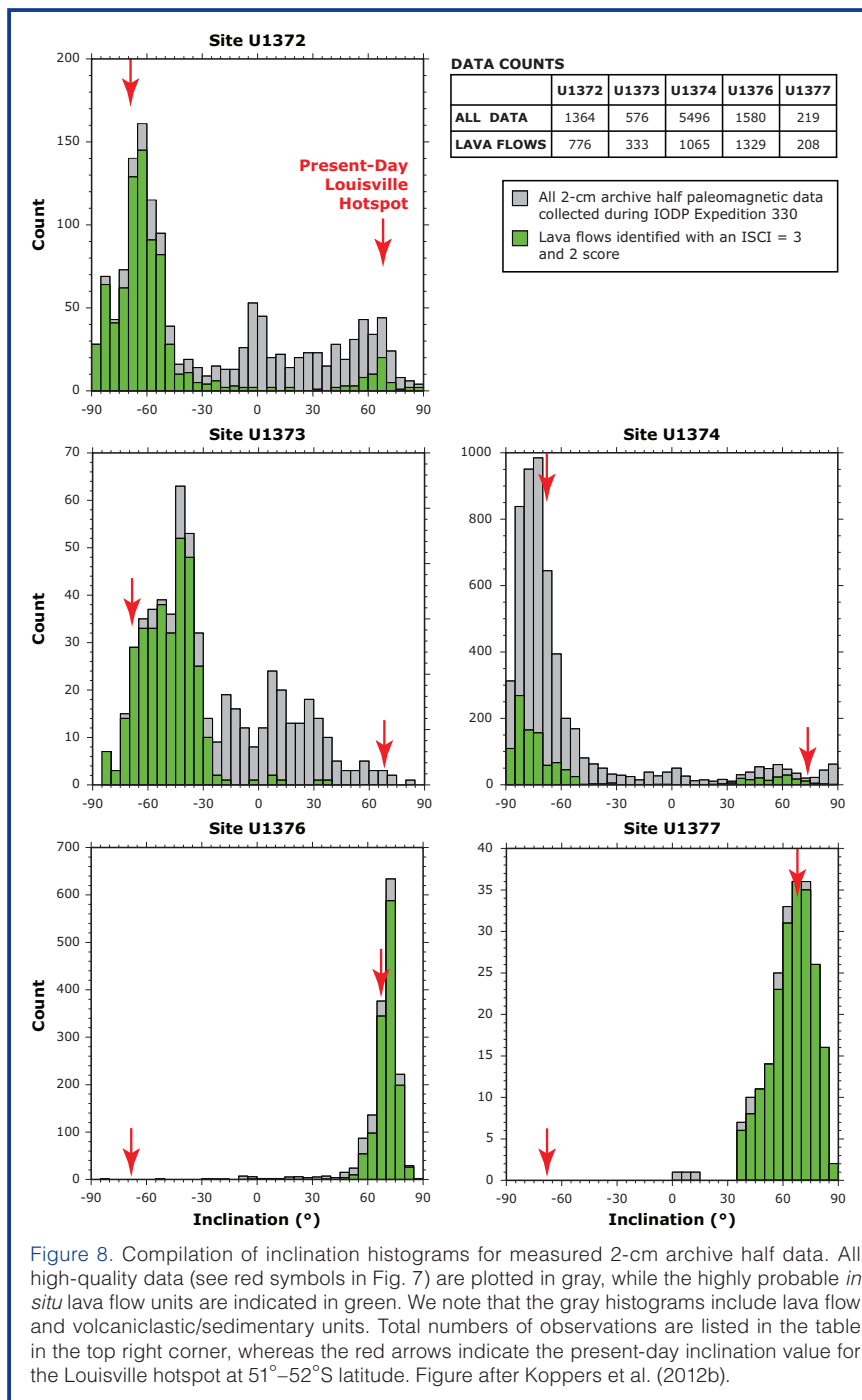
Figure 8. Compilation of inclination histograms for measured 2-cm archive half data. All high-quality data (see red symbols in Fig. 7) are plotted in gray, while the highly probable *in situ* lava flow units are indicated in green. We note that the gray histograms include lava flow and volcaniclastic/sedimentary units. Total numbers of observations are listed in the table in the top right corner, whereas the red arrows indicate the present-day inclination value for the Louisville hotspot at 51°–52°S latitude. Figure after Koppers et al. (2012b).

tiation in the Louisville seamounts. Both minerals are frequently observed as phenocrysts (Fig. 4) in the recovered lavas and are often well preserved (Koppers et al., 2012a). The high abundance of olivine phenocrysts in particular will allow post-cruise He (and Os) isotopic studies to further characterize the mantle source of the Louisville plume. Since no He isotopes have been previously published from Louisville, these studies will help to evaluate whether Louisville indeed represents a *primary* (deep?) hotspot (Courtillot et al., 2003). In addition, the composition of olivine phenocrysts (from less evolved samples) can be used to determine the Mg/Fe ratio of the parental magma, which is indicative of the potential temperature of the Louisville mantle plume source (Putirka et al., 2007).

Geomicrobiology of Seamounts

During Exp. 330 a large collection of igneous basement samples was devoted to microbiology studies to provide an excellent opportunity for studying living and extant microbial residents in old subseafloor volcanic rocks that make up the Louisville seamounts. Whole-round samples (5–20 cm long) were collected for microbiological analysis before the core sections were split into working and archive halves. Lithologies of the collected samples ranged from unconsolidated sediments to sedimentary conglomerates, volcaniclastics, volcanic breccias, and various kinds of basaltic lava flows and dike intrusions. All samples were preserved for shore-based cell counting, DNA analyses, and $\delta^{34}S$ and $\delta^{13}C$ isotope analyses. Some samples were used to inoculate culturing experiments with different types of cultivation media, and during shipboard analytical work microbial growth was detected in samples as deep as 400 mbsf in Rigil Guyot, particularly with media targeting sulfur-oxidizing bacteria and general heterotrophs. Other samples were prepared to set up stable isotope addition bioassays to determine rates of carbon and nitrogen utilization by subsurface microbes.

These studies are of great interest as differences in microbial populations between overlying (pelagic) sediments and volcaniclastic layers and the basaltic basement are so far largely unidentified, as are the largely unstudied variations between different seamount lithologies, depth into the seamount, and seamounts of different age. Because of the high number of fresh volcanic glass occurrences at most Exp. 330 drill sites, the search for and study of microbial fossil traces will provide new information on the activity of and boring patterns generated by glass-metabolizing microorganisms in the largely unstudied seamount subsurface environment.

Conclusions and Future Work

IODP Exp. 330 to the Louisville seamount trail most successfully cored 1114 m of sediment and igneous basement with an average 72.4% recovery at five seamounts. The cored materials are relatively unaltered, providing an affluence of well-preserved basaltic samples that contain, for example, pristine olivine crystals and fresh volcanic glass. The high recovery and superior sample conditions allowed us to carry out large numbers of shipboard paleomagnetic analyses on *in situ* lava flows that in turn provided direct evidence for a limited latitudinal motion of the Louisville hotspot between 70 Ma and 50 Ma (Koppers et al., 2012b). However, it is important to emphasize that at all drill sites large fractions of mostly submarine hyaloclastites, volcanic sandstone, and basaltic breccia were recovered, which makes estimating the paleolatitude for the Louisville hotspot more difficult than for the sites in the Hawaiian-Emperor seamount trail, where sequences of primarily subaerial lava flows were re-covered (Duncan et al., 2006). As shown in this paper, many of these volcaniclastic units in the Louisville seamounts have inclinations consistent with bracketing lava flows. Deciphering the origin and timing of the remanence acquisition in these volcaniclastic units will play a critical role in resolving the paleolatitude history for the Louisville hotspot. Following the shipboard inclination measurements and initial radiometric age dating, this will require additional $^{40}Ar/^{39}Ar$ age determinations, paleomagnetic and rock magnetic studies, and integration of additional shore-based and shipboard data (e.g., borehole magnetic anomalies).

Ultimately, the results of Exp. 330 provide a next step in testing the "fixed" hotspot hypothesis and to better understanding the large-scale mantle movements that occur over long geological intervals on Earth. Many questions still remain to be answered, and they will require future seamount drilling to establish paleolatitude histories for other long-lived hotspot systems (for example, the Walvis Ridge), located in the SE Atlantic. Such broader data sets will allow us to address the possibility of "true polar wander" (Besse, et al., 2002, and Torsvik, et al., 2002) that still is an often controversial but also largely untested science hypothesis.

The IODP Expedition 330 Scientific Party

Louise Anderson, Christoph Beier, David M. Buchs, Li-Hui Chen, Benjamin E. Cohen, Fabien Deschamps, Michael J. Dorais, Daniel Ebuna, Sebastian Ehmann, J. Godfrey Fitton, Patrick M. Fulton, Erdenesaikhan Ganbat, Jeffrey S. Gee, Cedric Hamelin, Takeshi Hanyu, Hiroyuki Hoshi, Lara Kalnins, Johnathon Kell, Shiki Machida, John J. Mahoney, Kazuyoshi Moriya, Alexander R.L. Nichols, Nicola Pressling, Svenja Rausch, Shin-ichi Sano, Jason B. Sylvan, and Rebecca Williams.

Acknowledgments

References

Bas, M. J. L., Maitre, R. W. L., Streckeisen, A., and Zanettin, B., 1986. A chemical classification of volcanic rocks based on the total alkali-silica diagram. *J. Petrol.*, 27(3):745–750. doi:10.1093/petrology/27.3.745

Beier, C., Vanderkluysen, L., Regelous, M., Mahoney, J. J., and Garbe-Schönberg, D., 2011. Lithospheric control on geochemical composition along the Louisville Seamount Chain. *Geochem. Geophys. Geosyst.*, 12(9):Q0AM01. doi:10.1029/2011GC003690

Besse, J., and Courtillot, V. (2002) Apparent and true polar wander and the geometry of the geomagnetic field over the 200 Myr. *J. Geophys. Res.*, 107, 2300, dpi:10.1029/2001JB000050.

Chen, C.-Y., and Frey, F. A., 1985. Trace element and isotope geochemistry of lavas from Haleakala Volcano, East Maui: Implications for the origin of Hawaiian basalts. *J. Geophys. Res.*, 90(B10):8743–8768. doi:10.1029/JB090iB10p08743

Cheng, Q., Park, K. H., Macdougall, J. D., Zindler, A., Lugmair, G. W., Staudigel, H., Hawkins, J., and Lonsdale, P., 1987. Isotopic evidence for a hot spot origin of the Louisville Seamount Chain. *In* Keating, B. H., Fryer, P., Batiza, R., and Boehlert, G. W. (Eds.), *Seamounts, Islands, and Atolls*, *Geophys. Monogr. Ser.*, 43:283–296. doi:10.1029/GM043p0283

Courtillot, V., Davaille, A., Besse, J., and Stock, J., 2003. Three distinct types of hotspots in the Earth's mantle. *Earth Planet. Sci. Lett.*, 205(3–4):295–308. doi:10.1016/S0012-821X (02)01048-8

Cowen, J. P., Giovannoni, S. J., Kenig, F., Johnson, H. P., Butterfield, D., Rappé, M. S., Hutnak, M., and Lam, P., 2003. Fluids from aging ocean crust that support microbial life. *Science*, 299(5603):120–123. doi:10.1126/science.1075653

Downey, N. J., Stock, J. M., Clayton, R. W., and Cande, S. C., 2007. History of the Cretaceous Osbourn spreading center. *J. Geophys. Res*, 112(B4):B04102. doi:10.1029/2006JB004550

Duncan, R. A., and Clague, D. A., 1985. Pacific plate motion recorded by linear volcanic chains. *In* Nairn, A. E. A., Stehli, F. L., and Uyeda, S. (Eds.), *The Ocean Basins and Margins:* New York (Plenum Press), 89–121. doi:10.1007/978-1-4613-2351-8_3

Duncan, R. A., Tarduno, J. A., and Scholl, D. W., 2006. Leg 197 synthesis: Southward motion and geochemical variability of the Hawaiian Hotspot. *In* Duncan, R. A., Tarduno, J. A., Davies, T. A., and Scholl, D. W., *Proc. ODP, Sci. Results*, 197: College Station, TX (Ocean Drilling Program). doi:10.2973/odp. proc.sr.197.001.2006

Expedition 330 Scientists, 2011. Louisville Seamount Trail: Implications for geodynamic mantle flow models and the geochemical evolution of primary hotspots. *IODP Prel. Rept.*, 330. doi:10.2204/iodp.pr.330.2011

Fisk, M. R., Giovannoni, S. J., and Thorseth, I., 1998. Alteration of oceanic volcanic glass: Textural evidence of microbial activity. *Science*, 281(5379):978–980. doi:10.1126/science. 281.5379.978

Geldmacher, J., Hoernle, K., Klügel., A., Bogaard, P.v.d., and Bernin, B., 2006. Origin and geochemical evolution of the Madeira-Tore Rise (eastern North Atlantic). *J. Geophys. Res.*, 111(B9):B09206. doi:10.1029/2005JB003931

Hawkins, J. W., Lonsdale, P. F., and Batiza, R., 1987. Petrologic evolution of the Louisville seamount chain. *In* Keating, B. H., Fryer, P., Batiza, R., and Boehlert, G. W. (Eds.), *Seamounts, Islands, and Atolls.* Geophys. Monogr., 43:235–254.

Kono, M., 1980. Paleomagnetism of DSDP Leg 55 basalts and implications for the tectonics of the Pacific Plate. *In* Shambach, J., Jackson, E. D., Koizumi, I., Avdeiko, G., Butt, A., Clague, D., Dalrymple, G. B., et al., *Init. Repts. DSDP*, 96: Washington, DC (U.S. Govt. Printing Office), 737–752.

Koppers, A. A. P., Duncan, R. A., and Steinberger, B., 2004. Implications of a non-linear ^{40}Ar/^{39}Ar age progression along the Louisville seamount trail for models of fixed and moving hotspots. *Geochem. Geophys. Geosyst.*, 5(6):Q06L02. doi:10.1029/2003GC000671

Koppers, A. A. P., Gowen, M. D., Colwell, L. E., Gee, J. S., Lonsdale, P. F., Mahoney, J. J., and Duncan, R. A., 2011. New ^{40}Ar/^{39}Ar age progression for the Louisville hot spot trail and implications for inter-hot spot motion. *Geochem. Geophys. Geosyst.*, 12(12):Q0AM02. doi:10.1029/2011GC003804

Koppers, A. A. P., Morgan, J. P., Morgan, J. W., and Staudigel, H., 2001. Testing the fixed hotspot hypothesis using ^{40}Ar/^{39}Ar age progressions along seamount trails. *Earth Planet. Sci. Lett.*, 185(3–4):237–252. doi:10.1016/S0012-821X(00) 00387-3

Koppers, A. A. P., Yamazaki, T., and Geldmacher, J., 2010. Louisville Seamount Trail: Implications for geodynamic mantle flow models and the geochemical evolution of primary hotspots. *IODP Sci. Prosp.*, 330. doi:10.2204/iodp.sp.330.2010

Koppers, A. A. P., Yamazaki, T., Geldmacher, J., and the Expedition 330 Scientists, 2012a. *Proc. IODP*, 330: Washington, DC (Integrated Ocean Drilling Program Management International, Inc.). doi:10.2204/iodp.proc.330.2012

Koppers, A. A. P., Yamazaki, T., Geldmacher, J., Gee, J. S., Pressiling, N., Hoshi, H., Anderson, L., et al., 2012b. Limited latitudinal mantle plume motion for the Louisville hotspot. *Nature Geosci.*, 5:911–917. doi:10.1038/ngeo1638

Lonsdale, P., 1988. Geography and history of the Louisville Hotspot Chain in the southwest Pacific. *J. Geophys. Res.*, 93(B4):3078–3104. doi:10.1029/JB093iB04p03078

Macdonald, G. A., and Katsura, T., 1964. Chemical composition of Hawaiian lavas. *J. Petrol.*, 5(1):82–133. doi:10.1093/ petrology/5.1.82

Mason, O. U., Nakagawa, T., Rosner, M., Van Nostrand, J. D., Zhou, J., Maruyama, A., Fisk, M. R., and Giovannoni, S. J., 2010. First investigation of the microbiology of the deepest layer of ocean crust. *PLoS ONE*, 5(11):e15399. doi:10.1371/journal. pone.0015399

Morgan, W. J., 1971. Convection plumes in the lower mantle. *Nature*, 230(5288):42–43. doi:10.1038/230042a0

Mortimer, N., Hoernle, K., Hauff, F., Palin, J. M., Dunlap, W. J., Werner, R., and Faure, K., 2006. New constraints on the age and evolution of the Wishbone Ridge, southwest Pacific Cretaceous microplates, and Zealandia–West Antarctica breakup. *Geology*, 34(3):185–188. doi:10.1130/G22168.1

Parkes, R. J., Cragg, B. A., Bale, S. J., Getlifff, J. M., Goodman, K., Rochelle, P. A., Fry, J. C., Weightman, A. J., and Harvey, S. M., 1994. Deep bacterial biosphere in Pacific Ocean sediments. *Nature*, 371(6496):410–413. doi:10.1038/371410a0

Phipps Morgan, J., 1999. Isotope topology of individual hotspot basalt arrays: Mixing curves or melt extraction trajectories? *Geochem. Geophys. Geosyst.*, 1:1003. doi:10.1029/1999 GC000004

Putirka, K. D., Perfit, M., Ryerson, F. J., and Jackson, M. G., 2007. Ambient and excess mantle temperatures, olivine thermometry, and active vs. passive upwelling. *Chemical Geology*, 241(3–4):177–206. doi:10.1016/j.chemgeo.2007.01.014

Rouxel, O., Ono, S., Alt, J., Rumble, D., and Ludden, J., 2008. Sulfur isotope evidence for microbial sulfate reduction in altered oceanic basalts at ODP Site 801. *Earth Planet. Sci. Lett.*, 268(1–2):110–123. doi:10.1016/j.epsl.2008.01.010

Steinberger, B., and Antretter, M., 2006. Conduit diameter and buoy-

ant rising speed of mantle plumes: Implications for the motion of hot spots and shape of plume conduits. *Geochem. Geophys. Geosyst.*, 7(11):Q11018. doi:10.1029/2006GC001409

Steinberger, B., and Calderwood, A.R., 2006. Models of large-scale viscous flow in the Earth's mantle with constraints from mineral physics and surface observations. *Geophys. J. Int.*, 167(3):1461–1481. doi:10.1111/j.1365-246X.2006.03131.x

Steinberger, B., and O'Connell, R. J., 1998. Advection of plumes in mantle flow: Implications for hotspot motion, mantle viscosity and plume distribution. *Geophys. J. Int.*, 132(2):412–434. doi:10.1046/j.1365-246x.1998.00447.x

Steinberger, B., Sutherland, R., and O'Connell, R. J., 2004. Prediction of Emperor-Hawaii seamount locations from a revised model of global plate motion and mantle flow. *Nature*, 430(6996):167–173. doi:10.1038/nature02660

Tarduno, J., Bunge, H.- P., Sleep, N., and Hansen, U., 2009. The bent Hawaiian-Emperor hotspot track: Inheriting the mantle wind. *Science*, 324(5923):50–53. doi:10.1126/science.1161256

Tarduno, J. A., 2007. On the motion of Hawaii and other mantle plumes. *Chem. Geol.*, 241(3–4):234–247. doi:10.1016/j.chemgeo.2007.01.021

Tarduno, J. A., and Cottrell, R. D., 1997. Paleomagnetic evidence for motion of the Hawaiian hotspot during formation of the Emperor seamounts. *Earth Planet. Sci. Lett.*, 153(3–4):171–180. doi:10.1016/S0012-821X(97)00169-6

Tarduno, J. A., Duncan, R. A., Scholl, D. W., Cottrell, R. D., Steinberger, B., Thordarson, T., Kerr, B. C., et al., 2003. The Emperor seamounts: Southward motion of the Hawaiian hotspot plume in Earth's mantle. *Science*, 301(5636):1064–1069. doi:10.1126/science.1086442

Torsvik, T.H., Van der Voo, R., and Redfield, T.F. (2002) Relative hotspot motions versus True Polar Wander. *Earth Planet. Sci. Lett.*, 202, 185–200.

Vanderkluysen, L., Mahoney, J., Koppers, A. A. P., and Lonsdale, P. F., 2007. Geochemical evolution of the Louisville seamount chain. *EOS Trans. AGU*, 88(52, Fall Meet. Suppl.): V42B-06.

Watts, A. B., Weissel, J. K., Duncan, R. A., and Larson, R. L., 1988. Origin of the Louisville Ridge and its relationship to the Eltanin Fracture Zone system. *J. Geophys. Res.*, 93(B4):3051–3077. doi:10.1029/JB093iB04p03051

Wessel, P., and Kroenke, L. W., 2008. Pacific absolute plate motion since 145 Ma: An assessment of the fixed hot spot hypothesis. *J. Geophys. Res.*, 113(B6):B06101. doi:10.1029/2007JB005499

Wessel, P., Harada, Y., and Kroenke, L., 2006. Toward a self-consistent, high-resolution absolute plate motion model for the Pacific. *Geochem. Geophys. Geosyst.*, 7(3):Q03L12. doi:10.1029/2005GC001000

Wilson, J. T., 1963. A possible origin of the Hawaiian Islands. *Canad. J. Phys.*, 41(6):863–870. doi:10.1139/p63-094

Worthington, T. J., Hekinian, R., Stoffers, P., Kuhn, T., and Hauff, F., 2006. Osbourn Trough: Structure, geochemistry and implications of a mid-Cretaceous paleospreading ridge in the South Pacific. *Earth Planet. Sci. Lett.*, 245(3–4):685–701. doi:10.1016/j.epsl.2006.03.018

Authors

Anthony A.P. Koppers, College of Oceanic & Atmospheric Sciences, Oregon State University, 104 CEOAS Administration Building, Corvallis, OR 97331-5503, U.S.A., e-mail:akoppers@coas.oregonstate.edu

Toshitsugu Yamazaki, (Currently) Atmosphere and Ocean Research Institute, University of Tokyo, 5-1-5 Kashiwanoha, Kashiwa, Chiba 277-8564, Japan

Jörg Geldmacher, (Currently) GEOMAR, Helmholtz Centre for Ocean Research Kiel, 24148 Kiel, Germany **and the IODP Expedition 330 Scientific Party**

IODP Expedition 334: An Investigation of the Sedimentary Record, Fluid Flow and State of Stress on Top of the Seismogenic Zone of an Erosive Subduction Margin

by Paola Vannucchi, Kohtaro Ujiie, Nicole Stroncik, and the IODP Exp. 334 Scientific Party

Abstract

The Costa Rica Seismogenesis Project (CRISP) is an experiment to understand the processes that control nucleation and seismic rupture of large earthquakes at erosional subduction zones. Integrated Ocean Drililng Program (IODP) Expedition 334 by R/V *JOIDES Resolution* is the first step toward deep drilling through the aseismic and seismic plate boundary at the Costa Rica subduction zone offshore the Osa Peninsula where the Cocos Ridge is subducting beneath the Caribbean plate. Drilling operations included logging while drilling (LWD) at two slope sites (Sites U1378 and U1379) and coring at three slope sites (Sites U1378–1380) and at one site on the Cocos plate (Site U1381). For the first time the lithology, stratigraphy, and age of the slope and incoming sediments as well as the petrology of the subducting Cocos Ridge have been characterized at this margin. The slope sites recorded a high sediment accumulation rate of 160–1035m m.y.$^{-1}$ possibly caused by on-land uplift triggered by the subduction of the Cocos Ridge. The geochemi-

cal data as well as the *in situ* temperature data obtained at the slope sites suggest that fluids are transported from greater depths. The geochemical profiles at Site U1381 reflect diffusional communication of a fluid with seawater-like chemistry and the igneous basement of the Cocos plate (Solomon et al., 2011; Vannucchi et al., 2012a). The present-day *in situ* stress orientation determined by borehole breakouts at Site U1378 in the middle slope and Site U1379 in the upper slope shows a marked change in stress state within ~12 km along the CRISP transect; that may correspond to a change from compression (middle slope) to extension (upper slope).

Introduction and Goals

Subduction megathrusts are responsible for the largest earthquakes on Earth and are often accompanied by devastating tsunamis. Erosive margins, which occur along at least 50% of the global subduction zones (Clift and Vannucchi, 2004), can generate magnitude 9.0 earthquakes, as shown by the 2011 Tohoku-Oki earthquake and tsunami, which occurred off the northeast coast of Japan. Typical of erosive convergent margins is the upper plate prov-enance of the material that is present along the megathrust at seismogenic depth. The upper plate material can be anything from crystalline rocks to sediments lithified and deformed in a previous, no longer active accretionary prism.

CRISP is designed to investigate the first-order seismogenic processes common to most faults, such as dynamic weakening processes as thermal pressurization (Wibberley and Shimamoto, 2005) or melt lubrication (Di Toro et al., 2006) and eventually those unique to erosional margins. The Costa Rica Margin is well studied (Fig. 1) and is currently the only known erosional end-member of convergent margins in which the seismogenic zone is realistically within reach of scientific drilling (~6 km depth, Ranero et al., 2006). With a fast convergence rate (90 mm yr^{1}, DeMets, 2001), abundant seismicity (DeShon et al., 2003), subduction erosion (Ranero and von Huene, 2000; Vannucchi et al., 2001), and change in
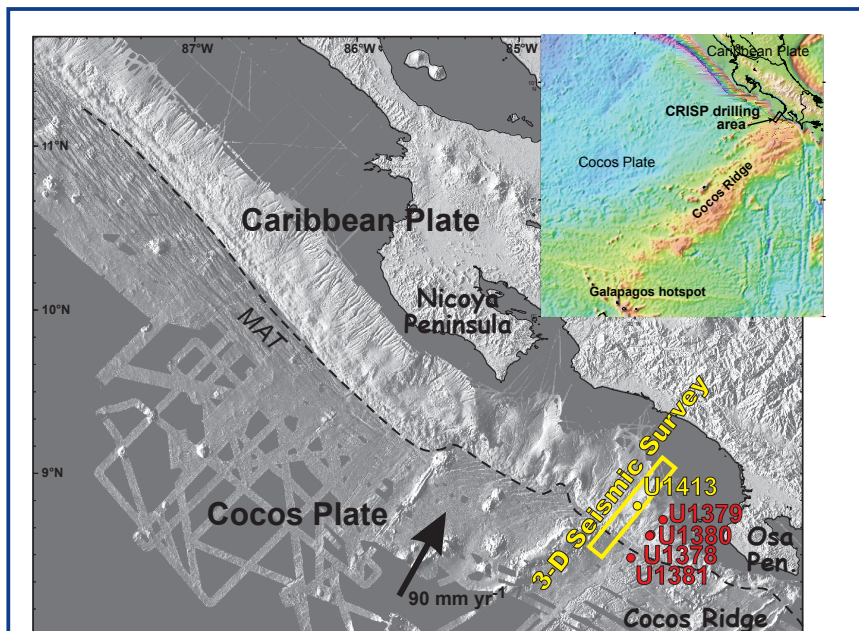
Figure 1. Bathymetric maps of the Cocos Ridge (inset) and of the Costa Rica area, showing the location of the Exp. 334 drilling transect, and the 3-D seismic survey area (Bangs et al., 2011). Seafloor bathymetry is based on swath mapping (Ranero et al., 2008). Note collision of the Cocos Ridge with the trench offshore the Osa Peninsula, which brings the trench very close to the Osa Peninsula coastline and the seismogenic zone within reach of IODP riser drilling capabilities. MAT=Middle America Trench. CRIS 13B is a possible location for deep riser drilling, targeting the seismogenic zone at ~6 km depth.

subducting plate relief along strike, the margin offshore southeast Costa Rica offers excellent opportunities to learn the mechanisms of earthquake nucleation and rupture propagation.

CRISP is conceived as a multiple platform drilling project with an initial exploration of the margin through riser-less drilling with the R/V *JOIDES Resolution* and a successive, deep penetration of the seismogenic portion of the megathrust with the riser drilling technology offered by D/V *Chikyu*. IODP Exp. 334 was planned as the riserless first phase of CRISP, called CRISP Program A.

Figure 2. Interpreted wide-angle seismic section from Stavenhagen et al. (1998). Schematic figure through the Osa Peninsula margin showing Sites U1381, U1378, U1380, and U1379. VE=vertical exaggeration, v=P-wave velocity (km s^{-1}).

The primary goals of Exp. 334 were as follows:

1. Characterization of lithological, physical, and frictional properties of upper plate material;

2. Estimation of subduction channel thickness and the rate of subsidence caused by subduction erosion;

3. Investigation of the fluid flow system and thermal structure of the erosive margin;

4. Determination of the change in the stress field across the updip limit of the seismogenic zone; and

5. Characterization of the influence of Cocos Ridge subduction on the evolution of the Central America volcanic arc and development of the volcanic arc gap inboard Cocos Ridge.

Tectonic, hydrologic, and physical conditions along this erosive convergent margin were investigated through continuous coring at three slope sites: Sites U1378 and U1380 on the middle slope and Site U1379 on the upper slope, and at one site on the Cocos plate, Site U1381 (Fig. 2). LWD was first conducted at Sites U1378 and U1379 to document the *in situ* physical properties, stratigraphic and structural features, and stress state of the material to be cored.

Geological Setting and Earlier Work

The oceanic Cocos plate subducting beneath Costa Rica has been formed at two different spreading centers, the East Pacific Rise (EPR) and the Cocos-Nazca Spreading Center (CNS), and it has been largely influenced by Galapagos hotspot volcanism. The largest feature formed by the passage of the Cocos plate over the Galapagos hotspot is the 2.5-km-high Cocos Ridge (Fig. 1). The oceanic crust beneath the ridge is about 20 km thick (i.e., three times thicker than normal oceanic crust; Sallares et al., 2003). The influence of Cocos Ridge subduction increases from the Nicoya Peninsula

in the northwest, where sills of Galapagos provenance abundantly infiltrate the igneous basement (Kimura et al., 1997; Morris et al., 2003), to the Osa Peninsula in the southeast (Fig. 1).

The CRISP transect is located along the northwest flank of the subducting Cocos Ridge, over a patch of shallow (updip limit ~4–5 km below the seafloor) seismically active megathrusts. The M6.4 June 2002 thrust earthquake off Caño Island, which occurred at a depth of ~9 km, and its aftershock sequence were located in the CRISP drilling area (Fig. 3; S.L. Bilek, pers. comm., 2003; I. Arroyo, pers. comm., 2009). GPS measurements on land indicated high stress over the subducted Cocos Ridge with most of the plate interface in the seismogenic region essentially fully locked (Dixon, 2003). In contrast, seismic profiles indicate fault geometries (i.e., angles between forethrusts, backthrusts, and the décollement), suggesting low values of plate boundary friction (von Huene et al., 2000, 2003, 2004). Fluids draining from the subducting lower plate are abundant, as indicated by numerous vents (Ranero et al., 2008). Using bottom-simulating reflector (BSR) depths as a proxy for heat flow, temperatures along the megathrust beneath the mid-slope drilling sites were estimated to range between 60°C and 90°C (Harris et al., 2010a, 2010b).

Drilling and seismic data indicate active and long-lived subduction erosion from Guatemala to Costa Rica (Ranero and von Huene, 2000; Ranero et al., 2000; Vannucchi et al., 2001, 2003, 2004). This interpretation is based on long-term subsidence of the continental slope offshore the Nicoya Peninsula. ODP Leg 170 provided direct evidence of shallow-water sedimentary rocks, now located in 3900 m water depth on the forearc and marking the slope apron–forearc basement unconformity, showing that the margin offshore the Nicoya Peninsula has experienced a net loss of crust since ~16 Ma (Vannucchi et al., 2001).

The forearc basement (i.e., the framework of the upper plate below the shelf/slope sediments) was the main target of IODP Exp. 334 (Fig. 2). The pre-expedition hypothesis

was that a high amplitude seismic reflector at the base of the well-stratified slope apron marks the unconformity between the forearc basement and the shelf/slope sediment. Drilling through the reflector disproved the pre-expedition hypothesis, as the cored material resulted as still infilling of the forearc basin. The forearc basement in the CRISP area, instead, has been interpreted from seismic profiles (Stavenhagen et al., 1998) to be composed of a middle Eocene–middle Miocene unit of oceanic lithologies accreted to the overriding plate (Vannucchi et al., 2006) very similar to the Osa Mélange. The Osa Mélange, dominated by basalt, radiolarite, and limestone, is the most seaward unit exposed on land close to the CRISP transect. The forearc basement, therefore, was not reached by drilling during Exp. 334.

On the incoming plate, the irregular topography of the Cocos Ridge has a direct effect on the thickness of its sedimentary cover. In areas of low seafloor topography on the northern flank of the Cocos Ridge, the sediment thickness reaches 200 m; by contrast, only a 100-m-thick sediment cover is found in areas of the northern flank of the ridge with high seafloor topography.

Preliminary Scientific Results

Exp. 334 drilled four sites in four weeks (Fig. 4): one on the Caribbean plate shelf into the upper slope (Site U1379), two into the middle slope (Sites U1378 and U1380), and one on the subducting Cocos Plate (U1381). Site U1381 also represents the first-ever penetration of the Cocos Ridge igneous basement. Acquisition of LWD logs prior to coring was successfully implemented at Sites U1378 and U1379 (Fig. 5).

Slope sediments at Sites U1378–U1380 were retrieved with a 100% recovery rate. At Site U1379 material marking the acoustic basement was reached below the high amplitude reflector. The recovery rate of this material was ~20%. Unfortunately, at Sites U1378 and U1380 both LWD and coring had to be stopped before reaching the target depth because of deteriorated hole conditions.

In the following paragraphs we summarize the five main accomplishments of IODP Exp. 334.

1. Estimating the composition, texture, and physical properties of the upper plate material

In erosive margins the upper plate material hosts the seismogenic portion of the plate boundary. The plate boundary itself is frequently addressed as a subduction channel where deformation is largely concentrated in a relatively thick layer of shearing; fluid driven processes weaken the upper plate
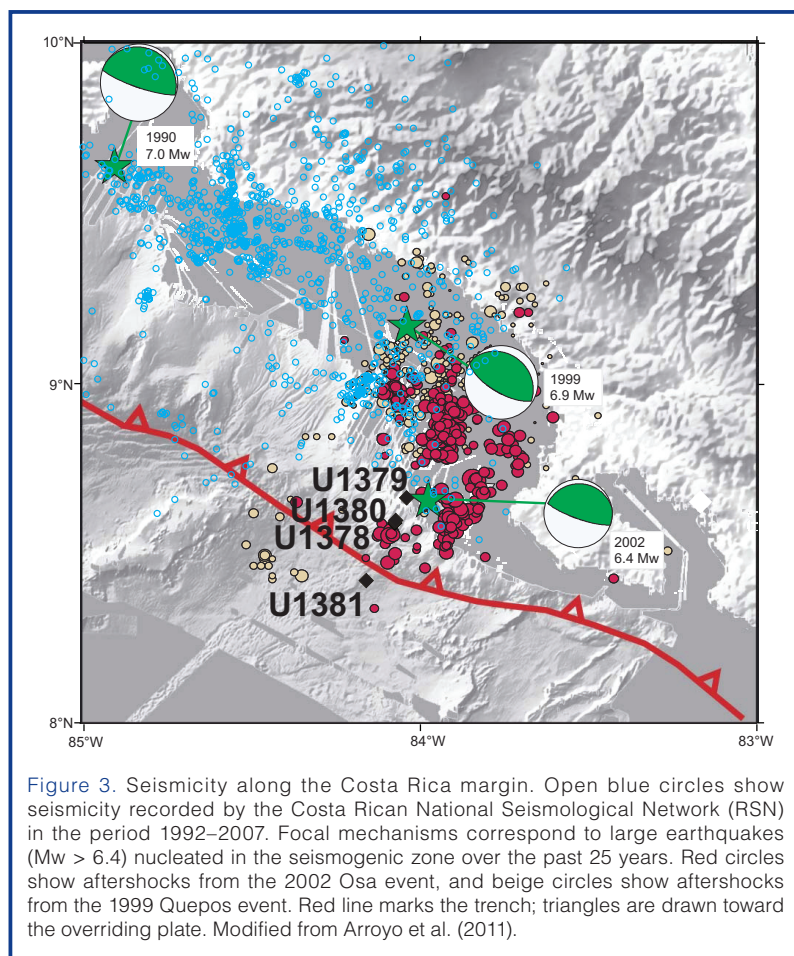
Figure 3. Seismicity along the Costa Rica margin. Open blue circles show seismicity recorded by the Costa Rican National Seismological Network (RSN) in the period 1992–2007. Focal mechanisms correspond to large earthquakes (Mw > 6.4) nucleated in the seismogenic zone over the past 25 years. Red circles show aftershocks from the 2002 Osa event, and beige circles show aftershocks from the 1999 Quepos event. Red line marks the trench; triangles are drawn toward the overriding plate. Modified from Arroyo et al. (2011).

and promote upward migration (i.e., toward the upper plate) of the active décollement. Sampling the upper plate material not only provides us with the opportunity to characterize its composition, texture, and physical properties and to conduct structural analysis and laboratory tests, but also with critical information in preparation for the deep riser drilling. The main objective of IODP Exp. 334 was to drill through the forearc sediments and reach the basement below the high amplitude reflector. At the shelf/upper slope Site U1379, located in 127 m water depth, both cores and LWD logs reached and penetrated below this reflector (Fig. 5b). LWD logs showed a marked increase in density and resistivity at ~892 meters below seafloor (mbsf). This change in physical properties was initially interpreted as penetration into the upper plate basement. Indeed, successive coring at Site U1379 showed a complex change in lithostratigraphy, going from the turbiditic sandstones with lithic fragments of igneous origin (Unit III) to near-shore sandstones with bioclasts (Unit IV), to a poorly sorted, well-lithified breccia with sandy matrix and igneous, calcareous, and mudstone clasts, to mudstone named Unit V (Fig. 4). The base of Unit IV was interpreted as marking the high amplitude reflector and laying unconformably on Unit V, which formed the acoustic basement at Site U1379. However, subsequent analysis of the cored material showed that we did not reach the forearc basement of the Caribbean plate, but rather an older forearc basin where clasts of basement were dispersed in fine, deep-water sediments.

A second penetration of the basement was attempted at Site U1378. Hole conditions did not allow reaching deeper than 457 mbsf during logging and 524 mbsf during coring at this site, whereas the expected depth of the top of the basement was ~750 mbsf. Detailed description of the cored sediments revealed the presence of a highly fractured and brecciated zone at 498–520 mbsf, interpreted as a fault zone, which may have caused the encountered drilling problems.

A final attempt to reach the basement was conducted at Site U1380, where the basement was expected to start at ~550 mbsf. Site U1380 is ~1 km upslope from site U1378, but the same drilling problems as at Site U1378 were encountered at this site, here at a depth of 482 mbsf. Therefore drilling of the middle slope was terminated.

2. Assess subduction channel thickness and the rate of subduction rrosion

In an erosive subduction margin, upper plate material is incorporated into the subduction channel because of basal erosion, resulting in subsidence of the upper plate. Thus, to assess the thickness of the subduction channel (Vannucchi et al., 2012b, and references therein) the mass removed from the upper plate has to be estimated, which can be achieved based on subsidence profiles determined from the cored slope sediments.

The first observation acquired from the cores indicates the formation of a well sediment-supplied forearc basin offshore the Osa Peninsula. The preliminary biostratigraphic

results obtained from the slope sites indicate high sediment accumulation rates in this terrestrially sourced slope sequence, ranging from 236–516 m m.y.$^{-1}$ at Site U1378 in the middle slope to 160–1035 m m.y.$^{-1}$ at Site U1379 in the shelf/upper slope (Fig. 6). In particular, the accumulation rate of the mainly clayey silt/silty clay slope sediments at Site U1379 at 1035 m m.y.$^{-1}$ is much higher than that of the middle slope sediments offshore the Nicoya Peninsula (38–99 m m.y.$^{-1}$, Kimura et al., 1997), and twice as high as the sediment accumulation rate along the sediment-rich trench off Muroto in the Nankai Trough (Fig. 5). This remarkably high accumulation rate offshore the Osa Peninsula could have its origin in the on-land uplift triggered by the subduction of the Cocos Ridge. On the other hand, the subduction of such topographic highs likely accelerates the basal erosion of the upper plate causing subsidence. The competition between subsidence and uplift of the forearc offshore the Osa Peninsula is recorded in the sedimentary and biostratigraphic characteristics of the slope sediments. The detailed analyses of sedimentary facies and benthic foraminifer fauna in slope sediments at Sites U1378 and U1379 are keys to estimate the mass removal associated with basal erosion and the thickness of the subduction channel.

3. Evaluate fluid/rock interaction, the hydrologic system, and the geochemical active within the upper plate

Fluid flow and fluid pressure in subduction zones can have a profound impact on the shallow thermal structure of the margin, on the content and distribution of fluids within the subducting and upper plates, and on the transfer of elements and isotopes to the ocean volcanic arc and mantle. It is also likely to, directly or indirectly, impact the partitioning of stable slip versus seismogenic slip along the plate boundary (Ranero et al., 2008). Changes in physical and mineralogical properties with depth and associated evolution of fluids in subduction zones may therefore be linked to the transition from aseismic to seismic behavior along the plate boundary (Moore and Saffer, 2001). Fluids advected along fault zones and other permeable horizons in the upper plate may record reactions occurring at greater depths in the subduction zone and can be used to constrain reactions occurring within the seismogenic zone (Vannucchi et al., 2010).

Based on the first results obtained during the shipboard geochemistry program of Exp. 334, two zones with fluid compositions indicative of transport from greater depths could be identified within the upper plate (Vannucchi et al., 2012a). At Site U1381 in the subducting plate, one zone of lateral flow of modified seawater in the igneous basement could be identified. Whereas pore fluids in the uppermost ~50 m at all sites drilled during Exp. 334 were dominated by reactions associated with the
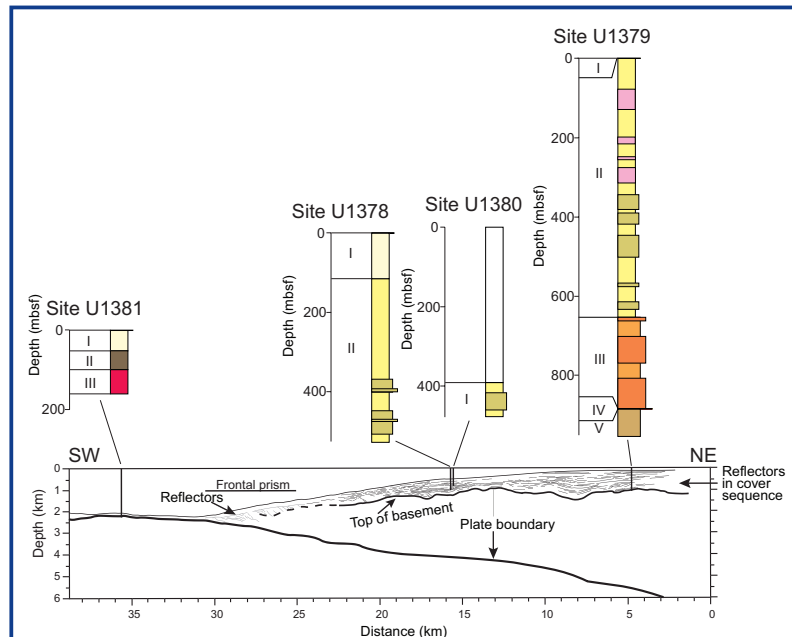
Figure 4. Lithostratigraphic columns from Exp. 334 sites. At Site U1378 Unit I is formed by clay, silt, and sand, Unit II by clay(stone), silt(stone), and sandstone. At Site U1379, Unit I is formed by coarse sand, Unit II by clay(stone), silt(stone), and sandstone, Unit III by fine to medium sandstone, Unit IV by medium to coarse sand, and Unit V by breccia. At Site U1380, Unit I is formed by clay(stone), silt(stone), and sandstone. At Site U1381, Unit I is formed by clay and silty clay, Unit II by siliceous to calcareous ooze, and Unit II by basalts.

cycling of organic carbon, deep fluid flow was also detected at each of the sites cored. This fluid flow overprints the general geochemical profiles that are associated with *in situ* diagenetic processes such as ion exchange, ongoing microbial metabolic reactions, volcanic ash alteration, and carbonate precipitation and dissolution. At Site U1379, a broad zone from ~600 mbsf to 800 mbsf contains a fluid with low Cl concentrations and peaks in the concentrations of thermogenic hydrocarbons (ethane, propane, *n*-butane, isobutane). The geothermal gradient at Site U1379 is too low to support the *in situ* production of thermogenic hydrocarbons or extensive clay dehydration, suggesting a deeper source of the fluid.

At Site U1381, the geochemical profiles below ~50 mbsf reflect diffusional communication of a fluid with seawater-like chemistry with the igneous basement (Vannucchi et al., 2012a).

4. Measure the stress field along the CRISP transect

We estimated present-day *in situ* stress orientation from borehole breakouts at Site U1378 in the middle slope and Site U1379 in the shelf/upper slope. Borehole breakouts in a vertical hole form in a direction perpendicular to the maximum horizontal principal stress (σ_{Hmax}) (Zoback et al., 2003). During Exp. 334, borehole breakouts were identified from LWD images of borehole radius and density. In addition, we determined types, orientations, and kinematics of faults from cores.

Figure 5. Summary of the lithostratigraphy and LWD measurements. [A] is for Site U1378, [B] for Site 1379C. GVR=geoVISION tool, ARC=arcVISION tool, PEF=photoelectric factor, IDRO=image-derived density (EcoScope tool), RHOB=bulk density, RING=resistivity measured by the ring electrode (geoVISION tool), P16B=phase-shift resistivity measured at a 16-inch source-receiver separation (arcVISION tool), A40B=attenuation resistivity measured at a 40-inch source-receiver separation (arcVISION tool).

The σ_{Hmax} orientation of slope sediments at Site U1379 down to a depth of 850 mbsf is east-northeast/west-southwest, below which σ_{Hmax} seems to rotate to north/south for about 50 m (Fig. 5). No obvious borehole breakouts appear below about 900 mbsf in the underlying acoustic basement (Fig. 5). Normal faults dominate the cores of the slope sediments at Site U1379 (Fig. 7). The kinematic analyses of the normal faults indicate a vertical maximum principal stress (σ_1), an intermediate principal stress (σ_2) oriented west-northwest/east-southeast, and a minimum principal stress (σ_3) oriented north-northeast/south-southwest (Fig. 7). The σ_{Hmax} orientation at Site U1379 for the upper 850 mbsf is consistent with north-northwest/south-southeast-directed horizontal extension, which is subparallel to the plate motion vector detected by GPS measurements northwest of the Osa Peninsula (LaFemina et al., 2009). On the other hand, the σ_3 orientation determined from kinematic analyses of core-scale normal faults is
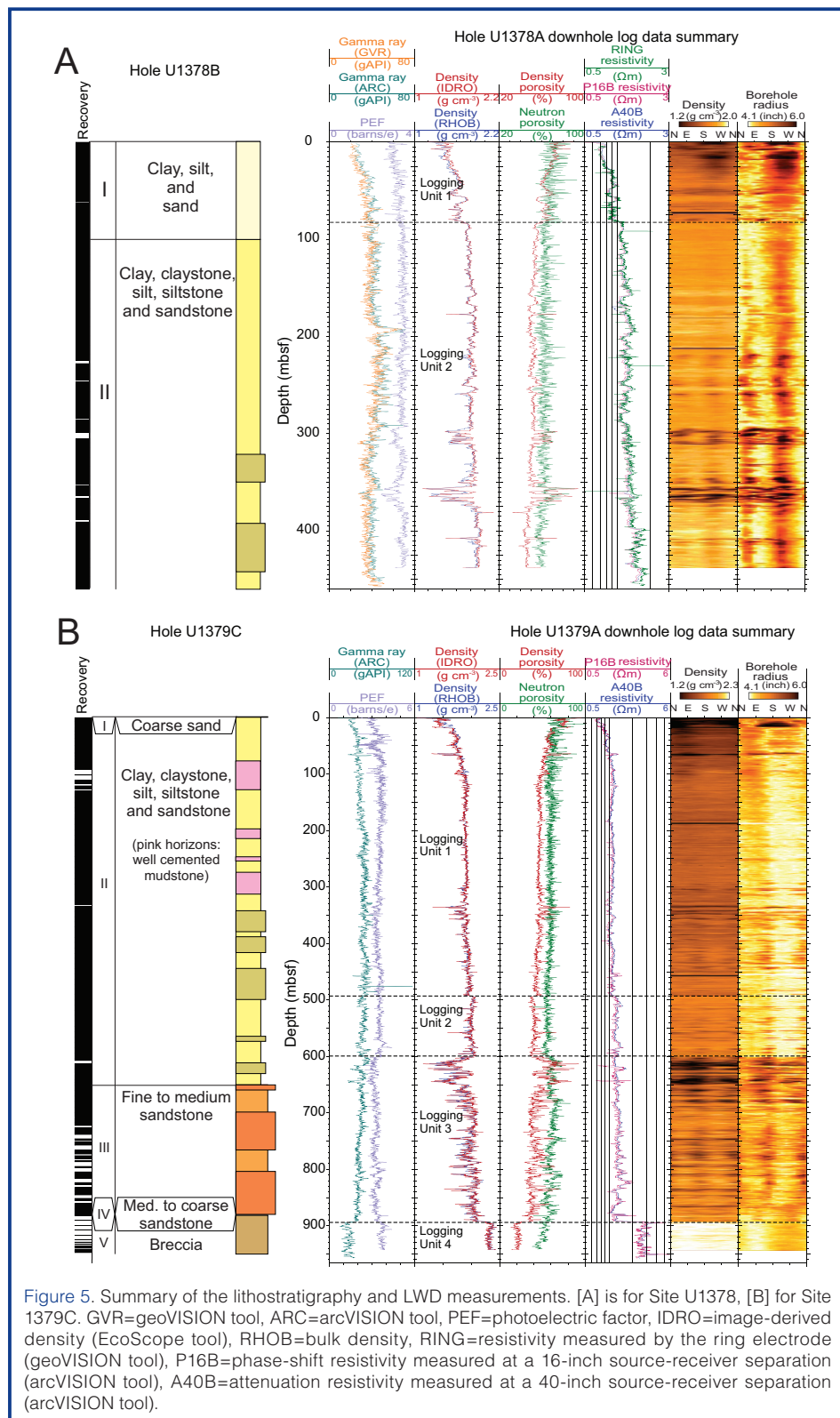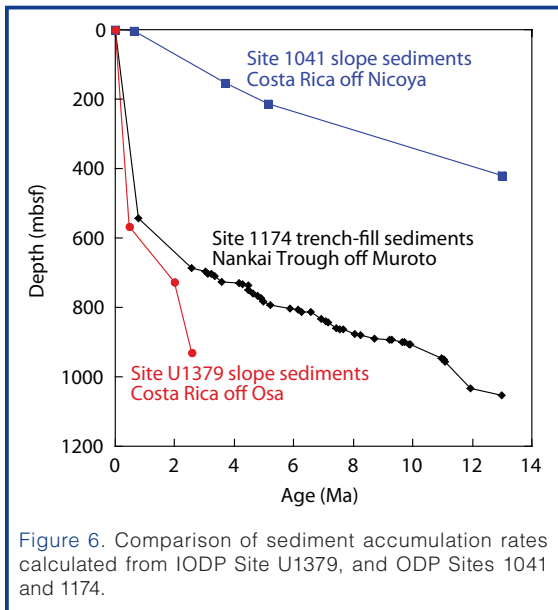
Figure 6. Comparison of sediment accumulation rates calculated from IODP Site U1379, and ODP Sites 1041 and 1174.

Figure 7. Summary of interpretations of borehole breakout for Sites U1378 and U1379 and of fault plane solution for Site U1379 fault data. Blue arrows represent the Cocos-Caribbean convergence direction. (VE=vertical exaggeration)

parallel to the convergence direction between the Cocos and Caribbean plates (DeMets, 2001). Core-scale normal faults record instantaneous stress conditions when the faults are active. Although stress data sets are derived from slope sediments overlying the upper plate basement, trench-normal extension in the upper section of Site U1379 is consistent with extensional faulting in the submarine wedge associated with basal erosion (Ranero and von Huene, 2000).

The *in situ* stress field configuration seems to be more complex considering the 50-m interval between 850 mbsf and 900 mbsf. Borehole breakouts, in fact, seem to indicate about a 90° rotation of σ_{Hmax} orientation, very similar to the breakout orientation of slope sediments at Site U1378. There, σ_{Hmax} is oriented north-northwest/south-southeast (Fig. 7). At Site U1378 both normal and reverse faults are observed in cores from the slope sediments. The σ_{Hmax} orientation at Site U1378 and possibly in the deeper portion of U1379 is consistent with the north-northwest-directed plate motion vector detected by the GPS measurement northwest of the Osa Peninsula (LaFemina et al., 2009) and is oblique to the convergence direction (north-northeast) between the Cocos and Caribbean plates (DeMets, 2001). The Cocos Ridge is con-sidered to act as a rigid indenter to the Caribbean plate, resulting in a change in plate motion from north-northeast-directed trench-normal motion in southern Costa Rica to trench-parallel motion in central Costa Rica where plate convergence is normal to the trench (LaFemina et al., 2009). North-northwest-oriented σ_{Hmax} at Sites U1378 and U1379 may represent the shortening of the middle slope opposite the northwestern flank of the Cocos Ridge (thrust faulting stress regime), where plate motion likely deviates from trench-normal motion, although strike-slip and/or normal stress states are also possible.
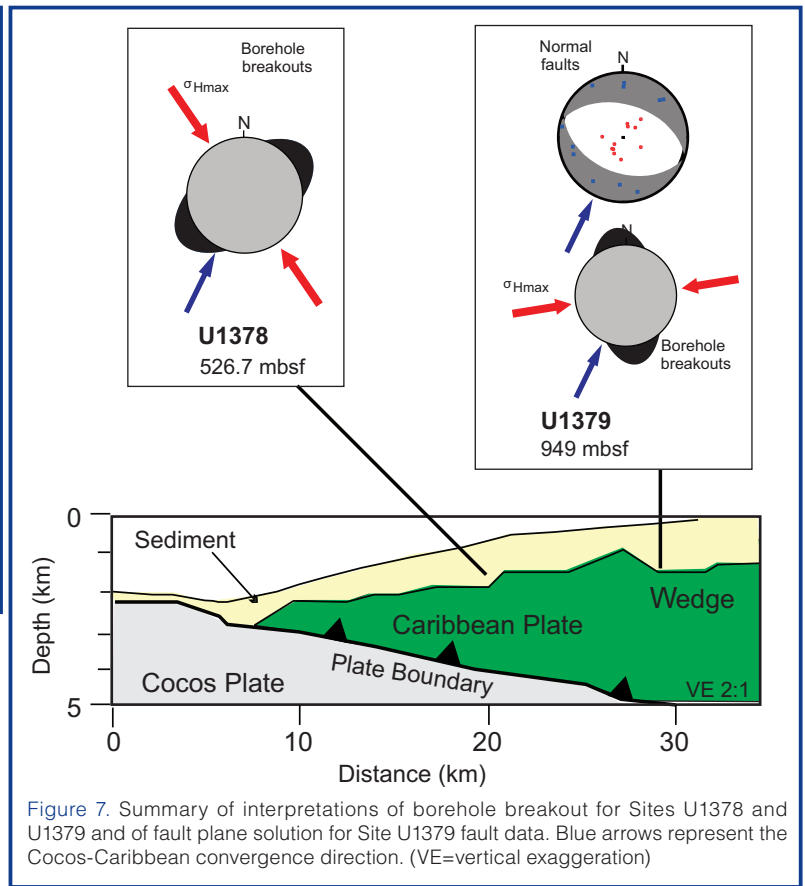
5. Reconstruct the Cocos Ridge subduction: evolution of the Central American volcanic arc and development of the volcanic arc gap inboard Cocos Ridge

Site U1381 sampled the sediments and basalts of the Cocos Ridge, which represents the trace of the Galapagos hotspot on the Cocos plate. Approximately eighty meters of basalts were recovered from below ~100 m of biogenic pe-lagic sediments consisting mainly of siliceous to calcareous oozes. Investigations are currently being conducted to study the petrogenesis and geochemistry of these basalts as well as fluid/rock interaction processes that may be occurring.

In addition to the igneous rocks cored at Site U1381, approximately 170 tephra layers were retrieved, described, and sampled from the holes cored at the four different sites visited during Exp. 334. Tephra ages range from middle Miocene to the present. Post-cruise analyses of the tephra will shed light on the evolution of the magmatic arc, including the deactivation of the volcanoes located on the present-day location of the Talamanca Cordillera.

Plans for Future Investigations

Because of an abbreviated operation schedule of IODP Exp. 334, the original CRISP Program A plan was reduced and kept mainly focused on the middle and shelf/upper slope region off the Osa Peninsula. IODP Exp. 344 returned to the Costa Rica margin with the aim to complete CRISP Program

A (Expedition 344 Scientists, 2013) in preparation of later, deep and riser-supported drilling into the basement, and ultimately through the plate interface in locations of both aseismic and seismogenic fault behavior. A 3-D reflection seismic survey conducted in April 2011 over the Costa Rica margin (Bangs et al., 2011) will provide further information on potential locations for such deep drilling. One potential site, IODP Site U1413, at a water depth of 540 m and located over the up-dip end of the seismogenic zone has already been identified and cored during Exp. 344 (Fig. 1).

The IODP Expedition 334 Scientific Party

Alberto Malinverno, Ivonne Arroyo, Udo Barckhausen, Marianne J. Conin, Susan Murr Foley, Michael J. Formolo, Robert N. Harris, Arnauld Heuret, Gary J Huftile, Jun Kameda, Gil Young Kim, Steffen O. Kutterolf, Amanda J. Martino, Gillian A. McCay, Marianne Nuzzo, Ken'ichi Ohkushi, Saneatsu Saito, Peter B. Sak, Evan A. Solomon, Michael Stipp, Marta E. Torres, Akito Tsutsumi, Masaoki Uno, Yoichi Usui, Yatheesh Vadakkeyakath, Yuzuru Yamamoto, Xixi Zhao, Junjiang Zhu and Jenifer Saltman (Education and Outreach)

References

Arroyo, I. G., Grevemeyer, I., von Huene, R., Husen, S., Ranero, C. R., and Behrmann, J. H., 2011. Interplate seismicity at the CRISP site: The 2002 Osa earthquake sequence. [Paper presented at the American Geophysical Unon Fall 2011 Meeting, San Francisco, 5–9 December 2011]. Abstract T21B-2348.

Bangs, N. L.; McIntosh, K. D.; Silver, E. A.; Ranero, C. R.; Kluesner, J. W.; von Huene, R., Cavanaugh, S. et al., 2011. Preliminary results of the CRISP 3D seismic experiment, offshore Costa Rica. [Paper presented at the American Geophysical Union Fall Meeting, San Francisco, CA, 5–9 December 2011]. Abstract T21B-2341.

Clift, P. D., and Vannucchi, P., 2004. Controls on tectonic accretion versus erosion in subduction zones: Implications for the origin and recycling of the continental crust: *Rev. Geophys.*, 42:RG2001. doi:2010.1029/2003RG000127

DeMets, C., 2001. A new estimate for present-day Cocos-Caribbean plate motion: Implications for slip along the Central American volcanic arc. *Geophys. Res. Lett.*, 28:4043–4046. doi:10.1029/2001GL013518

DeShon, H. R., Schwartz, S. Y., Bilek, S. L., Dorman, L. M., Gonzalez, V., Protti, J. M., Flueh, E. R., and Dixon, T. H., 2003. Seismogenic zone structure of the southern Middle America Trench, Costa Rica. *J. Geophys. Res. B Solid Earth*, 108:2491. doi:10.1029/2002JB002294

Di Toro, G., Hirose, T. Nielsen, S., Pennacchioni, G., and Shimamoto, T. 2006. Natural and experimental evidence of melt lubrication of faults during earthquakes. *Science*, 311:647–649. doi: 10.1126/science.1121012

Dixon, T. H., 2003. Relations between seismic coupling and mountain building based on GPS observations in Costa Rica. *Geophys. Res. Abstr.*, 5:4374.

Expedition 344 Scientists, 2013. Costa Rica Seismogenesis Project, Program A Stage 2 (CRISP-A2): Sampling and quantifying lithologic inputs and fluid inputs and outputs of the seismogenic zone. *IODP Prel. Rept.,* 344. doi:10.2204/iodp. pr.344.2013

Harris, R. N., Grevemeyer, I., Ranero, C. R., Villinger, H., Barckhausen, U., Henke, T., Muller, C., and Neben, S., 2010a. The thermal regime of the Costa Rican convergent margin: 1. Along-strike variations in heat flow from probe measurements and estimated from bottom-simulating reflectors. *Geochem. Geophys. Geosyst.*, 11:Q12S28.

Harris, R. N., Spinelli, G., Ranero, C. R., Grevemeyer, I., Villinger, H., and Barckhausen, U., 2010b. The thermal regime of the Costa Rican convergent margin: 2. Thermal models of the shallow Middle America Subduction Zone offshore Costa Rica. *Geochem. Geophys. Geosyst.*, 11:Q12S29.

Kimura, G., Silver, E. A., Blum, P., et al., 1997. *Proc. ODP, Init. Repts.*, 170: College Station, TX (Ocean Drilling Program). doi:10.2973/odp.proc.ir.170.1997

LaFemina, P., Dixon, T. H., Govers, R., Norabuena, E., Turner, H., Saballos, A., Mattioli, G., Protti, M., and Strauch, W., 2009. Fore-arc motion and Cocos Ridge collision in Central America. *Geochem. Geophys. Geosyst.*, 10:Q05S14. doi:10.1029/2008GC002181

Moore, J. C., and Saffer, D., 2001. Updip limit of the seismogenic zone beneath the accretionary prism of southwest Japan: An effect of diagenetic to low-grade metamorphic processes and increasing effective. *Geology*, 29:183–186. doi: 10.1130/0091-7613

Morris, J. D., Villinger, H. W., Klaus, A., et al., 2003. *Proc.ODP, Init. Repts.*, 205: College Station, TX (Ocean Drilling Program), 75 (CD-ROM).

Ranero, C. R., and von Huene, R., 2000. Subduction erosion along the Middle America convergent margin. *Nature*, 404:748–752. doi:10.1038/35008046

Ranero, C. R., Grevemeyer, I., Sahling, U., Barckhausen, U., Hensen, C., Wallmann, K., Weinrebe, W., Vannucchi, P., von Huene, R., and McIntosh, K., 2008. The hydrogeological system of erosional convergent margins and its influence on tectonics and interplate seismogenesis. *Geochem. Geophys. Geosyst.*, 9:Q03S04. doi:10.1029/2007GC001679

Ranero, C. R., Marone, C., Bilek, S., Barckhausen, U., Charvis, P., Collot, J-Y, DeShon, H., at al. 2006. CRISP Program B: The transition from stable to unstable slip at erosional convergent plate boundaries. IODP Proposal 537B-Full4

Ranero, C. R., von Huene, R., Flueh, E., Duarte, M., Baca, D., and McIntosh, K., 2000. A cross section of the convergent Pacific margin of Nicaragua. *Tectonics*, 19:335–357. doi:10.1029/1999TC900045

Sallares, V., Charvis, P., Flueh, E. R., and Bialas, J., 2003. Seismic structure of Cocos and Malpelo Volcanic Ridges and implications for hot spot-ridge interaction. *J. Geophys. Res.*, 108:2564. doi:10.1029/2003JB002431

Solomon, E. A., Torres, M. E., Harris, R. N., Formolo, M., Nuzzo, M., and the Expedition 334 Scientists, 2011. Geochemical constraints on fluid-rock reactions, fluid sources, and flow

pathways along the CRISP transect; IODP Expedition 334. [Paper presented at the American Geophysical Union Fall Meeting, San Farncisco, CA, 5–9 December 2011] Abstract T14B-06.

Stavenhagen, A. U., Flueh, E. R., Ranero, C. R., McIntosh, K. D., Shipley, T., Leandro, G., Schulze, A., and Dañobeitia, J. J., 1998. Seismic wide-angle investigations in Costa Rica - A crustal velocity model from the Pacific to the Caribbean. *Zbl. Geol. Paläont.*, 1:393–408.

Vannucchi, P., Fisher, D. M., Gardner, T. W., and Bier, S., 2006. From seamount accretion to tectonic erosion: Formation of Osa Mélange and the effects of Cocos Ridge subduction in southern Costa Rica. *Tectonics*, 25:TC2004. doi:10.1029/2005TC001855

Vannucchi, P., Galeotti, S., Clift, P. D., Ranero, C., and von Huene, R., 2004. Long-term subduction-erosion along the Middle America Trench. *Geology*, 32:617–620. doi:10.1130/G20422.1

Vannucchi, P., Ranero, C. R., Galeotti, S., Straub, S. M., Scholl, D. W., and McDougall-Ried, K., 2003. Fast rates of subduction erosion along the Costa Rica Pacific margin: Implications for nonsteady rates of crustal recycling at subduction zones. *J. Geophys. Res.*, 108:2511, doi:10.1029/2002JB002207

Vannucchi, P., Remitti, F., Bettelli, G., Boschi, C., and Dallai, L., 2010. Fluid history related to the early Eocene-middle Miocene convergent system of the Northern Apennines (Italy): Constraints from structural and isotopic studies. *J. Geophys. Res.*, 115:B05405. doi:10.1029/2009JB006590

Vannucchi, P., Sage, F., Morgan, J. P., Remitti, F., and Collot, J. Y., 2012b. Toward a dynamic concept of the subduction channel at erosive convergent margins with implications for inter-plate material transfer. *Geochem. Geophys. Geosyst.*, 13:Q02003. doi:10.1029/2011GC003846

Vannucchi, P., Scholl, D. W., Meschede, M., and McDougall-Reid, K., 2001. Tectonic erosion and consequent collapse of the Pacific margin of Costa Rica: Combined implications from ODP Leg 170, seismic offshore data, and regional geology of the Nicoya Peninsula. *Tectonics*, 20:649–668. doi:10.1029/2000TC001223

Vannucchi, P., Ujiie, K., Stroncik, N., and the Expedition 334 Scientists, 2012a. *Proc. IODP*, 334: Washington, DC (Integrated Ocean Drilling Program Management International, Inc.). doi:10.2204/iodp.proc.334.2012

von Huene, R., Alvarado, G., Brown, K., Harris, R., Kinoshita, M., Suyehiro, K., McIntosh, K., et al., 2003. Discussions of ODP Leg 205 and drilling of Middle America seismogenic zone. *Eos Trans. AGU*, 84:91–92.

von Huene, R., Ranero, C. R., and Vannucchi, P., 2004. Generic model of subduction erosion. *Geology*, 32:913–916. doi:10.1130/G20563.1

von Huene, R., Ranero, C. R., Weinrebe, W., and Hinz, K., 2000. Quaternary convergent margin tectonics of Costa Rica, segmentation of the Cocos Plate, and Central American volcanism. *Tectonics*, 19:314–334. doi:10.1029/1999TC001143

Wibberley, C., and Shimamoto, T., 2005. Earthquake slip weakening and asperities explained by thermal pressurization, *Nature*, 436:689-692. doi:10.1038/nature03901

Zoback, M. D., Barton, C. A., Brudy, M., Castillo, D. A., Finkbeiner, T., Grollimund, B. R., Moos, D. B., Peska, P., Ward, C. D., and Wiprut, D. J., 2003. Determination of stress orientation and magnitude in deep wells. *Int. J. Rock Mech. Min. Sci.*, 40:1049–1076. doi:10.1016/j.ijrmms.2003.07.001

Authors

Paola Vannucchi, (Currently) Department of Earth Sciences, Royal Holloway, University of London, Egham, Surrey, TW20 0EX, U.K., e-mail: paola.vannucchi@rhul.ac.uk

Kohtaro Ujiie, Graduate School of Life and Environmental Sciences, University of Tsukuba, 1-1-1 Tennodai, Tsukuba 305-0006, Japan, e-mail: kujiie@geol.tsukuba.ac.jp

Nicole Stroncik, Integrated Ocean Drilling Program, Texas A&M University, 1000 Discovery Drive, College Station, TX 77845-9547, U.S.A., e-mail: stroncik@iodp.tamu.edu

and the IODP Exp. 334 Scientific Party

IODP Expedition 340T: Borehole Logging at Atlantis Massif Oceanic Core Complex

by Donna Blackman, Angela Slagle, Alistair Harding, Gilles Guerin, and Andrew McCaig

Abstract

Integrated Ocean Drilling Program (IODP) Expedition 340T returned to the 1.4-km-deep Hole U1309D at Atlantis Massif to carry out borehole logging including vertical seismic profiling (VSP). Seismic, resistivity, and temperature logs were obtained throughout the geologic section in the footwall of this oceanic core complex. Reliable downhole temperature measurements throughout and the first seismic coverage of the 800–1400 meters below seafloor (mbsf) portion of the section were obtained. Distinct changes in velocity, resistivity, and magnetic susceptibility characterize the boundaries of altered, olivine-rich troctolite intervals within the otherwise dominantly gabbroic se-quence. Some narrow fault zones also are associated with downhole resistivity or velocity excursions. Small deviations in temperature were measured in borehole fluid adjacent to known faults at 750 mbsf and 1100 mbsf. This suggests that flow of seawater remains active along these zones of faulting and rock alteration. Vertical seismic profile station coverage at zero offset now extends the full length of the hole, including the uppermost 150 mbsf, where detachment processes are expected to have left their strongest imprint. Analysis of wallrock pro-

perties, together with alteration and structural characteristics of the cores from Site U1309, highlights the likely interplay between lithology, structure, lithospheric hydration, and core complex evolution.

Geologic Setting and Motivation

The Atlantis Massif oceanic core complex (OCC) was drilled during IODP Expedition 304/305 (Blackman et al., 2006). It formed due to spatial and temporal variability in magmatism and faulting within the axial zone of the slow-spreading Mid-Atlantic Ridge at 30°N (Cann et al., 1997). Long-lived strain localization along select axial faults allowed development of a detachment zone that unroofed intrusive crust 0.5–1.5 Ma (Grimes et al., 2008). High fracture intensity in the detachment zone enabled circulation of seawater (McCaig et al., 2010), and associated alteration included formation of low-strength minerals that enhanced strain localization. Geophysical studies (Blackman et al., 2008; Canales et al., 2008; Collins et al., 2009; Blackman and Collins, 2010; Henig et al., 2012), seafloor mapping and sampling (Blackman et al., 2002; Schroeder and John, 2004; Boschi et al., 2006; Karson et al., 2006), and deep basement drilling and logging (Blackman et al., 2011; Ildefonse et al.,
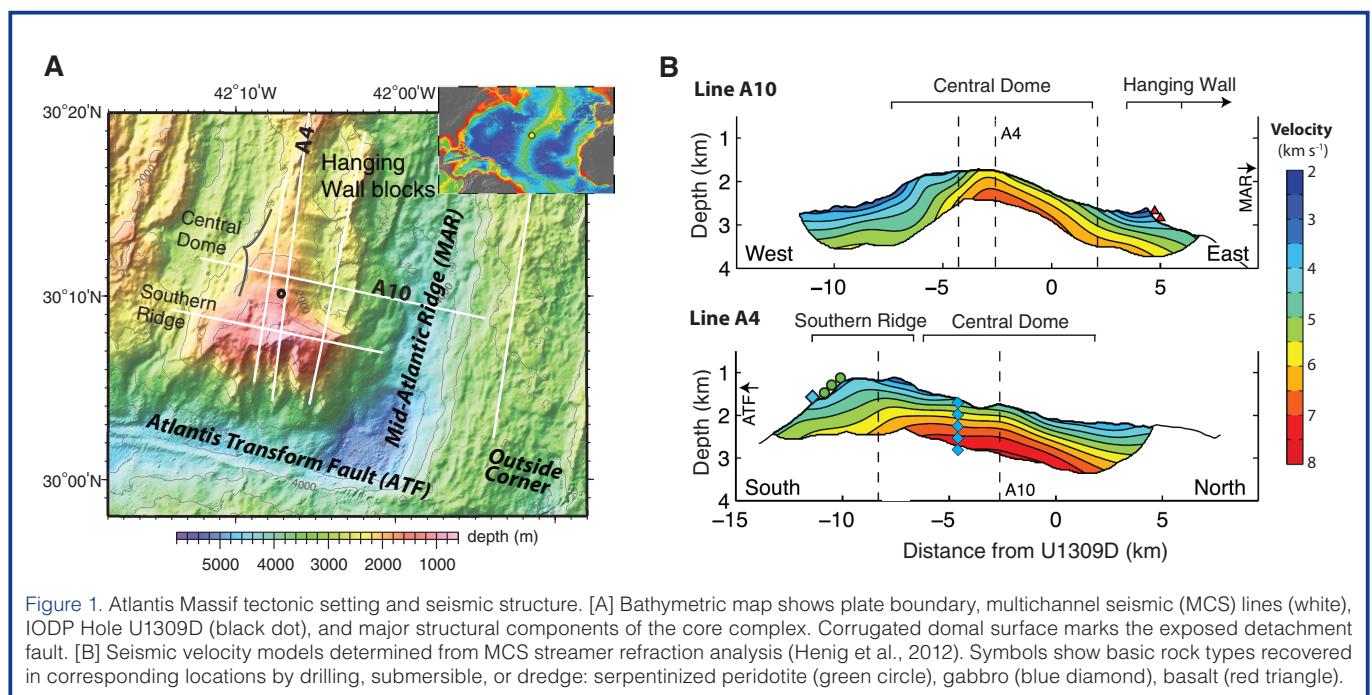
Figure 1. Atlantis Massif tectonic setting and seismic structure. [A] Bathymetric map shows plate boundary, multichannel seismic (MCS) lines (white), IODP Hole U1309D (black dot), and major structural components of the core complex. Corrugated domal surface marks the exposed detachment fault. [B] Seismic velocity models determined from MCS streamer refraction analysis (Henig et al., 2012). Symbols show basic rock types recovered in corresponding locations by drilling, submersible, or dredge: serpentinized peridotite (green circle), gabbro (blue diamond), basalt (red triangle).

2007) all contribute to the model of how the Atlantis Massif OCC evolved.

Figure 1 illustrates the structural components of the Atlantis Massif and the variability in shallow velocity field; a lack of a conventional seismic Layer 2 within the core complex is evident. The domal core is capped by the corrugated, exposed detachment fault that unroofed the intrusive crust drilled at Site U1309 on the Central Dome. This gabbroic body has seismic velocity of 5.5–7 km s^{-1} and shoals to the seafloor in the eastern part of the central and southern portions of the domal core (Henig et al., 2012). The exposed detachment fault bounds the high velocity gabbroic body on the east, dipping beneath the basaltic hanging wall blocks toward the axis of the Mid-Atlantic Ridge. The steeper, western boundary of the body may be an intrusive contact that was originally near horizontal, but other interpretations are also under investigation (Harding et al., 2012). Paleomagnetic results indicate that at least the upper 400 m, and likely the full 1.4-km section, of Hole U1309D has rotated a minimum of 45° counterclockwise about a horizontal axis that parallels the rift valley (Morris et al., 2009). Seven narrow fault zones (several centimeters to a few meters in scale) within the interval 100–1100 mbsf were documented within the core and by earlier logging data (Blackman et al., 2006; Hirose and Hayman, 2008; Michibayashi et al., 2008). But the limited extent of these faults might imply that they did not dominate the development of the OCC. An eighth fault was identified at 1346 mbsf from logs obtained during Exp. 340T. However, some of these narrow intervals are associated with notable downhole change in degree/style of alteration and wallrock properties, so the implications of this are a subject for further investigation in which the Exp. 340T logs will play a significant role (Blackman et al., 2012).

Prior multi-channel seismic imaging (Canales et al., 2004) and application of a novel wide-angle stacking method (Singh et al., 2004; Masoomzadeh et al., 2010) suggested that there is considerable seismic reflectivity within the footwall of this oceanic core complex. This was somewhat surprising given the dominantly gabbroic section recovered from Hole U1309D. The Exp. 340T logging program was designed to document whether olivine-rich, highly altered intervals, and/or narrow, possibly fluid-bearing fault zones within the formation might contribute to regional reflectivity, thus potentially enabling use of the seismic sections for assessing former and current hydrological flow fields within the OCC.

Figure 2. Borehole fluid temperature in Hole U1309D. Solid black line shows IODP 340T MTT measurements. Dashed gray line is predicted gradient at position of Site U1309 from 3-D model of plate-driven mantle flow and lithospheric cooling. The ridge-transform-ridge model had geometry and spreading rate of the study region (calculation of Blackman et al., 2008).

Logging Operations

On approach for the initial reentry of Hole U1309D during Exp. 340T (February 2012), we monitored the video carefully for possible fluid flow into/out of the well. No flow was apparent, and the reentry cone had just a light sediment cover accrued since the end of drilling operations in 2005. Hole U1309D was found to be in good condition, and an initial, minimal-disturbance borehole fluid temperature measurement was achieved on the first logging run into the borehole. The triple combination tool string employed for that run included the Modular Temperature Tool (MTT) that documented the borehole fluid temperature at centimeter-scale resolution. Additional temperature measurements were made during each subsequent logging run using a sensor in the logging cable head. All standard log measurements were recorded and are in excellent agreement with data from Exp. 304/305. Intervals that are out of bore or unusually ragged match those recognized during the 2004–2005 drilling. Electrical resistivity was measured with the High-Resolution Laterolog Array (HRLA) during Exp. 340T, a newer resistivity tool than that used during Exp. 304/305. The HRLA provides six resistivity measurements at different depths of penetration into the wall rock, including one measurement of the borehole fluid.

Seismic velocity was measured during Exp. 340T throughout the section. The 800–1400 mbsf interval that had not been possible to cover at the end of Exp. 305 was logged with the Dipole Shear Sonic Imager, which was run with a low frequency sequence that generated Stoneley waves in addition to compressional and shear waves. A zero-offset Vertical Seismic Profile (VSP) experiment was conducted using the *JOIDES Resolution* two-gun 250-in^3 cluster as the source and the Versatile Seismic Imager (VSI) triaxial geophone as the receiver. The VSP was carried out during daylight hours over two days, in keeping with the marine mammal hazard mitigation plan. Differences in weather/ship conditions and problems with the VSI anchoring arm appear to have impacted data quality. High quality recordings were obtained during a VSP run when sea/wind state was calmest. The next day, most recordings had only fair signal-to-noise ratio, although initial analysis indicates that it will be possible to determine velocities to VSI stations throughout the section (Expedition 340T Scientists, 2012).

A newly constructed Magnetic Susceptibility Sonde (MSS) was run for the first time in seawater during Exp. 340T. Limits on operating temperature

restricted its use to the upper 750 mbsf. The data appear to be high quality, with intervals showing significant excursion in measured value agreeing closely with the multi-sensor track record of core susceptibility obtained during Exp. 304/305.

More detailed information on the logged properties, logging tools, and logging operations may be found in the IODP Exp. 340T Preliminary Report (Expedition 340T Scientists, 2012).

Highlighted Initial Results

Exp. 340T extended *in situ* seismic velocity measurement of intrusive oceanic crust, which typically comprises Layer 3, beyond one km, a depth where closure of micro-fractures eliminates bias associated with shallow exposure. Earlier work had documented gabbroic wallrock velocities to sub-seafloor depths of 0.5–0.8 km (Itturino et al., 2002; Blackman et al., 2006). The new logs indicate that the little-altered section from 800 mbsf to 1400 mbsf at Site U1309 has a mean compressional velocity of 6.6 km s^{-1} and mean shear velocity of 3.7 km s^{-1}. These averages excludes the oli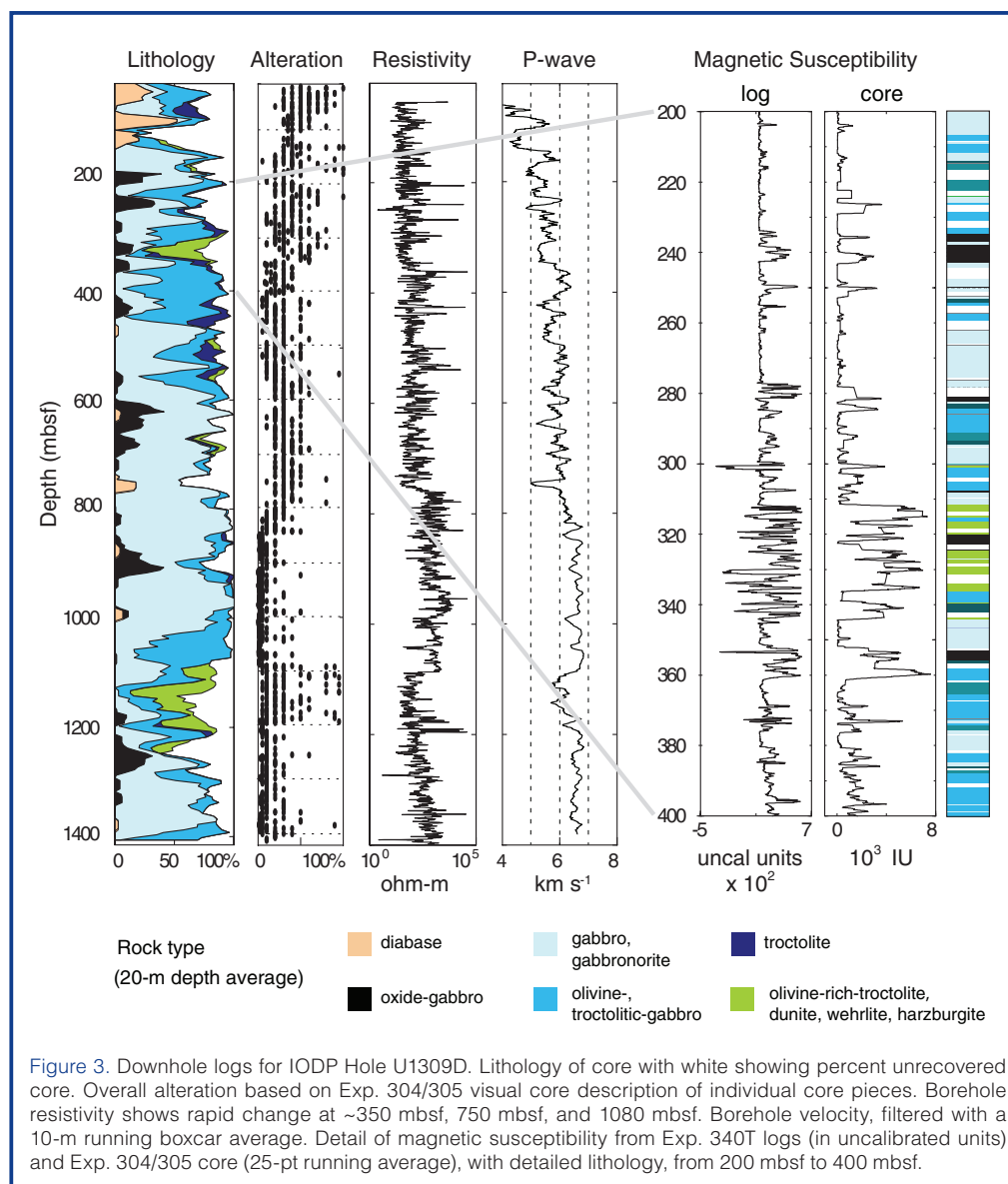vine-rich troctolite interval at 1080–1220 mbsf that has several highly serpen-tinized intervals. This multimeter-scale average represents the inherent seismic properties of this (and likely most oceanic) gabbroic section. When post-processing of the VSP data is complete, a site average compressional velocity for this intrusive crustal section will be obtained that includes the effects of fracturing at the 100-m scale that the sonic log does not measure.

The temperature at the base of Hole U1309D at 1400 mbsf is ~146°C. The downhole gradient (Fig. 2) is nearly linear—just under 100°C km^{-1} (Expedition 340T Scientists, 2012)—but closer examination, after removing a linear trend, shows some interesting downhole thermal structure. Small deviations in borehole fluid temperature measured adjacent to a few narrow faults, documented in the core and/or Exp. 304/305 Formation MicroScanner (FMS) images, suggest that seawater presently percolates through these zones.

Integration of the new log data with a prior geologic description of Hole U1309D core indicates that boundaries of highly altered olivine-rich troctolite intervals mark distinct changes in seismic velocity, resistivity, and magnetic susceptibility within the gabbroic section (Fig. 3). There are two zones where olivine-rich troctolite occurs repeatedly throughout an interval that is tens of meters thick: 310–350 mbsf and 1080–1220 mbsf. Other ultramafic intervals are tens of centimeters to ~3 m thick, with dunite and harzburgite only recovered above 224 mbsf. A fault zone at 750 mbsf (Michibayashi et al., 2008) is also associated with a significant local drop in seismic velocity, and below it resistivity increases rapidly. This is one of the faults where a small deviation in borehole fluid temperature was confirmed during Exp. 340T, and another occurs at ~1100 mbsf. Both these faults were documented by deformation structures in core samples and by fault gouge. The ~1100 mbsf fault and another newly identi-

Figure 3. Downhole logs for IODP Hole U1309D. Lithology of core with white showing percent unrecovered core. Overall alteration based on Exp. 304/305 visual core description of individual core pieces. Borehole resistivity shows rapid change at ~350 mbsf, 750 mbsf, and 1080 mbsf. Borehole velocity, filtered with a 10-m running boxcar average. Detail of magnetic susceptibility from Exp. 340T logs (in uncalibrated units) and Exp. 304/305 core (25-pt running average), with detailed lithology, from 200 mbsf to 400 mbsf.

fied narrow fault zone at ~1345 mbsf have sharply distinct seismic properties that cause reflection of the borehole Stoneley wave (Fig. 4).

The thickness of the lower velocity interval associated with the altered olivine-rich troctolite zone at 1080–1220 mbsf is sufficient that, if laterally extensive, would be detectable within regional, far-field seismic data. Compressional velocities are 0.5–1 km s^{-1} lower than the surrounding rock. Similarly, the olivine-rich troctolite interval at 310–350 mbsf has velocity notably lower than adjacent rock. Much of the section shallower than 350 mbsf is highly altered, so it is possible that structure or processes associated with the base of this olivine-rich troctolite zone are more relevant in controlling seismic properties than alteration within the zone itself. Nevertheless, there is a distinct drop of over 0.5 km s^{-1} at 310 mbsf, the top of the zone, and an increase of ~1 km s^{-1} below the base. The seismic velocity of the moderately altered section at 350–750 mbsf varies modestly around a value of ~6 km s^{-1}. As noted above, the little-altered section deeper than 800 mbsf has an average velocity of 6.6 km s^{-1}, with a maximum discrete velocity of ~6.8 km s^{-1}. Primary lithology would dictate that the highest velocities accompany the olivine-rich intervals, but we find that alteration plays the dominant role in determining present-day seismic velocity in the upper kilometer and a half of the domal core at Atlantis Massif.
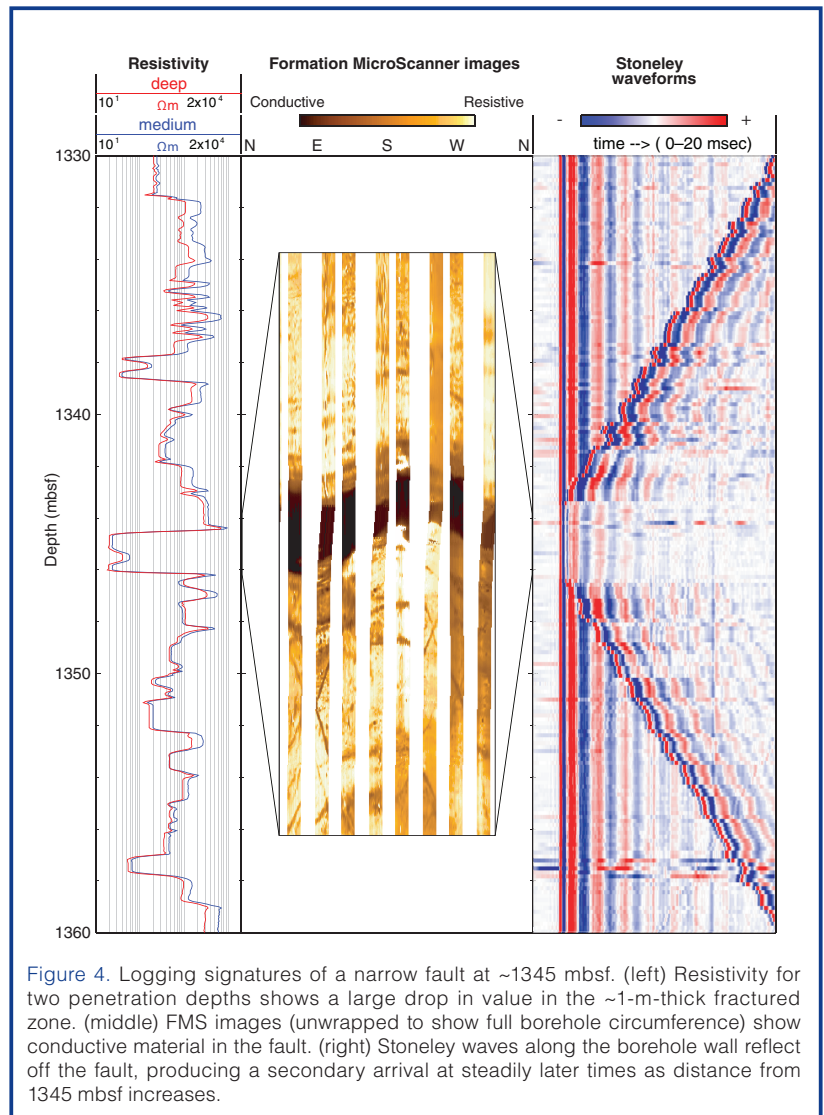

Figure 4. Logging signatures of a narrow fault at ~1345 mbsf. (left) Resistivity for two penetration depths shows a large drop in value in the ~1-m-thick fractured zone. (middle) FMS images (unwrapped to show full borehole circumference) show conductive material in the fault. (right) Stoneley waves along the borehole wall reflect off the fault, producing a secondary arrival at steadily later times as distance from 1345 mbsf increases.

References

Blackman, D., Slagle, A., Guerin, G., and Harding, A., 2012. Formation and early evolution of oceanic lithosphere- multi-faceted study of tectonic, magmatic, and hydrologic processes at Atlantis Massif, MAR 30°N, [Paper presented at 2012 Fall Meeting AGU San Francisco, 3–7 December 2012]. Abstract OS44A-01

Blackman, D. K., and Collins, J. A., 2010. Lower crustal variability and the crust/mantle transition at the Atlantis Massif oceanic core complex. *Geophys. Res. Lett.*, 37(24):L24303. doi:10.1029/2010GL045165

Blackman, D. K., Ildefonse, B., John, B. E., Ohara, Y., Miller, D. J., Abe, N., Abratis, M., et al., 2011. Drilling constraints on lithospheric accretion and evolution at Atlantis Massif, Mid-Atlantic Ridge 30°N. *J. Geophys. Res.*, 116:B07103. doi:10.1029/2010JB007931

Blackman, D. K., Ildefonse, B., John, B. E., Ohara, Y., Miller, D. J., MacLeod, C. J., and the Expedition 304/305 Scientists, 2006. *Proc. IODP*, 304/305: Washington, DC (Integrated Ocean Drilling Program Management International, Inc.). doi:10.2204/iodp.proc.304305.2006

Blackman, D. K., Karner, G., and Searle, R. C., 2008. Three-dimensional structure of oceanic core complexes: Effects on gravity signature and ridge flank morphology, Mid-Atlantic Ridge 30°N. *Geochem. Geophys. Geosyst.*, 9:Q06007. doi:10.1029/2008GC001951

Blackman, D. K., Karson, J. A., Kelley, D. S., Cann, J. R., Früh-Green, G. L., Gee, J. S., Hurst, S., et al., 2002. Geology of the Atlantis Massif (Mid-Atlantic Ridge, 30°N): Implications for the evolution of an ultramafic oceanic core complex. *Mar. Geophys. Res.*, 23(5–6):443–469. doi:10.1023/B:MARI.0000018232.14085.75

Boschi, C., Früh-Green, G. L., Delacour, A., Karson, J. A., and Kelley, D. S., 2006. Mass transfer and fluid flow during detachment faulting and development of an oceanic core complex, Atlantis Massif (MAR 30°N). *Geochem. Geophys. Geosyst.*, 7(1):Q01004. doi:10.1029/2005GC001074

Canales, J. P., Tucholke, B. E., and Collins, J. A., 2004. Seismic reflection imaging of an oceanic detachment fault: Atlantis megamullion (Mid-Atlantic Ridge, 30°10' N). *Earth Planet. Sci. Lett.*, 222(2):543–560. doi:10.1016/j.epsl.2004.02.023

Canales, J. P., Tucholke, B. E., Xu, M., Collins, J. A., and Dubois, D. L., 2008. Seismic evidence for large-scale compositional heterogeneity of oceanic core complexes. *Geochem. Geophys. Geosyst.*, 9(8):Q08002. doi:10.1029/2008GC002009

Cann, J. R., Blackman, D. K., Smith, D. K., McAllister, E., Janssen, B., Mello, S., Avgerinos, E., Pascoe, A. R., and Escartin, J., 1997. Corrugated slip surfaces formed at ridge–transform intersections on the Mid-Atlantic Ridge. *Nature*, 385:329–332. doi:10.1038/385329a0

Collins, J. A., Blackman, D. K., Harris, A., and Carlson, R. L., 2009. Seismic and drilling constraints on velocity structure and reflectivity near IODP Hole U1309D on the central dome of Atlantis Massif, Mid-Atlantic Ridge 30°N. *Geochem. Geophys. Geosyst.*, 10(1):Q01010. doi:10.1029/2008GC002121

Expedition 340T Scientists, 2012. Atlantis Massif Oceanic Core Complex. Velocity, porosity, and impedance contrasts within the domal core of Atlantis Massif: Faults and hydration of lithosphere during core complex evolution. *IODP Prel. Rept,* 340T. doi:10.2204/iodp.pr.340T.2012

Grimes, C. B., John, B. E., Cheadle, M. J., and Wooden, J. L., 2008. Protracted construction of gabbroic crust at a slow spreading ridge: Constraints from $^{206}Pb/^{238}U$ zircon ages from Atlantis Massif and IODP Hole U1309D (30°N, MAR). *Geochem. Geophys. Geosyst.*, 9(8):Q08012. doi:10.1029/2008GC002063

Harding, A., Arnulf, A., and Expedition 340T Science Party, 2012. Crustal structure in the vicinity of Hole U1309D, Atlantis Massif [Paper presented at 2012 Fall Meeting AGU San Francisco, 3–7 December 2012]. Abstract OS11E-08.

Henig, A. S., Blackman, D. K., Harding, A. J., Canales, J- P., and Kent, G. M., 2012. Downward continued multi-channel seismic refraction analysis of Atlantis Massif oceanic core complex, 30°N Mid-Atlantic Ridge. *Geochem. Geophys. Geosyst.*, 13(5):Q0AG07. doi:10.1029/2012GC004059

Hirose, T., and Hayman, N. W., 2008. Structure, permeability, and strength of a fault zone in the footwall of an oceanic core complex, the Central Dome of the Atlantis Massif, Mid-Atlantic Ridge, 30°N. *J. Struct. Geol.*, 30(8):1060–1071. doi:10.1016/j.jsg.2008.04.009

Ildefonse, B., Blackman, D. K., John, B. E., Ohara, Y., Miller, D. J., MacLeod, C. J., and IODP Expeditions 304/305 Science Party, 2007. Oceanic core complexes and crustal accretion at slow-spreading ridges. *Geology*, 35:623–626.

Itturino, G. J., Ildefonse, B., and Boitnott, G., 2002. Velocity structure of the lower oceanic crust: Results from Hole 735B, Atlantis II Fracture Zone. *In* Natland, J. H., Dick, H. J. B., Miller, D. J., and Von Herzen, R. P., *Proc. ODP, Sci. Results*, 176: College Station, TX (Ocean Drilling Program), 1–71.

Karson, J. A., Früh-Green, G. L., Kelley, D. S., Williams, E. A., Yoerger, D. R., and Jakuba, M., 2006. Detachment shear zone of the Atlantis Massif core complex, Mid-Atlantic Ridge, 30°N. *Geochem. Geophys. Geosyst.*, 7(6):Q06016. doi:10.1029/2005GC001109

Masoomzadeh, H., Barton P. J., and Singh, S. C., 2010. Non-stretch moveout correction of long-offset multi-channel seismic data for subsalt imaging: Example from the North Atlantic. *Geophysics*, 75(4):R83–R91. doi:10.1190/1.3443579

McCaig, A. M., Delacour, A., Fallick, A. E., Castelain, T., and Früh-Green, G. L., 2010. Fluid circulation and isotopic alteration in and beneath oceanic detachment faults in the Central Atlantic: Implications for the geometry and evolution of high-temperature hydrothermal circulation cells at slow-spreading ridges. *In* Rona, P. A., Devey, C. W., Dyment, J., and Murton, B. J. (Eds.), *Diversity of Hydrothermal Systems on Slow Spreading Ocean Ridges*. AGU Geophys. Monogr. Ser., 188:207–239.

Michibayashi, K., Hariagane, Y., Escartin, J., Delius, H., Linek, M., Hirose, T., Nozaka, T., and Ohara, Y., 2008. Hydration due to high-T brittle failure within in situ oceanic crust, 30°N Mid-Atlantic Ridge. *Earth Planet. Sci. Lett.*, 275(3–4):348–354. doi:10.1016/j.epsl.2008.08.033

Morris, A., Gee, J. S., Pressling, N., John, B. E., MacLeod, C. J., Grimes, C. B., and Searle, R. C., 2009. Footwall rotation in an oceanic core complex quantified using reoriented Integrated Ocean Drilling Program core samples. *Earth Planet. Sci. Lett.*, 287(1–2):217–228. doi:10.1016/j.epsl.2009.08.007

Schroeder, T., and John, B. E., 2004. Strain localization on an oceanic detachment fault system, Atlantis Massif, 30°N, Mid-Atlantic Ridge. *Geochem. Geophys. Geosyst.*, 5(1):Q11007. doi:10.1029/2004GC000728

Singh, S. C., Collins, J. A., Canales, J. P., Tucholke, B. E., and Detrick, R. S., 2004. New insights into serpentinization at Atlantis Massif using wide-angle seismic method. *Eos Trans. AGU*, 85(47, Fall Meet. Suppl.):V23B-0628.

Authors

Donna Blackman, and **Alistair Harding**, Scripps Institution of Oceanography, University of California San Diego, 9500 Gilman Drive, La Jolla, CA 92093, U.S.A., e-mail: dblackman@ucsd.edu

Angela Slagle, and **Gilles Guerin**, Lamont Doherty Earth Observatory, Columbia University, 61 Route 9W, P.O. Box 1000, Palisades, NY 10964-8000, U.S.A.

Andrew McCaig, School of Earth and Environment, Maths/Earth and Environment Building, The University of Leeds, Leeds LS2 9JT, U.K.

First Results from HOTSPOT: The Snake River Plain Scientific Drilling Project, Idaho, U.S.A.

by John W. Shervais, Douglas R. Schmitt, Dennis Nielson, James P. Evans, Eric H. Christiansen, Lisa Morgan, W. C. Pat Shanks, Alexander A. Prokopenko, Thomas Lachmar, Lee M. Liberty, David D. Blackwell, Jonathan M. Glen, Duane Champion, Katherine E. Potter, and James A. Kessler

Abstract

HOTSPOT is an international collaborative effort to understand the volcanic history of the Snake River Plain (SRP). The SRP overlies a thermal anomaly, the Yellowstone-Snake River hotspot, that is thought to represent a deep-seated mantle plume under North America. The primary goal of this project is to document the volcanic and stratigraphic history of the SRP, which represents the surface expression of this hotspot, and to understand how it affected the evolution of continental crust and mantle. An additional goal is to evaluate the geothermal potential of southern Idaho.

Project HOTSPOT has completed three drill holes. (1) The Kimama site is located along the central volcanic axis of the SRP; our goal here was to sample a long-term record of basaltic volcanism in the wake of the SRP hotspot. (2) The Kimberly site is located near the margin of the plain; our goal here was to sample a record of high-temperature rhyolite volcanism associated with the underlying plume. This site was chosen to form a nominally continuous record of volcanism when paired with the Kimama site. (3) The Mountain Home site is located in the western plain; our goal here was to sample the Pliocene-Pleistocene transition in lake sediments at this site and to sample older basalts that underlie the sediments.

We report here on our initial results for each site, and on some of the geophysical logging studies carried out as part of this project.

Introduction

Mantle plumes are thought to play a crucial role in the Earth's thermal and tectonic evolution. They have long been implicated in the rifting and breakup of continents, and plume-derived melts play a significant role in the creation and modification of the continental crust and mantle lithosphere (DePaolo and Manga, 2003; DePaolo and Weis, 2007). Much of our understanding of mantle plumes comes from plume tracks in oceanic lithosphere, but oceanic lithosphere is recycled back into the mantle by subduction, and evidence for mantle plumes in the oceanic realm is destroyed. Thus, if we are to understand plume-related volcanism prior to 200 Ma, we must learn how plume-derived magmas inter-
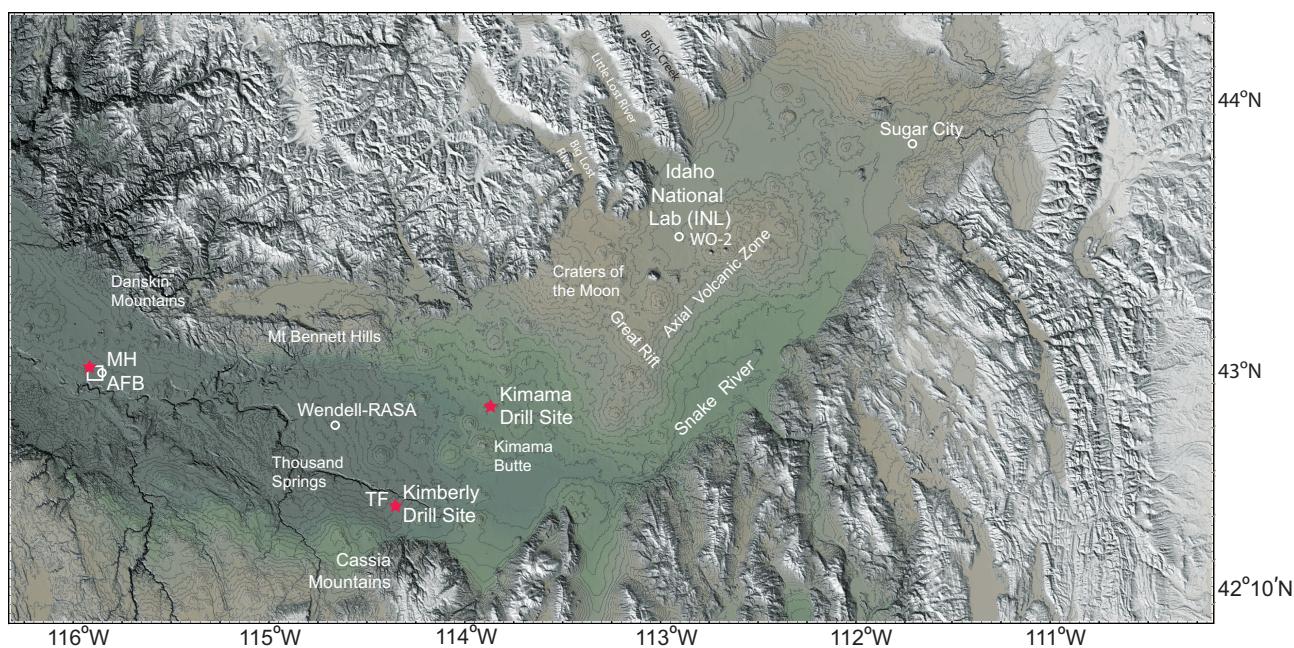

Figure 1. Shaded relief-topographic map of Snake River Plain derived from NASA 10-m DEM data and contoured at 30-m intervals. Red stars=new drill sites of this project; open circles=legacy drill sites discussed in text. TF=city of Twin Falls, MH AFB=Mountain Home Air Force Base.

act with continental lithosphere, and how this interaction affects the chemical and isotopic composition of lavas that erupt on the surface.

Hotspot volcanism in oceanic lithosphere has been the subject of studies by the International Continental Drilling Program (ICDP)—e.g., the Hawaii Drilling Project and the Reykjanes Drilling Project—and by the Integrated Ocean Drilling Program (IODP) and its predecessors (Neal et al., 1997; DePaolo et al., 2001; Elders et al., 2011). A variety of geochemical evidence from oceanic hotspots suggests that the source of volcanism involves mantle that is distinct from the shallowest upper mantle (DePaolo and Manga, 2003). Hotspot volcanism within continental lithosphere has not been studied in such detail, and it is undoubtedly more complex (Burov et al., 2007).

Project HOTSPOT is an effort by an international group of investigators to understand the long-term volcanic, tectonic, and thermal history of the Snake River volcanic province (Fig. 1) and its relationship to the Yellowstone hotspot, which sits above a sub-continental mantle plume (Shervais et al., 2006a). The SRP preserves a record of volcanic activity extending back to 16 Ma, and with basalts as recent as 200 ky in the western SRP graben, and as young as 2000 years at Craters of the Moon in the central SRP.

The central questions addressed by Project HOTSPOT are as follows: how do mantle hotspots interact with continental lithosphere, and how does this interaction affect the geochemical evolution of mantle-derived magmas and of the continental lithosphere?

Project HOTSPOT: The Snake River Volcanic Province

The Snake River volcanic province formed in response to movement of the continental lithosphere over the Yellowstone "mantle plume," which has thinned the lithosphere and fueled the intrusion of hot basaltic magma into the lower and middle crust, forming a sill complex up to 10 km thick. The onset of "hotspot"-related volcanism is generally marked by the eruption of large volumes of dry, high-temperature rhyolites as ignimbrites, lavas, and lava-like ignimbrites (Branney et al., 2008). The oldest rhyolites exposed (in western Idaho, eastern Oregon, and northern Nevada) are preceded by basalt; all of the younger rhyolites are overlain by up to a kilometer of "post-hotspot" basalts that erupted after the lithosphere moved to position southwest of the active plume source (Geist et al., 2002; Hughes et al., 2002; Shervais et al., 2005, 2006b).

Geologic mapping has documented widespread Quaternary volcanism throughout the central SRP (Shervais et al., 2005). Basaltic vents are dominant along the axial volcanic zone, forming a distinct topographic high that confines sediments and river drainages to topographic lows on
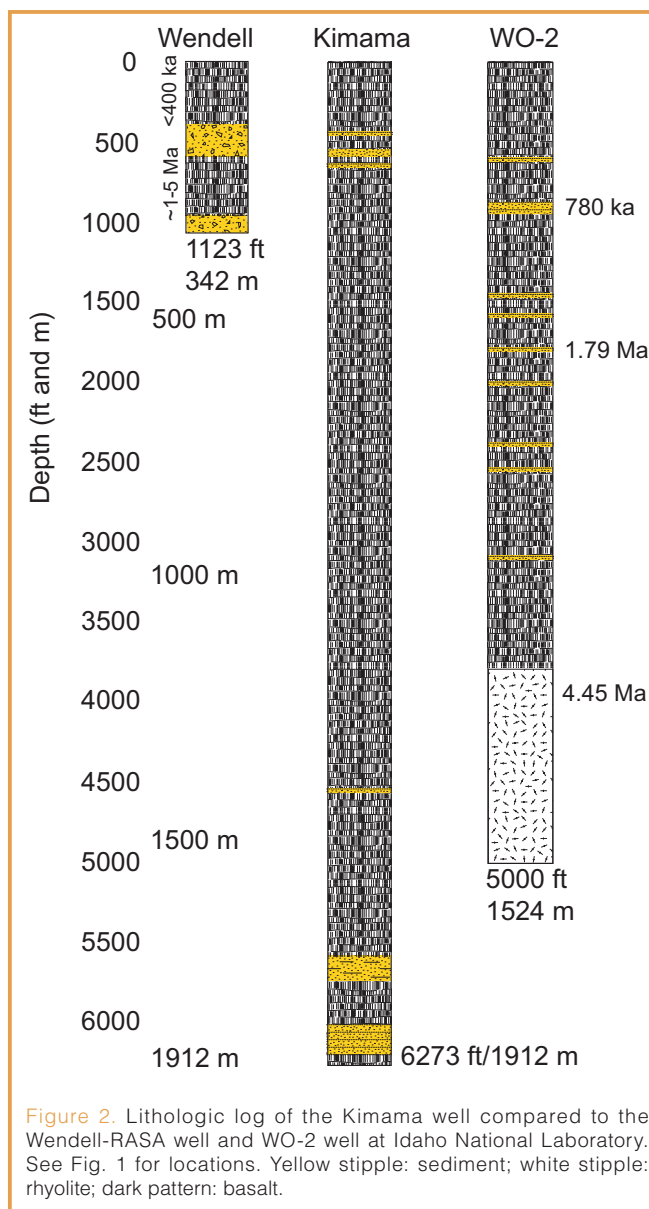
Figure 2. Lithologic log of the Kimama well compared to the Wendell-RASA well and WO-2 well at Idaho National Laboratory. See Fig. 1 for locations. Yellow stipple: sediment; white stipple: rhyolite; dark pattern: basalt.

the north and south (Fig. 1; Kauffman et al., 2005a, 2005b; Cooke et al., 2006a, 2006b; Matthews et al., 2006a, 2006b; Shervais et al., 2006c, 2006d). The basalt section thins northwest of Twin Falls, Idaho and becomes intercalated with fluvial and lacustrine sediments of the western SRP domain. For example, the Wendell-RASA well (342 m), which lies 40 km northwest of Twin Falls, has 122 m of Quaternary basalt (<400 ka) separated from older basalts (1.0–2.5 Ma) by 60 m of sediment; the older basalts are themselves underlain by more sediment (Whitehead and Lindholm, 1985).

Basalt flows also thin towards the margins of the plain, where they may sit directly on rhyolite or on sediment horizons that rest on rhyolite (Shervais et al., 2005). This is in contrast to the 1500-m-deep WO-2 Idaho well site of the Idaho National Lab (INL), which contains ~1200 m of basalt with minor intercalated sediments on top of 300 m of rhyolite, with no intervening sediments and no major sediment horizons within the basalt (Morgan, 1990; Hackett et al., 2002).

One of the primary goals of Project HOTSPOT was acquisition of continuous core in the central SRP that documents the long-term volcanic and sedimentary record of hotspot passage, from the early rhyolitic volcanism (which marks arrival of the plume over a given location) to the later, post-plume basaltic volcanism (Shervais et al., 2006a). This record will be combined with existing core to the west and east to produce a four-dimensional (space and time) synthesis of mantle plume-continental lithosphere interaction. It is this plume-continental lithosphere interaction that leads to the eruption of early A-type rhyolites, rather than basalt, as the dominant volcanic signature of the subcontinental plume, in contrast to oceanic plumes. Basalts post-date the rhyolites and form after the locus of rhyolite volcanism has shifted to the northwest in response to the southwestward movement of the North American plate (Smith and Braille, 1994).

Another primary goal was recovery of a similar long-term record in the western SRP, including lacustrine sediments thought to span the Pliocene-Pleistocene transition, and the onset of North American glaciation (Shervais et al., 2006a). This paleo-climate goal targeted the lacustrine sedimentary record of "Lake Idaho," a large long-lived lake that filled the western SRP graben during the Neogene.

In addition to these scientific goals, drilling was planned to validate new exploration techniques for geothermal resources and to document the existence of new geothermal resources in a setting that has no previous development of high-temperature geothermal prospects. Heat flow in shallow drill holes is high along the margins of the plain (80–100 mW m^{-2} s^{-1}) and low along the axis of the plain (20–30 mW m^{-2} s^{-1}). However, previous deep drillholes (>1 km) in the axial portion of the plain have high geothermal gradients similar to the margins of the plain below ~200–500 m depth (75–110 mW m^{-2} s^{-1}; Blackwell, 1989). This contrast between the shallow and deep parts of the axial portion of the plain is caused by the Snake River aquifer, a massive aquifer system that extends under the plain and emerges at Thousand Springs, Idaho.

An offset drilling strategy was employed, with our first hole drilled along the central volcanic axis (to capture the most complete record of basaltic volcanism), and our second
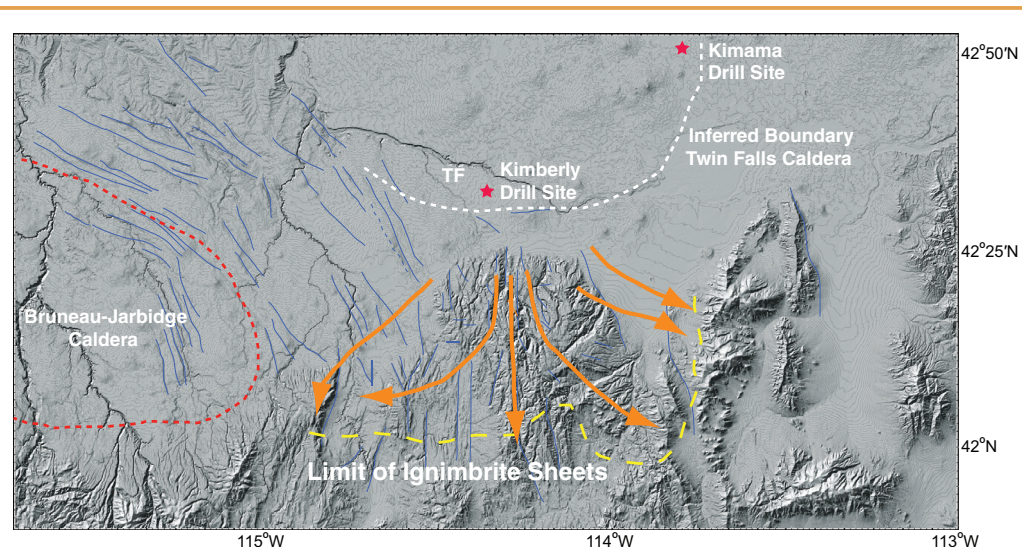

Figure 3. Shaded relief map of Twin Falls area, with 10-m contours calculated from NASA 10-m DEM data in GeoMapApp. Blue lines show mapped faults and lineaments mapped in 10-m data. Orange arrows show flow directions on ash flow tuff sheets in the Cassia Mountains, mapped by McCurry et al. (1996), with southern extent of sheets marked by long-dashed yellow line at the bottom. Bruneau-Jarbidge caldera marked by dashed red line. Southern margin of the Twin Falls caldera complex, inferred from regional Bouger gravity anomaly, shown with short-dashed white line. Drill sites marked with red stars; TF=city of Twin Falls.

hole drilled along the southern margin of the plain, where rhyolite is exposed beneath basalt in the Snake River Canyon (Fig. 1). This approach allowed us to drill almost 4 km of section at a significantly lower cost than a single continuous drill hole in the central SRP and to complete an additional 1.8 km drillhole in the western plain.

Preliminary Results

Drilling was completed between September 2010 and January 2012. In all, three deep holes were completed, collecting over 5.9 km of core for further study with better than 98% core recovery (Fig. 1). Geophysical studies carried out in conjunction with the drilling effort included (1) high-resolution gravity and magnetic surveys, (2) high-resolution shallow seismic surveys, and (3) borehole geophysical logs. The borehole data will be used to correlate the surface geophysical studies and extend the cored stratigraphy away from the drill sites.

Cores from all three sites were moved to the Core Laboratory of the Utah State University in Logan for processing, which includes high-resolution photographs, high-resolution image scans of whole round core sections, and detailed lithologic and structural logging. All data are entered into ICDP's Drilling Information System (DIS) database.

1. Kimama – Continuous Basalt Core from the Axial Volcanic Zone

The Kimama drill site was set up to acquire a continuous record of basaltic volcanism along the central volcanic axis and to test the extent of geothermal resources beneath the Snake River aquifer. Elevated groundwater temperatures

beneath the central volcanic axis (15°C–17°C) imply a significant flux of conductive heat flow from below (Potter et al., 2012).

Lindholm (1996) used potential field, resistivity, and well data to infer a basalt thickness of 1.2–1.4 km in the axial volcanic zone (Fig. 1). The topographic axial volcanic high is apparently mirrored by a keel of basalt that runs from the central plain to the eastern plain, and thins toward the margins and the ends. The hole was spudded into late Pleistocene basalts around 174 ky in age and was anticipated to encounter rhyolite between 1.2 km and 1.4 km depth. The plan was to continue drilling a few hundred meters into underlying rhyolite to allow correlation with the Kimberly drill site; however, the results of drilling forced changes to this plan.

Drilling at Kimama was completed between September 2010 and January 2011 with a final depth of 1912 m. An original target depth (TD) of ~1500 m for this site was based on an expected depth of ~1200 m to the basalt-rhyolite contact. However, no basalt-rhyolite contact was recovered, and budget constraints prevented further deepening of the hole. Borehole logging was carried out through the drillstring by a U.S. Geological Survey team (Twining and Barthomay, 2011). Cased (i.e., through drillstring) and open hole logging were carried out in the deepest parts of the Kimana hole. Open hole logging was carried out by the ICDP Operational Support Group in June–July 2011 in the upper sections.

The Kimama section consists almost entirely of basalt, with thin intercalations of loess-like sediment in the upper 200 m of the hole, and with somewhat thicker intercalated beds of fluvial gravels, sands, and silts in the lower 300 m (Fig. 2). Very thin silt intercalations are scattered throughout the intervening depths. Potter et al. (2011) have documented 557 basalt flow units in this section, based on natural gamma logs, neutron logs, and the recovered core, with a total thickness of 1803 m. Preliminary geochemical studies and paleomagnetic results suggest at least thirty flow groups representing distinct time periods, and magma batches are present, with the oldest lavas ~6 Ma in age (Bradshaw et al., 2012; Champion and Duncan, 2012; Potter et al., 2012).

The thickness of basalt plus intercalated sediment in the Kimama drillhole (1912 m) is almost 70% more than in the WO-2 drillhole at the Idaho National Laboratory, about 90 km to the northeast. It is also over five times greater than the section sampled by the Wendell-RASA drillhole (Fig. 2). This large thickness of basalt was completely unexpected, and its existence suggests the presence of a deep, possibly fault-controlled accommodation space.

The electrical resistivity (ER) maps are thought to define the depth to water-saturated basalt—generally interpreted to represent the base of the younger Quaternary basalts, excluding older Pliocene basalts which have limited porosity (Lindholm, 1996). Our data suggest that the ER measure-

ments most likely correspond to the base of the Snake River aquifer. Below the aquifer, basalt porosity is sealed by authigenic mineralization that restricts permeability (Morse and McCurry, 2002). Based on these ER maps, the depth to base of the aquifer at the Kimama site was estimated to be ~850 m. However, thermal gradient logs of the Kimama drillhole document a near-isothermal gradient from the top of the aquifer to ~980 m depth, which is now interpreted to reflect the true base of the aquifer (Nielson et al., 2012). This is almost twice the documented thickness of the Snake River aquifer in other locales.

Temperatures (15°C–17°C) within this thick aquifer are elevated relative to groundwater temperatures farther east and along the margins of the plain (~9°C). However, even this modest temperature increase must reflect a significant flux of heat from lower in the crust (Blackwell, 1989), which is consistent with the thermal gradient of ~75°C–80°C per
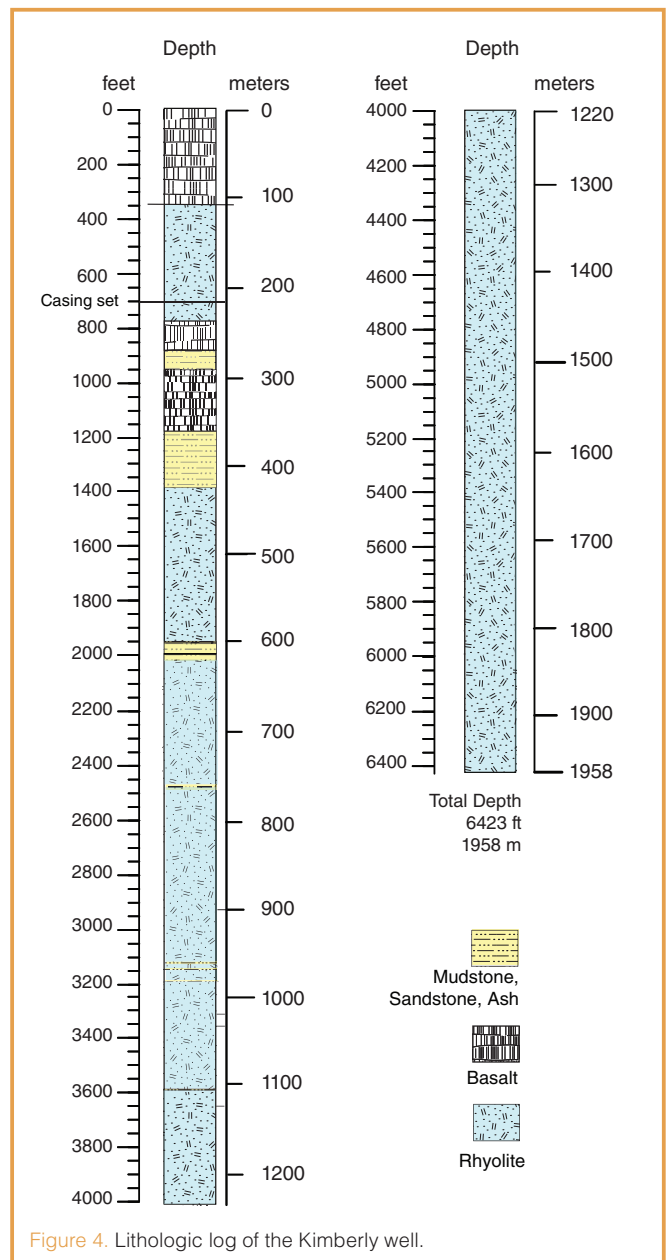

Figure 4. Lithologic log of the Kimberly well.

km below the aquifer, and a bottom hole temperature of ~98°C (Nielson et al., 2012).

2. Kimberly – The Basalt-Rhyolite Transition and Plume-Driven Rhyolite Volcanism

The primary goal of the Kimberly drillhole was to core the lower portion of the composite basalt-rhyolite section that characterizes the central and eastern SRP. A section exposed in the Snake River Canyon documents about 100 m of basalt overlying rhyolite 6.25 Ma old (Shervais et al., 2005). Regional Bouguer gravity anomalies and mapped flow directions in ignimbrites exposed south of Kimberly in the Cassia Mountains suggest that this site lies on the southern margin of the Twin Falls eruptive complex, an immense Yellowstone-scale rhyolite eruptive center inferred to underlie the central SRP north of Twin Falls (Fig. 3). The Kimberly site was selected to lie just outside the margin of this eruptive center, so that core would capture proximal rhyolite ash-flows.

An additional goal was to assess the geothermal potential of up-flow zones along a buried caldera margin. The Kimberly drill site lies south of the Snake River, where groundwater flow is dominated by water that originates in the Cassia Mountains to the south and penetrates deeply into the crust where it is heated before upwelling in the Twin Falls low-temperature geothermal district (Street and DeTar, 1987; Lewis and Young, 1989; Baker and Castelin, 1990). Geothermal wells in the Twin Falls Groundwater Management Area range in temperature from around 30°C to 72°C.

Kimberly drilling was completed between January 2011 and June 2011; it reached a total depth of 1958 m (uppermost 214 m not cored; similar section exposed in the nearby Snake River Canyon). This deep hole is dominated by massive rhyolite lava and welded ashflow tuffs, with basalt/sediment intercalations at 241 m to 424 m depth, and thin altered ash interbeds around 610 m depth (Fig. 4). The lower 900 m (from 1050 m to 1958 m) has no apparent flow contacts and may represent a single, thick welded ashflow tuff. There is no indication of granophyric textures that would suggest an intrusive origin, even in the deepest recovered core.

Temperature measurements, made while drilling with the Drilling, Observation and Sampling of the Earths Continental Crust (DOSECC) core barrel temperature tool, and wireline temperature logging document a cool water aquifer in the upper 400 m of the Kimberly drillhole, underlain by an immense, 55°C–60°C water aquifer extending from 400 m to TD at 1958 m (Nielson et al., 2012).

3. Mountain Home – Basalts and Lacustrine Sediments of the Western SRP

Basaltic volcanism in the western SRP occurred early in the history of the hotspot and continued throughout the Neogene, with basalts as young as 200 ky that erupted across a wide area (Shervais et al., 2005). A major goal of our project in the western plain was to capture a record of the older basalts and the lacustrine sediments which overlie them (Lewis and Stone, 1988). Sampling of the Neogene lacustrine deposits will test hypotheses for changes in moisture transport to inland North America from the Pacific initiation of Northern Hemisphere glaciation, and examine the response of the Great Basin hydrological system to the Pliocene climatic optimum. The lacustrine record will also allow us to infer the chronology of biotic recovery in the post-eruption intervals following some of the largest explosive volcanic eruptions
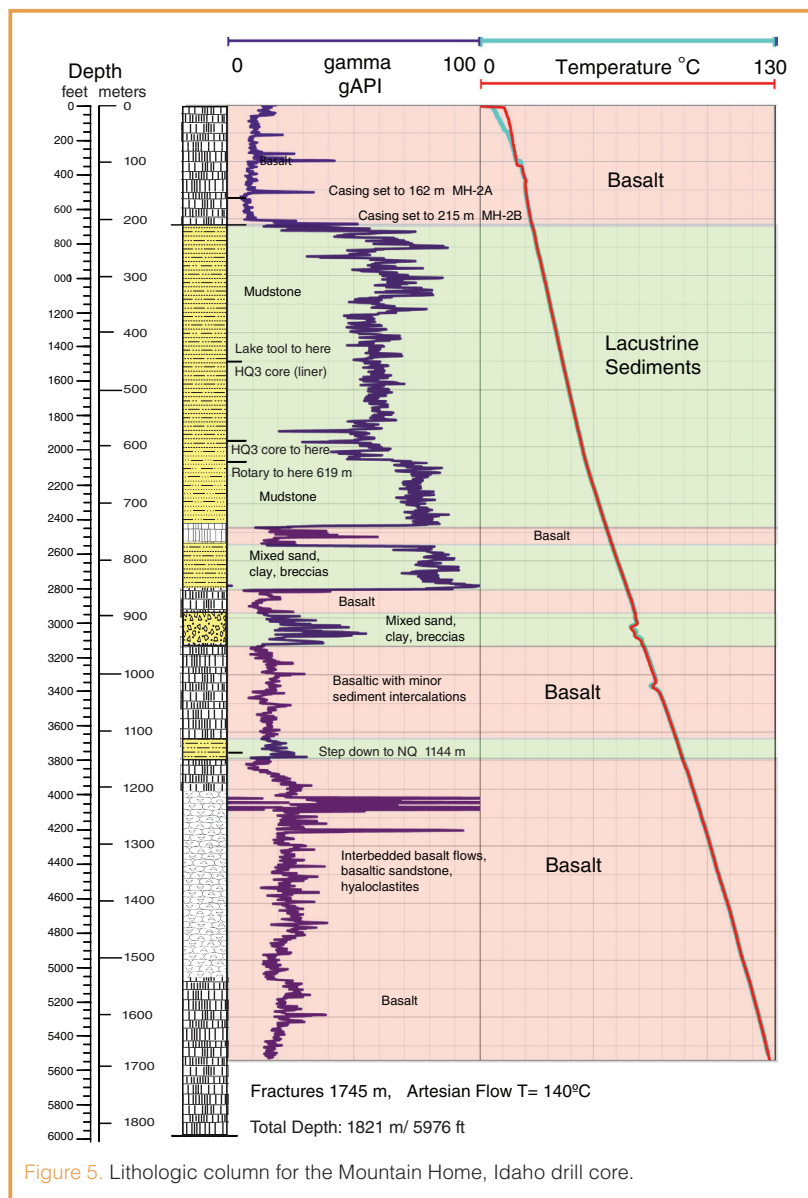

Figure 5. Lithologic column for the Mountain Home, Idaho drill core.

known. Finally, this core will allow us to resolve late Neogene records of biotic and landscape evolution in response to tectonic and magmatic processes related to SRP-Yellowstone hotspot evolution, and to develop a reference section for regional biostratigraphy.

Drilling operations at Mountain Home were completed between July 2011 and January 2012. A first hole was abandoned at 599 m depth because of drilling problems, but a second hole offset 7 m from the first hole successfully reached a final depth of 1821 m. Borehole logging was first carried out in January 2012 to a depth of 1690 m, prior to final deepening of the hole. Temperature and natural gamma-ray logs were recorded within the drillstring; open hole logging was restricted to the lower 1200 m of the drillhole because sediments in the upper part of the hole were too unstable to remove the casing before the plug-and-abandon process. A second logging campaign in November 2012 attempt-

Figure 6. Comparison of geophysical and core scan logs through a massive basalt flow, 1362–1378 m in the Kimama 1B borehole. The logs shown are the observed natural gamma radioactivity (in counts per second, CPS), the returning scattered neutron response (in reversed counts per second), the lateral electrical resistivity log (linear scale in Ω–m), and the Spontaneous Potential (SP) log (in reversed mV). The borehole televiewer (BHTV) amplitudes are normalized, and black indicates lost signal; the BHTV log has been rotated to align with geographic north. The unwrapped core scans are from RGB images; these have not been oriented. In the sonic log display the arrivals of the P- and S-waves are highlighted by right and left pointing arrows, respectively.

ed additional logging to the final TD of 1821 m, but temperatures in the lower 200 m exceeded the stability limits on the tools. However, open hole logging with a high-T borehole televiewer was successful between 1200 m and 1600 m.

The Mountain Home drill section consists of an upper basalt unit with minor interbedded sediments at 0–215 m, overlying interbedded sands and clays, with minor gravels and thin basalt layers at 215–850 m. From 850 m to 1250 m, basalt horizons alternate with sandstone, gravels, and volcanic ash. Below 1250 m the section consists of basalt flows, basalt hyaloclastites, and basaltic sands that are compact and well-indurated but less dense than massive basalt (Fig. 5).

A fracture system was encountered at 1745 m with artesian flow of geothermal fluids (Nielson et al., 2012). Temperature readings with the bottom hole temperature

(BHT) tool indicated temperatures ~150°C when the geothermal zone was encountered; later temperature logging indicates temperatures of ~135°–140°C, possibly as the result of downward flow of cold water (Nielson et al., 2012). Chemical analysis of the geothermal waters shows that they are sulfate-rich, indicative of steam-heated volcanic waters, and have a high pH (9.6), consistent with interaction with altered basalt (Lachmar et al., 2012). Calculated equilibrium temperatures are 140°–150°C (Giggenbach, 1988, 1997), consistent with measured temperatures in the geothermal zone.

Geophysical Logging

An ambitious borehole geophysics program was implemented to support the geological interpretations and to provide additional information on modern-day tectonic regimes in the SRP. The logs obtained include total natural

γ–radiation (including some spectral γ logging for U, Th, and K contents), neutron hydrogen index, γ–γ density, resistivity, magnetic susceptibility and full vector magnetic field, 4-arm caliper (i.e., dipmeter), full waveform sonic, and ultrasonic borehole televiewer imaging (Schmitt et al., 2012).

The neutron and γ–γ density logs employ radioactive sources. As such, and in the interest of minimizing any risk they would be lost in the open hole, both of these were run in the drillstring. While this precludes accurate quantitative assessment of density or hydrogen index, it does provide useful semi-quantitative comparisons for purposes of mapping the lithology. Figure 6 compares a variety of different logs through a massive basalt flow between 1362 m and 1378 m in the Kimama 1B borehole. Through this zone, the lithologies are simplified into three categories of sediment interbeds, seen as the reddish tinged layer between 1374.5 m and 1376.5 m, the low porosity massive basalt above 1374.5 m to 1364 m, and a more porous basalt with precipitate-filled vesicles (above 1364 m and also below 1376.5 m). The latter lithology is related to the top of the flows where porosity can exist from both rubble and vesiculation. The interbedded sediment consists of mostly loess deposits laid down in periods between subsequent flows.

The neutron response is primarily sensitive to the density of hydrogen nuclei in the surrounding fluids, clays, and hydrous alteration products. As such, and somewhat unexpectedly, the relative neutron log intensity could indicate individual basalt flows primarily because of porosity and clay content differences between the dense massive basalt and the rubbly and sediment-containing flow tops. This is apparent in the neutron log of Fig. 6, where high returning neutron fluxes (indicative of low H content) correlate well with the massive basalt, particularly above 1373 m. This signal decays towards the top of the flow where the higher porosity can contain more fluids and possibly hydrous minerals. The sediment layer, too, has higher porosity, and it contains clay minerals that produce a low neutron response.

Natural γ-ray radiation is produced by the decay of various isotopes of uranium, thorium, and potassium. The concentration of these elements is typically low in basalt except for horizons of "Craters of the Moon"-type evolved basalts with high K_2O (>1 wt%; Potter et al., 2011). Spectral γ-logging through the thick rhyolites at Kimberly, however, gave K_2O concentrations of 2.5–3.5 wt% that contributes to a relatively high total response often in excess of 200 API (American Petroleum

Institute) units. In the basalt sections, the natural γ-ray log was usually, but not always, a strong indicator of sediment intercalations. This is also seen in Fig. 6 where the natural radioactivity is low everywhere except for the sediment layer.

The electrical resistivity, measured by the lateral log (Fig. 6), is high in the massive basalts due to their low porosity and lack of conductive minerals. The lateral log resistivity mirrors the neutron responses to some degree. The sediments are much more conductive.

The borehole televiewer image quality also correlates well with the lithology. The signal is lost due to washing of the borehole during the coring operations through the softer sediments. Images through massive basalt and rhyolite are mostly featureless except for fractures that appear mostly to be filled by precipitates in the core (Fig. 7). Vesicles near the tops of the basalt flows are more apparent.

The full-waveform acoustic log also displays interesting correlations with the lithology through this section. In Fig. 6, the arrivals of the P- and S-waves are highlighted by the right and left pointing arrows, respectively. Traveltimes are short within massive basalt, indicative of a high sonic log velocity. Strong S-waves also appear throughout the massive basalt. A possible existence of split shear waves (e.g., the section between 1374 m and 1372 m) could indicate stress-induced seismic anisotropy around the borehole. Only the P-wave first arrival is seen within the sediment layer, and no clear S-wave can be unambiguously interpreted through the sediments.

Figure 7. Examples of BHTV and core images from the Kimama 2A corehole. Comparison of ultrasonic borehole televiewer images through naturally fractured rhyolite with the corresponding unwrapped core scans. The core scans have been oriented based on the televiewer images. Note that the core image mirrors that of the televiewer.

Figure 6 is just one example of the logging data obtained. The Kimberly logging campaign was the most extensive carried out and is a rare, if not unique, set of geophysical logs through a thick sequence of rhyolitic ignimbrites. The relative uniformity of the thick rhyolite sequence provided for a high quality borehole and consequently exceptional borehole televiewer images. Comparisons between the core and televiewer images allow the former to be oriented, greatly supporting stress and fracture related studies. In addition, numerous drilling-induced fractures indicating the horizontal principal stress directions were observed.

High-resolution surface and borehole seismic data were acquired in order to provide additional structural information in the immediate vicinity of each of the three boreholes. These typically included (when possible), 2-D seismic profiles
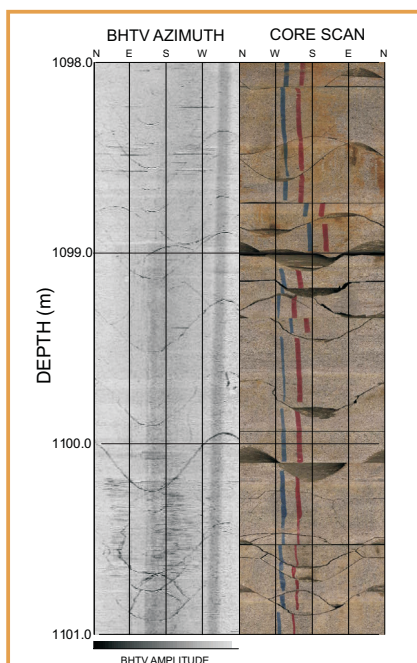
crossing near the borehole as well as closely spaced (2-m) zero-offset and walk-a-way vertical seismic profile (VSP) data.

The results of the processed VSP from Kimama (Fig. 8) display strong seismic reflectors associated with the sediment interbeds and prove that substantial seismic energy in fact does transmit through the basalts. Lack of proper seismic images within basalt flows is due to scattering effects in the near surface.

Summary and Conclusions

The Kimama and Kimberly core holes were selected to produce a composite section through volcanic crust in the central SRP that replicated a slice through time and the eruptive history of the plain in this location. We succeeded in this goal—basalts near the bottom of the Kimama core hole are ~6 Ma in age, while rhyolite lava overlain by basalt in the uppermost Kimberly core hole has been dated at 6.25 Ma (Shoshone Falls rhyolite; Bonnichsen et al., 2008). Basalts in the Kimama hole are at least 50% thicker than anticipated, and they preserve a remarkable record of essentially contin-uous mafic volcanism within the Axial Volcanic Zone. The occurrence of clastic fluvial sediments at ~1800 m depth in Kimama shows that during its earliest history, the Axial Volcanic Zone was not a topographic high but a basin with a through-going drainage system. The repeated occurrence of highly evolved "Craters of the Moon"-type lavas in the Kimama hole at three depth horizons in the well shows that these highly evolved flows form repeatedly during evolution of volcanic province, not just towards the end of volcanism.

The Kimberly core hole is notable because it documents the intercalation of basalt and rhyolite immediately after the initial phase of rhyolite volcanism, and because it reveals the occurrence of massive rhyolite ignimbrites that may be up to 900 m thick. The Mountain Home well confirms the occurrence of an older basaltic basement, which underlies Pliocene-Pleistocene paleo-lake sediments that are over 600 m thick. Comparison with dated sections exposed in outcrop suggests that the lower basalts are 6–8 Ma in age, while basalts that overlie the paleo-lake sediments are less than 2 Ma. Geochemical and paleomagnetic studies are just beginning on the Kimberly and Mountain Home core samples.

Drilling and geophysical surveys have been largely completed, and we are currently evaluating the results. The Kimama well, completed at 1912 m, samples an aquifer that is twice as deep as the next deepest part of the aquifer (960 m vs. 500 m at the INL site), suppressing the thermal gradient. Nonetheless, a temperature gradient of 80°C km^{-1} underlies the aquifer, reflecting a deep buried resource that
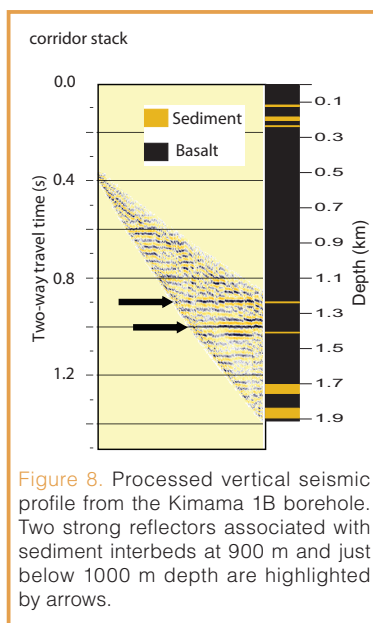
Figure 8. Processed vertical seismic profile from the Kimama 1B borehole. Two strong reflectors associated with sediment interbeds at 900 m and just below 1000 m depth are highlighted by arrows.

may be tapped where the aquifer is thinner. The Kimberly well (1958 m) taps a warm water aquifer at 55°C–60°C that is too cool for power generation but may represent an immense passive resource (Nielson et al., 2012). Finally, the Mountain Home well (1821 m) in-tersected a 135°C–140°C (or higher) geothermal resource with artesian flow to the surface. Combined with data from older explora-tion efforts, this docu-ments a significant electric-grade geother-mal resource that lies outside existing geo-thermal resource areas.

The central questions addressed by Project HOTSPOT—how mantle hotspots interact with continental lithosphere, and how this interaction affects the geochemical evolution of mantle-derived magmas and of the continental lithosphere—must await completion of the geochemical and isotopic studies before they can be answe-red. However, the excellent core recovery achieved (>98% of cored intervals) has provided the HOTSPOT Science Team with the material it needs to address this question, and the geophysical campaign places these results within the broader context of stratigraphic and tectonic evolution.

References

Baker, S. J., and Castelin, P. M., 1990. Geothermal resource analysis in Twin Falls County, Idaho, Part II. Idaho Dept. Water

Resources, Water Information Bulletin No. 30, Part 16, 36 pages.

Blackwell, D. D., 1989. Regional implications of heat flow of the Snake River Plain, northwestern United States. *Tectonophysics*, 164(2–4):323–343. doi:10.1016/0040-1951(89)90025-5

Bonnichsen, B., Leeman, W., Honjo, N., McIntosh, W., and Godchaux, M., 2008. Miocene silicic volcanism in southwestern Idaho: Geochronology, geochemistry, and evolution of the central Snake River Plain. *Bull. Volcanol.*, 70(3):315–342.

Bradshaw, R. W., Christiansen, E. H., Dorais, M. J., Shervais, J. W., and Potter, K. E., 2012. Source and crystallization characteristics of basalts in the Kimama core: Project Hotspot Snake River Scientific Drilling Project, Idaho. *Eos Trans. AGU*, V13B-2840.

Branney, M., Bonnichsen, B., Andrews, G., Ellis, B., Barry, T., and McCurry, M., 2008. 'Snake River (SR)-type' volcanism at the Yellowstone hotspot track: Distinctive products from unusual, high-temperature silicic super-eruptions. *Bull. Volcanol.*, 70(3):293–314. doi:10.1007/s00445-007-0140-7

Burov, E., Guillou-Frottier, L., d'Acremont, E., Le Pourhiet, L., and Cloetingh, S., 2007. Plume head–lithosphere interactions near intra-continental plate boundaries. *Tectonophysics*, 434(1–4):15–38. doi:10.1016/j.tecto.2007.01.002

Champion, D., and Duncan, R.A., 2012. Paleomagnetic and 40Ar/39Ar studies on tholeiite basalt samples from "HOTSPOT" core-hole taken at Kimama, Idaho, central Snake River Plain. *Eos Trans.AGU*, V13B-2842.

Cooke, M. F., Shervais, J. W., Kauffman, J. D., and Othberg, K. L., 2006a. Geologic map of the Dietrich Butte Quadrangle, Lincoln County, Idaho. 1:24,000. *Idaho Geological Survey*, Digital Web Map-63.

Cooke, M. F., Shervais, J. W., Kauffman, J. D., and Othberg, K. L., 2006b. Geologic map of the Dietrich Quadrangle, Lincoln County, Idaho. 1:24,000. *Idaho Geological Survey*, Digital Web Map-66.

DePaolo, D. J., and Manga, M., 2003. Deep origin of hotspots–The mantle plume model. *Science*, 300(5621):920–921. doi:10.1126/science.1083623

DePaolo, D. J., and Weis, D., 2007. Hotspot volcanoes and large igneous provinces. *In* Harms, U., Koeberl, C., and Zoback, M. D. (Eds.), *Continental Scientific Drilling: A Decade of Progress, and Challenges for the Future:* Berlin-Heidelberg (Springer-Verlag), 259–288.

DePaolo, D. J., Bryce, J. G., Dodson, A., Shuster, D. L., and Kennedy, B. Mack, 2001. Isotopic evolution of Mauna Loa and the chemical structure of the Hawaiian plume. *Geochem. Geophys. Geosyst.*, 2:1044. doi:10.1029/2000GC000139

Elders, W. A., Frithleifsson, G. O., Zierenberg, R. A., Pope, E. C., Mortensen, A., K., Guthmundsson, A., Lowenstern, J. B., et al., 2011. Origin of a rhyolite that intruded a geothermal well while drilling at the Krafla volcano, Iceland. *Geology*, 39(3):231–234. doi:10.1130/G31393.1

Geist, D., Sims, E., and Hughes, S., 2002. Open-system evolution of a single cycle of Snake River Plain magmatism. *GSA Special Paper*, 353:193–204.

Giggenbach, W. F., 1988. Geothermal solute equilibria. Derivation of Na-K-Mg-Ca geoindicators. *Geochem. Cosmochem. Acta*, 52(12):2749–2765. doi:10.1016/0016-7037(88)90143-3

Giggenbach, W. F., 1997. The origin and evolution of fluids in magmatic-hydrothermal systems, *In* Barnes, H. L. (Ed.), *Geochemistry of Hydrothermal Ore Deposits* (3rd ed.): New York (John Wiley and Sons), 737–796.

Hackett, W. R., Smith, R. P., and Khericha, S., 2002. Volcanic hazards of the Idaho National Engineering and Environmental Laboratory, southeast Idaho. *In* Bonnichsen, B., White, C. M., and McCurry, M. (Eds.), *Tectonic and Magmatic Evolution of the Snake River Plain Volcanic Province: Idaho,* Geol. Surv. Bull. 30:461–482.

Hughes, S. S., McCurry, M., and Geist, D. J., 2002. Geochemical correlations and implications for the magmatic evolution of basalt flow groups at the Idaho National Lab. *GSA Special Paper*, 353:151–173.

Kauffman, J. D., Othberg, K. L., Gillerman, V. S., and Garwood, D. L., 2005a. Geologic map of the Twin Falls 30×60 minute Quadrangle, Idaho. 1:100,000. *Idaho Geological Survey*, Digital Web Map-43.

Kauffman, J. D., Othberg, K. L., Shervais, J. W., and Cooke, M. F., 2005b. Geologic map of the Shoshone Quadrangle, Lincoln County, Idaho. 1:24000. *Idaho Geological Survey*, Digital Web Map-44.

Lachmar, T. L., Freeman, T., Shervais, J. W., and Nielson, D. E., 2012. Preliminary results: Chemistry and thermometry of geothermal water from MH-2B test well. *Geotherm. Resources Council Trans.*, 36:689–692.

Lewis, R. E., and Stone, M. A. J., 1988. Geohydrologic data from a 4,403-foot geothermal test hole, Mountain Home Air Force Base, Elmore County, Idaho. U.S. Geological Survey Open-File Report 88–166, 30 p.

Lewis, R. E., and Young, H. W., 1989. The hydrothermal system in central Twin Falls County, Idaho. USGS Water-Resources Investigations Report 88-4152, 44 p.

Lindholm, G. F., 1996. Summary of the Snake River regional aquifer-system analysis in Idaho and eastern Oregon. U.S. Geological Survey Professional Paper 1408-A, 59 p.

Matthews, S. H., Shervais, J. W., Kauffman, J. D., and Othberg, K. L., 2006a. Geologic map of the Shoshone SE Quadrangle, Jerome and Lincoln Counties, Idaho. 1:24,000. *Idaho Geological Survey*, Digital Web Map-62.

Matthews, S. H., Shervais, J. W., Kauffman, J. D., and Othberg, K. L., 2006b. Geologic map of the Star Lake Quadrangle, Jerome and Lincoln Counties, Idaho. 1:24,000. *Idaho Geological Survey*, Digital Web Map-67.

McCurry, M., Watkins, A. M., Parker, J. L., Wright, K., and Hughes, S. S., 1996. Preliminary volcanological constraints for sources of high-grade rheomorphic ignimbrites of the Cassia Mountains, Idaho: Implications for the evolution of the Twins Falls volcanic center. *Northwest Geology*, 26:81–91.

Morgan, L. A., 1990. Lithologic description of the "Site E Corehole" Idaho National Engineering Laboratory, Butte County, Idaho. USGS Open-File Report 90–487.

Morse, L.H., and McCurry, M., 2002. Genesis of alteration of Quaternary basalts within a portion of the eastern Snake River Plain Aquifer. *In* Link, P. K., and Mink, L. L. (Eds.), *Geology, Hydrogeology, and Environmental Remediation; Idaho National Engineering and Environmental Laboratory, Eastern Snake River Plain, Idaho*. GSA Special Paper, 353:213–224.

Neal, C. R., Mahoney, J. J., Kroenke, L. W., Duncan, R. A., and Patterson, M. G., 1997. The Ontong Java Plateau, *In*

Mahoney, J., and F. Coffin (Eds.), *Large Igneous Provinces: Continental, Oceanic, and Planetary Flood Volcanism*. Geophys. Monogr. Ser., 100:183–216.

Nielson, D. L., Delahunty, C., and Shervais, J. W., 2012. Geothermal systems in the Snake River Plain, Idaho, characterized by the Hotspot Project. *Geotherm. Resources Council Trans.*, 36:727–730.

Potter, K. E., Bradshaw, R., Sant, C. J., King, J., Shervais, J. W., and Christiansen, E. J., 2011. Project HOTSPOT: Insight into the subsurface stratigraphy and geothermal potential of the Snake River plain. *Geotherm. Resources Council Trans.*, 35:967–971.

Potter, K. E., Shervais, J. W., Champion, D., Duncan, R. A., and Christiansen, E. H., 2012. Project Hotspot: Temporal compositional variation in basalts of the Kimama Core and implications for magma source evolution, Snake River Scientific Drilling Project, Idaho. *Eos Trans. AGU*, V13B-2839.

Schmitt, D. R., Liberty, L. M., Kessler, J. E., Kück, J., Kofman, R., Bishop, R., Shervais, J. W., Evans, J. P., and Champion, D. E., 2012. The ICDP Snake River Geothermal Drilling Project: Preliminary overview of borehole geophysics. *Geotherm. Resources Council Trans.*, 36:1017–1022.

Shervais, J. W., Branney, M. J., Geist, D., Hanan, B. B., Hughes, S. S., Prokopenko, A. A., and Williams, D. F., 2006a. HOTSPOT: The Snake River Scientific Drilling Project–Tracking the Yellowstone hotspot through space and time. *Sci. Drill.*, 3:56–57. doi:10.2204/iodp.sd.3.14.2006

Shervais, J. W., Cooke, M. F., Kauffman, J. D., and Othberg, K. L., 2006c. Geologic map of the Owinza Butte Quadrangle, Jerome and Lincoln Counties, Idaho. 1:24,000. *Idaho Geological Survey*, Digital Web Map-65.

Shervais, J. W., Cooke, M. F., Kauffman, J. D., and Othberg, K. L., 2006d. Geologic map of the Owinza Quadrangle, Lincoln County, Idaho, Idaho Geological Survey, Moscow Idaho. 1:24,000. *Idaho Geological Survey*, Digital Web Map-64.

Shervais, J. W., Kauffman, J. D., Gillerman, V. S., Othberg, K. L., Vetter, S. K., Hobson, V. R., Zarnetske, M., Cooke, M. F., Matthews, S. H., and Hanan, B. B., 2005. Basaltic volcanism of the central and western Snake River plain: A guide to field relations between Twin Falls and Mountain Home, Idaho. *In* Pederson, J., and Dehler, C. M. (Eds.), *Guide to Field Trips in the Western United States, Field Guide* (vol. 6)*:* Boulder, Colorado (Geological Society of America), 26 p.

Shervais, J. W., Vetter, S. K., and Hanan, B. B., 2006b. Layered mafic sill complex beneath the eastern Snake River Plain: Evidence from cyclic geochemical variations in basalt. *Geology*, 34(5):365–368. doi:10.1130/G22226.1

Smith, R. B., and Braille, L. W., 1994. Yellowstone hotspot. *J. Volcanol. Geotherm. Res.*, 61:121–187.

Street, L. V., and DeTar, R. E., 1987. Geothermal resource analysis in Twin Falls County, Idaho. IDWR Water Information Bulletin 30, Part 15, 46 p.

Twining, B.V., and Bartholomay, R. C., 2011. Geophysical logs and water-quality data collected for boreholes Kimama-1A and -1B, and a Kimama water supply well near Kimama, southern Idaho. U.S. Geological Survey Data Series 622 (DOE/ID 22215), 18 p., plus appendix.

Whitehead, R. L., and Lindholm, G. F., 1985. Results of geohydrologic test drilling in the eastern Snake River Plain, Gooding County, Idaho. U.S. Geological Survey Water Resources Investigations Report 84–4294, 30 p., 1 plate.

Authors

John W. Shervais, **James P. Evans**, **Thomas Lachmar**, **Katherine E. Potter**, and **James A. Kessler**, Department of Geology, Utah State University, 4505 Old Main Hill, Logan, UT 84322-4505, U.S.A., e-mail: john.shervais@usu.edu.

Douglas R. Schmitt, Department of Physics, CCIS 3-091, University of Alberta, Edmonton, Alberta, T6G 2E1, Canada.

Dennis Nielson, DOSECC, Inc., 2075 Pioneer Road, Suite B, Salt Lake City, UT 84104-4231, U.S.A.

Eric H. Christiansen, Department of Geological Sciences, Brigham Young University, Provo, UT 84602, U.S.A.

Lisa Morgan, and **W. C. Pat Shanks**, U.S. Geological Survey, Central Mineral and Environmental Resources Science Center, Box 25046, MS-973, Denver Federal Center, Denver, CO 80225, U.S.A.

Lee M. Liberty, Center for Geophysical Investigation of the Shallow Subsurface, Boise State University, 1910 University Drive, Boise, ID 83725-1536, U.S.A.

David D. Blackwell, Huffington Department of Earth Sciences, Southern Methodist University, P.O. Box 750395, Dallas, TX 75275-0395, U.S.A.

Jonathan M. Glen, and **Duane Champion**, U.S. Geological Survey, 345 Middlefield Road, Menlo Park, CA 94025-3591, U.S.A.

Alexander A. Prokopenko, Department of Earth and Ocean Sciences, University of South Carolina, Columbia, South Carolina, 29208, U.S.A.

Performance of the Wireline Heave Compensation System Onboard D/V *JOIDES Resolution*

by Gerardo Iturrino, Tanzhuo Liu, David Goldberg, Louise Anderson, Helen Evans, Annick Fehr, Gilles Guerin, Jenny Inwood, Johanna Lofi, Alberto Malinverno, Sally Morgan, Stefan Mrozewski, Angela Slagle, and Trevor Williams

Introduction

During wireline logging operations, the up-and-down motion of the ship causes a similar motion (heave) of the downhole logging tools unless properly compensated. If the amplitude of this motion is large (greater than a few tens of centimeters), depth discrepancies can be introduced into the logging data (for example, in bed thicknesses, precise depths of lithological boundaries, and angles of dipping fractures). Also, large and irregular downhole tool motions increase the risk of damaging downhole instruments, particularly those with relatively fragile caliper arms. It is therefore critical to minimize downhole tool motion for high quality logging data acquisition.

Figure 1. Photographs showing [A] the Proteus™ compensator unit, [B] wireline winch, and [C] hydraulic power unit (HPU). These units are located on a starboard side platform above the rig floor onboard the *JOIDES Resolution*. The Proteus unit is a hydraulic ram-type compensator with a set of sheaves mounted in an overhead flying head that moves vertically in opposite direction to the ship's motion. The sheave assembly contains six active cable legs that reduce the compensator stroke-to-heave movement by 6:1. A high-performance Vickers/Eaton servo valve controls a pump supplying the hydraulic rams and operates on signals originating from the position control system. To control the servo valve, the AHC system uses ship motion information acquired by the motion reference unit (MRU) and its accelerometer package that is located in the ship's center of rotation.

During the Ocean Drilling Program (ODP) and the Integrated Ocean Drilling Program (IODP), Lamont-Doherty Earth Observatory (LDEO) of Columbia University designed and maintained wireline heave compensating systems that supported efficient and high-quality logging data acquisition (Goldberg, 1990; Guerin and Goldberg, 2002; Myers et al., 2001; Sarker et al., 2006). The U.S. Implementing Organization (USIO) decided to replace the previous active heave compensating systems during the 2006–2007 extensive conversion of the D/V *JOIDES Resolution* in order to reduce rig-up time, improve monitoring quality, and, if possible, improve compensation efficiency. An active heave compensation (AHC) system was developed as part of the drilling vessel conversion project. The goal for this new AHC system was to provide (1) a more efficient and reliable heave compensation system located closer to the rig floor, and (2) a robust quantitative methodology for routine assessment of the AHC, including the system's performance at variable water depth, sea state, cable length, logging speed, and direction.

In this report we present the compensation performance results from the new AHC system on the *JOIDES Resolution* during 2009–2012 IODP operations and compare the results to those obtained during ODP and early IODP operations. Assessments were based on stationary tests where uphole and downhole data were collected while the tool string was held at a predetermined depth, and during normal logging operations when the tool strings were raised or lowered at conventional logging speeds of a few hundreds of meters per hour. Based on these data, we find that the new AHC system reduces 65%–80% of downhole tool displacement under stationary conditions and 50%–60% during normal logging operations. These results indicate that the new system's compensation efficiency is as good as or better than that of previous systems, with additional advantages that include upgradable compensation control software and the capability for continued assessment under varying logging conditions.

Heave Compensation Systems and Performance

The original LDEO Wireline Heave Compensator (LWHC) was designed and installed on the *JOIDES Resolution* in 1986; it worked for almost twenty years. It was a horizontally oriented unit that used a hydraulic cylinder to
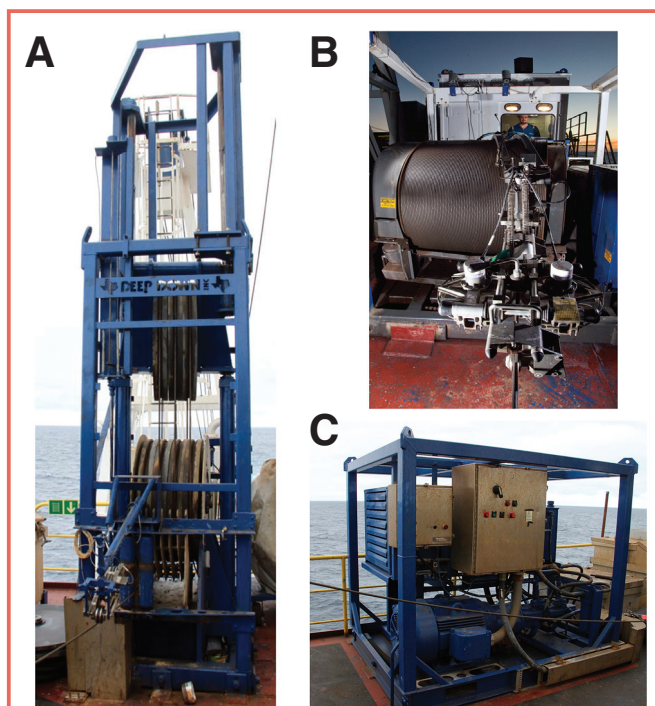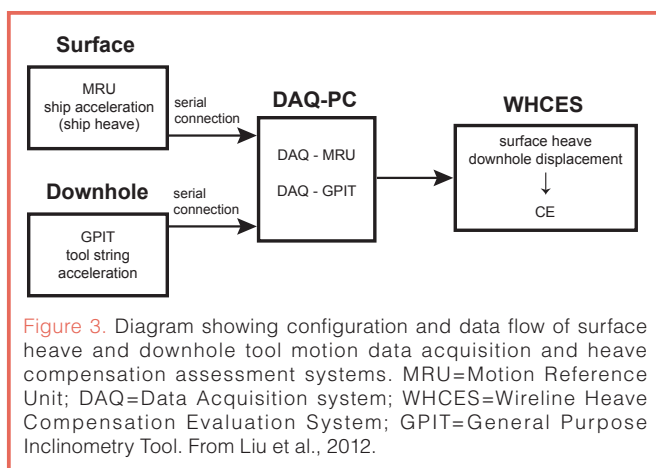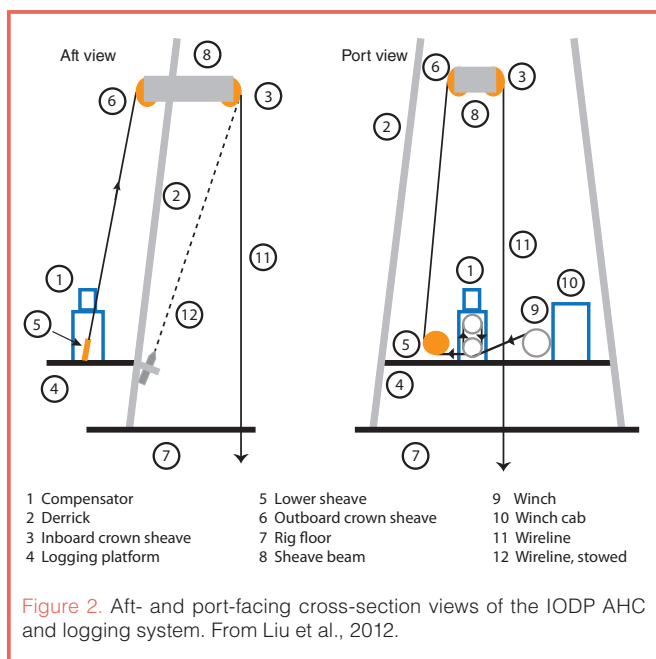
Figure 2. Aft- and port-facing cross-section views of the IODP AHC and logging system. From Liu et al., 2012.

1 Compensator	5 Lower sheave	9 Winch	
2 Derrick	6 Outboard crown sheave	10 Winch cab	
3 Inboard crown sheave	7 Rig floor	11 Wireline	
4 Logging platform	8 Sheave beam	12 Wireline, stowed	

Figure 3. Diagram showing configuration and data flow of surface heave and downhole tool motion data acquisition and heave compensation assessment systems. MRU=Motion Reference Unit; DAQ=Data Acquisition system; WHCES=Wireline Heave Compensation Evaluation System; GPIT=General Purpose Inclinometry Tool. From Liu et al., 2012.

move a piston and sheave that paid out or retrieved logging cable according to acceleration-derived heave. The piston's single sheave limited its stroke to 3 m and its ultimate heave compensation to ~6 m. In 2005, a replacement prototype was tested on the *JOIDES Resolution*—the rotary Smart Wireline Heave Compensator (SWHC). Previous assessments of wireline heave compensation systems compared the performance of the LWHC and SWHC (Sarker et al., 2006) and reported that the LWHC performed consistently at a high level with a variety of logging tool strings. Results indicated that the LWHC reduced downhole tool displacement by more than 50% of surface heave (Sarker et al., 2006). Initial results showed that the SWHC reduced downhole tool motion even further (Sarker et al., 2006). However, after analyzing additional data from IODP Phase I operations, it was determined that the SWHC was unable to compensate sufficiently to acquire high-resolution Formation MicroScanner (FMS) images (Liu et al., 2012). As a result, the LWHC was chosen as the main compensation system for the rest of the IODP Phase I operations ending in 2005, and efforts were directed to develop a new, third system. It should be noted, however, that during both prior LWHC and SWHC tests heave condi-

tions were within ±1.8–2.5 m and that analyses were performed using short time windows, potentially limiting how representative those tests were with respect to their respective routine performances.

The AHC active wireline heave compensation system uses two primary components, the Proteus™ compensator unit and a hydraulic power unit (HPU), operating in series with the Schlumberger winch (Fig. 1). Figures 2 and 3 show schematics of the complete wireline logging heave-compensating system setup and the data flow of the surface and downhole components, respectively.

Data Acquisition and Compensation Efficiency (CE) Evaluation

Measurements of downhole tool string displacement, uphole (surface) heave of the ship, and ideally a means for real-time comparison of motion dynamics are all required to properly assess the performance of the AHC. Downhole acceleration and borehole inclination data are typically acquired during logging using Schlumberger's General Purpose Inclinometry Tool (GPIT). Modifications to the Schlumberger acquisition software allow for real-time output of these data at a sampling rate of 15 Hz, which is suitable for heave compensation assessment. Surface (ship) acceleration and heave are measured by the Motion Reference Unit (MRU) and recorded using LabView utilities in the Downhole Measurements Laboratory (Fig. 3). Lastly, the USIO-LDEO developed the MATLAB-based Wireline Heave Compensation Evaluation System (WHCES), which assesses the performance of the AHC system in real time. Liu et al. (2012) described the capabilities of the WHCES synchronously accessing GPIT and MRU data at ~5-s intervals and computing the compensation efficiency of the AHC in real time.

For this study, the compensation efficiency (CE) is defined as

$$CE = [1 - std(d) / std(h)] \times 100,$$

where d is the downhole displacement of the tool string, h the uphole or surface heave of the vessel, and std is the standard deviation.

To test the reliability of the GPIT- and MRU-derived displacement measurements, the GPIT is lowered to the same level as the MRU (9.7 meters below rig floor, or mbrf) for 5–15 min prior to logging operations. Results typically show that surface heave computed from both acceleration measurements is similar in magnitude, phase, and within their 4% measurement uncertainties (Liu et al., 2012). Both measurements can therefore be used reliably for computation of real-time compensation efficiency. The CE can be computed in the time domain as the percent reduction in downhole displacement, or in the frequency domain as a reduction in

variance. Previous studies reported 50%–80% heave compensation in terms of variance reduction (Goldberg, 1990; Sarker et al., 2006), which is equivalent to a 30%–55% reduction in downhole tool displacement.

Results

The performance assessment of the AHC consisted of four types of tests.

- Static CE evaluation with the tool string in a stationary position at different depths in the drill pipe or in open hole. During such tests, the logging tool string is positioned at a pre-determined depth, and uphole and downhole acceleration data are collected with the AHC turned on and off.

- Dynamic CE evaluation in open hole when logging up or down with the AHC for the entire logging operation and continuously collecting both uphole and downhole acceleration data

- Evaluation of factors that may affect the CE performance while logging up or down at different speeds and using different tool strings

- Qualitative analysis of AHC performance by evaluation of field logging data

Overall, the performance evaluation was based on logging data obtained aboard the *JOIDES Resolution* during IODP Expeditions 320T through 340. Detailed assessments of the system's performance are given from Liu et al. (2012).

Assessment during Stationary Tests

Real-time CE evaluations using the WHCES were carried out during stationary tests under varying water depths and sea conditions. In shallow water (575 mbrf) and low peak-to-peak heave conditions (±0.2–0.4 m), the system was able to perform at CE = 68% (Fig. 4a), indicating that the compensated downhole displacement was less than ±0.1 m. In shallower water (300 mbrf) and moderate heave (±1.0–1.5 m), the system was able to perform at CE = 65%, with compensated downhole displacement of ±0.3–0.4 m (Fig. 4b). In this particular case, the downhole displacement increased to ±1.3 m without heave compensation (Liu et al., 2012). In deep water (4590 mbrf) and low heave conditions (±0.5–1.0 m), the system performed at CE = 75%, and the compensated downhole displacement was ±0.2–0.3 m (Fig. 4c). Overall, the highest compensation efficiency obtained by the AHC during the stationary tests was CE = 80%, with a maximum instantaneous CE of 86% (Liu et al., 2012). In depths of 775 mbrf and low heave of ±0.15 m, the compensator was able to reduce downhole tool motion to less than ±0.03 m (Liu et al., 2012), demonstrating its full capability and high CE potential. In summary, during stationary tests, the new AHC system performed in a CE range of 65%–80%.

Assessment during Dynamic Tests

Figure 5 shows a typical real-time CE evaluation and display by the WHCES during a triple combination tool string deployment during IODP Exp. 340, in Hole U1395B, at water depth of 1209 mbrf and heave of ±0.3–0.6 m. During the first downlog (elapsed time, ET = 1–10 min), the logging speed was 600 m hr^{-1} and the AHC best performed in a CE range of 30%–50%, with a mean of 40% (ET = 3–9 min). During the subsequent uplogs (ET = 10–27 min and ET = 32–55 min), the logging speed was 300 m hr^{-1}, and the AHC best performed in a CE range of 35%–50%, with a mean of 46% for log Pass 1 (ET = 12–26 min) and 42% for log Pass 2 (ET = 33–55 min). Two sharp drops in CE (below -60%) before and after log Pass 1 were caused by the temporary shutdown of the AHC. As a result, the downhole displacement of the tool string jumped from ±0.2 m to ±0.6 m, while ship heave remained the same (±0.3–0.5 m). At the end of logging operations (ET = 55–70 min) and when the AHC was turned off, the system was not compensating; thus, the software recorded higher downhole displacement than surface heave, resulting in the negative CE values (-20% to -40%).

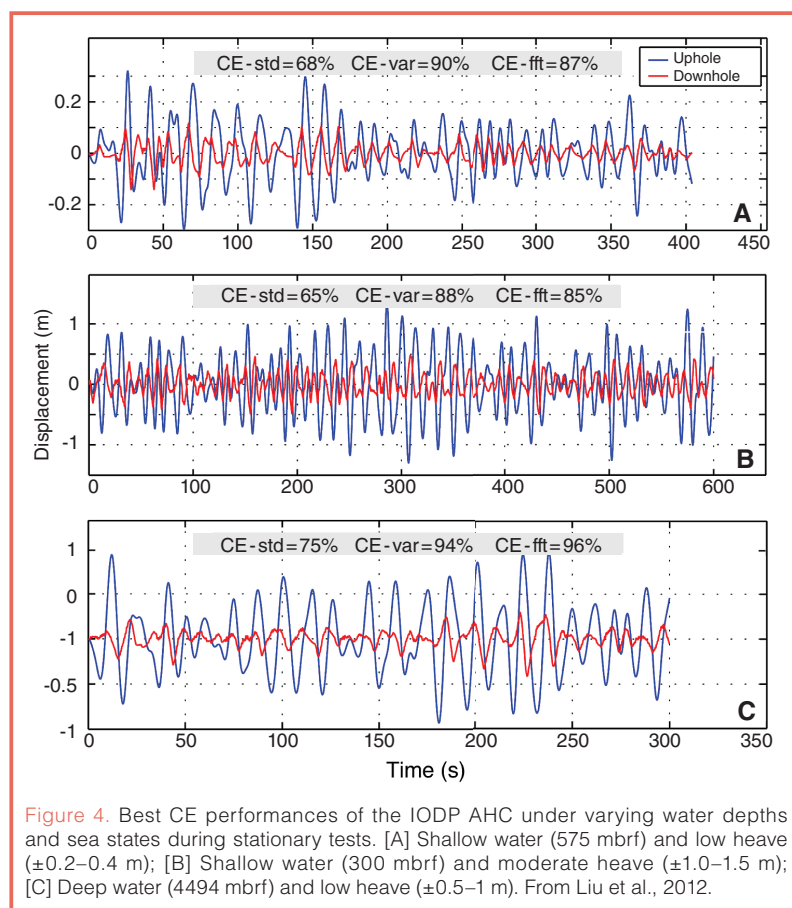Overall, dynamic test results indicate that, at normal logging speeds (300–600 m hr^{-1}), the

Figure 4. Best CE performances of the IODP AHC under varying water depths and sea states during stationary tests. [A] Shallow water (575 mbrf) and low heave (±0.2–0.4 m); [B] Shallow water (300 mbrf) and moderate heave (±1.0–1.5 m); [C] Deep water (4494 mbrf) and low heave (±0.5–1 m). From Liu et al., 2012.

new AHC system performed at a CE range of 50%–60% (Liu et al., 2012). A comparison between stationary tests and logging operations reveals a 15%–20% reduction in CE while logging, due to the upward or downward motion ("stick and slip") of the tool string, where factors such as friction or borehole rugosity likely contributed to such differences.

Factors Affecting the CE Performance

Many factors such as water depth, sea state, cable length, cable payload, logging direction, and speed can influence the CE. Therefore, routine assessments of the wireline heave compensator's effectiveness are essential. Based on results from this study, water depth does not appear to have a
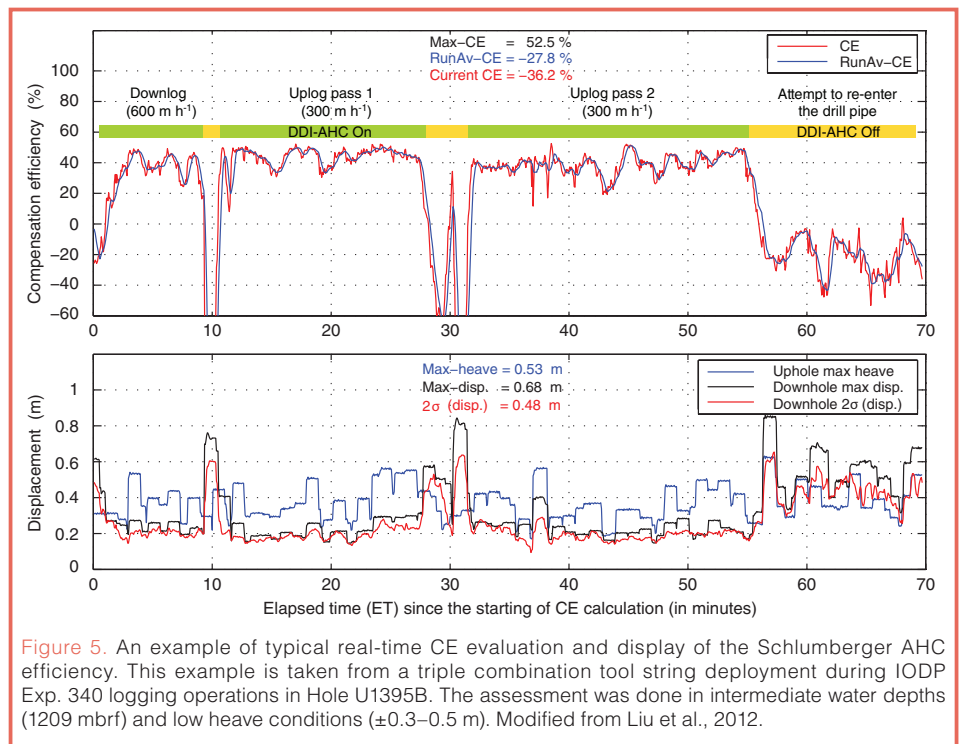

Figure 5. An example of typical real-time CE evaluation and display of the Schlumberger AHC efficiency. This example is taken from a triple combination tool string deployment during IODP Exp. 340 logging operations in Hole U1395B. The assessment was done in intermediate water depths (1209 mbrf) and low heave conditions (±0.3–0.5 m). Modified from Liu et al., 2012.

significant effect on the overall performance of the AHC (Liu et al., 2012). The system performed well (CE = 65%–80%) in both shallow and deep waters after optimization of the operating parameters. Furthermore, CE is generally independent of cable length and payload, including the weight of tool strings (Liu et al., 2012). The sea state and heave period also do not appear to affect the overall performance of the heave compensator when using the optimal operational parameters obtained from all the testing. This may be because the AHC receives its input driving function from surface heave conditions, and as a result, it effectively compensates heave-induced downhole tool motion.

Logging direction and speed can affect the compensator's performance, however. Based on these test results, logging

down at high speeds of 1000–1200 m hr^{-1} in open holes reduces CE values by about 55%–65%, whereas logging down or up at low speeds (300–600 m hr^{-1}) as well as logging up at high speed (~1600 m hr^{-1}) reduces CE values by only 15%–20%. Such large CE reductions during high-speed downlogging are likely due to cable slack and resonances. Other factors such as borehole shape, size, centralizers, and open caliper arms may also contribute to higher CE values when logging at faster speeds or under atypical conditions.

Qualitative Analysis Using Logging Data

Ultimately, heave compensation efficiency contributes to the quality of logging data recorded, and, therefore, log data quality can provide a qualitative measure of the AHC performance. Under given borehole conditions, the quality of FMS images, which are recorded at a 2.5-mm sampling interval, is largely controlled by variations in tool speed that must be corrected during post-logging processing. Such depth corrections are calculated using acceleration data provided by the GPIT and can also be used as a representative measure to evaluate the effectiveness of heave compensation during logging operations. FMS image data acquired while using the AHC (Fig. 6) show excellent resolution between successive passes in Hole U1330A. Distinct features over the lower
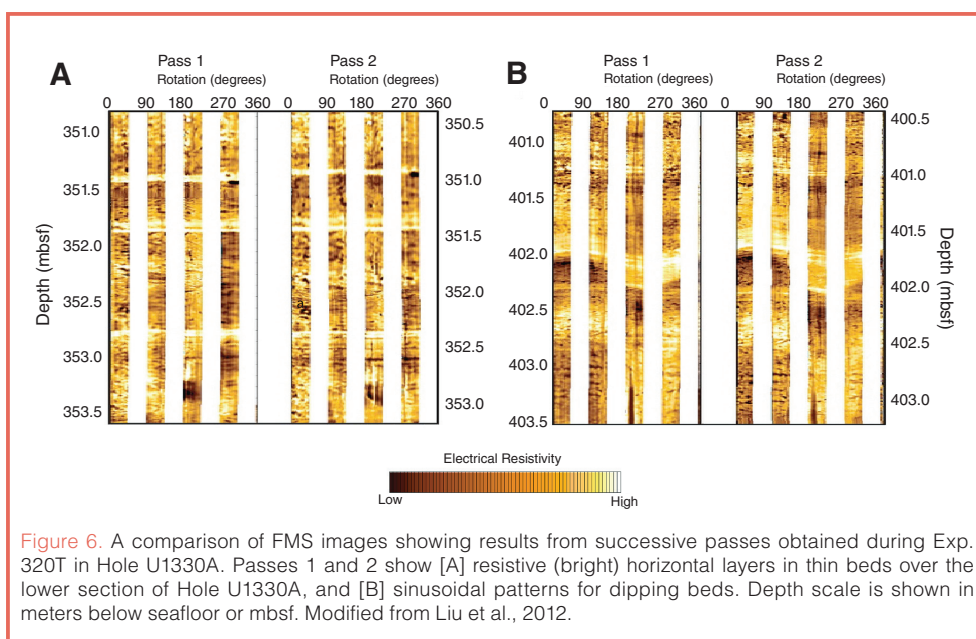

Figure 6. A comparison of FMS images showing results from successive passes obtained during Exp. 320T in Hole U1330A. Passes 1 and 2 show [A] resistive (bright) horizontal layers in thin beds over the lower section of Hole U1330A, and [B] sinusoidal patterns for dipping beds. Depth scale is shown in meters below seafloor or mbsf. Modified from Liu et al., 2012.

section of the hole (Passes 1 and 2) show resistive horizontal layers (bright) in thin beds (Fig. 6a) and sinusoidal patterns for dipping beds (Fig. 6b). Note that each distinctive pattern is reproduced with the same sharpness in each pass. This repeatability was not attainable with the SWHC, because the rotary system could not produce accurate cable speed measurements that are necessary for making the proper speed corrections in FMS image processing. These data suggest that the AHC produces proper depth controls that lead to successful heave-induced depth-shift corrections of FMS images (Liu et al., 2012).

Conclusion

Based on the test results obtained from this study, the new AHC system is capable of reducing 65%–80% of down-hole tool displacement under stationary conditions and 50%–60% during normal logging operations, a result that is better than that of previous wireline compensation systems used on board the *JOIDES Resolution*. The highest CE in downhole tool motion reduction achieved so far is 80%. The new AHC system is also more versatile and upgradable in design, and it facilitates real-time assessment of compensation efficiency. Optimal AHC performance reduces downhole tool motion to less than ±0.5 m, independent of water depth and sea state; this can be effectively corrected with post-logging data processing. The repeatability of high-resolution FMS images acquired during the tests attests to high quality log data acquisition. Overall, the new AHC system enables sound scientific interpretations of stratigraphy, structure, and petrophysical properties based on high quality marine geophysical downhole logging data obtained from a floating platform subjected to considerable vertical movements during operations.

Acknowledgments

References

Goldberg, D., 1990. Test performance of the Ocean Drilling Program wireline heave motion compensator. *Sci. Drill.*, 1:206–209.

Guerin, G., and Goldberg, D., 2002. Heave compensation and formation strength evaluation from downhole acceleration measurements while coring. *Geo-Mar. Lett.*, 22:133–141. doi:10.1007/s00367-002-0104-z

Liu, T., Iturrino, G., Goldberg, D., Meissner, E., Swain, K., Furman, C., Fitzgerald, P., et al., 2012. Performance evaluation of active wireline heave compensation systems in marine well logging environments. *Geo-Mar. Lett.*, 33(1):83–93. doi:10.1007/s00367-012-0309-8. http://www.springerlink.com/content/m2734t03081h3617/

Myers, G., Gaillot, P., and Goldberg, D., 2001. Ship heave effects on ODP drilling dynamics: Analysis of MWD data in the Nankai Trough. *Eos Trans. AGU*, 82(47, Fall Meet. Suppl.):T41A-0852.

Sarker, G., Myers, G., Williams, T., and Goldberg, D., 2006. Comparison of heave motion compensation systems on scientific ocean drilling ship and their effects on wireline logging data. *Proc. – 2006 Offshore Technol. Conf.*, abstract 17916.

Authors

Gerardo Iturrino, **Tanzhuo Liu**, **David Goldberg**, **Helen Evans**, **Gilles Guerin**, **Alberto Malinverno**, **Stefan Mrozewski**, **Angela Slagle**, and **Trevor Williams**, Lamont-Doherty Earth Observatory of Columbia University, Borehole Research Group, Palisades, NY 10964, U.S.A., e-mail: iturrino@ldeo.columbia.edu

Louise Anderson, **Jenny Inwood**, and **Sally Morgan**, Borehole Research Group, Department of Geology, University of Leicester, Leicester LE1 7RH, U.K.

Annick Fehr, Institute for Applied Geophysics and Geothermal Energy, E.ON Energy Research Center, RWTH Aachen University, D-52074 Aachen, Germany

Johanna Lofi, Géosciences Montpellier, UMR5243, Bât. 22, Université de Montpellier II, Place Eugene Bataillon, 34095 Montpellier Cedex 5, France

Photo Credits

Fig. 1b: William Crawford, IODP-TAMU

The Motion Decoupled Delivery System: A New Deployment System for Downhole Tools is Tested at the New Jersey Margin

by Peter B. Flemings, Peter J. Polito, Thomas L. Pettigrew, Gerardo J. Iturrino, Eric Meissner, Robert Aduddell, Donald L. Brooks, Chris Hetmaniak, David Huey, John T. Germaine, and the IODP Expedition 342 Scientists

Overview

The Motion Decoupled Hydraulic Delivery System (MDHDS) is a new downhole tool delivery system that is deployed by wireline and uses drillstring pressure to advance a penetrometer (or other downhole tool) into the formation at the bottom of offshore boreholes. After hydraulic deployment of the penetrometer, it is completely decoupled from the BHA; this eliminates the adverse effects of ship heave. We tested the MDHDS at Site U1402 (the location of Site 1073, ODP Leg 174A), offshore New Jersey, during two days of ship time during Integrated Ocean Drilling Program (IODP) Expedition 342. In one deployment we emplaced a penetrometer successfully and documented that it was decoupled from drillstring movement. Based on this successful field test, the MDHDS has been certified by the U.S. Implementing Organization (USIO) for shipboard use. The MDHDS will replace the previous deployment system, the Colletted Delivery System. The MDHDS is an IODP-funded engineering development led by The University of Texas at Austin, in conjunction with the USIO and Stress Engineering Services. This sea trial was the culmination of a seven-year development effort that included extensive engineering design and fabrication.

Introduction

We make downhole measurements in the IODP with 1) wireline logging or logging-while-drilling (LWD) tools that profile the borehole, 2) permanent observatories at the seafloor, and 3) downhole tools that interact with the formation at specific depths. Wireline logging or LWD is used throughout the drilling program to measure physical properties and for interpreting everything from formation pressure (Moore et al., 1995) to sedimentology and climate change (Hesselbo, 1996). We generally rely on oil field service company products for logging. However, tools also have been developed specifically for deployment within the IODP (Goldberg et al., 2004). Over the last two decades, we have made extraordinary investments in borehole observatories to measure geochemical and hydrological properties (Becker and Davis, 2005). Finally, we have a limited number of downhole tools that make measurements at specific depths when a borehole is drilled. The Advanced Piston Corer Temperature tool (APCT) and the Sediment Temperature tool (SET), previously known as the Davis-Villinger Temperature Probe (DVTP), are used to take temperature measurements. The Sediment Temperature Pressure tool (SET-P), previously known as the Davis-Villinger Temperature Pressure Probe (DVTP-P), the Temperature Two Pressure probe (T2P), and the Piezoprobe are used to take pressure measurements in semi-consolidated rocks. More recently, with the use of wide diameter drillpipe or riser drilling system, we have also begun to make direct pressure and stress measurements with the Modular Formation Dynamics Tester (MDT) of Schlumberger (Boutt et al., 2012; Lin et al., 2010).

The SET, SET-P, Piezoprobe, and T2P are borehole penetrometers. They are lowered down the borehole inside the drill pipe to the bottom of the borehole and driven vertically downwards by the weight of the drillstring into the formation. The SET records the frictional heating that results when the tool is driven in and the subsequent temperature dissipation; *in situ* temperature and the thermal diffusivity can be derived from these data. The SET-P, Piezoprobe, and T2P record pore pressure during insertion and during subsequent dissipation from which the *in situ* pressure and the coefficient of consolidation can be derived. The SET-P and T2P also record temperature. The SET-P was deployed during ODP Legs 190, 201, and 204 (D'Hondt et al., 2003; Moore et al., 2001;
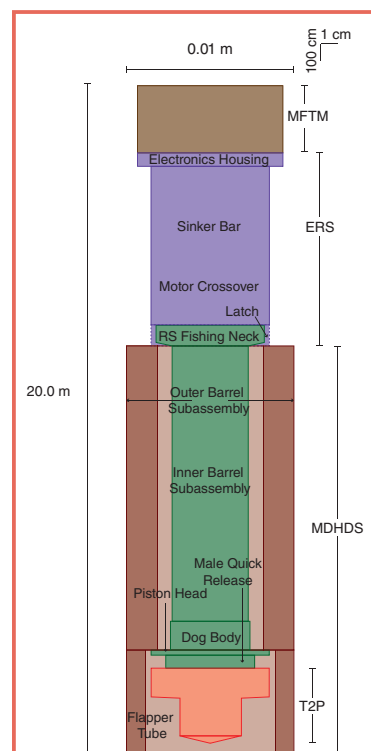
Figure 1. The deployment system has three components—the Multi-Function Telemetry Module (MFTM), the Electronic RS (ERS), and the Motion Decoupled Hydraulic Delivery System (MDHDS)—and the attached tool (in this case the T2P penetrometer). The MFTM is attached directly to the electric wireline and is in turn attached to the ERS. The MDHDS is composed of an Outer Barrel (Brown) and an Inner Barrel (green). The top of the Inner Barrel is capped by the RS Fishing Neck. The pore pressure penetrometer (red) is shown in this example as the T2P, but the SET-P or SET can also be used.

Tréhu et al., 2003). The Piezoprobe was deployed during ODP Leg 204 (Long et al., 2007), whereas the DVTP-P and T2P were deployed during IODP Expedition 308 (Flemings et al., 2005, 2008; Long et al., 2008).

The ability to measure *in situ* pressure and temperature rapidly and at multiple depths during an expedition provides an important capability to address problems described in the new IODP Science Plan. These measurements allow us to map heat and fluid flow, provide valuable constraints for analyzing climate change, and help in our understanding of the Earth's dynamic systems, which are themes within the 2013–2023 IODP Science Plan. For example, we can determine slope stability (when and how submarine landslides form), interpret whether recent warming has occurred from the temperature profile, and illuminate how pore pressure impacts deformation in convergent margins.

Although penetrometer deployments in the IODP have yielded exciting results, they have also been challenging because the penetrometer is often dislodged from the formation. During IODP Exp. 308, in more than half of all deployments—and in all deployments at less than 100 mbsf—the penetrometer was dislodged (Flemings et al., 2008). Uncoupling is recorded by a rapid drop in the measured pressure and by tool movement (recorded by the accelerometer) when the BHA is raised after the penetrometer is inserted. This compromises the measurement of *in situ* pressure. The DVTP-P pressure records from Legs 201 and 204 also show that tool dislodgement has been a persistent problem (D'Hondt et al., 2003; Tréhu et al., 2003). In addition, when a narrow diameter penetrometer such as the T2P is used, the tip is often bent or destroyed, either because the tool is poorly aligned when it is pushed into the formation or because it is bent when it passes through the flapper valve at the drill bit (Flemings et al., 2006).

The T2P and SET-P penetrometers have been deployed by wireline on the Colleted Delivery System (CDS). The CDS is analogous to an old-style pointer, in which a series of cylinders slide past each other to increase or decrease the system's length. In this configuration, the penetrometer is pushed into the formation by the drillstring, and then the drillstring is raised several meters. Decoupling of the drillstring from the penetrometer is achieved by the expansion and contraction of the CDS. We attribute the dislodgement of the penetrometer to be due to friction within the CDS that pulls the penetrometer out when the drillstring is raised, or to "swabbing" (the suction induced by raising the drillstring).

In 2005 we began a seven-year project to design, build, and test a new deployment system called the Motion

Figure 2. [A] The Inner Barrel Subassembly (IBS) and the Outer Barrel Subassembly (OBS). [B] Left: the IBS lies inside the OBS. The fishing neck of the IBS is shown on the lower left. Right: the ERS is connected to the MFTM, which is connected to the logging line. The ERS Latch is at the bottom of the ERS assembly. [C] The MDHDS Latch and latching tool. The latch is set on the rig floor, and this fixes the IBS to the OBS. When the drillstring is pressurized, this latch is released, and the IBS slides freely from the OBS. [D] The SET-P and the T2P are two pore pressure penetrometers available for use in the drilling program.

Decoupled Hydraulic Delivery System (MDHDS). This wireline-deployed system uses drillstring pressure to advance a penetrometer into the formation. After hydraulic deployment of the penetrometer, it is completely decoupled from the BHA to eliminate the adverse effects of ship heave. We completed three separate land tests at Schlumberger's Sugarland Test Facility and numerous other bench-top tests at Stress Engineering Services, LDEO, and The University of Texas at Austin. In June 2012, we held a final field test on the *JOIDES Resolution* during IODP Expedition 342. A full description of this engineering development is available (Shipboard Scientific Party, 2013). We summarize the MDHDS development and the final field test at Site U1302 below.

The New Deployment System

The MDHDS is part of a three-component system (Fig. 1). The Multi-Function Telemetry Module (MFTM) allows real-time communication with the ERS and other tools. The Electronic "RS" (the ERS; "RS" is an oil field designation for a particular geometry of fishing tool) delivers and retrieves the MDHDS and the attached downhole tool to the Bottom Hole Assembly (BHA). The MDHDS, once seated in the BHA, is the platform from which the penetrometer (or some tool to be designed in the future) is deployed.

Multi-Function Telemetry Module (MFTM)

The MFTM (Fig. 1) is a downhole sonde that allows real-time communication with downhole tools through the Schlumberger armored 7-conductor cable. The MFTM was developed by the Lamont-Doherty Earth Observatory (LDEO) Borehole Research Group, and it is used to activate the latching of the ERS and to capture data streams from probes attached to the inner core barrel of the MDHDS assembly.

Electronic RS (ERS) System

The ERS tool (Figs. 1, 2) was developed for use with the Simple Cabled Instrument for Measuring Parameter In-situ (SCIMPI) system, and the MDHDS. The ERS deploys and retrieves the MDHDS (or any downhole tool) within the drill-pipe on the electric wireline. The ERS has a snap-lock and is latched at the surface; the tool is low-ered into the borehole, where an electric motor within the ERS is commanded from the surface to rotate until the RS pulling neck on the downhole instrument is released. This motor can unlock the ERS from the down-hole tool and return the ERS to a locked position so that it can be used to retrieve the downhole tool. The ERS consists of an electronics section, wired through sinker bars, and a motor section that contains the latching mechanism at the bottom of the tool. A prototype of the ERS was used on IODP Expedition 327 to successfully deploy the Hole U1301B CORK system (Expedition 327 Scientists, 2011).

The Motion Decoupled Hydraulic Delivery System

The MDHDS is composed of an Inner Barrel Subassembly (IBS, Figs. 1, 2a), an Outer Barrel Subassembly (OBS, Fig. 1), and the MDHDS Latch. The penetrometer is attach-ed to the IBS. On the rig floor, before the MDHDS is deployed, the IBS is latched to the OBS. The latching system (MDHDS Latch), near the bottom of the MDHDS (Fig. 1), is cocked by shifting a latch piston, compressing a spring within the MDHDS Latch, and then shifting an internal sleeve to lock the latch piston in place (Fig. 2c). The internal sleeve is then held in place by shear pins. The latched MDHDS is conveyed by wireline by the ERS to sit on the landing shoulder of the standard BHA. The MDHDS Latch is activated by raising the drillstring pressure. This severs the two shear pins, which allow the internal sleeve to move, unlocking the latch piston, which remains held in place by the drillstring pressure. Relieving the drillstring pressure allows the spring to expand, moving the latch piston, and opening the latch. The IBS is then freed from the OBS.
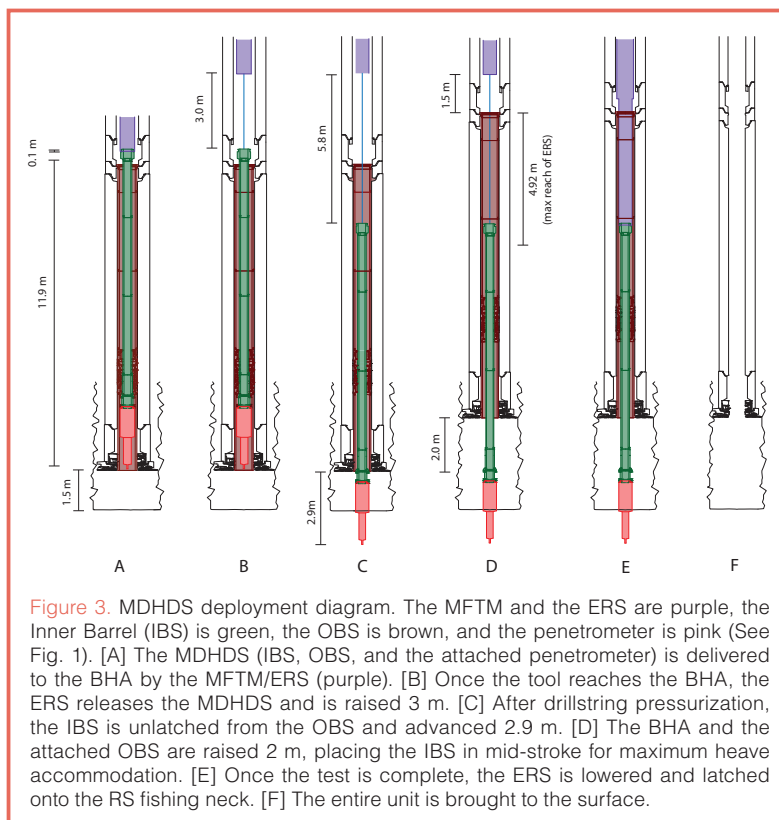

Figure 3. MDHDS deployment diagram. The MFTM and the ERS are purple, the Inner Barrel (IBS) is green, the OBS is brown, and the penetrometer is pink (See Fig. 1). [A] The MDHDS (IBS, OBS, and the attached penetrometer) is delivered to the BHA by the MFTM/ERS (purple). [B] Once the tool reaches the BHA, the ERS releases the MDHDS and is raised 3 m. [C] After drillstring pressurization, the IBS is unlatched from the OBS and advanced 2.9 m. [D] The BHA and the attached OBS are raised 2 m, placing the IBS in mid-stroke for maximum heave accommodation. [E] Once the test is complete, the ERS is lowered and latched onto the RS fishing neck. [F] The entire unit is brought to the surface.

The IBS and penetrometer is then pumped into the forma-tion by raising the drillstring pressure. When using a narrow diam-eter penetrometer like the T2P, the bottom of the MDHDS can be outfitted with a flapper guide tube. This tube protects the penetrometer as it passes through the flapper at the drill bit and acts as a guide to ensure vertical deploy-ment. For larger diameter penetrometers like the SET-P, the flapper guide tube is not used.

During this test, we installed a tension device inside the IBS to house a communications tether. The tether allowed real-time communication from the penetrometer to the rig floor. This tension device—consisting of a rigid and elastic cable and a series of pulleys—held the communications tether in tension at all times, taking up slack as the drill-string heaved downward and letting it out as it heaved upward. The tether connected to the top of the T2P and the bottom of the ERS.

Deployment Procedure

The MDHDS is first latched at the rig floor (Fig. 2c). The penetrometer is then attached to the bottom of the IBS. The MDHDS and the penetrometer are then hung vertically on the rig floor in the drillpipe. The cable head, MFTM, and ERS assembly are then snap-locked to the IBS, and the MDHDS is lowered on the electric wireline. The MDHDS is landed in the BHA with the BHA positioned 1.5 m above the bottom of the hole (Fig. 3a).

The MFTM actuates the ERS to unlatch the MDHDS, and the ERS is raised 3 m (Fig. 3b). With the MDHDS

latched and landed in the BHA, all the drillstring fluid is forced through the center of the OBS through a contact seal between the MDHDS landing shoulder and the wall of the BHA. Next, the drillstring is slowly pressurized to approximately 8 MPa (1160 psi) and held for several minutes to actuate the latch mechanism. Pressure is then released and, upon pressure reduction, the latch is opened. Next, the drillstring is re-pressurized, and the probe is pumped into the formation (Fig. 3c). The probe can be driven a maximum of 2.9 m because after that a circulation path is established and there is no longer any driving pressure. The BHA is then raised 2 m (Fig. 3d), allowing for +/- 2.5 m of vertical motion. At this point in the deployment, the OBS is fixed relative to the BHA, and the IBS is fixed relative to the bottom of the hole. There are no seals in contact between the IBS and OBS; thus, no seal friction exists that could induce heave motion into the probe.

The probe is extracted by using the MFTM for actuating the ERS into a closed position, lowering the MFTM-ERS assembly until latching with the RS fishing neck that is attached to the IBS (Fig. 3e). The probe is then pulled from the formation into the OBS (Fig. 3f), where it is well protected during the trip out of the hole. If the probe is embedded so firmly into the formation that the wireline cannot lift, then the BHA can be raised to dislodge the probe from the bottom.

The MDHDS is retrieved by wireline. On deck, it is laid out as a normal core barrel would be. The flapper tube is removed to allow access to the T2P, which is then detached from the IBS by disconnecting a quick-release connection.

Figure 4. MDHDS deployment record. Zero time is set to the onset of pressure dissipation. At Pt. A (-400 s), the MDHDS latch is released, and the IBS and the attached T2P descend by gravity driving the tip a small distance into the formation. As a result, the tip pressure (blue) and the shaft pressure (red) rise abruptly. The accelerometer (green) records rapid changes in acceleration. At Pt. B, the drillstring is re-pressurized, and the penetrometer is driven into the formation (e.g., Fig. 3c). At Pt. C, we interpret that the penetrometer has been driven the maximum 2.9 m of stroke that is possible (Fig. 3c). Between Pt. C and Pt. D, there is ongoing circulation but no longer any significant driving force. At Pt. D, the circulation pumps are turned off, and pressure dissipation begins.

The MDHDS latch is then reset in preparation for the next deployment.

Site U1402 Deployment

At Site U1402, the continental slope is smooth, draped by sediments from the Hudson River apron, and the water depth is 639 m. During ODP Leg 174A, Advanced Piston Cores (APC) were taken to 215 mbsf (meters below sea floor). Sediments within the first 200 mbsf were dominated by silty clay (Shipboard Scientific Party, 1998).

The new hole at the previous Site 1073 was named Site U1402 and was spudded on 7 June 2012. The seafloor was recorded at 650 meters below rig floor (mbrf). The hole was washed down to 96.4 mbsf (746.4 mbrf), and the MDHDS, T2P, and the ERS were assembled and deployed. The MDHDS was lowered by the ERS to the BHA. The ERS was unlatched with the tether system in place and raised two meters above the BHA. The drillstring pressure was raised, and the T2P penetrometer was deployed (Fig. 4).

After the MDHDS Latch was released, the T2P and IRS passed through the BHA and into the formation under their own weight, driving the tip of the T2P into the formation, but not far enough to drive the shaft pressure port into the formation (Fig. 4, Pt. A). After we increased the drillstring pressure a second time, the entire tool was driven approximately 2.9 m farther into the formation until circulation was established (Fig. 4, Pt. B). Between Points C and D (Fig. 4), circulation was maintained, and pore pressure varied but declined slightly. At Pt. D, the pumps were shut off, and the pressure data recorded a dissipation characteristic of a penetrometer deployment.

When circulation was re-established to clear the BHA of settled sediment, the tool jammed. The ERS was released and the wireline was pulled from the hole; the top drive was then set back, and the drillstring was tripped from the hole. After drillpipe retrieval, we found that the tether within the IBS had snapped and worked between the tool and the inside of the BHA aperture, jamming the tool in place and preventing recovery.

Interpretation of Results

The MFTM, ERS, and MDHDS worked well in this deployment. The IBS and T2P successfully unlatched and were deployed after drillstring pressurization (Fig. 4, Pt. A). When the drill string was re-pressurized, the penetrometer was successfully driven into the formation (Fig. 4, Pt. B). After penetration, both the tip and shaft pressure sensors recorded smooth pressure dissipation profiles. The lack of any motion in the accelerometer (green triangles, Fig. 4) during the dissipa-
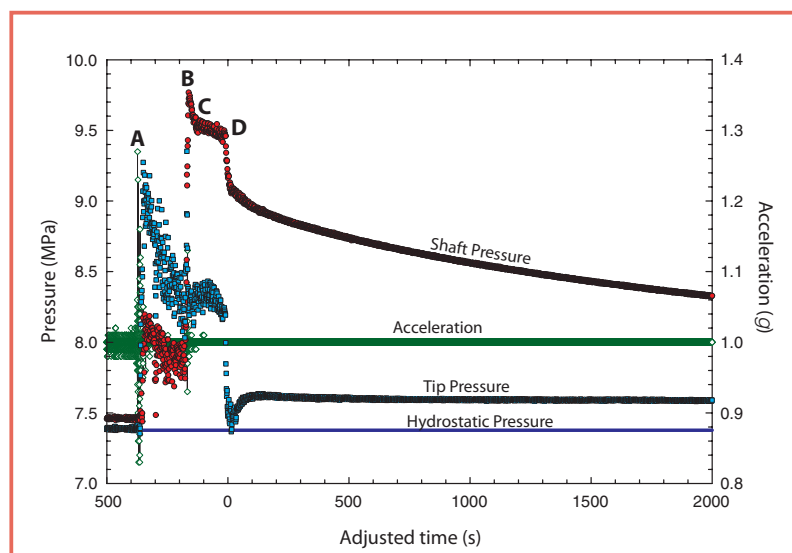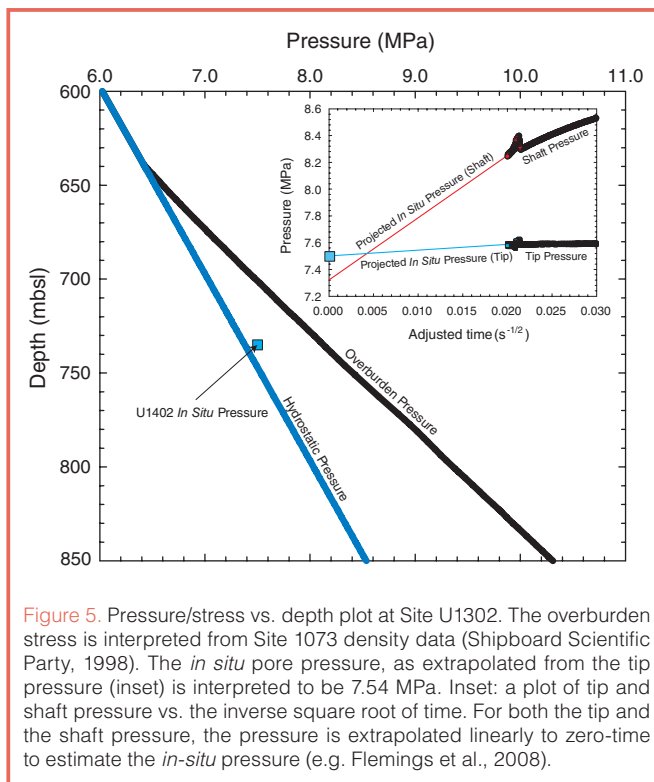
Figure 5. Pressure/stress vs. depth plot at Site U1302. The overburden stress is interpreted from Site 1073 density data (Shipboard Scientific Party, 1998). The *in situ* pore pressure, as extrapolated from the tip pressure (inset) is interpreted to be 7.54 MPa. Inset: a plot of tip and shaft pressure vs. the inverse square root of time. For both the tip and the shaft pressure, the pressure is extrapolated linearly to zero-time to estimate the *in-situ* pressure (e.g. Flemings et al., 2008).

tion interval is evidence that the drillstring completely decoupled from the penetrometer. Finally, the penetrometer was undamaged when it was recovered, which indicates that it was driven straight downward and that there were no problems with the flapper valve at the bottom of the BHA.

The pressure records are characteristic of those recorded by successful T2P deployments (Flemings et al., 2008). The shaft pressure (Fig. 4) is higher than the tip pressure because the larger diameter shaft induced a larger pore pressure during penetration. The pressure rebound recorded at the tip (0–50 seconds, Fig. 4) is due to the unloading that resulted when circulation stopped. Extrapolation of the tip pore pressure record (Fig. 5, inset) results in a predicted *in situ* pressure of 7.54 MPa (blue square, Fig. 5), which is slightly above hydrostatic pressure. Similar results were predicted by Dugan and Flemings (2000) based on an indirect measurement with respect to bulk density.

Long-Term Application

Based on the outcome of this engineering test, the MDHDS, the T2P, and MFTM have been certified for deployment on board the *JOIDES Resolution*. Although real-time data were acquired through the tethered system, failure of the tether during drillstring pressurization shows that a tethered real-time telemetry configuration is not ready for regular shipboard use. Stress Engineering Services is completing final modifications to the ERS to improve its latching operation. Once the modifications are complete, this tool will also be certified for onboard deployment by USIO. The ERS will be used to deploy the SCIMPI during

IODP Expedition 331S in May of 2013. We hope that the advances in tool delivery allowed by the MDHDS will result in rich pore pressure and temperature data sets in future expeditions and will engender the development of new downhole tools that can be deployed by the MDHDS.

The IODP Expedition 342 Scientists

R.D. Norris (Co-chief Scientist), P.A. Wilson (Co-chief Scientist), P. Blum (Expedition Project Manager/Staff Scientist), A. Fehr, C. Agnini, A. Bornemann, S. Boulila, P.R. Bown, C. Cournede, O. Friedrich, A.K. Ghosh, C.J. Hollis, P.M. Hull, K. Jo, C.K. Junium, M. Kaneko, D. Liebrand, P.C. Lippert, Z. Liu, H. Matsui, K. Moriya, H. Nishi, B.N. Opdyke, D. Penman, B. Romans, H.D. Scher, P. Sexton, H. Takagi, S.K. Turner, J.H. Whiteside, T. Yamaguchi, Y. Yamamoto

References

Becker, K., and Davis, E. E., 2005. A review of CORK designs and operations during the Ocean Drilling Program. *In* Fisher, A. T., Urabe, T., Klaus, A., and the Expedition 301 Scientists, *Proc. IODP*, 301: Washington, DC (Integrated Ocean Drilling Program Management International, Inc.). doi:10.2204/iodp.proc.301.104.2005

Boutt, D. F., Saffer, D., Doan, M.- L., Lin, W., Ito, T., Kano, Y., Flemings, P. B., et al., 2012. Scale dependence of *in situ* permeability measurements in the Nankai accretionary prism: The role of fractures. *Geophys. Res. Lett.*, 39:L07302. doi:10.1029/2012GL051216

D'Hondt, S. L., Jørgensen, B. B., Miller, D. J., et al., 2003. *Proc. ODP, Init. Repts.*, 201: College Station, TX (Ocean Drilling Program), [CD-ROM].

Dugan, B., and Flemings, P. B., 2000. Overpressure and fluid flow in the New Jersey continental slope: Implications for slope failure and cold seeps. *Science*, 289(5477):288–291. doi:10.1126/science.289.5477.288

Expedition 327 Scientists, 2011. Expedition 327 summary, *In* Fisher, A. T., Tsuji, T., Petronotis, K., and the Expedition 327

Scientists, *Proc. IODP*, 327: Washington, DC (Integrated Ocean Drilling Program Management International, Inc.). doi:10.2204/iodp.proc.327.101.2011

Flemings, P. B., Behrmann, J., Davies, T., John, C., and the Expedition 308 Project Team, 2005. Gulf of Mexico hydrogeology—overpressure and fluid flow processes in the deepwater Gulf of Mexico: Slope stability, seeps, and shallow-water flow. *IODP Sci. Prosp.*, 308. doi:10.2204/iodp.sp.308.2005

Flemings, P. B., Behrmann, J., John, C. M., and the Expedition 308 Scientists, 2006. *Proc. IODP*, 308: Washington, DC (Integrated Ocean Drilling Program Management International, Inc.). doi:10.2204/iodp.proc.308.2006

Flemings, P. B., Long, H., Dugan, B., Germaine, J., John, C. M., Behrmann, J. H., and Sawyer, D., 2008. Erratum to "Pore pressure penetrometers document high overpressure near the seafloor where multiple submarine landslides have occurred on the continental slope, offshore Louisiana, Gulf of Mexico" [*Earth and Planetary Science Letters* 269/3–4 (2008) 309–32]. *Earth Planet. Sci. Lett.*, 274(1–2):269–283. doi:10.1016/j.epsl.2008.06.027

Goldberg, D., Meltser, A., Myers, G., and Masterson, W., 2004. Comparison of Multi-Sensor Spectral Gamma Ray Tool (MGT) and conventional spectral gamma ray logs, ODP Site 1179. *Proc. ODP*, *Sci. Results*, 191: College Station, TX (Ocean Drilling Program).

Hesselbo, S. P., 1996. *Proc. ODP, Sci. Results*, 150: College Station, TX (Ocean Drilling Program).

Lin, W., Doan, M.-L., Moore, J. C., McNeill, L., Byrne, T. B., Ito, T., Saffer, D., et al., 2010. Present-day principal horizontal stress orientations in the Kumano forearc basin of the southwest Japan subduction zone determined from IODP NanTroSEIZE drilling Site C0009. *Geophys. Res. Lett.*, 37:L13303. doi:10.1029/2010GL043158

Long, H., Flemings, P. B., and Germaine, J. T., 2007. Interpreting in situ pressure and hydraulic properties with borehole penetrometers in ocean drilling: DVTPP and Piezoprobe deployments at southern Hydrate Ridge, offshore Oregon. *J. Geophys. Res.*, 112:B04101. doi:10.1029/2005JB004165

Long, H., Flemings, P. B., Dugan, B., Germaine, J. T., and Ferrell, D., 2008. Data report: Penetrometer measurements of in situ temperature and pressure, IODP Expedition 308. *In* Flemings, P. B., Behrmann, J. H., John, C. M., and the Expedition 308 Scientists, *Proc. IODP*, 308: Washington, DC (Integrated Ocean Drilling Program Management International, Inc.). doi:10.2204/iodp.proc.308.203.2008

Moore, G. F., Taira, A., Bangs, N. L., Kuramoto, S., Shipley, T. H., Alex, C. M., Gulick, S. S., et al., 2001. Structural setting of the Leg 190 Muroto Transect. *In* Moore, G.F., Taira, A., Klaus, A., et al., *Proc. ODP, Init. Repts.*, 190:College Station, TX (Ocean Drilling Program), [CD-ROM].

Moore, J. C., Shipley, T. H., Goldberg, D., Ogawa, Y., Filice, F., Fisher, A., Jurado, M. J., et al., 1995. Abnormal fluid pressures and fault-zone dilation in the Barbados accretionary prism: Evidence from logging while drilling. *Geology*, 23(7):605–608. doi:10.1130/0091-7613(1995)023<0605:AFP AFZ>2.3.CO;2

Shipboard Scientific Party, 1998. Site 1073. *In* Austin, Jr., J. A., Christie-Blick, N., Malone, M. J., et al., *Proc. ODP, Init. Repts.*, 174A: College Station, TX (Ocean Drilling Program), 153–191. doi:10.2973/odp.proc.ir.174a.105.1998

Shipboard Scientific Party, in press. Site 342. *In* Norris, R., Wilson, P., and Blum, P., *Proc. ODP, Init. Repts.*, 211: College Station, TX (Ocean Drilling Program).

Tréhu, A. M., Bohrmann, G., Rack, F. R., and Torres, M. E., 2003. *Proc. ODP, Init. Repts.*, 204: College Station, TX (Ocean Drilling Program). doi:10.2973/odp.proc.ir.204.102.2003

Authors

Peter B. Flemings, **Peter J. Polito**, and **Donald L. Brooks**, Jackson School of Geosciences, The University of Texas at Austin, 1 University Station C1100, Austin, TX 78712-0254, U.S.A., e-mail: pflemings@jsg.utexas.edu, peter.polito@jsg.utexas.edu, brodon@ig.utexas.edu

Thomas L. Pettigrew, Pettigrew Engineering, 479 Nine Mile Road, Milam TX 75959, U.S.A., e-mail:tom.pettigrew@ windstream.net

Gerardo J. Iturrino, and **Eric Meissner**, Borehole Research Group, Lamont-Doherty Earth Observatory of Columbia University, P.O. Box 1000, 61 Route 9W, Palisades, NY 10964, U.S.A., e-mail:iturrino@ldeo.columbia.edu, meissner@ldeo.columbia.edu

Robert Aduddell, Integrated Ocean Drilling Program, Texas A&M University, 1000 Discovery Drive, College Station, TX 77845-9547, U.S.A., e-mail:aduddell@iodp.tamu. edu

Chris Hetmaniak, and **David Huey**, Stress Engineering Services, 13800 Westfair East Drive Houston, TX 77041, U.S.A., e-mail:chris.hetmaniak@stress.com, dave.huey@ stress.com

John T. Germaine, Department of Civil and Environmental Engineering, Massachusetts Institute of Technology, Cambridge, MA 02139, U.S.A., e-mail:jgermain@mit.edu
and the IODP Expedition 342 Scientists

Photo Credits

Fig. 2a–c: Peter Flemings, The Unicersity of Texas at Austin
Fig. 2d: William Crawford, IODP-TAMU

Related Web Links

http://www.iodp.org/Science-Plan-for-2013-2023/
http://www.ig.utexas.edu/research/facilities/downhole/mdhds.htm

Assessment and Use of NGR Instrumentation on the *JOIDES Resolution* to Quantify U, Th, and K Concentrations in Marine Sediment

by Ann G. Dunlea, Richard W. Murray, Robert N. Harris, Maxim A. Vasiliev, Helen Evans, Arthur J. Spivack, and Steven D'Hondt

Introduction

Concentrations of uranium (U), thorium (Th), and potassium (K) in geological materials provide insight into many important lithological characteristics and geologic processes. In marine sediment, they can aid in identifying clay compositions, depositional environments, and diagenetic processes. They can also yield information about the alteration and heat production of rocks (Ketcham 1996; Barr et al., 2002; Revillon et al., 2002; Brady et al., 2006; Bartetzko, 2008). Measurements of the concentrations of these elements in geological materials are relatively straightforward in shore-based laboratories. Rapidly determining their abundance within cores of sedimentary and igneous rock sequences onboard a research vessel is a more challenging but potentially very useful method to non-destructively and quickly provide important geochemical information about the concentrations of U, Th, and K within the sequences being cored.

When ^{238}U, ^{232}Th, and ^{40}K radioisotopes decay, they and their daughter products emit gamma rays at specific energy levels unique to each isotope. Natural gamma-ray (NGR) spectroscopy measures a wide energy spectrum that can be used to estimate the abundance of each isotope based on the strength of the signal at characteristic energies (Blum et al., 1997; Gilmore, 2008). Although intensities measured by an NGR system are proportional to the elemental concentrations, converting total counts in the energy spectrum to absolute elemental concentrations can be challenging due to low concentrations in the targeted lithologies and the time

constraints of core processing. Measuring ^{238}U, ^{232}Th, and ^{40}K in marine sediment and rock is particularly difficult because certain marine lithologies are commonly an order of magnitude less radioactive than continental material (Kogan et al., 1971; Taylor and McLennan, 1985; Rudnick and Gao, 2003).

Since 1993, an NGR system on the Ocean Drilling Program (ODP)/Integrated Ocean Drilling Program (IODP) drillship *JOIDES Resolution* has successfully been measuring NGR emitted by marine sediment and rocks of varying lithologies (Blum et al., 1997). Additionally, there is a history through Deep Sea Drilling Project (DSDP)/ODP/IODP of downhole logging with NGR tools (Gealy, 1973; Hoppie et al., 1994; Blum et al., 1997; Sakamoto et al., 2003). However, the shipboard NGR system used prior to 2009 often required excessive NGR measurement time in order to produce reliable counting statistics, and hence conflicted with the flow of core processing otherwise imposed by the shipboard operations. Because of their composition in general, deep-sea sediments in particular pose a problem in this regard. This caused the NGR system to be underutilized.

In 2009, a new NGR system was installed on the *JOIDES Resolution* to quicken the pace of NGR measurements while providing the statistical reliability and quality of data needed (Fig. 1, Vasiliev et al., 2011). Now, each core section (up to 1.5 m in length) requires only 10–60 minutes of instrument time to produce a high-resolution energy spectrum. This data from this spectrum can be rapidly converted to concentrations by combining analytical and modeling techniques. Due to instrument design, NGR counts for each set of spectral data are integrated over 40 cm of core length. Vasiliev et al. (2011) details the geometric layout of the improved system and provides an overview of its analytical capabilities, including spatial resolution.

While the new NGR system is a significant step forward, it is important to assess the instrument's performance by comparing NGR-derived results to those from independent measurements. Here we compare the concentrations of U, Th, and K derived from the shipboard NGR instrument to shore-based inductively coupled plasma-mass spectrometer (ICP-MS) and inductively coupled plasma-emission spectrometer (ICP-ES) analyses of 38 samples collected during IODP Expedition 329 to the South Pacific Gyre. The samples are metalliferous pelagic clays and carbonate oozes (D'Hondt et al., 2011). We highlight several simple, yet vital, correc-
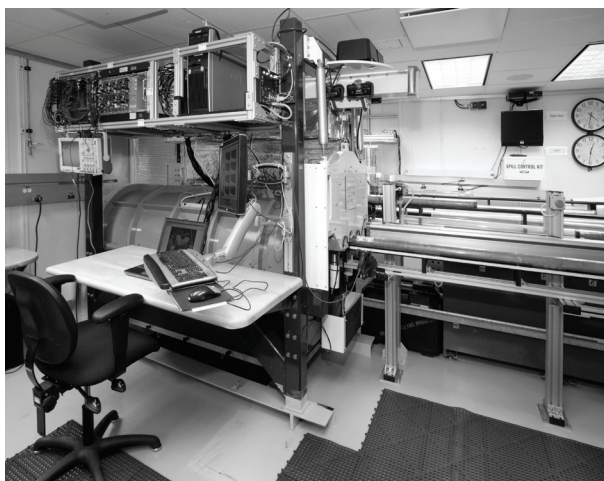

Figure 1. The natural gamma radiation (NGR) system on the *JOIDES Resolution* (from Vasiliev et al., 2011).

tions that must be applied to the raw shipboard NGR data to improve their quality. Our goal is to assess the accuracy and improve the precision of shipboard NGR estimates of U, Th, and K concentrations so future expeditions may more fully use this new NGR system.

NGR Measurements on the *JOIDES Resolution* during Expedition 329

The improved NGR instrument (Vasiliev et al., 2011) was used during IODP Expedition 329. Prior to analyzing each set of sediment core sections, we measured the NGR background spectra for ~5.5 hours to account for cosmic and environmental sources. Twice during the expedition, we calibrated each NaI(Tl) detector using a set of 1-mkCi ^{137}Cs and ^{60}Co gamma-ray calibration sources. Measurements of

cylindrical core-shaped standards with known abundances of ^{40}K allowed us to convert NGR counts per second (cps) to concentrations of total K, assuming natural abundances of K isotopes. We obtained the NGR data reported in this study (Table 1) by measuring the energy spectrum emitted by each core section (1.5 m maximum) for 60 minutes. Additional information is described by D'Hondt et al. (2011).

The decay of ^{40}K to ^{40}Ar produces a distinct peak at 1460 keV on the NGR spectrum. ^{238}U and ^{232}Th do not emit detectable gamma rays when they decay, but some of their daughter products emit a gamma-ray energy signal that is apparent in the measured spectrum. We used the daughter products with the most obvious energy signal, ^{214}Bi (1.76 MeV) and ^{208}Tl (2614 keV) to indicate the presence of the parent isotopes ^{238}U and ^{232}Th, respectively (Kogan,

Table 1. Concentrations of U, Th, and K from the ICP-MS, ICP-ES, and NGR measurements.

Site/ Hole	Depth (mbsf)	K ICP-ES Not Normalized wt%	K ICP-ES Normalized wt%	Th ICP-MS ppm	U ICP-MS ppm	K NGR Uncorrected wt%	Th NGR Uncorrected ppm	U NGR Uncorrected ppm	Bulk/Dry MAD Density	K NGR Corrected %	Th NGR Corrected ppm	U NGR Corrected ppm
1366B	0.1	2.27	2.85	16.00	1.66	0.75	2.80	0.90	3.32	2.49	9.31	2.99
	1.8	2.43	2.88	15.56	1.94	0.96	4.80	1.60	3.32	3.19	15.95	5.32
	3.5	2.65	3.16	14.70	1.93	0.97	2.80	0.80	3.32	3.22	9.31	2.66
	5.1	2.71	3.25	12.09	1.94	1.28	6.00	1.50	3.32	4.25	19.94	4.99
	6.2	2.66	3.29	13.33	2.30	0.98	4.80	1.70	3.32	3.26	15.95	5.65
	7.9	1.60	2.18	12.92	2.77	0.63	3.50	1.20	3.32	2.09	11.63	3.99
	10.1	1.91	2.42	17.64	3.81	0.87	6.40	1.20	3.32	2.89	21.27	3.99
	13.1	2.58	3.45	5.59	2.33	1.25	2.20	1.60	2.36	2.95	5.19	3.78
	15.8	3.01	3.67	3.79	20.4	1.43	1.80	1.50	2.36	3.38	4.25	3.54
1367B	0.2	1.99	2.58	15.90	3.87	1.43	6.00	20.40	2.78	3.97	16.67	56.66
	1.2	1.94	2.54	7.93	3.85	0.92	2.50	1.60	2.78	2.56	6.94	4.44
	1.8	2.02	2.64	7.56	3.81	1.14	3.10	2.90	2.78	3.17	8.61	8.05
	3.3	2.17	2.74	7.77	3.87	1.05	2.90	2.60	2.78	2.92	8.05	7.22
	6.5	0.08	0.26	0.43	0.29	0.69	2.60	2.90	1.63	1.12	4.24	4.73
	7.2	0.08	0.24	0.43	0.37	0.15	0.60	0.60	1.63	0.24	0.98	0.98
	7.7	0.21	0.45	1.41	1.81	0.12	0.50	0.90	1.63	0.20	0.82	1.47
	12.1	0.05	0.14	0.15	0.60	0.05	0.30	0.60	1.63	0.08	0.49	0.98
	17.1	0.06	0.16	0.08	1.15	0.08	0.20	1.20	1.63	0.13	0.33	1.96
	21.5	0.16	0.46	0.05	0.79	0.09	0.20	1.20	1.63	0.15	0.33	1.96
1368B	0.2	0.23	0.56	2.04	1.26	0.10	0.25	3.33	1.82	0.18	0.46	6.08
	0.5	0.08	0.25	0.37	0.85	0.10	0.25	1.33	1.82	0.18	0.46	2.43
	2.6	0.06	0.17	0.07	0.94	0.07	0.20	0.93	1.82	0.13	0.36	1.70
	3.9	0.06	0.18	0.12	0.50	0.04	0.11	0.44	1.82	0.07	0.20	0.80
	6.3	0.06	0.15	0.05	0.99	0.04	0.20	0.48	1.82	0.07	0.36	0.88
	8.2	0.05	0.15	0.03	0.71	0.01	0.03	0.07	1.82	0.02	0.05	0.13
	10.5	0.06	0.15	0.04	1.39	0.06	0.15	0.72	1.82	0.11	0.27	1.31
	11.2	0.07	0.17	0.08	2.56	0.09	0.23	1.11	1.82	0.16	0.42	2.03
	12.9	0.09	0.20	0.07	1.97	0.09	0.21	1.01	1.82	0.16	0.38	1.84
	15.3	0.55	0.58	1.36	0.91	0.25	0.36	1.85	1.82	0.46	0.66	3.38
1369B	0.2	2.35	2.85	14.27	1.61	1.31	9.70	32.80	3.42	4.48	33.15	112.11
	2.8	2.68	3.24	11.99	1.38	1.05	3.90	1.31	3.42	3.59	13.33	4.48
	3.3	2.99	3.63	12.11	1.47	1.22	4.50	1.01	3.42	4.17	15.38	3.45
	5.6	2.70	3.32	16.07	1.96	1.01	3.75	1.01	3.42	3.45	12.82	3.45
	7.2	3.20	3.74	13.82	1.81	1.85	5.93	1.54	2.48	4.58	14.69	3.81
	8.8	2.79	3.31	17.01	2.45	1.16	5.10	1.45	2.48	2.87	12.63	3.59
	11.3	3.12	3.72	12.97	2.24	1.83	5.49	1.83	2.48	4.53	13.60	4.53
	14.1	3.43	4.11	11.92	2.44	1.99	7.37	1.65	2.48	4.93	18.26	4.09
	16.5	3.24	3.91	12.66	2.56	1.59	4.78	1.07	2.48	3.94	11.84	2.65

The freeze-dried concentrations of major oxides determined by ICP-ES were normalized to 100% to represent dry, volatile-free concentrations of K to better compare with concentrations from samples dried in a convective oven (see text). Column 3 reports the freeze-dried ICP-ES K (wt%, measured at λ=766.490nm) concentrations prior to normalization, and column 4 reports the normalized K (wt%) concentrations. Columns 7–9 report the raw NGR estimates of U, Th, and K concentrations. Column 10 reports the bulk density to dry density ratio from the MAD data that was used to correct the NGR data from wet concentration to dry concentrations. There was limited moisture and density (MAD) data that was co-located with our samples, so we averaged the density data from similar samples at each site that showed a consistent gamma-ray attenuation (GRA) density. Columns 11–13 report the density-corrected NGR results.

1971). By measuring decays of daughter products as a proxy for [238]U and [232]Th concentrations, it is assumed that the analyzed sediment is in a state of secular equilibrium. However, this assumption is not always valid, as discussed below.

For each NGR-measured [40]K peak, we converted the area under the background-corrected spectral peak (Vasiliev et al., 2011) to concentrations based on the cps/concentration ratio of a K standard (with natural abundances of K isotopes) and the mass of the sediment that contributed to the radiation received by each NaI detector. Each detector receives radiation from ~20 cm of core on either side of the detector, and thus all NGR measurements are integrated over ~40 cm (Vasiliev et al., 2011).

The mass of sediment is determined by convolving the NGR detector response function with core densities and core volumes. The "core volume" term in the calculation is the volume of the cylindrical K standard in the visible range of the NaI detector, where core densities are measured with the shipboard gamma-ray attenuation (GRA) system. The statistical error of GRA densities is estimated to be less than 0.5%, and errors in accuracy are less than 5% (Blum, 1997). The error in the GRA density combined with statistical counting and systematic error for the NGR measurements is estimated to be ~7%–8% for K.

For much marine sediment, including those we describe here from the South Pacific Gyre, U and Th cannot be calibrated by simple comparison to a standard because the concentrations are too low given a reasonable measurement time, and the dynamic range of available standard reference materials is too narrow. Instead, we estimated U/K and Th/K ratios by comparing the measured NGR spectra to spectra generated by Monte Carlo simulations (Sambridge and Mosegaard, 2002).

The Monte Carlo simulations were performed on the *JOIDES Resolution* using the GEANT 3.21 simulation tool designed at CERN (Brun et al., 1994; Vasiliev et al., 2011). A single Monte Carlo-simulated spectrum that was generated using a unique combination of [238]U, [232]Th, and [40]K activity ratios will best match the experimentally measured spectrum and reveal the U/K and Th/K ratios. The concentrations of U and Th can then be calculated by multiplying these ratios by the concentrations of K determined from the calibration standard. The spectral analysis for the NGR system that computes elemental concentrations for U, Th, and K are based on natural abundances of the isotopes [238]U, [232]Th, and [40]K (Vasiliev et al., 2011). The statistical error for the Monte Carlo simulations is negligible, but systematic errors are ~10% and in many cases may be much lower.

ICP-MS and ICP-ES Quantification of U, Th, and K Concentrations

To assess the accuracy of the U, Th, and K concentrations generated from the shipboard NGR, we selected 38 samples from discrete depth intervals from Holes U1366B, U1367B,

U1368B, and U1369B (Table 1). We used well-established ICP-MS and ICP-ES methods to determine accurate and precise concentrations of these 38 samples (Murray and Leinen, 1996; Martinez et al., 2007; Ziegler et al., 2007). We freeze-dried, powdered, and digested the samples in a sealed heated acid cocktail containing HNO_3, HCl, HF, and H_2O_2. Additions of boric acid after the initial digestion neutralized the HF. We analyzed the solutions at Boston University on a VG PlasmaQuad Excell ICP-MS for U and Th concentrations, and on a Jobin Yvon Ultima C ICP-ES for K concentrations. Based on replicate analysis from the powder weighing step onward, the precision of the K measurement is 4% of the measured value, and the precision of both U and Th is 2% of their respective measured values. To ensure accuracy, we analyzed the BHVO-2 Standard Reference Material (Wilson, 1997; U.S. Geological Survey) independent from our calibrations. Our measured values agree with the reported values (and their reported uncertainty) within analytical precision. Because of this high precision and accuracy, in our discussion we consider the ICP-MS and ICP-ES data (Table 1) to be the benchmark against which we assess the NGR results.

Importance of Accurate Sediment Density Measurements

Sediment density is a critical parameter when comparing U, Th, and K concentrations from NGR measurements to ICP-MS and ICP-ES methods. The concentrations derived from NGR are based on a GRA density, which represents a bulk, *wet* density. In contrast, the ICP-MS and ICP-ES analyses require that the samples be freeze-dried before dissolution, and thus the ICP-MS and ICP-ES data are a concentration based on a *dry* sample weight. Therefore, a density correction (wet to dry) is required prior to comparing shipboard NGR-based concentrations to shore-based ICP-MS and ICP-ES concentrations. This density correction is theoretically straightforward, but in reality there are a number of different parameters that need to be considered throughout the density correction process due to the density measurement techniques, the physical nature of core material, and other aspects of NGR analysis.

We took advantage of the moisture and density (MAD) data collected during Exp. 329 to determine the bulk wet density/dry bulk density ratio (ρ_{bulk}/ρ_{dry}) and to correct the NGR-based measurements for direct comparison with the ICP-ES based concentrations according to the following relationship:

$$[K(wt\%)_{ICP-ES}] = (\rho_{bulk} / \rho_{dry})[K(wt\%)_{NGR}].$$

Different methods of drying sediment can lead to disparities between data sets. Following typical standard protocol, the Exp. 329 shipboard scientific party measured the wet and dry sediment densities by weighing ~7 cm^3 of wet sediment, drying the sample in a convection oven at $105°C \pm 5°C$ for more than 24 hours, cooling it in a desiccator, and then reweighing it to determine the MAD bulk and dry densities.

The accuracy and precision of the MAD masses determined on the *JOIDES Resolution* while at sea are both stat-ed to be ~0.1% (Blum, 1997), which are likely to be low estimates.

Baking the sediment in a convective oven to measure dry density (ρ_{dry}) removes an undeter-mined amount of the interlayer water from clay minerals and also potentially drives off some CO_2 from carbonates, regardless of mineralogy. However, freeze-drying the sediment for ICP-MS and ICP-ES analyses retains the interlayer water and CO_2. Therefore, the dry weights on which the ICP-MS and ICP-ES concentrations are based are different from the dry weights on which the NGR calcula-tions are based, even after the ρ_{bulk}/ρ_{dry} correction is employed. This difference can be fairly substantial, yet variable depending on sedi-ment composition.

To account for this weight difference, we deter-mined the concentrations of all ten major element oxides in the sediment using the ICP-ES and nor-malized the oxides (including K_2O) to sum to 100%. Calculating this "volatile-free" ICP-ES data yields the most appropriate K_2O data to compare to the
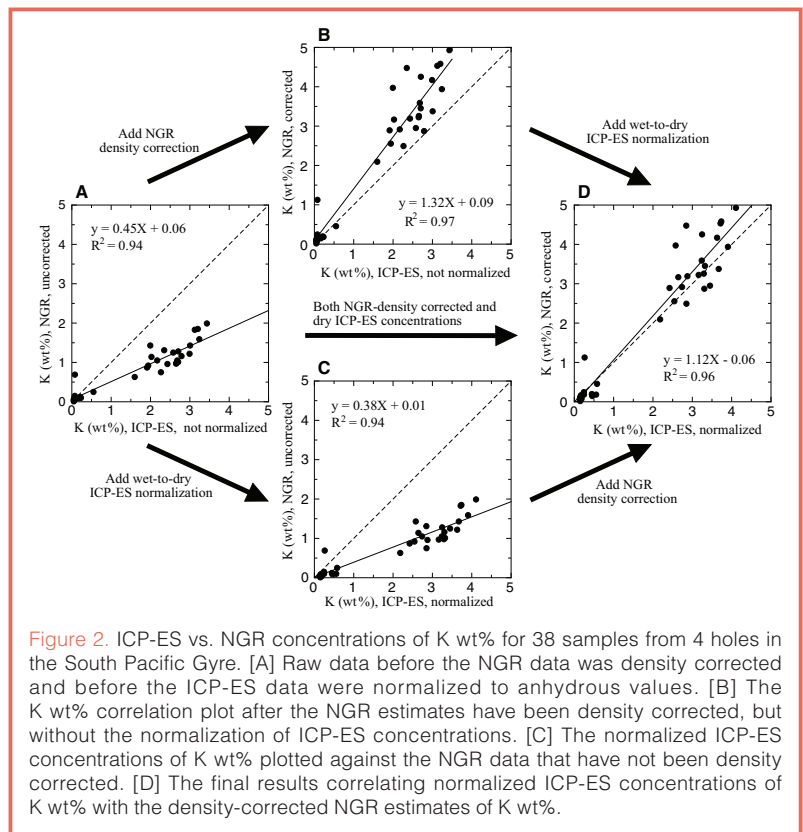

Figure 2. ICP-ES vs. NGR concentrations of K wt% for 38 samples from 4 holes in the South Pacific Gyre. [A] Raw data before the NGR data was density corrected and before the ICP-ES data were normalized to anhydrous values. [B] The K wt% correlation plot after the NGR estimates have been density corrected, but without the normalization of ICP-ES concentrations. [C] The normalized ICP-ES concentrations of K wt% plotted against the NGR data that have not been density corrected. [D] The final results correlating normalized ICP-ES concentrations of K wt% with the density-corrected NGR estimates of K wt%.

density-corrected NGR data. Performing this correction is important not only for comparing NGR and ICP measure-ments in our study, but is also critical to consider when using NGR data as a scientific data set; because the NGR data taken alone at face value is based on a *wet* measurement, comparison to literature data may not be straightforward. It also means that in order to effectively calibrate the NGR to shore-based analyses of K, *all* major oxides need to be analy-zed even if K is the only element of scientific interest to a particular investigator.

Comparison of NGR Data with ICP-MS and ICP-ES Data

The complete raw data generated from shipboard NGR measurements and shore-based ICP-ES and ICP-MS analy-ses are presented in Table 1. We discuss our K results first because the U and Th data are based on the K concentrations in the NGR measurements (see previous section). Figure 2 illustrates the combined significance of the density correc-tion and use of anhydrous ICP-ES concentrations. Prior to any correction, comparing the raw shipboard-produced NGR data to the non-normalized ICP-ES data (Fig. 2a) shows that the NGR data is offset significantly from the ICP-ES data. The correlation between the data is strong (R^2=0.94), yet the raw NGR values are approximately one-half of the ICP-ES concentrations (slope=0.45). Performing the density correction alone (Fig. 2b) slightly improves the correlation (R^2=0.97) but causes the NGR estimates to be ~30% higher than the ICP-ES concentrations (slope=1.32). Performing the anhydrous correction to ICP-ES data with-out the density correction (Fig. 2c) causes the NGR results

to underestimate ICP-ES concentrations, decreasing the accuracy (slope=0.38) but leaving the correlation un-changed (R^2=0.94). Application of *both* the density correc-tion and the anhydrous correction (Fig. 2d) results in the best comparison between datasets (slope=1.12) and essen-tially retains the best correlation (R^2=0.96).

While seemingly straightforward, the density measure-ments themselves also contain nuances that affect the data (Blum, 1997) and are the likely cause of the 1.12 slope value. Since we use the MAD bulk density and dry density as a ratio in Equation 1, any errors in the bulk volume measure-ment arithmetically cancel and do not affect the results. However, the GRA bulk densities used in converting NGR cps to concentrations can be skewed toward lower values by fractures, gaps, or expansion/compression in the sediment cores that result from pressure changes, mechanical stretch-ing, gas escaping, or other disturbances during the coring process. Additionally, the gamma-ray attenuation (GRA) measurements assume that the average attenuation coeffi-cient is constant for the measured material, which may not be the case if the characteristics of the sediment core vary (Blum, 1997). These factors, coupled with the fact that MAD and NGR data are not always co-located, contribute to the observed scatter between the NGR and ICP-ES data for K.

Additional sources of error may originate from the differ-ences in sampling resolution between the NGR system and ICP-MS and ICP-ES analyses. As noted previously, the NGR measurements integrate over ~40 cm of core length (Vasiliev et al., 2011). In this study, the ICP-MS and ICP-ES methods sampled over 10-cm intervals. The different resolutions

alone may produce error of up to 5%–10% between the two data sets, with stratigraphic lithological contrasts being smeared in the NGR data. Contrasts in lithology, either within one site or between the sites, may also influence the scatter.

Thus, there are a number of factors contributing to the inconsistencies between the NGR and ICP data. Because we calculate the NGR-based U and Th data from the ratio to K concentrations, the scatter within the K dataset will propagate through to the U and Th data as well (Fig. 3). Comparisons between our NGR and ICP-MS values of Th reveal good accuracy (slope=1.05) but a degraded correlation (R^2=0.87) relative to the K comparison. U comparisons show less accuracy (slope=1.20) and a poorer correlation (R^2=0.67) between the datasets. We further note that the U comparative plot is the only one that has a significant y-intercept (Fig. 3). This may reflect the impacts of secular disequilibrium, as described in the next section, or merely that U is the lowest concentration element of the three measured by NGR and thus may be expected to be the least precise.

U-Series Secular Disequilibrium

Several samples from shallow depths in the cores show large disparities between NGR and ICP-MS concentrations of U, which we interpret as indicating that the system is not in secular equilibrium. This trend arises from the difference in chemical properties of ^{238}U and ^{230}Th in seawater and manifests itself in our data because of the inherent differences between what each technique measures. ICP-MS measures ^{238}U directly, while NGR *infers* ^{238}U concentrations by measuring the decay of ^{214}Bi, its daughter product.

A system is in secular equilibrium when the concentration of each radioactive isotope in a decay chain series is solely dictated by the amount of decay of its parent isotope (Faure and Mensing, 2004). Over time, an isolated radioactive system will approach secular equilibrium, typically taking about six times the half-life of the longest-lived daughter to fully equilibrate (Bourdon et al., 2003). Thus, the ^{238}U- and ^{232}Th-decay series require approximately 1.5 Myr and 40 years, respectively, to reach secular equilibrium.

The equilibration process is disrupted if there is a separation between parent and daughter isotopes in the system, which commonly occurs between U and Th in seawater. When ^{238}U dissolved in seawater eventually decays to ^{230}Th, the ^{230}Th daughter product is rapidly scavenged and deposited on the seafloor (Bacon, 1984). Thus, the surface of the seafloor becomes enriched in ^{230}Th and subsequent daughter products relative to the concentration of the ^{238}U parent present. At the seafloor, the initial system is not in secular equilibrium, but as time passes and the sediment is buried, the system approaches a state of equilibrium.

The most shallowly buried samples analyzed in this study in Holes U1367B, U1368B, and U1369B show significantly

higher U concentrations estimated from NGR than from ICP-MS (Fig. 4). We interpret that this difference results from the excess of ^{238}U-decay daughter products on the seafloor and can be measured by NGR spectroscopy before the system has reached secular equilibrium. In contrast, ICP-MS analysis of ^{238}U only measures the parent product (and not the daughter products) and thus more accurately quantifies U concentrations in samples that are not at secular equilibrium. Our interpretation is supported by the complete NGR profiles from Exp. 329 (D'Hondt et al., 2011) that show a more gradual decline in ^{214}Bi gamma radiation deeper down each hole.

Sedimentation rates in the South Pacific Gyre are on the order of 0.1–1 m Myr^{-1} (Expedition 329 Scientists, 2011) and consequently, the sediment reaches secular equilibrium in less than 1.5 meters below the seafloor. NGR measurements of sediment from other regions with higher sedimentation rates may give the appearance that ^{238}U and ^{232}Th concentrations decline over a greater depth below the seafloor. For example, during the Pacific Equatorial Age Transect (PEAT) IODP expeditions (Pälike et al., 2010), the NGR system measured high concentrations of ^{238}U-series isotopes near the seafloor, due to the enrichment in the daughter product ^{230}Th, and exponentially decayed to a low concentration at depth as secular equilibrium was achieved (T. Williams, G. Winckler, and M. Lyle, pers. comm., 2012; Williams and Winckler, 2012).

Considerations for Future Applications

Our study shows that after employing the various corrections, use of the NGR/Monte Carlo technique onboard the *JOIDES Resolution* has the potential to rapidly determine U, Th, and K concentrations in marine sedimentary sequences, and thus contribute to the successful achievement of drilling objectives.

The accuracy and precision of the required NGR density corrections, however, depends on the accuracy and precision of both the wet and dry weight measurements. Accurate characterization of the wet vs. dry density in core materials is therefore essential to ensure the accuracy of U, Th, and K concentrations determined from the NGR measurements.
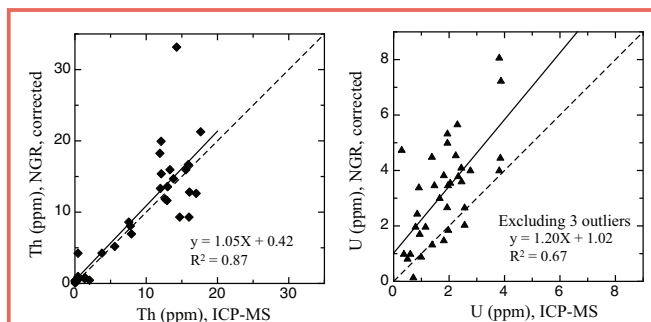

Figure 3. Total U and Th concentrations measured by ICP-MS vs. density-corrected U and Th concentrations measured by NGR for the 38 samples from 4 sites in the South Pacific Gyre that were analyzed for this study. Three outliers were removed from the U graph and are discussed in the section about secular disequilibrium.

One methodological improvement in this regard would be to dry sediment for MAD data on the *JOIDES Resolution* using a freeze-drier rather than a convection oven. Indeed, this was originally suggested by Blum (1997) and would eliminate the need for the anhydrous correction shown in Fig. 2c.

Figure 4. Depth profiles of the concentrations of K, Th, and U for Holes U1366B, U1367B, U1368B, and U1369B showing ICP-MS and ICP-ES data (circles) and NGR density-corrected data (triangles). Additional NGR total cps data from Expedition 329 (not shown here) illustrates a more continuous equilibration trend from the highest NGR emitted from sediment at the sediment-water interface and declining with depth.

Reported values should fully describe how density was measured.

Quantifying the wet to dry density ratio should be done as precisely as possible for a variety of samples from different lithologies throughout the sediment sequence that is being analyzed for NGR to reduce scatter produced by different lithologies and their transitional boundaries. Additionally, the shipboard ICP-ES could be used to quantify concentrations of elemental K in the core material, thereby checking the NGR system's accuracy while at sea. If the ICP samples are freeze-dried and the NGR samples continue to be oven-dried, then all ten major elements will need to be determined by ICP in order to facilitate the anhydrous-based data conversion. When incorporating the various data sets (GRA, MAD, NGR, ICP-ES and/or ICP-MS), samples must be co-located when possible to further enhance appropriate application of the density and anhydrous corrections.

Secular disequilibrium in young marine sediment near the seafloor should also be considered when determining the U and Th concentrations with the NGR system because it measures the daughter products of ^{238}U and ^{232}Th instead of the parent isotope. In the South Pacific Gyre, slow sedimentation rates cause the upper several decimeters of sediment cores from three sites to be in ^{238}U-series secular disequilibrium, while the ^{232}Th-series appears to be fully equilibrated throughout the sediment column.

Acknowledgements

References

Bacon, M. P., 1984. Glacial to interglacial changes in carbonate and clay sedimentation in the Atlantic Ocean estimated from ^{230}Th measurements. *Chem. Geol.*, 46(2):97–111. doi:10.1016/0009-2541(84)90183-9

Barr, S. R., Revillon, S., Brewer, T. S., Harvey, P. K., and Tarney, J., 2002. Determining the inputs to the Mariana Subduction Factory: Using core-log integration to reconstruct basement lithology at ODP Hole 801C. *Geochem. Geophys. Geosyst.*, 3(11):8901. doi:10.1029/2001GC000255

Bartetzko, A., 2008. Gamma ray spectrometric analysis of hydrothermally altered dacite samples from the PACMANUS hydrothermal field: Implications for the interpretation of gamma ray wireline measurements. *J. Volcanol. Geotherm. Res.*,
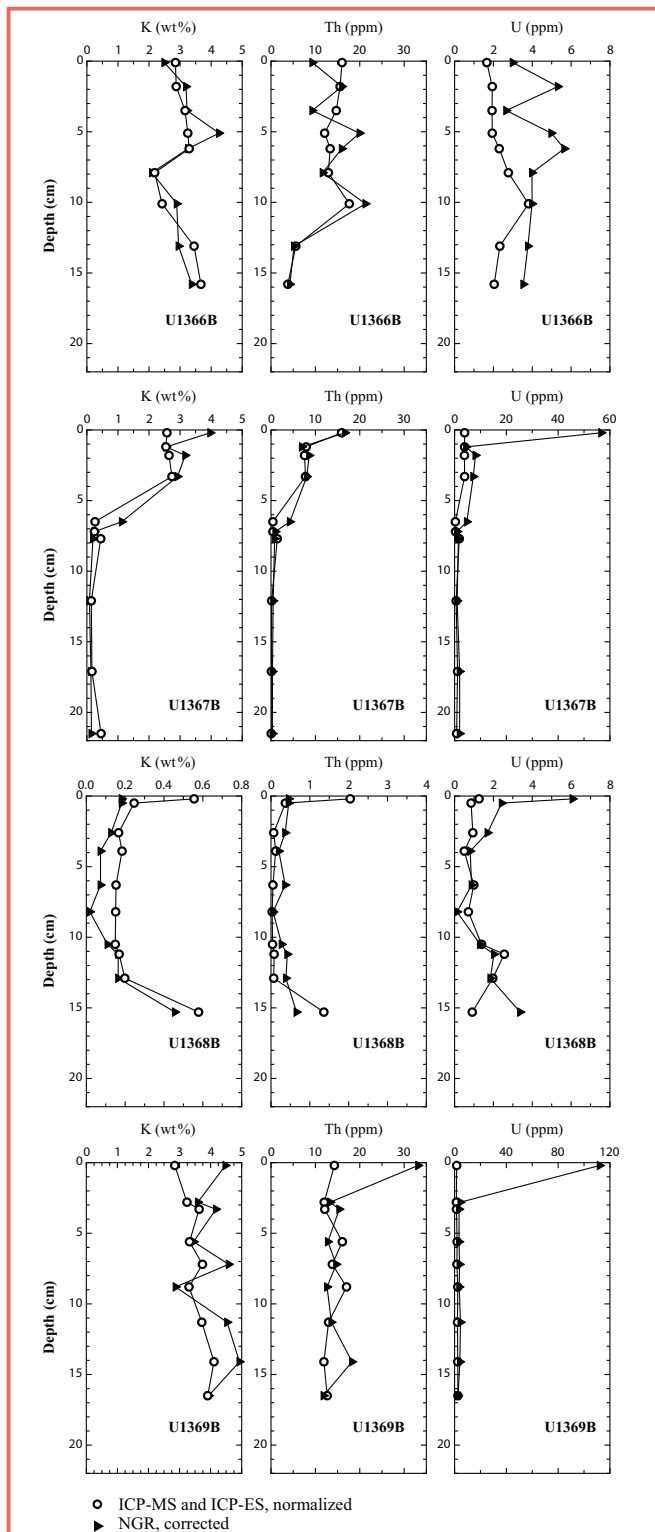
175(3):269–277. doi:10.1016/j.jvolgeores.2008.03.014

Blum, P., 1997. Physical properties handbook. *ODP Tech. Note*, 26. doi:10.2973/odp.tn.26.1997

Blum, P., Rabaute, A., Gaudon, P., and Allan, J. F., 1997. Analysis of natural gamma-ray spectra obtained from sediment cores with the shipboard scintillation detector of the Ocean Drilling Program: Example from Leg 156. *In* Shipley, T. H., Ogawa, Y., Blum, P., and Bahr, J. M., *Proc. ODP, Sci. Results,* 156: College Station, TX (Ocean Drilling Program), 183–195.

Bourdon, B., Turner, S., Henderson, G. M., and Lundstrom, C. C., 2003. Introduction to U-series geochemistry. *Rev. Mineral. Geochem.*, 52:1–21. doi:10.2113/0520001

Brady, R., Ducea, M., Kidder, S., and Saleeby, J., 2006. The distribution of radiogenic heat production as a function of depth in the Sierra Nevada Batholith, California. *Lithos*, 86(3–4):229–244. doi:10.1016/j.lithos.2005.06.003

Brun, R., Bruyant, F., and Marie, M., 1994. GEANT – Detector Description and Simulation Tool. CERN Program Library Long Writeup W5013, CERN, Geneva, Switzerland.

D'Hondt, S., Inagaki, F., Alvarez Zarikian, C. A., and the Expedition 329 Scientists, 2011. *Proc. IODP,* 329: Washington, DC (Integrated Ocean Drilling Program Management International, Inc.). doi:10.2204/iodp.proc.329.2011

Expedition 329 Scientists, 2011. South Pacific Gyre subseafloor life. *IODP Prel. Rept.,* 329. doi:10.2204/iodp.pr.329.2011

Faure, G., and Mensing, T. M., 2004. *Isotopes: Principles and Applications* (3rd ed.): Hoboken (John Wiley & Sons).

Gealy, E. L., 1973. Natural gamma radiation of sediments from the Western Equatorial Pacific: Leg 7, *Glomar Challenger. In* Winterer, E. L., et al., *Init. Repts. DSDP*, 7: Washington, DC (U.S. Government Printing Office), 1037–1080. doi:10.2973/dsdp.proc.7.123.1971

Gilmore, G., 2008. *Practical Gamma-Ray Spectrometry* (2nd ed.): Hoboken (John Wiley & Sons). doi:10.1002/9780470861981

Hoppie, B., Blum, P., and Party, S. S., 1994. Natural gamma-ray measurements on ODP cores: Introduction to procedures with examples from Leg 150. *In* Mountain, G. S., Miller, K. G., Blum, P., et al., *Proc. ODP, Init. Repts.*, 150: College Station, TX (Ocean Drilling Program), 51–59.

Ketcham, R. A., 1996. Distribution of heat-producing elements in the upper and middle crust of southern and west central Arizona: Evidence from the core complexes. *J. Geophys. Res.*, 101(B6):13611–13632.

Kogan, R. M., Nazarov, I. M., and Fridman, Sh. D., 1971. Gamma spectrometry of natural environments and formations: Theory of the method applications to geology and geophysics. Israel Program for Scientific Translations (Jerusalem), No. 5778. Translated from Russian.

Martinez, N. C., Murray, R. W., Thunell, R. C., Peterson, L. C., Muller-Karger, F., Astor, Y., and Varela, R., 2007. Modern climate forcing of terrigenous deposition in the tropics (Cariaco Basin, Venezuela). *Earth Planet. Sci. Lett.*, 264:438–451. doi:10.1016/j.epsl.2007.10.002

Murray, R.W., and Leinen, M., 1996. Scavenged excess aluminum and its relationship to bulk titanium in biogenic sediment from the central equatorial Pacific Ocean. *Geochim. Cosmochim. Acta*, 60(20):3869–3878. doi:10.1016/0016-7037(96)00236-0

Pälike, H., Lyle, M., Nishi, H., Raffi, I., Gamage, K., Klaus, A., and the Expedition 320/321 Scientists, 2010. *Proc. IODP,* 320/321: Washington, DC (Integrated Ocean Drilling Program Management International, Inc.). doi:10.2204/iodp.proc.320321.2010

Revillon, S., Barr, S., Brewer, T., Harvey, P., and Tarney, J., 2002. An alternative approach using integrated gamma-ray and geo-chemical data to estimate the inputs to subduction zones from ODP Leg 185, Site 801. *Geochem. Geophys. Geosyst.*, 3(12):8902. doi:10.1029/2002GC000344

Rudnick, R. L., and Gao, S., 2003. Composition of the continental crust. *In* Rudnick, R.L. (Ed.), *Treatise on Geochemistry, vol. 3, The Crust*. Amsterdam (Elsevier), 1–64.

Sakamoto, T., Saito, S., Shimada, C., and Yamane, M., 2003. Core-log integration of natural gamma ray intensity to construct a 10-my continuous sedimentary record off Sanriku, Western Pacific Margin, ODP Sites 1150 and 1151. *Proc. ODP, Sci. Results,* 186: College Station, TX (Ocean Drilling Program).

Sambridge, M., and Mosegaard, K., 2002. Monte Carlo methods in geophysical inverse problems. *Rev. Geophys.*, 40(3):1–29. doi:10.1029/2000RG000089

Taylor, S. R., and McLennan, S. M., 1985. *The Continental Crust: Its Composition and Evolution. An Examination of the Geochemical Record Preserved in Sedimentary Rocks:* Oxford (Blackwell Scientific Publications, Inc.).

Vasiliev, M. A., Blum, P., Chubarian, G., Olsen, R., Bennight, C., Cobine, T., Fackler, D., et al., 2011. A new natural gamma radiation measurement system for marine sediment and rock analysis. *J. Applied Geophys.*, 75(3):455–463. doi:10.1016/j.jappgeo.2011.08.008

Williams, T. J., and Winckler, G., 2012. Characterization of natural gamma radioactivity and [230]Th in the top of the sediment column in the eastern equatorial Pacific [Paper presented at 2012 Fall Meeting, AGU, San Francisco, 3–7 December 2012]. Abstract PP22A-03.

Wilson, S. A., 1997. Data compilation for USGS reference material BHVO-2, Hawaiian Basalt: *U.S. Geol. Survey Open-File Rept.*

Ziegler, C. L., Murray, R. W., Hovan, S. A., and Rea, D. K., 2007. Resolving eolian, volcanogenic, and authigenic components in pelagic sediment from the Pacific Ocean. *Earth Planet. Sci. Lett.*, 254:416–432. doi:10.1016/j.epsl.2006.11.049

Authors

Ann G. Dunlea, and **Richard W. Murray**, Department of Earth and Environment, Boston University, Boston, MA 02066, U.S.A., e-mail: adunlea@bu.edu; rickm@bu.edu

Robert N. Harris, College of Earth, Ocean, and Atmospheric Sciences, Oregon State University, Corvallis, OR 97331, U.S.A., e-mail: rharris@coas.oregonstate.edu

Maxim A. Vasiliev, (Currently) Baker Hughes, Inc., Houston, TX 77073, U.S.A., e-mail: maxim.vasilyev@baker hughes.com

Helen Evans, Lamont-Doherty Earth Observatory, Palisades, NY 10964, U.S.A., e-mail: helen@ldeo.columbia.edu

Arthur J. Spivack, and **Steven D'Hondt**, Graduate School of Oceanography, University of Rhode Island, Narragansett, RI 02882, U.S.A., e-mail: spivack@gso.uri.edu; dhondt@gso.uri.edu

Scientific Drilling and Related Research in the Samail Ophiolite, Sultanate of Oman

by Peter Kelemen, Ali Al Rajhi, Marguerite Godard, Benoit Ildefonse, Jürgen Köpke, Chris MacLeod, Craig Manning, Katsu Michibayashi, Sobhi Nasir, Everett Shock, Eiichi Takazawa, and Damon Teagle

Summary

This workshop report describes plans for scientific drilling in the Samail ophiolite in Oman in the context of past, current, and future research. Long-standing plans to study formation and evolution of the Samail crust and upper mantle, involving igneous and metamorphic processes at an oceanic spreading center, have been augmented by recent interest in ongoing, low temperature processes. These include alteration and weathering, and the associated sub-surface biosphere supported by chemical potential energy due to disequilibrium between mantle peridotite and water near the surface. This interest is motivated in part by the possibility of geological carbon capture and storage via engineered, accelerated mineral carbonation in Oman.

Our International Continental Drilling Program (ICDP) proposal led to the Workshop on Scientific Drilling in the Samail Ophiolite in Palisades, New York, on 13–17 September 2012. There were seventy-seven attendees from eleven countries, including twenty early career scientists.

After keynote presentations on overarching science themes, participants in working groups and plenary sessions outlined a ~U.S.$2 million drilling plan that practically addresses testable hypotheses and areas of frontier discovery in the following areas.

- understanding the subsurface biosphere
- characterizing the rates and mechanisms of ongoing mineral hydration and carbonation
- characterizing chemical and physical processes of mass transfer across a subduction zone
- evaluating well-posed hypotheses on hydrothermal circulation, cooling, and emplacement mechanisms of igneous rocks in the lower crust
- investigating key problems in the dynamics of mantle flow and melt transport beneath oceanic spreading ridges

This report places these goals in the context of complementary research via ocean drilling and ongoing studies of active processes at oceanic spreading centers, subduction zones, and peridotite-hosted hydrothermal systems. We end

with an outline of the synergy between Oman drilling and the specific drilling proposed in the Integrated Ocean Drilling Program (IODP) proposal "Mohole to Mantle Project (M2M)", IODP Proposal 805-MDP.

Workshop Proceedings and Results

Keynote speakers outlined hypotheses and areas of frontier scientific exploration to be addressed via drilling, including

- the nature of mantle upwelling,
- the chemical and physical mechanisms of mantle melt transport,
- the processes of lower crustal accretion and cooling,
- the frequency and magnitude of microseismicity during weathering,
- the rate and location of ongoing alteration, and
- the composition, density, and spatial distribution of subsurface microbial communities.

Additional keynote talks covered state-of-the-art geological logging of drillcore, geophysical logging in boreholes, and data management.

Breakout groups considered overarching science themes, then designed idealized projects to address these themes,
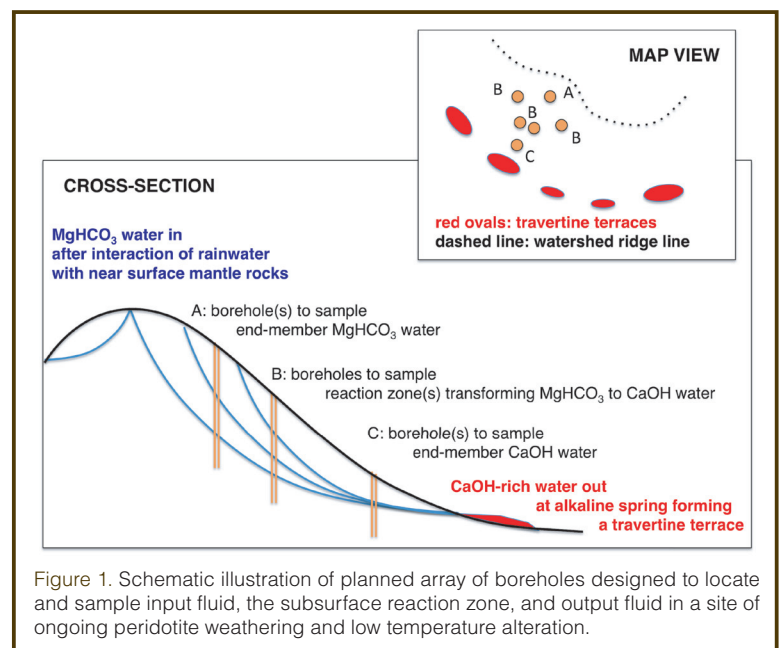

Figure 1. Schematic illustration of planned array of boreholes designed to locate and sample input fluid, the subsurface reaction zone, and output fluid in a site of ongoing peridotite weathering and low temperature alteration.

and finally considered practical constraints. We agreed to focus on studies relevant to global processes. There was a consensus that to achieve the desired goals for this project, core must be logged to the IODP standard by dedicated science teams, and there must be extensive geophysical logging and experiments in boreholes. We planned for individual holes extending to a maximum of 600 m using local drilling technology and expertise, reasoning that current understanding of variation with depth does not warrant the extra expense required to import specialized equipment and engineers required for deeper holes. After wireline diamond drilling with continuous coring, it will be necessary to widen some holes or to drill parallel holes without coring, by rotary-drilling in order to obtain the ~15-cm diameter required for many geophysical logging tools and likely downhole experiments.

We derived an approximate value of USD $250 per meter for continuous coring, based on approximate, informal estimates from two contractors operating in Oman. Using this estimate, the three final breakout groups were charged with designing a "Phase I" drilling program costing USD $2 million. In a striking demonstration of consensus, all three recommended similar plans. Despite interest in the more complex, polygenetic northern massifs of the ophiolite, all three groups focused on drilling in the simpler southern massifs during Phase I.

To investigate active peridotite weathering, all three groups favored drilling multiple holes of moderate length in a peridotite catchment hosting alkaline springs to locate reaction zones where $MgHCO_3$ ground water is transformed to CaOH alkaline water (Fig. 1). A few holes would later be deepened to investigate the variation of processes with depth, and widened to permit geophysical logging and downhole experiments. "Clean" rotary holes, drilled using air or high purity drinking water as lubricants, might be used to supplement diamond-cored holes to allow for easier and more accurate characterization of fluid compositions and the subsurface biosphere.

All groups prioritized 600-m holes through key transitions in the ophiolite: the dike-gabbro transition, the crust-mantle transition, and the basal thrust. They also prioritized 600-m holes in selected parts of the more homogeneous lower crustal gabbro and mantle sections. Some of these would be widened for logging to learn the nature of gaps in core recovery and allow for regional characterization of variability in hydrology, fluid composition, and subsurface biosphere as a function of lithology and location. All groups recommended that some of these longer "lithology" holes should be supplemented by shorter holes to characterize the nature and extent of lateral heterogeneity.
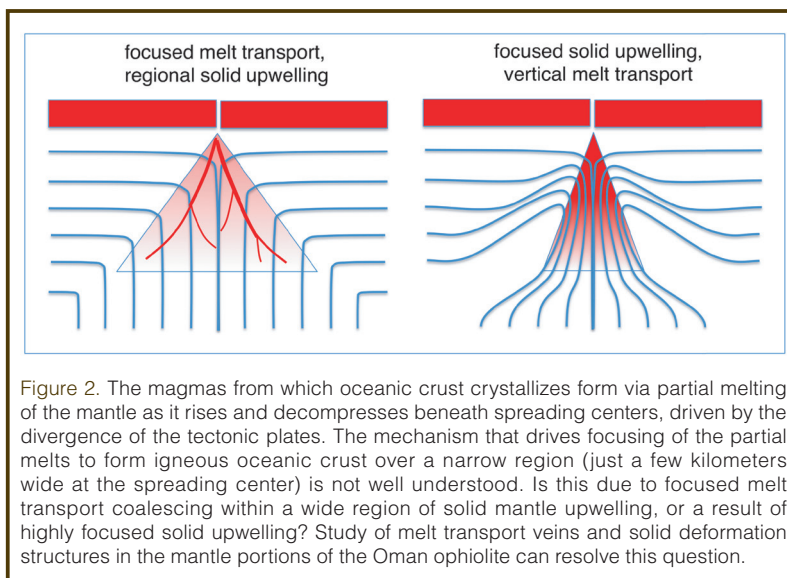

Figure 2. The magmas from which oceanic crust crystallizes form via partial melting of the mantle as it rises and decompresses beneath spreading centers, driven by the divergence of the tectonic plates. The mechanism that drives focusing of the partial melts to form igneous oceanic crust over a narrow region (just a few kilometers wide at the spreading center) is not well understood. Is this due to focused melt transport coalescing within a wide region of solid mantle upwelling, or a result of highly focused solid upwelling? Study of melt transport veins and solid deformation structures in the mantle portions of the Oman ophiolite can resolve this question.

A popular idea among workshop participants was to send both core and scientists to use the IODP research drilling vessel *JOIDES Resolution* (JR) during the time that the vessel is in port (approximately four months per year). In addition to the efficiency of using the dedicated core logging facilities on the JR, this idea appealed to us because it would include housing, meals, and potential 24-hour operations for a science party dedicated to the task at hand. This plan is incorporated in our full proposal to the ICDP.

Processes at Oceanic Spreading Centers

The Samail ophiolite, in the Sultanate of Oman and the United Arab Emirates, is the world's largest subaerial exposure of oceanic crust and upper mantle. As for other ophiolites, the presence of continuous layers of pelagic and metalliferous sediments, submarine lavas, sheeted dikes, and cumulate gabbros overlying residual mantle peridotite is similar to crust formed at intermediate- to fast-spreading, mid-ocean ridges (Nicolas et al., 2000). Geochemical data suggest that the crust also has affinities with magmatic rocks in back-arc or fore-arc basins (Koepke et al., 2009; Pearce et al., 1981). The ophiolite has long been a testing ground for hypotheses about processes at spreading centers, including the following.

- ductile flow in the upper mantle (focused vs. plate-driven upwelling; Fig. 2)
  [Ceuleneer et al., 1996; Nicolas and Violette, 1982]
- melt extraction and transport in the mantle (cracks vs. porous conduits)
  [Braun and Kelemen, 2002; Kelemen et al., 1995; Nicolas, 1986]
- accumulation of melt in the crust-mantle transition zone
  [Boudier and Nicolas, 1995; Korenaga and Kelemen, 1997]
- deformation of the lower crust (gabbro glacier vs. sheeted sills; Fig. 3)

[Kelemen et al., 1997; Nicolas et al., 1988]

- near-ridge hydrothermal circulation and alteration (shallow vs. deep; Fig. 4)
  [Bosch et al., 2004; Coogan et al., 2002; Manning et al., 2000; VanTongeren et al., 2008]
- melt transport, porosity, and crystallization in lower crustal cumulates
  [Korenaga and Kelemen, 1998; Nicolas and Ildefonse, 1996]
- freezing, intrusion, stoping, and metamorphism at the dike-gabbro transition (Fig. 5)
  [Boudier and Nicolas, 2011; France et al., 2009; MacLeod and Rothery, 1992; MacLeod and Yaouancq, 2000]
- formation of chemical layering within the volcanic section
  [Alabaster et al., 1982; Godard et al., 2003]

Given the evident similarities and differences between the Samail ophiolite and mid-ocean ridges, investigations of the Samail ophiolite have generated hypotheses about ridge processes that are tested via seagoing research, and in turn observations from the oceans lead to refinement or modification of ideas about the ophiolite.

Proposed investigations in drillcore samples of the Oman mantle section include studies combining geochemistry to characterize mantle heterogeneity and crystallographic pre-ferred orientations indicative of solid state mantle flow trajectories, and studies of the relative age and spatial relationships of melt transport features. The results will allow us to evaluate the nature and importance of "mantle diapirs" in Oman and to test hypotheses for the processes by which partial melt from a region hundreds of kilometers wide in the mantle is focused into a 2–4 km-wide zone of crustal accretion along oceanic spreading ridges (Fig. 2).

Analyses of drillcore from the Oman lower crust will be used to address well-posed, long-standing, unresolved questions. These pertain to (1) the extent of porous flow versus magmatic injection in dikes and sills, (2) the extent of solid-state versus crystal mush deformation of the lower crust and its variation with depth in the crustal section (Fig. 3), (3) the modification of lower crustal composition during hydrothermal alteration, (4) the transition from relatively coarse gabbros to fine-grained sheeted dikes, and (5) the role of fluids in controlling the nature and rate of cooling of the lower crust. These factors provide the primary controls on heat and mass input from the mantle to the oceans, but their extent and interplay remain controversial after decades of discussion. Study of the pattern of chemical variation with depth, the extent of crystallographic preferred orientation, and zoning within minerals indicative of cooling rates over a variety of different temperature intervals should provide clear resolution of these issues, or at least comprehensive constraints on remaining hypotheses.
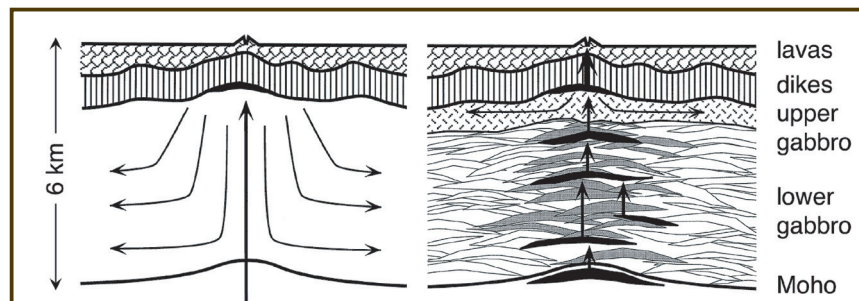

Figure 3. The lower oceanic crust forms from subsurface crystallization of igneous rock beneath spreading centers, forming gabbros. The site of crystallization is poorly known. Does all of the crystallization occur in a "shallow melt lens" near the surface, where heat can be extracted efficiently, after which gabbros undergo ductile flow downward and outward (left), or do gabbros crystallize in many stacked melt lenses throughout the crust (right)? Studies of chemical variation and crystal orientation in the lower crust of the Oman ophiolite can resolve this question. Modified from Kelemen et al. (1997).
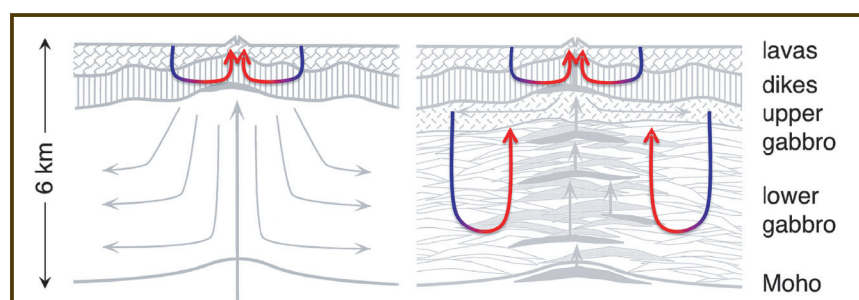

Figure 4. Crystallization of gabbros in a shallow melt lens requires rapid removal of heat by hydrothermal convection in the upper crust. Crystallization of gabbros at a range of depths requires hydrothermal circulation down to the base of the crust. Measurement of mineral zoning in Oman gabbros, interpreted in terms of cooling rates, will resolve which was predominant.

Mass Transfer into the Shallow Mantle above Subduction Zones

A close correspondence between 96–95-Ma igneous ages in the crust, and the oldest ages of metamorphic rocks along the basal thrust (~95–94 Ma), indicate that thrusting of the ophiolite over adjacent oceanic crust and nearby sedimentary rocks began during or immediately after initial formation of igneous crust (Rioux et al., 2012a, 2012b). Metamorphic rocks emplaced along the basal thrust, between overlying peridotite and underlying metasediments, record hot subduction zone conditions up to $800°C–900°C$ and $650–900$ MPa (Ghent and Stout, 1981; Hacker and Gnos, 1997). In some localities at much shallower depths and lower temperatures, hanging wall peridotites underwent 100% carbonation at $100°C–200°C$ to form rocks composed entirely of magnesite + quartz + chromite (Kelemen et al., 2011; Fig. 6), suggesting that the "leading edge of the mantle wedge" may be a globally important, hitherto unappreciated reservoir for carbon.

Mapping and sampling outcrops of the basal thrust, spanning the contact between metasediments and the overlying mantle (Fig. 7), will allow direct study of chemical and physical processes of mass transfer in a subduction zone. Because the thrust beneath the Samail ophiolite was young and hot, observations there will be interpreted in the context provided by investigations of other settings, especially along active subduction zones in different stages of evolution. In the context of research to be addressed via drilling in Oman, ideas and observations outlined above can be quantified via detailed 1-D geochemical and structural transects in drillcore(s), combined with detailed mapping of the surrounding 3-D geology. Of particular interest will be identifying the footwall source(s) of carbon-rich fluids, the mechanical processes of fluid migration, the diffuse or localized nature of hanging wall alteration, the overall balance of low temperature mass transfer, the pressure and temperature range over which mass transfer was active, and the extent to which Oman observations can be extrapolated to subduction zones worldwide.

Figure 5. Gabbros intruding and stoping blocks of hydrothermally altered sheeted dikes in the Wadi Gideah section of the Wadi Tayin massif. Studies of such dike-gabbro transitions will provide essential information on the nature of heat and mass transfer between oceanic lower crust, upper crust, and the oceans. From France et al. (2009).

Ongoing Weathering and Present-Day Hydrology

Pioneering studies of peridotite-hosted alkaline springs (Neal and Stanger, 1985; Fig. 8a) and bedrock hydrology (Dewandel et al., 2005) in the ophiolite are now commonly-cited foundations for research on weathering of peridotites, focused primarily on mineral hydration (serpentinization), mineral carbonation, and generation of H_2 and CH_4 (Boudier et al., 2010; Kelemen et al., 2011; Oeser et al., 2012). Closed-system interpretation of ^{14}C data yields ages of 0 kyr to >50 kyr for carbonate veins in serpentinized peridotites (Fig. 8b), with an average of about 26 kyr, and a similar range in ages of travertine terraces at alkaline
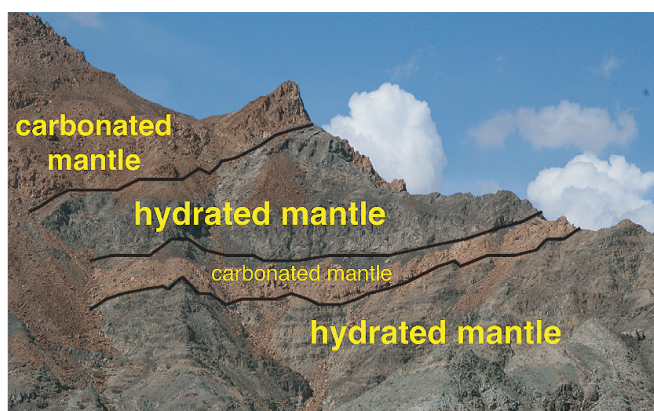

Figure 6. Fully carbonated lenses (magnesite + quartz + chromian spinel) within partially serpentinized mantle peridotite, near the base of the Samail mantle section where peridotites were thrust over metasediments. The lenses are parallel to the basal thrust. The thinner lower lens is about 10 m thick; the thicker upper lens is about 200 m thick. Together, they contain about one billion tons of CO_2 in solid carbonate minerals.

springs (Clark and Fontes, 1990; Kelemen and Matter, 2008; Kelemen et al., 2011). These young ages are consistent with mineral thermometry indicating near-surface crystallization at 20°C to 60°C (Streit et al., 2012), and with observations of alkaline spring water (Paukert et al., 2012), demonstrating that subsurface serpentinization and mineral carbonation are active, ongoing processes in Oman. Perhaps this is not surprising, given the huge reservoir of chemical potential energy represented by outcrops of peridotite far from equilibrium with the high fO_2, fH_2O and fCO_2 in the atmosphere and surface waters. Presumably, the resulting steep chemical gradients, particularly in redox potential, support an abundant and unique subsurface microbial ecosystem, but in Oman this is essentially terra incognita, and studies of similar niches elsewhere have yielded strikingly low cell densities and species diversity (D. Cardace, M. Schrenk, A. Templeton, I. Tiago, pers. comm., 2012).

Biogeoscience

There is increasing recognition that investigating ongoing alteration and the related subsurface microbial ecosystem in the Samail ophiolite holds as much promise—for contributing to fundamental understanding of global processes—as studying the Cretaceous formation and evolution of oceanic plates in Oman. On-land studies will complement observations from similar, submarine systems. Thus, proposed IODP drilling of Atlantis Massif in the vicinity of the Lost City hydrothermal system (IODP Proposal 758-Full2), a site of ongoing peridotite alteration near the Mid-Atlantic Ridge, will form a fertile partnership with studies of similar systems in Oman.

Investigations of ongoing alteration and the associated subsurface biosphere are ideally suited to studies of cores and in boreholes. Cores will be used to observe the vertical extent and distribution of vein lithologies and diffuse alteration, small-scale variation of fracture density and permeability, and the pore-scale habitat of microbial communities. Downhole measurements and fluid sampling will determine the multi-scale variation of fluid composition and flow, crack-aperture, porosity, permeability, temperature, stress, microbial density, and species diversity. In-hole experiments will determine geochemical transport properties and allow

microbial culture and incubation experiments. Hole-to-hole measurements will characterize the nature and frequency of natural fracture events due to volume changes during ongoing alteration, changing temperature, and precipitation events. They will also monitor microseismicity induced by fluid injection for permeability and geomechanical measurements, and monitor the results of reactive tracer experiments.

Figure 7. Reddish area indicates approximate position of the Samail mantle section during thrusting over the metamorphic sole and metasediments of the Hawasina Group. Study of alteration of hanging wall peridotites underlying metasediments will provide an essential complement to studies of mass transfer in subduction zones worldwide. Modified from Oakley et al. (2007).

Again, this very specific list of achievable, observational goals can be placed in a broader context. The factors we will measure control mass transfer between the atmosphere, the hydrosphere, and the lithosphere in the near surface environment. They determine why some rocks preserve high temperature and pressure mineral equilibria, while others undergo complete hydration and carbonation to form mineral assemblages in equilibrium with surface waters, generating microbial habitats in the process. They control the rates of chemical and mechanical weathering and feedback between these processes.

From a biogeoscience point of view, there is plenty of energy available for chemosynthesis in Samail peridotites near the surface (Ménez et al., 2012; Okland et al., 2012; Schulte et al., 2006; Shock, 1996). And, strikingly, the combination of low fO_2, reduced carbon species, and the presence of FeNi metal alloys (common during peridotite alteration) promotes abiotic synthesis of complex hydrocarbon species (McCollom et al., 2010). Why have studies of peridotite alteration environments elsewhere found so little life? Are there nutrient limitations, or toxic constituents? Have investigators looked in the wrong places, or is this energetic but geochemically extreme environment inaccessible along almost all available evolutionary pathways?

Mineral Carbonation in Peridotite for Geological Carbon Capture and Storage

The previous sections of this paper describe natural systems in which alteration has converted silicates in peridotite into Mg-Ca carbonate minerals, both in a ~200°C subduction zone setting and in the present day weathering environment. It has been proposed that understanding these natural mineral carbonation systems in Oman, which in some cases have formed carbonate minerals from all of the Mg and Ca present in peridotite protoliths, can provide insight into design of potential, engineered systems for geological capture and storage of carbon springs (Kelemen and Matter, 2008; Kelemen et al., 2011). It seems likely that reactions that increase solid mass and decrease solid density will grind to a halt, consuming porosity, destroying permeability, and armoring reactive surfaces with reaction products. However,
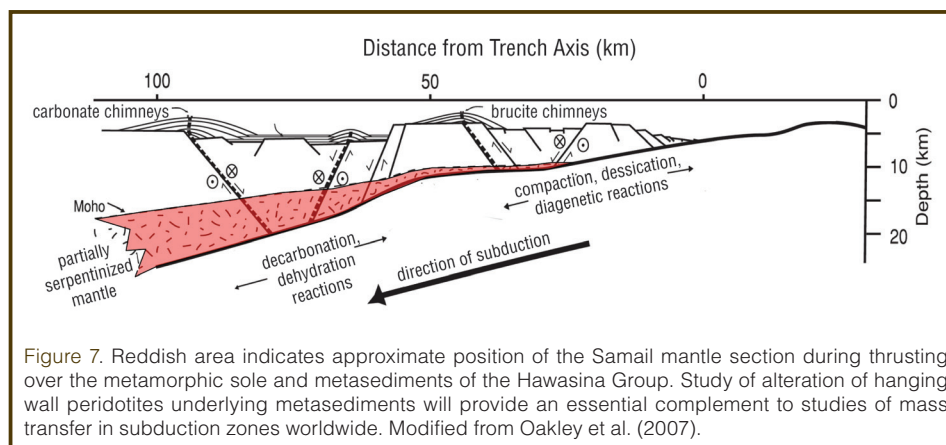
the presence of fully carbonated and hydrated (serpentinized) peridotites demonstrate that this is not always the case.

Under what conditions do natural systems avoid these negative feedbacks and produce 100% carbonation? One key seems to be that, under some circumstances, increasing solid volume—due to addition of H_2O and CO_2, and to decreasing solid density—leads to increasing stress and fracture, which in turn provides continuing access for fluids to reactive mineral surfaces in a positive feedback mechanism that produces a network of fractures at the grain scale (Kelemen and Hirth, 2012). Understanding reaction-driven cracking is important for engineered, *in situ* mineral carbonation but also could be applied to extraction of unconventional hydrocarbon resources and improving geothermal power generation. However, the conditions that lead to runaway, reaction-driven cracking are poorly understood.

How might we engineer these conditions? What would be the environmental impacts of rapid, large-scale peridotite carbonation, for example, in terms of fluid composition and/or rock deformation?

More information on this topic can be found in the report of the Workshop on Geological Carbon Capture and Storage in Mafic and Ultramafic Rocks (see Related Web Links).
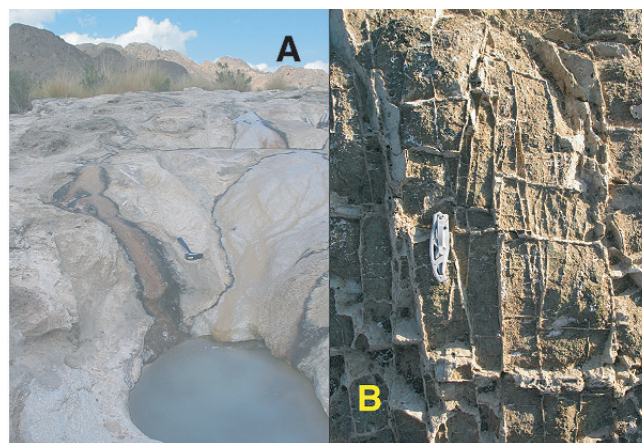

Figure 8. [A] Travertine at an alkaline spring in a peridotite catchment, near the village of Falaij, Oman. [B] Carbonate veins in serpentinized peridotite, near the town of Birkat al Mawz, Oman.

Synergy with the IODP Science Plan

Finally, most of the proposed drilling within the Samail ophiolite and associated scientific objectives should be seen in the context of the IODP Science Plan 2013–2023 and the specific IODP drilling Proposal 805-MDP, which proposed the Mohole to the Mantle Project (M2M), for drilling a complete section of oceanic crust into the underlying mantle in the Pacific. While Oman drilling and ocean drilling into the mantle are very different in their overall scale, technological requirements, and associated budgets, they are also extremely complementary. Oman drilling provides an opportunity to evaluate IODP strategies at a relatively low risk. Scientists often ask, what can be learned from a one-dimensional sample through a three-dimensional object such as an oceanic plate? One clear and valid answer, of course, is that if you don't go, you won't ever know. But scientific drilling in the Samail ophiolite provides opportunities for a more subtle and quantitative response. In Oman, we can make observations in drillcore, and then in many cases map the surrounding three-dimensional geology at any desired scale. Thus, we can determine—just as a simple example—the statistics of serpentine vein density in olivine in 100 m of drillcore, and compare them to the values for samples from surrounding outcrops with significant structural relief at a density of one sample (or 10, or 100, or 1000) per km^3. Such comparisons can provide a statistically valid answer to the question, how representative is a single drillcore, and hence, help guide coring and offset hole strategies and the choice of geophysical logging techniques within a full crustal drill hole in the oceans.

Likewise, the hypothesis that ophiolites are closely analogous to *in situ* oceanic crust has often been challenged because most, if not all, ophiolites are believed to have formed in supra-subduction zone environments. Also, the Samail ophiolite was affected by thrust tectonics during or very soon after its formation. Yet, the layered structure of ophiolites, and particularly the Samail ophiolite, has been central to our paradigm for the structure of Pacific Ocean crust. How representative are specific features of ophiolites, with respect to "normal" oceanic crust formed at mid-ocean ridges such as the East Pacific Rise? This question can be dramatically addressed by sampling oceanic lower crust and upper mantle in the Pacific. This endeavor is one of the major challenges highlighted in the IODP Science Plan 2013–2023, and the topic of IODP Proposal 805-MDP. Meanwhile, we will continue the decades-long, highly productive dialogue in which ophiolite studies lead to hypotheses and issues best addressed by seagoing studies, and in which marine observations inform ongoing ophiolite research. Ophiolite drilling can provide a 3-D understanding of the scale of crustal and mantle heterogeneity that is difficult or impossible to achieve via ocean drilling. Drilling in Oman will use simple, locally available technology, at about two orders of magnitude lower cost than drilling through Pacific crust. By contrast, drilling through the crust and into the mantle in the Pacific will pro-vide unique samples from an environment that has never been visited, and which is more inaccessible and much less well known than the surface of the Moon.

Conclusion

Our workshop and the related full proposal to the ICDP have outlined a community consensus plan for scientific drilling in the Samail ophiolite in the Sultanate of Oman. Drilling will address long-standing, well-posed questions about the nature of solid upwelling and focused melt transport in the mantle beneath spreading centers, the igneous and metamorphic processes essential to the formation of oceanic lower crust in an intermediate- to fast-spreading environment, and ongoing processes of weathering and alteration of mantle peridotite exposed to reaction with surface waters. Understanding natural weathering processes, including mineral carbonation, can aid in future design of proposed engineered systems for geological carbon capture and storage and, more generally, design of systems using "reaction-driven cracking" to create a fracture network at the grain scale to extract unconventional hydrocarbon resources and improve geothermal power generation. We will explore the frontier area of microbial ecology within peridotite undergoing active alteration, with implications for abiotic hydrocarbon synthesis, the origin of life, and life in extreme environments. Oman drilling has synergies with IODP projects, including proposed drilling at the Lost City hydrothermal system in the Atlantic. It will provide an inexpensive and immediate opportunity to greatly optimize hole design, coring and logging programs for drilling into the mantle within Pacific ocean crust, and thus additionally provide a much needed context for reaping the maximum scientific benefits from that huge technical and financial endeavor in the future.

Acknowledgements

References

Alabaster, T., Pearce, J. A., and Malpas, J., 1982. The volcanic stratigraphy and petrogenesis of the Oman ophiolite complex. *Contrib. Mineral. Petrol.*, 81(3):168–183. doi:10.1007/BF00371294

Bosch, D., Jamais, M., Boudier, F., Nicolas, A., Dautria, J.- M., and Agrinier, P., 2004. Deep and high-temperature hydrothermal circulation in the Oman ophiolite: Petrological and isotopic evidence. *J. Petrol.*, 45(6):1181–1208. doi:10.1093/petrology/egh010

Boudier, F., and Nicolas, A., 1995. Nature of the Moho transition zone

in the Oman ophiolite. *J. Petrol.*, 36(3):777–796. doi:10.1093/petrology/36.3.777

Boudier, F., and Nicolas, A., 2011. Axial melt lenses at oceanic ridges - A case study in the Oman ophiolite. *Earth Planet. Sci. Lett.*, 304(3–4):313–325. doi:10.1016/j.epsl.2011.01.029

Boudier, F., Baronnet, A., and Mainprice, D., 2010. Serpentine mineral replacements of natural olivine and their seismic implications: Oceanic lizardite versus subduction-related antigorite. *J. Petrol.*, 51(1–2):495–512. doi:10.1093/petrology/egp049

Braun, M. G., and Kelemen, P. B., 2002. Dunite distribution in the Oman ophiolite: Implications for melt flux through porous dunite conduits. *Geochem. Geophys. Geosyst.*, 3:8603. doi:10.1029/2001GC000289

Ceuleneer, G., Monnereau, M., and Amri, I., 1996. Thermal structure of a fossil mantle diapir inferred from the distribution of mafic cumulates. *Nature*, 379:149–153. doi:10.1038/379149a0

Clark, I. D., and Fontes, J.- C., 1990. Paleoclimatic reconstruction in northern Oman based on carbonates from hyperalkaline groundwaters. *Quat. Res.*, 33(3):320–336. doi:10.1016/0033-5894(90)90059-T

Coogan, L., Jenkin, G. R. T., and Wilson, R. N., 2002. Constraining the cooling rate of lower oceanic crust: A new approach applied to the Oman ophiolite. *Earth Planet. Sci. Lett.*, 199(1–2):127–146. doi:10.1016/S0012-821X(02)00554-X

Dewandel, B., Lachassagne, P., Boudier, F., Al-Hattali, S., Ladouche, B., Pinault, J.- L., and Al-Suleimani, Z., 2005. A conceptual hydrogeological model of ophiolite hard-rock aquifers in Oman based on a multiscale and a multidisciplinary approach. *Hydrogeol. J.*, 13(5–6):708–726. doi:10.1007/s10040-005-0449-2

France, L., Ildefonse, B., and Koepke, J., 2009. Interactions between magma and hydrothermal system in Oman ophiolite and in IODP Hole 1256D: Fossilization of a dynamic melt lens at fast spreading ridges. *Geochem. Geophys. Geosyst.*, 10:Q10O19, doi:10.1029/2009GC002652

Ghent, E. D., and Stout, M. Z., 1981. Metamorphism at the base of the Samail ophiolite, southeastern Oman mountains. *J. Geophys. Res.*, 86(B4):2557–2571. doi:10.1029/JB086iB04p02557

Godard, M., Dautria, J.- M., and Perrin, M., 2003. Geochemical variability of the Oman ophiolite lavas: Relationship with spatial distribution and paleomagnetic directions. *Geochem. Geophys. Geosyst.*, 4:8609. doi:10.1029/2002GC000452

Hacker, B. R., and Gnos, E., 1997. The conundrum of samail: Explaining the metamorphic history. *Tectonophysics*, 279(1–4):215–226. doi:10.1016/S0040-1951(97)00114-5

Kelemen, P. B., and Hirth, G., 2012. Reaction-driven cracking during retrograde metamorphism: Olivine hydration and carbonation. *Earth Planet. Sci. Lett.*, 345:81–89. doi:10.1016/j.epsl.2012.06.018.

Kelemen, P. B., and Matter, J., 2008. In situ mineral carbonation in peridotite for CO_2 storage. *Proc. Natl. Acad. Sci. U.S.A.*, 105(45):17295–17300. doi:10.1073/pnas.0805794105

Kelemen, P. B., Koga, K., and Shimizu, N., 1997. Geochemistry of gabbro sills in the crust-mantle transition zone of the Oman ophiolite: Implications for the origin of the oceanic lower crust. *Earth Planet. Sci. Lett.*, 146(3–4):475–488. doi:10.1016/S0012-821X(96)00235-X

Kelemen, P. B., Matter, J., Streit, E. E., Rudge, J. F., Curry, W. B., and Blusztajn, J., 2011. Rates and mechanisms of mineral carbonation in peridotite: Natural processes and recipes for enhanced, *in situ* CO_2 capture and storage. *Ann. Rev. Earth Planet. Sci.*, 39:545–576. doi:10.1146/annurev-earth-092010-152509

Kelemen, P. B., Shimizu, N., and Salters, V. J. M., 1995. Extraction of mid-ocean-ridge basalt from the upwelling mantle by focused flow of melt in dunite channels. *Nature*, 375:747–753. doi:10.1038/375747a0

Koepke, J., Schoenborn, S., Oelze, M., Wittmann, H., Feig, S.T., Hellebrand, E., Boudier, F., and Schoenberg, R., 2009. Petrogenesis of crustal wehrlites in the Oman ophiolite: Experiments and natural rocks. *Geochem. Geophys. Geosyst.*, 10:Q10002, doi:10.1029/2009GC002488

Korenaga, J., and Kelemen, P. B., 1997. Origin of gabbro sills in the Moho transition zone of the Oman ophiolite: Implications for magma transport in the oceanic lower crust. *J. Geophys. Res.*, 102(B12):27729–27749. doi:10.1029/97JB02604

Korenaga, J., and Kelemen, P. B., 1998. Melt migration through the oceanic lower crust: A constraint from melt percolation modeling with finite solid diffusion. *Earth Planet. Sci. Lett.*, 156(1–2):1–11. doi:10.1016/S0012-821X(98)00004-1

MacLeod, C. J., and Rothery, D. A., 1992. Ridge axial segmentation in the Oman ophiolite: Evidence from along-strike variations in the sheeted dyke complex. *Geol. Soc. London Spec. Publ.*, 60:39–63. doi:10.1144/GSL.SP.1992.060.01.03

MacLeod, C. J., and Yaouancq, G., 2000. A fossil melt lens in the Oman ophiolite: Implications for magma chamber processes at fast spreading ridges. *Earth Planet. Sci. Lett.*, 176(3–4):357–373. doi:10.1016/S0012-821X(00)00020-0

Manning, C. E., MacLeod, C. J., and Weston, P. E., 2000. Lower-crustal cracking front at fast-spreading ridges: Evidence from the East Pacific Rise and the Oman ophiolite. *Geol. Soc. Am. Spec. Pap.*, 349:261–272. doi:10.1130/0-8137-2349-3.261

McCollom, T. M., Sherwood-Lollar, B., Lacrampe-Couloumem, G., and Seewald, J. S., 2010. The influence of carbon source on abiotic organic synthesis and carbon isotope fractionation under hydrothermal conditions. *Geochim. Cosmochim. Acta*, 74(9):2717–2740. doi:10.1016/j.gca.2010.02.008

Ménez, B., Pasini, V., and Brunelli, D., 2012. Life in the hydrated sub-oceanic mantle. *Nature Geosci.*, 5:133–137. doi:10.1038/ngeo1359

Neal, C., and Stanger, G., 1985. Past and present serpentinization of ultramafic rocks: An example from the Semail ophiolite nappe of northern Oman. *In* Drever, J. I. (Ed.), *The Chemistry of Weathering:* Dordrecht (D. Reidel Publishing Company), 249–275. doi:10.1007/978-94-009-5333-8_15

Nicolas, A., 1986. A melt extraction model based on structural studies in mantle peridotites. *J. Petrol.*, 27(4):999–1022. doi:10.1093/petrology/27.4.999

Nicolas, A., and Ildefonse, B., 1996. Flow mechanism and viscosity in basaltic magma chambers. *Geophys. Res. Lett.*, 23(16):2013–2016. doi:10.1029/96GL02073

Nicolas, A., and Violette, J. F., 1982. Mantle flow at oceanic spreading centers: Models derived from ophiolites. *Tectonophysics*, 81:319–339. doi:10.1016/0040-1951(82)90136-6

Nicolas, A., Boudier, F., Ildefonse, B., and Ball, E., 2000. Accretion of Oman and United Arab Emirates ophiolite: Discussion of a new structural map. *Mar. Geophys. Res.*, 21(3–4):147–179. doi:10.1023/A:1026769727917

Nicolas, A., Reuber, I., and Benn, K., 1988. A new magma chamber model based on structural studies in the Oman ophiolite. *Tectonophysics*, 151(1–4):87–105. doi:10.1016/0040-1951 (82)90136-6

Oakley, A. J., Taylor, B., Fryer, P., Moore, G. F., Goodliffe, A. M., and Morgan, J. K., 2007. Emplacement, growth, and gravitational deformation of serpentinite seamounts on the Mariana forearc. *Geophys. J. Int.*, 170(2):615–634. doi:10.1111/j.1365-246X.2007.03451.x

Oeser, M., Strauss, H., Wolff, P. E., Koepke, J., Peters, M., Garbe-Schönberg, D., and Dietrich, M., 2012. A profile of multiple sulfur isotopes through the Oman ophiolite. *Chem. Geol.*, 312–313:27–46. doi:10.1016/j.chemgeo.2012.04.008

Okland, I., Huang, S., Dahle, H., Thorseth., I. H., and Pedersen, R. B., 2012. Low temperature alteration of serpentinized ultramafic rock and implications for microbial life. *Chem. Geol.*, 318–319:75–87. doi:10.1016/j.chemgeo.2012.05.015

Paukert, A. N., Matter, J. M., Kelemen, P. B., Shock, E. L., and Havig, J. R., 2012. Reaction path modeling of enhanced in situ CO_2 mineralization for carbon sequestration in the peridotite of the Samail Ophiolite, Sultanate of Oman. *Chem. Geol.*, 330–333:86–100. doi:10.1016/j.chemgeo.2012.08.013

Pearce, J. A., Alabaster, T., Shelton, A. W., and Searle, M. P., 1981. The Oman Ophiolite as a Cretaceous arc-basin complex: Evidence and implications. *Phil. Trans. Roy. Soc. London*, *Ser. A*, 300(1454):299–317. doi:10.1098/rsta.1981.0066

Rioux, M., Bowring, S., Kelemen, P., Gordon, S., Dudás, F., and Miller, R., 2012a. Rapid crustal accretion and magma assimilation in the Oman-U.A.E. ophiolite: High precision U-Pb zircon geochronology of the gabbroic crust. *J. Geophys. Res.*, 117:B07201. doi:10.1029/2012JB009273

Rioux, M., Bowring, S., Kelemen, P., Gordon, S., Miller, R., and Dudás, F., 2012b. Tectonic development of the Samail ophiolite: High precision U-Pb zircon geochronology of crustal growth and ophiolite emplacement, *J. Geophys. Res.*, submitted.

Schulte, M., Blake, D., Hoehler, T., and McCollom, T., 2006. Serpentinization and its implications for life on the early Earth and Mars. *Astrobiology*, 6(2):364–376. doi:10.1089/ast.2006.6.364

Shock, E. L., 1996. Hydrothermal systems as environments for the emergence of life, *In* Bock, G. R., and Goode, J. A. (Eds.), *Evolution of Hydrothermal Systems on Earth (and Mars):* Chichester, U.K. (J. Wiley & Sons Ltd.), vol. 202, 40–60. doi: 10.1002/9780470514986.ch3

Streit, E., Kelemen, P., and Eiler, J., 2012. Coexisting serpentine and quartz from carbonate-bearing serpentinized peridotite in the Samail Ophiolite, Oman. *Contrib. Mineral. Petrol.*, 164(5):821–837. doi:10.1007/s00410-012-0775-z

VanTongeren, J. A., Kelemen, P. B., and Hanghøj, K., 2008. Cooling rates in the lower crust of the Oman ophiolite: Ca in olivine, revisited. *Earth Planet. Sci. Lett.*, 267(1–2):69–82. doi:10.1016/j.epsl.2007.11.034

Authors

Peter Kelemen, Department of Earth & Environmental Sciences, Columbia University, Lamont Doherty Earth Observatory, 211 Comer, 61 Route 9W, P.O. Box 1000, Palisades, NY 10964-8000, U.S.A., e-mail: peterk@ldeo. columbia.edu

Ali Al Rajhi, Geological Survey, Directorate General of Minerals, Ministry of Commerce & Industry, Oman, e-mail: alialrajhi69@yahoo.com

Marguerite Godard, and **Benoit Ildefonse**, Géosciences Montpellier, UMR CNRS-UM2 5243 Université de Montpellier II, cc60, Place Eugéne Bataillon, 34095 Montpellier cedex 5, France, e-mail: mgodard@univ-montp2. fr

Jürgen Köpke, Institut für Mineralogie, Leibniz Universität, Callinstr. 3, D-30167 Hannover, Germany, e-mail: koepke@ mineralogie.uni-hannover.de

Chris MacLeod, School of Earth & Ocean Sciences, Cardiff University, Park Place, Cardiff CF10 3AT, U.K., e-mail: Macleod@cardiff.ac.uk

Craig Manning, Department of Earth & Space Sciences, UCLA, Los Angeles, CA 90095-1567, U.S.A., e-mail: manning@ess.ucla.edu

Katsu Michibayashi, Institute of Geosciences, Shizuoka University, 836 Oya, Suruga-ku, Shizuoka 422-8529, Japan, e-mail: sekmich@ipc.shizuoka.ac.jp

Sobhi Nasir, Department of Earth Sciences, Sultan Qaboos University, Oman, e-mail: sobhi@squ.edu.om

Everett Shock, Department of Chemistry & Biochemistry, Arizona State University, Physical Sciences Building, Room D-102, P.O. Box 871604, Tempe, AZ 85287-1604, U.S.A., e-mail: Everett.Shock@asu.edu

Eiichi Takazawa, Department of Geology, Faculty of Science, Niigata University, Nishi-ku, Igarashi, 2-8050, Niigata 950-2181, Japan, e-mail: takazawa@geo.sc.niigata-u. ac.jp

Damon Teagle, National Oceanography Centre, Southampton, University of Southampton Waterfront Campus, European Way, Southampton SO14 3ZH, U.K., e-mail: Damon.Teagle@southampton.ac.uk

Related Web Links

http://www.iodp.org/abc
http://www.icdp-online.org
http://www.ldeo.columbia.edu/gpg/projects/icdp-workshop-oman-drilling-project
http://www.ldeo.columbia.edu/files/uploaded/image/Oman%20mineral%20carbonation%20workshop%20report.pdf
http://www.mohole.org
http://www.iodp.org/700
http://www.iodp.org/science-plan-for-2013-2023

Photo Credits

All photos of outcrops are by Peter Kelemen

DeepCHALLA: Two Glacial Cycles of Climate and Ecosystem Dynamics from Equatorial East Africa

by Dirk Verschuren, Daniel O. Olago, Stephen M. Rucina, Peter O. Odhengo,
on behalf of the ICDP DeepCHALLA Consortium

Scientific Rationale in Relation to Scientific Themes of the ICDP Workshop

Documenting the geographical variation of past climate change and the structure of its temporal variability is critical for understanding how various external climate forcings, on inter-annual to orbital timescales, are translated into regional climate variability. Long climate records from tropical and sub-tropical continental regions provide a particularly im-portant complement to the polar ice-core records, as they are crucial to resolving long-standing questions about the relative importance of tropical and high-latitude climate processes in generating spatial patterns in climate. This high priority is exemplified by completed International Continental Scientific Drilling Program (ICDP) lake-drilling projects in South and Central America (e.g., Titicaca, Peten Itza) and Africa (e.g., Bosumtwi, Malawi).

One specific geographical area where long continental climate records are still notably scarce is the inter-tropical zone near the equator, where twice-annual passage of tropical convective activity known as the Intertropical Convergence Zone (ITCZ) creates a bimodal seasonal rainfall regime of two wet seasons and two dry seasons. Equatorial East Africa is perhaps the most appropriate region to pursue this equatorial record, because here seasonal ITCZ migration spans the widest latitude range in the world, and hence atmospheric dynamics associated with Northern and Southern Hemisphere monsoon systems most strongly interact. Specifically, these systems are the northeasterly monsoon bringing rainfall during Northern Hemisphere autumn –winter, and the southeasterly monsoon bringing rainfall during its spring–summer.

An extraordinarily well-suited location for an ICDP lake-drilling project near the equator would be Lake Challa (3°S, 36°E), a 4.2-km^2, 94-m-deep crater lake situated at 840 m altitude near Mt. Kilimanjaro (Fig. 1) in eastern equatorial Africa. From 10 to 13 September 2012, twenty-five scientists from eight countries joined twenty-three colleagues and government representatives from Kenya at an ICDP-funded workshop in Nairobi and Taveta to develop the scientific objectives of an ICDP deep-drilling project on Lake Challa (DeepCHALLA), and to discuss technical and logistical issues concerning both the recovery of this sedimentary archive and the establishment of a lake-system monitoring program.

The workshop started with a full day of formal presentations at the National Museums of Kenya on the aims and structure of ICDP itself and the DeepCHALLA project (Fig. 2). In addition, high-resolution (3.5-kHz GeoPulse) seismic data collected in 2005 were used to identify preferred and alternative drilling sites where the profundal sediment stratigraphy is continuous and complete (Fig. 3). On the second day the group visited Lake Challa, where a lively discussion developed on the equipment and logistics

Figure 2. Clockwise: [A] Group photo of participants in the ICDP DeepCHALLA workshop, in front of the Louis Leakey Auditorium of the National Museums of Kenya, host of the workshop. [B] Dr. Gerald Haug presenting the ICDP program. [C] Opening speech by Dr. Idle Omar Farah, Director General of the National Museums of Kenya.
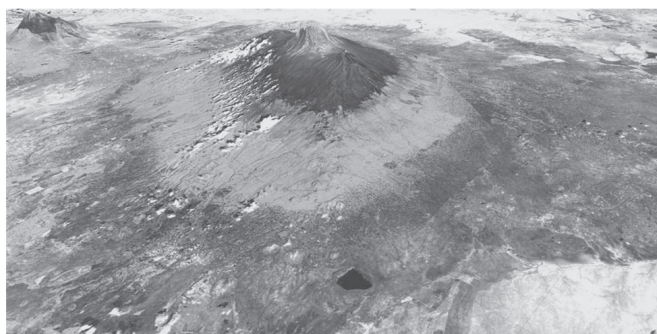
Figure 1. Lake Challa occupying a volcanic caldera, of 2.7 km diameter, at 840 m elevation on the lower east slope of Mt. Kilimanjaro, viewed from the southeast; gray shading reflect vegetation zones.

required to successfully drill the lake's sediment record. Lake Challa is a relatively difficult ICDP target site in terms of access with heavy instrumentation, but this is compensated by quiet lake-surface conditions and the relatively shallow depth of sub-bottom drilling (~210 m; Fig. 3) from an anchored platform. On day three in Taveta, technical presentations were provided by invited scientists. The discussions elaborated the scientific work program and revealed new synergies between different proxies and analytical methods to more reliably reconstruct past climate and ecosystem components. In the final morning session, a strategy was developed for financing of the project via formal collaborations between teams working jointly on particular portions of the project, followed by discussion of outreach and knowledge-transfer opportunities. The workshop ended with an overview of the project consortium, which includes thirty-four principal investigators from eleven countries, of which six are ICDP member countries.
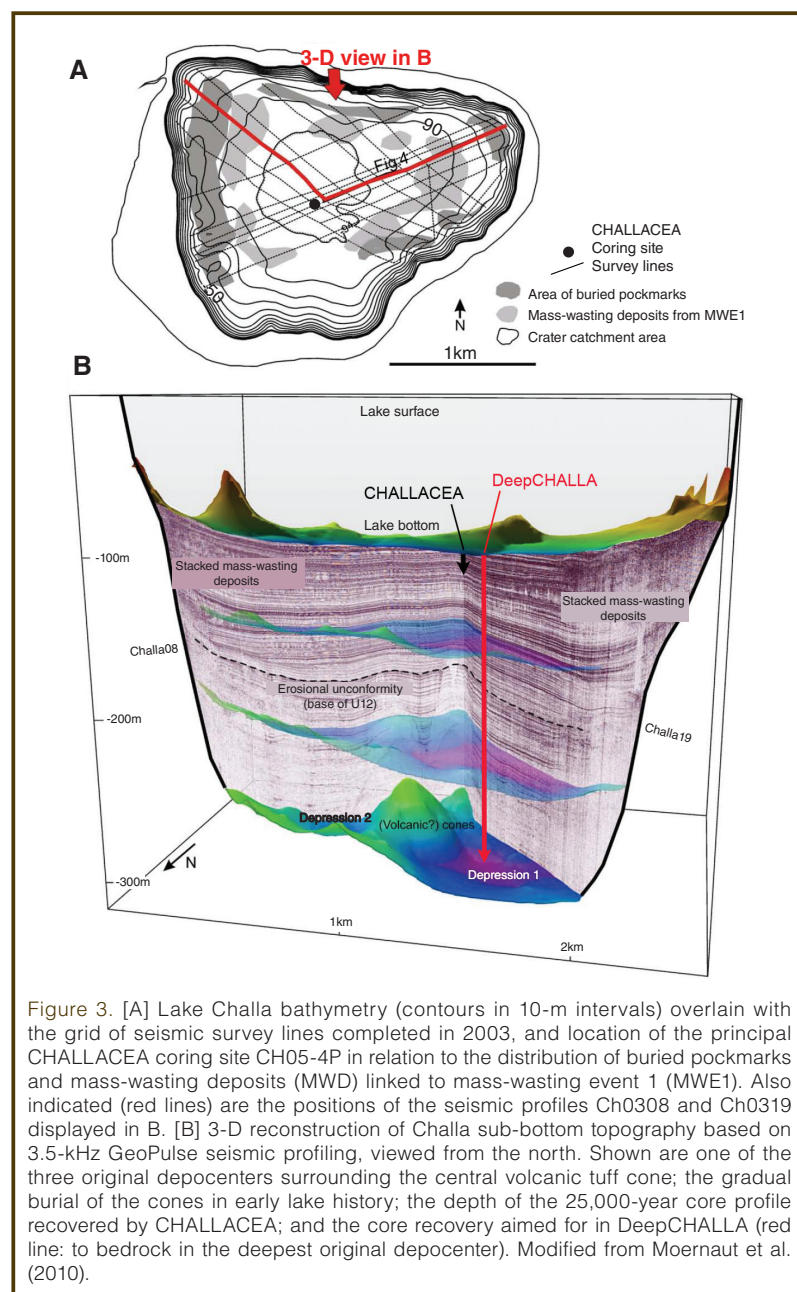

Figure 3. [A] Lake Challa bathymetry (contours in 10-m intervals) overlain with the grid of seismic survey lines completed in 2003, and location of the principal CHALLACEA coring site CH05-4P in relation to the distribution of buried pockmarks and mass-wasting deposits (MWD) linked to mass-wasting event 1 (MWE1). Also indicated (red lines) are the positions of the seismic profiles Ch0308 and Ch0319 displayed in B. [B] 3-D reconstruction of Challa sub-bottom topography based on 3.5-kHz GeoPulse seismic profiling, viewed from the north. Shown are one of the three original depocenters surrounding the central volcanic tuff cone; the gradual burial of the cones in early lake history; the depth of the 25,000-year core profile recovered by CHALLACEA; and the core recovery aimed for in DeepCHALLA (red line: to bedrock in the deepest original depocenter). Modified from Moernaut et al. (2010).

The principal objective of the DeepCHALLA project is to acquire high-resolution and accurately dated proxy data of continental climate and ecosystem change near the Equator over at least one complete glacial-interglacial cycle (150,000 years), with an aim towards extracting the complete record spanning >250,000 years. Such a climate record would encompass the entire known existence of modern humans (*Homo sapiens*) in East Africa.

Lake Challa's proximity to the Indian Ocean ensures that the Congo Air Boundary (CAB), the mostly north-south oriented zone of convection between Atlantic and Indian Ocean moisture sources, is always located to the west. Consequently, the Lake Challa region is little impacted by the climatic effects of changes in tropical Atlantic thermohaline circulaeon, through which signatures of northern hemisphere glaciation are transferred to the adjacent low-latitude continents (Verschuren et al., 2009). This Atlantic influence extends well into the eastern half of the African continent to the Ethiopian highlands and western portions of the East African Plateau (Tierney et al., 2011); therefore, only in the far east of equatorial Africa can we expect to find a climate history relatively unaffected by a strong northern high-latitude signature. DeepCHALLA thus presents unique opportunities to further scientific understanding of long-term climate change within the inter-tropical zone.

Origin and Development of the DeepCHALLA Project

DeepCHALLA is a follow-up initiative to the CHALLACEA project (2005–2008), which used a suite of 22-m hammer-driven piston cores to reconstruct climate and environmental history near the East African equator over the past 25,000 years. CHALLACEA was funded via the EuroCLIMATE program of the European Science Foundation (ESF), and was executed by six principal investigators from four European countries (Belgium, Denmark, Germany, and The Netherlands), plus associate partners in Canada, Kenya, the U.K., and the U.S.A. The project proved highly successful, due partly to the exceptionally well-constrained chronological framework (Blaauw et al., 2011) and partly to integration of a large number of sedimentol-ogical, geochemical, isotopic, and biological proxies, permitting highly detailed palaeoen-vironmental reconstructions and a level of proxy cross-validation that is usually elusive. While CHALLACEA's principal and associate investigators constitute the logical core of the DeepCHALLA collaborative effort, the ICDP exploratory workshop provided the opportunity to solicit involvement from researchers with relevant expertise not presently available in the consor-

tium, such that the expanded consortium covers all the research niches that recovery of the complete Lake Challa sediment record will generate.

Previous Investigations and State of the Art

The long lake records produced by ICDP projects in Africa and South America, plus excellent palaeodata extracted from South American and East Asian speleothems (Cruz et al., 2005; Wang et al., 2008), show that northern and southern tropical regions experienced anti-phased 23,000-year-long moisture-balance cycles. This supports the idea that on orbital timescales the mean annual position of the ITCZ and associated tropical monsoon rainfall mostly responded to precession-driven changes in low-latitude summer insolation (Ruddiman, 2006). The ICDP records from tropical Africa (Cohen et al., 2007; Scholz et al., 2007) also revealed the occurrence of African mega-droughts during the period of incipient glaciation—Marine Isotope Stage (MIS) 5a-d—compared to which the iconic Last Glacial Maximum (LGM) drought may have been quite modest, at least in certain parts of the continent. Geophysical surveying of profundal lacustrine deposits in Lake Challa by the CHALLACEA project produced an exquisite seismic-reflection stratigraphy of lake-level changes over the last 150,000 years (Moernaut et al., 2010). In itself this seismic record (Fig. 4) has sufficient detail already to constrain important aspects of the long-term moisture-balance history of equatorial East Africa, including signatures of local drought during MIS 6 (Peak Penultimate Glaciation), MIS 5a-d (African mega-drought), and MIS 2 (LGM). A striking observation is that near-constant high lake level (inferred moist climate conditions) prevailed between about 98,000 and 20,000 years ago, interrupted only by eight short-lived dry spells, five of which match the timing of Heinrich events 2 to 6. These data demonstrate the high quality of the Lake Challa sediment record with regard to temporal continuity and the stability of sedimentation rates.
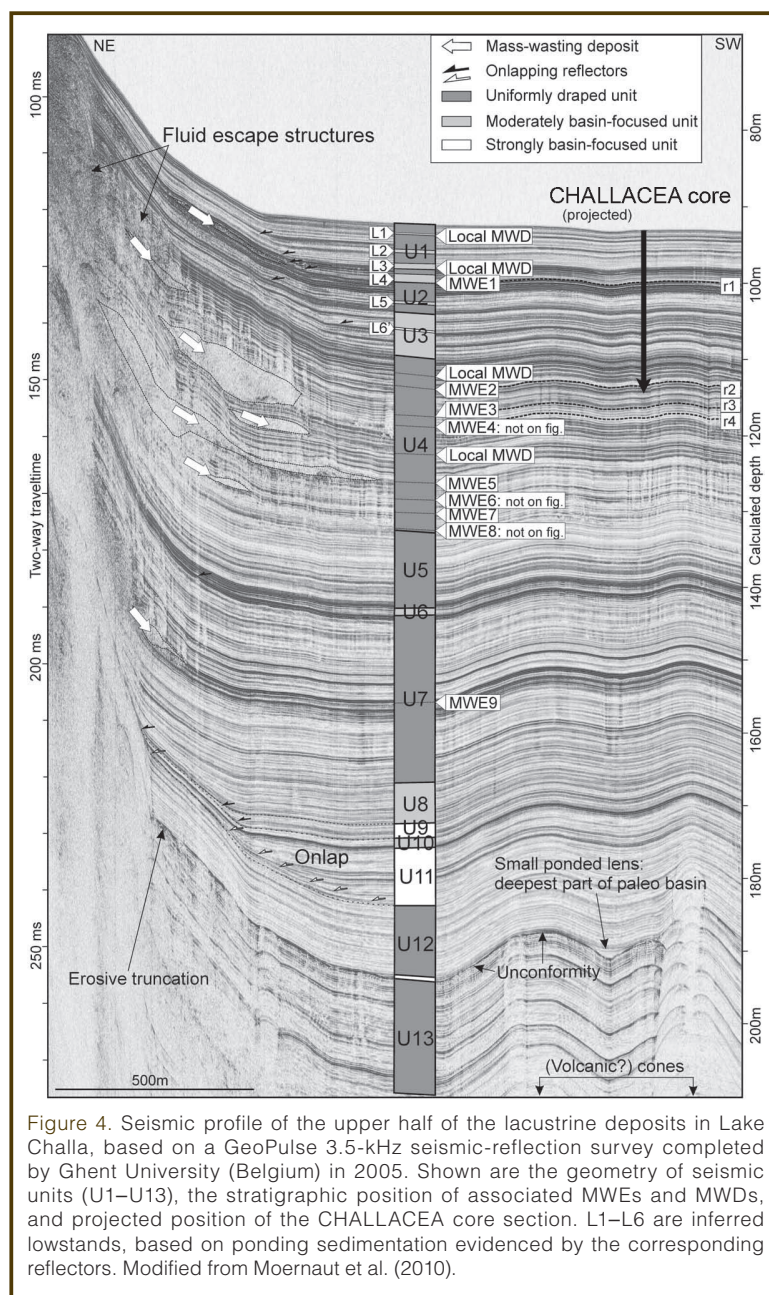

Figure 4. Seismic profile of the upper half of the lacustrine deposits in Lake Challa, based on a GeoPulse 3.5-kHz seismic-reflection survey completed by Ghent University (Belgium) in 2005. Shown are the geometry of seismic units (U1–U13), the stratigraphic position of associated MWEs and MWDs, and projected position of the CHALLACEA core section. L1–L6 are inferred lowstands, based on ponding sedimentation evidenced by the corresponding reflectors. Modified from Moernaut et al. (2010).

Analysis of two independent paleohydrological proxies in the cored upper portion of the Lake Challa sediment sequence (Verschuren et al., 2009) revealed that over the past 25,000 years, rainfall variability in easternmost equatorial Africa followed a hybrid pattern of those typically documented for the northern and southeastern African tropics. Some millennial-scale climate events of high northern-latitude origin impacted strongly on East Africa, such as the Younger Dryas cold episode which is recorded as a severe drought between 13,000 and 11,650 years ago. Overall, however, Challa's moisture-balance history predominantly reflects longer-term variation in low-latitude insolation. Noting that wet and dry episodes alternated at half-precessional (~11,500-year) intervals, Verschuren et al. (2009) suggested that the region enjoyed high rainfall when peak summer insolation over either northern or southern subtropical Africa strengthened southeasterly or northeasterly monsoon flow advecting moist air from the Indian Ocean. Dry climate conditions prevailed between 20,500 and 16,500 years ago and between 8500 and 4500 years ago, when neither monsoon was strong and a minimum in local March or September insolation caused the ensuing rain season to wither.

The clear expression of this characteristically equatorial signature at Lake Challa is attributed to the unique combination of the site's position east of the CAB and the strongly bimodal rainfall seasonality of this semi-arid equatorial region. Also, in this system both the seismic stratigraphy of lake-level fluctuation and the Branched Isoprenoid Tetraether

(BIT) index of glycerol dialkyl glycerol tetraether (GDGT) membrane lipids preserved in bottom sediments appear to reflect past variation in the amount of annual rainfall.

By contrast, a paleohydrological reconstruction based on the oxygen-isotope (δ^{18}O) signature of diatom silica, which in this system mainly reflects the duration and severity of the main dry season (Barker et al., 2011), displayed an increasing trend throughout most of the Holocene. Combination of the BIT and diatom δ^{18}O records showed how decoupled variation in annual rainfall and seasonal drought controlled long-term variation in the region's savanna fire regimes (Nelson et al., 2012). Comparison of the δ^{13}C record of plant leaf-wax alkanes preserved in Lake Challa with the BIT record, the TEX$_{86}$ record of central African temperature from Lake Tanganyika (Tierney et al., 2008; Sinninghe Damsté et al., 2012), and the ice-core record of atmospheric pCO$_2$ allowed assessing principal environmental controls on the proportion of regional plants using the C$_3$ or C$_4$ photosynthetic pathway (Sinninghe Damsté et al., 2011). These and other studies have demonstrated Lake Challa's status as a tropical climate archive of global significance, and they create confidence that the deeper Lake Challa sediments will reveal a truly unique record of quintessentially equatorial climate change and ecosystem dynamics over glacial-interglacial timescales.

Lake Challa is also the only long climate archive from equatorial Africa with a demonstrated annual rhythm of sediment deposition, allowing reconstruction of high-frequency (inter-annual) climate variability over long periods of time. Our work on this aspect (Wolff et al., 2011) showed that variation in the thickness of annual layers deposited over the past century significantly correlates with historical sea-surface temperatures in the western Indian Ocean and El Niño–Southern Oscillation (ENSO) dynamics in the Pacific Ocean, demonstrating that Lake Challa sediments contain signatures of past regional climate variability with the highest possible time resolution. In this semi-arid tropical region, the magnitude of inter-annual rainfall variability is a primary determinant of agricultural success. Detailed study of this short-term variability and the recurrence time of climate extremes in past time windows with colder and warmer mean climate than today has evident socio-economic value for this water-stressed, densely populated region of equatorial East Africa.

Collection of data on the geology, physical limnology, chemistry, and biology of Lake Challa started with a first surveying trip in September 1999 and now comprises twelve field campaigns. Lake-monitoring efforts were stepped up in November 2006 with the installation of air and water temperature loggers and a sediment trap and with the monthly collection of water-level data and water samples for stable-isotope analysis. The monthly sediment-trap samples provided invaluable information on seasonal variation in phytoplankton composition, carbonate precipitation, min-

eral dust, and organic matter deposition (Barker et al., 2011; Wolff et al., 2011), and on the influx of organic biomarkers derived from a variety of aquatic and terrestrial micro-organisms (Sinninghe Damsté et al., 2009). All these data and samples are used to calibrate and validate climate and environmental proxies extracted from the sediment record. We aim to continue this monitoring effort for a total of ten years (2006–2015), i.e., through a full ENSO rainfall cycle.

Scientific Objectives of the ICDP DeepCHALLA Project

The four principal research objectives identified during the workshop are as follows.

To reconstruct at least one complete glacial-interglacial cycle of tropical monsoon dynamics over the western Indian Ocean, allowing assessment of the equatorial signatures of i) low-latitude insolation forcing vs. long-distance impacts of northern hemisphere and Antarctic glaciation; ii) the MIS 5 African mega-droughts; and iii) inter-annual climate variability and extreme events under a range of different mean climate states. We specifically focus on differentiating the histories of three fundamental aspects of the tropical hydrological cycle: annual rainfall, effective moisture, and the duration/severity of seasonal drought.

To document long-term biodiversity patterns and ecological dynamics of a tropical grassland-woodland ecosystem in response to changes in atmospheric CO$_2$, temperature, moisture balance, and fire. As we exploit the full range of terrestrial paleoecological proxies available, our results will help explain/predict the present-day/future prevalence of C$_3$ and C$_4$ plant species using the photosynthetic pathway in tropical grasslands, and the past/future persistence of biodiversity hotspots in eastern Africa, in particular the montane forest ecosystems of the Eastern Arc Mountains in Tanzania.

To reconstruct the long-term dynamics of a tropical freshwater ecosystem in response to climate-driven changes in water-column temperature and stratification, palaeohydrology, and nutrient budget, with special attention to the colonization of an isolated crater lake by cichlid fish, and their morphological adaptation to long-term variation in available habitat.

To drill to the bottom of the sedimentary infill in Lake Challa (Fig. 3; ~210 m below the lake floor) and determine the age of its caldera, which may help constrain the history of Mt. Kilimanjaro volcanism. Given the >250,000-year paleoenvironmental record contained in Lake Challa, the DeepCHALLA project will show exactly how often, when, and how much the East African landscape has changed throughout the entire existence of modern humans (currently dated at 190,000 years). Specifically, documentation of the magnitude and geographical distribution of severe drought across tropical Africa during MIS 6 and MIS 5 is critical to reconstructing the tempo and mode of their exodus from Africa into Eurasia ~100,000 years ago.

References

Barker, P. A., Hurrell, E. R., Leng, M. J., Wolff, C., Cocquyt, C., Sloane, H. J., and Verschuren, D., 2011. Seasonality in equatorial climate over the last 25,000 years revealed by oxygen isotope records from Mount Kilimanjaro. *Geology*, 39:1111–1114. doi:10.1130/G32419.1

Blaauw, M., van Geel, B., Kristen, I., Plessen, B., Lyaruu, A., Engstrom, D. R., van der Plicht, J., and Verschuren, D., 2011. High-resolution ^{14}C dating of a 25,000-year lake-sediment record from equatorial East Africa. *Quat. Sci. Rev.*, 30:3043–3059. doi:10.1016/j.quascirev.2011.07.014

Cohen, A. S., Stone, J. R., Beuning, K. R. M., Park, L. E., Reinthal, P. N., Dettman, D., Scholz, C. A., et al., 2007. Ecological consequences of Early Late-Pleistocene megadroughts in Tropical Africa. *Proc. Nat. Acad. Sci. U.S.A.*, 104:16422–16427. doi:10.1073/pnas.0703873104

Cruz, Jr., F. W., Burns, S. J., Karmann, I., Sharp, W. D., Vuille, M., Cardoso, A. O., Ferrari, J. A., Silva Dias, P.L., and Viana, Jr., O., 2005. Insolation-driven changes in atmospheric circulation over the past 116,000 years in subtropical Brazil. *Nature*, 434:63–66. doi:10.1038/nature03365

Moernaut, J., Verschuren, D., Charlet, F., Kristen, I., Fagot, M., and De Batist, M., 2010. The seismic-stratigraphic record of lake-level fluctuations in Lake Challa: Hydrological stability and change in equatorial East Africa over the last 140 kyr. *Earth Planet. Sci. Lett.*, 290:214–223. doi:10.1016/j.epsl.2009.12.023

Nelson, D. M., Verschuren, D., Urban, M. A., and Hu, F. S., 2012. Long-term variability and rainfall control of savanna fire regimes in equatorial East Africa. *Glob. Change Biol.*, 18:3160–3170. doi:10.1111/j.1365-2486.2012.02766.x

Ruddiman, W. F., 2006. What is the timing of orbital-scale monsoon changes? *Quat. Sci. Rev.*, 25:657–658. doi:10.1016/j.quascirev.2006.02.004

Scholz, C. A., Johnson, T. C., Cohen, A. S., King, J. W., Peck, J. A., Overpeck, J. T., Talbot, M. R., et al., 2007. East African megadroughts between 135 and 75 thousand years ago and bearing on early-modern human origins. *Proc. Nat. Acad. Sci. U.S.A.*, 104:16416–16421. doi:10.1073/pnas.0703874104

Sinninghe Damsté, J. S., Ossebaar, J., Abbas, B., Schouten, S., and Verschuren, D., 2009. Fluxes and distribution of tetraether lipids in an equatorial African lake: Constraints on the application of the TEX_{86} palaeothermometer and BIT index in lacustrine settings. *Geochim. Cosmochim. Acta*, 73:4232–4249. doi:10.1016/j.gca.2009.04.022

Sinninghe Damsté, J. S., Ossebaar, J., Schouten, S., and Verschuren, D., 2012. Distribution of tetraether lipids in the 25-kyr sedimentary record of Lake Challa: Extracting reliable TEX_{86} and MBT/CBT palaeotemperatures from an equatorial African lake. *Quat. Sci. Rev.,* 50:43–54. doi:10.1016/j.quascirev.2012.07.001

Sinninghe Damsté, J. S., Verschuren, D., Ossebaar, J., Blokker, B., van Houten, R., van der Meer, M. T. J., Plessen, B., and Schouten, S., 2011. A 25,000-year record of climate-induced changes in lowland vegetation of eastern equatorial Africa revealed by the stable carbon-isotopic composition of fossil plant leaf waxes. *Earth Planet. Sci. Lett.*, 302:236–246. doi:10.1016/j.epsl.2010.12.025

Tierney, J. E., Russell, J. M., Huang, Y. S., Sinninghe Damsté, J. S., Hopmans, E. C., and Cohen, A. S., 2008. Northern hemisphere controls on tropical southeast African climate during the past 60,000 years. *Science*, 322:252–255.

Tierney, J. A., Russell, J. M., Sinninghe Damsté, J. S., Huang, Y., and Verschuren, D., 2011. Late Quaternary behavior of the East African monsoon and the importance of the Congo Air Boundary. *Quat. Sci. Rev.*, 30:798–807. doi:10.1016/j.quascirev.2011.01.017

Verschuren, D., Sinninghe Damsté, J. S., Moernaut, J., Kristen, I., Blaauw, M., Fagot, M., Haug, G. H., and CHALLACEA project members, 2009. Half-precessional dynamics of monsoon rainfall near the East African equator. *Nature*, 462:637–641. doi:10.1038/nature08520

Wang, Y. J., Cheng, H., Lawrence Edwards, R., Kong, X., Shao, X., Chen, S., Wu, J., Jiang, X., Wang, X., and An, Z., 2008. Millennial- and orbital-scale changes in the East Asian monsoon over the past 224,000 years. *Nature*, 451:1090–1093. doi:10.1038/nature06692

Wolff, C., Haug, G. H., Timmermann, A., Sinninghe Damsté, J. S., Brauer, A., Sigman, D. M., Cane, M. A., and Verschuren, D., 2011. Reduced interannual rainfall variability in East Africa during the last ice age. *Science*, 333:743–747. doi:10.1126/science.1203724

Authors

Dirk Verschuren, Ghent University, Limnology Unit, K.L. Ledeganckstraat 35, B-9000 Ghent, Belgium, e-mail:dirk.verschuren@UGent.be

Daniel O. Olago, University of Nairobi, Department of Geology, Chiromo Campus, P.O. Box 30197, Nairobi 00100, Kenya, e-mail:dolago@uonbi.ac.ke

Stephen M. Rucina, Palynology and Palaeobotany Section, National Museums of Kenya, P.O. Box 40658, Nairobi 00100, Kenya, e-mail: stephenrucina@yahoo.com

Peter O. Odhengo, Office of the Prime Minister, P.O. Box 74434, Nairobi 00200, Kenya, e-mail:odhengo@yahoo.co.uk

Related Web Links

http://www.ecology.ugent.be/limno/challacea.htm
http://www.esf.org/activities/eurocores/completed-programmes/euroclimate/projects/challacea-fp28.html

Photo Credit

Fig. 2: National Museums of Kenya.

Conference on ICDP's New Science Plan

by Ulrich Harms and Thomas Wiersberg

icdp **I**

Imaging the Past to Imagine our Future

2013

The Earth science community is invited to take part in the development of the International Continental Scientific Drilling Program's new Science Plan by contributing to the conference "Imaging the Past to Imagine our Future", to be held 11–14 November 2013 in Potsdam, Germany.

Over the past fifteen years the International Continental Scientific Drilling Program (ICDP) has served the scientific community through financial and operational support for high-profile international drilling projects. ICDP projects have significantly contributed to major advances in understanding Earth's cycles, structure, and evolution including its environment and life. Since 2005, sixteen drilling projects have been conducted, and more than thirty workshops were held with ICDP support under the umbrella of ICDP's current Science Plan (Fig. 1).
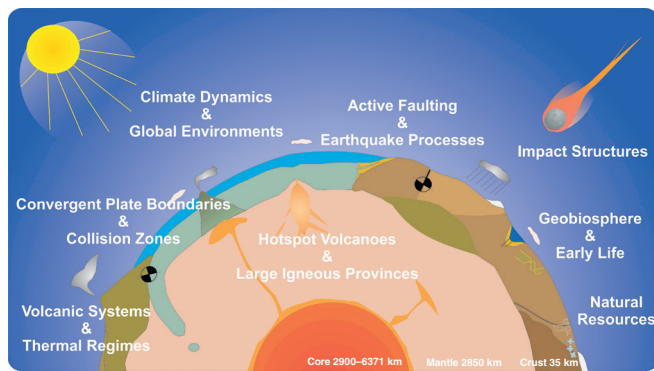

Figure 1. Summary of key themes of the ICDP since the year 2005

The ICDP conference in November 2013 will define the new Science Plan, and it will be structured to link the themes shown in Figure 1 into two major categories: **Understanding of Geoprocesses** and **Societal Challenges**. The former includes faulting and earthquake processes, heat and mass transfer, global cycles, and the hidden biosphere; the latter theme involves topics such as water quality and availability, climate and ecosystem evolution, energy and mineral resources, and natural hazards. This matrix format of the meeting is illustrated in Fig. 2.

The conference will start with keynote talks on ICDP's achievements and present scientific projects, followed by discussions of the four subtopics in Understanding of

Figure 2. Matrix structure for ICDP's new science plan showing in green where Societal Challenges topics meet the themes of Understanding of Geoprocesses.

Geoprocesses each in plenary half-day sessions including perspectives on how societal and economic criteria apply. Further topics addressed in separate sessions will be Technology at Work (drilling, logging, monitoring), Industry Perspectives of Scientific Drilling, and Information Transfer and Outreach.

"Imaging the Past to Imagine our Future" will bring together scientists, ICDP stakeholders, media representatives, policymakers, and industry professionals. The number of conference attendees is limited, but keynote talks, discussions, and the planned media conference can be followed worldwide via live video webcasts including interactive capabilities through the ICDP Web site.

The conference will produce a white paper explaining the new ICDP Science Plan to stakeholders, funding organizations, politicians, and decision makers, as well as serving the science community as a guideline for developing ICDP proposals. In addition, a special issue of a scientific journal will address overviews of the state of the art and highlight the scientific achievements of ICDP over past years.

Details of the conference are explained at www.icdp-online.org/conference2013

Authors

Ulrich Harms, and **Thomas Wiersberg**, German Research Centre for Geosciences GFZ, Potsdam, e-mail: ulrich.harms@gfz-potsdam.de

Joint ECORD/IODP-ICDP Activities EGU 2013

7–12 April 2013, Vienna, Austria

With more than 13,000 participants from 95 countries in 2012, the European Geosciences Union (EGU) General Assembly is a major conference to present IODP and ICDP to the science community in Europe. For the fourth year ECORD/IODP and ICDP will join their efforts to promote ocean and continental research drilling at the European Geosciences Union General Assembly 2013 in Vienna, Austria.

IODP-ICDP Exhibition Booth (#52-53-54 in the Main Hall): will provide a focal point for the scientific drilling community and also for scientists from other fields of research (biology, oceanology, etc.). Visitors can collect the most recent information about the programs (expeditions, projects, workshops, summer schools, training courses, etc.) and meet IODP and ICDP participants and representatives. Lively downhole-logging demonstrations will be organized by ICDP and ECORD.

Joint IODP-ICDP Townhall Meeting: Co-convenors Gilbert Camoin and Uli Harms will provide updates on recent scientific achievements and upcoming new projects, as well as sharing views on the exciting challenges of both programs.

Interdivision IODP-ICDP session (CL5.9): will be co-organized by Convenor Carlota Escutia, and Co-Convenors Ursula Röhl, Ulrich Harms, Thomas Wiersberg, and Rüdiger Stein. The session will address major achievements and perspectives in scientific ocean and continental drilling with special emphasis on the European contributions to IODP and ICDP. Perspectives and visions for drilling projects using a multi-platform approach will be tackled.

Times, dates and locations will be announced on the ECORD website at http://www.ecord.org/pi/egu13.html
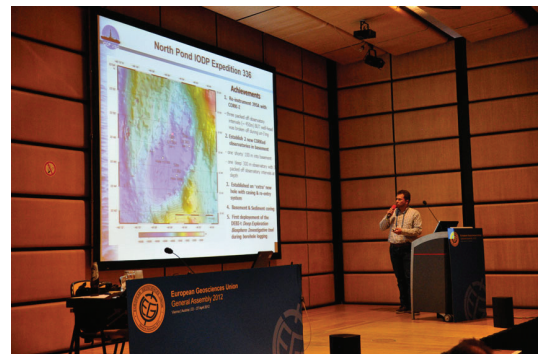
CHIKYU+10 International Workshop

21–23 April 2013, Tokyo, Japan

Beginning in October 2013, the unique deep-sea drilling vessel *Chikyu* (www.jamstec.go.jp/chikyu/eng/CHIKYU) will continue deep drilling, logging, and observatory deployment beneath the world's oceans for the new International Ocean Discovery Program, IODP (www.iodp.org/new-program). To assist in decadal planning, the workshop CHIKYU+10 (www.jamstec.go.jp/chikyu+10), organized by the Japan Agency for Marine-Earth Science and Technology (JAMSTEC) with coordination assistance by IODP Management International, is being held in April 2013.

CHIKYU+10 brings international researchers together to discuss D/V *Chikyu*'s next decade of exploration. The five workshop themes encompass completed, active, or proposed *Chikyu* projects—Active Faults, Earth's Mantle, Deep Life, Continent Formation, Sediment Secrets—as well as a "blue sky" area for new ideas. Thematic discussions will highlight D/V *Chikyu*'s accomplishments during the Integrated Ocean Drilling Program, current science proposals, and new ideas to use *Chikyu*'s deep riser capability. Presentations at the workshop combine invited keynote talks with white papers submitted by the international community. CHIKYU+10 will emphasize participation by early career researchers.

The workshop report, containing scientific perspectives and recommendations developed by the participants, will be made available to JAMSTEC and other governmental officials who have the task of creating the financial and operational models for *Chikyu*'s next decade of deep exploration.

MagellanPlus Workshop Series Programme

15–17 April 2013, London, U.K.
6–8 May 2013, Brisighella, Italy
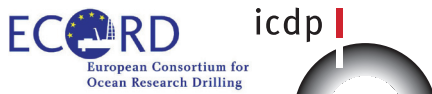
The ECORD/ICDP MagellanPlus Workshop Series Programme is designed to support European and Canadian scientists in developing new and innovative science proposals for submission to IODP and ICDP.

Two Workshops are planned for the 2013 spring:

(1) Exploring the Cretaceous Greenhouse through Scientific Drilling (by Stuart Robinson and Timothy Bralower) 15–17 April, 2013—London, United Kingdom) http://iodp-usssp.org/workshop/cretaceous/

(2) Deep-sea Record of Mediterranean Messinian Events (DREAM) (by A. Camerlenghi, G. deLange, R. Flecker, D. Garcia-Castellanos, C. Hübscher, W. Krijgsman, J. Lofi, S. Lugli, V. Manzi, T. McGenity, G. Panieri, M. Rabineau, M. Roveri and F.J. Sierro), 6–8 May 2013—Brisighella, Italy.

Calls for MagellanPlus workshop proposals are issued twice a year in February and July. For more information visit: http://www.essac.ecord.org/index.php?mod=workshop&page=call-workshop

ECORD–Urbino Summer School: Palaeoclimatology

10–30 July 2013, Urbino, Italy
Registration Deadline: 30 April 2013

With eight years of experience, the Faculty of Sciences and Technologies of the University of Urbino, Italy, has organized the Urbino Summer School in Paleoclimatology (USSP) for the 2013 summer.

The course is designed to provide early-career graduate students from around the world with an intensive educational experience in reconstructing Cretaceous-Neogene paleoclimate dynamics and history. World experts in the diverse disciplines subsumed within paleoclimatology (e.g., paleontology, sedimentology, geochemistry, climatology, etc.) converge to provide a combination of lecturing on paleoclimate related topics and mentoring on exploration, integration, and synthesis of disparate paleoclimate data and modeling. With this goal, an introductory part presents the general evolution of climates from both a proxy and model perspective to provide the students with a view of model-data disparities as targets for additional investigation and opportunities for improved understanding.

ECORD-ESSAC-USSP fellowships are available for high-potential graduate students. ECORD-based scholarships are available for participants from ECORD countries to attend the international USSP. Scholarships are competitively awarded and cover student accommodation and tuition expenses. More information is available at the ESSAC webpage: http://www.essac.ecord.org/index.php?mod=education&page=scolarships

Urbino's location within the Umbria-Marche Basin provides exceptional field access to regional stratigraphic records of the Cenozoic paleoclimatic history and events focused upon by the USSP.

The USSP will include a field trip led by Professors Galeotti (University

Urbino) and Brinkhuis (Utrecht University), who have published extensively on the region and its paleoclimatic record.

The deadline for early registration in the Urbino Summer School is 30 April 2013. Details at: http://www.urbinossp.it/, and contact: simone.galeotti@uniurb.it

ECORD Summer School 2013 in Bremen

9–20 September 2013, Bremen, Germany
Registration Deadline: 30 April 2013

"Deep-Sea Sediments: From Stratigraphy to Age Models"

The Center for Marine Environmental Sciences (Marum) at the University of Bremen, Germany, will host the 7th ECORD Summer School for early career scientists (PhD students and young post-docs) interested in the understanding of past environmental conditions based on the study of ocean sediment cores.

Because the IODP Bremen Core Repository (BCR) and the MARUM Laboratories offer unique analytical facilities, this summer school will combine lab exercises on IODP-style "shipboard" methodologies with interactive discussions on the field of the stratigraphy and age models for the testing of climate related hypotheses in the context scientific drilling.

The students will be trained through a "virtual ship", getting familiarized with the "real" IODP shipboard techniques and core description methods.

A large pool of qualified teachers from prestigious institutions around the world will be guiding the students in this exciting experience.

The deadline to apply for participation in the Summer School is 30 April 2013. More information about the program and how to apply is available at: http://www.marum.de/en/ECORD_Summer_School_2013.html#Section51214

Contact: jbuelten@marum.de
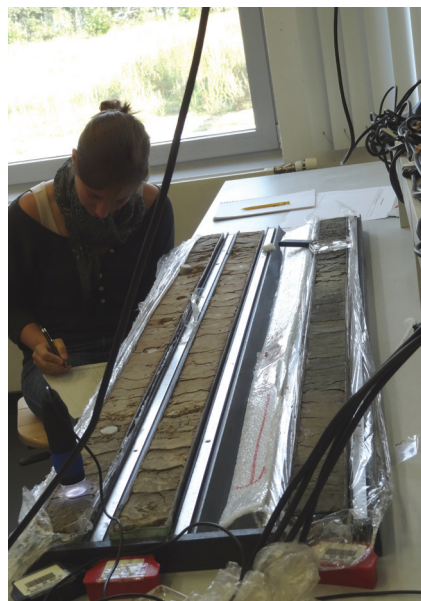
Moreover, students are encouraged to apply for ECORD scholarships to attend the Summer School. For more information visit the ESSAC webpage: http://www.essac.ecord.org/index.php?mod=education&page=scolarships

New Science Plan in Chinese to be Available

The science plan for the International Ocean Discovery Program (IODP, 2013–2023), "illuminating the Earth's Past, Present, and Future", now has the Chinese version. This Science Plan, originally published in English in June 2011, will guide multidisciplinary, international collaboration in scientific ocean drilling during the period 2013 to 2023.

To encourage more Chinese scientists to get involved in this international program and attract more attention from the public, the IODP-China Office has organized senior scientists to translate this Science Plan into Chinese. The translation will be published in early 2013.

"I sincerely hope and invite our Chinese colleagues to read this plan and propose bold new ideas and methods to advance our understanding of the Earth and participate in IODP expeditions of discoveries in the spirit of Zheng He". Kiyoshi Suyehiro, the president of IODP-MI, offers his best wishes to Chinese scientists and writes the preface for the Chinese version of this science plan.
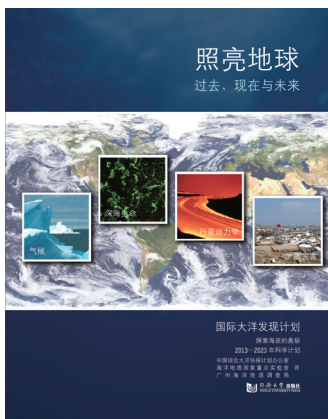
Start of a New Moroccan Middle and High Atlas Lake Drilling Program

In September 2012, new lake sediment cores were recovered from Lake Sidi Ali in the Middle Atlas mountains of Morocco. A German-British-Belgian team from Leipzig University and the universities of Potsdam, Osnabrück, Manchester and Ghent obtained a 20-m-long core from the 38-m-deep southwestern part of the lake and two parallel 9-m-long cores from the shallow northeastern sub-basin at 10 m water depth using a UWITEC coring device. Coring sites were selected following a detailed seismic sub-bottom sediment profiling survey.

Seismic surveys and short-core sampling were also conducted on lakes Tislit, Isli and Afourgagh in the High and Middle Atlas mountains to prepare further drilling campaigns in 2013. However, the 2012 campaign focused on Lake Sidi Ali which was previously investigated by Prof. Henry Lamb (University of Aberystwyth) and his team in the 1990s. They recovered a 6-m-long core from a third very shallow sub-basin of the lake and conducted pioneering work on the mid and late Holocene lake and regional climate history. The new study of sediment cores from Lake Sidi Ali seeks to address glacial and late glacial millennial-scale cooling events in the western Mediterranean-Saharan transition zone, Holocene Rapid Climate Changes, and the regional pastoral-

ism, forest clearance and fire activity history. Initial funding is provided to Christoph Zielhofer and Steffen Mischke by a grant from the Deutsche Forschungsgemeinschaft (DFG) and to William Fletcher by a grant from the Natural Environment Research Council (NERC).

## First Phase of Scientific Drilling at Koyna, India

A major program including scientific drilling has been launched to investigate reservoir-triggered earthquakes in the Konya area, located in the Deccan Flood Basalt Province of western India. As a prelude to setting up of a deep borehole observatory, drilling of a set of four exploratory boreholes surrounding the Koyna-Warna reservoir area (called Koyna) started in mid-December 2012. Each borehole is planned to a depth of about 1500 m, so that they penetrate the Deccan basaltic pile and go a few hundred meters in the underlying basement rocks. Measurements in the boreholes would help provide unprecedented information about the thickness and properties of the Deccan Traps in the area and the nature of the basement that has remained elusive so far. Scientific experiments to be carried out in the basement sections would enable precise subsurface imaging of the rock volume where earthquakes are occurring in Koyna.

Koyna Borehole-1 (KBH-1) is located ~2.5 km SSW of the Koyna Dam and is in close vicinity to the epicenter of the 1967 M6.3 Koyna earthquake (See the map on the next page). Starting on 17 December 2012, KBH-1 reached the granitic basement at a depth of 933 m on 17 January 2013. It went through several lava flows and inter-trappean red bole horizons. The thickness of the Deccan Traps is consistent with the inference from recent broadband seismic monitoring in the area that shows a conspicuous absence of earthquakes in the top ~1 km. Cores recovered from the borehole have revealed a flood basalt pile com-

prising a number of lava flows of variable thicknesses, with each flow characterized by a vesicular and/or amygdaloidal layer underlain by fine-grained massive basalt. Inter-trappean red bole beds up to several tens of centimeters in thickness have been observed at multiple depths. This borehole has provided answers to two important questions. The thickness of lava pile in this area is 933 m, and there are no sediments between the thick lava pile and the granitic basement.

The work is being carried out by the CSIR-National Geophysical Research Institute, Hyderabad, India, with support from the Ministry of Earth Sciences (MoES), Government of India. The results, although preliminary, mark a significant progress on the action plan that emerged after the MoES- and ICDP-supported "International Workshop on Scientific Deep Drilling in the Koyna Region" held at Hyderabad and Koyna during March 2011.
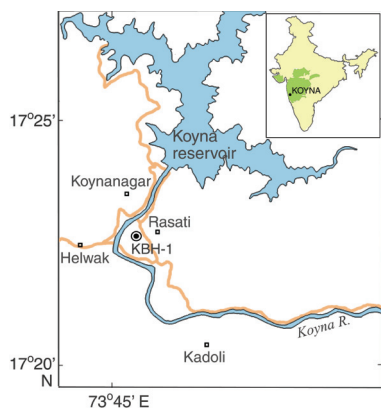
The map shows the location of KBH-1 in the Deccan Traps of India.

Southwest Pacific IODP Workshop

8–11 October 2012, Sydney, Australia

Recent geophysical surveys and geological studies in the Southwest Pacific have helped to crystallize new research goals. In the current phase of IODP there have been five regional expeditions: 317, 318, 325, 329 and 330.

Of six current IODP proposals in this region, four are ready to drill. In order to initiate compelling new drilling proposals, a workshop was organized at the University of Sydney with a diverse group of 80 scientists. The likely presence of *JOIDES Resolution* in the region in 2015–2016 helped generate a sense of urgency.

The workshop covered all fields of geoscience, and drilling targets that extended from the Equator to Antarctica. High-quality contributions and a positive and cooperative atmosphere ensured its success. The four science themes of the new IODP Science Plan were addressed. An additional resource-oriented theme considered possible co-investment opportunities involving IODP vessels.

Various potential new full and add-on proposals were identified:

Climate and Ocean Change: marine Paleogene proposals, namely Lord Howe Rise and Campbell Plateau; and a Wilkes Land continental shelf Neogene proposal.

Deep Biosphere: biosphere in organic-rich Gulf of Papua sediments; and several ancillary proposals.

Earth Connections: formation of the Greater Ontong Java large igneous province; initiation of subduction and origin of sedimentary basins in the Lord Howe Rise region; and structure and dynamics of mantle flow in the northern Australian-Antarctic Discordance.

Earth in Motion: the active Brothers Volcano system in the Kermadec Arc; active volcanic systems in the Manus Basin; the nature of the Tuaheni Landslides off northeast New Zealand; and near-trench-axis comparative drilling around the Pacific Ocean.

Marine Resources: the nature and resource potential of gas hydrates off northeast New Zealand; and deep stratigraphic drilling on the Lord Howe Rise related to both petroleum potential and research.

Many proposals are broad and multidisciplinary: those related to active volcanic systems in the Brothers Volcano and Manus Basin; the Cretaceous-Paleocene paleoenvironment, tectonic history, and petroleum

potential of the Lord Howe Rise region; and slow-slip subduction, fluid flow, landslides and gas hydrate potential of the Hikurangi Subduction Margin.

The workshop was hosted by the Australian and New Zealand IODP Consortium (ANZIC) and the University of Sydney, with additional funding from IODP-MI, USSSP and J-DESC. Abstracts and program are available on http://www.iodp.org.au. The workshop results will be published in detail on the IODP Web site in early 2013 and later in *Scientific Drilling*.

ICDP Training Course on Lake Drilling

The 2012 ICDP Training Course was carried out 15–19 October in Minneapolis in close cooperation with the National Lacustrine Core Facility (LacCore) from the University of Minnesota and focused on soft and lacustrine sediments from lake drilling. Thirty participants from 19 countries attended the training course. Ten international experts gave lectures on lake drilling engineering, downhole logging basics, application of downhole logging data, pre-site surveys, drill core sampling, handling, storage and analysis, data management, application strategies, and pro-ject planning and management. Reports were also presented from completed and currently planned ICDP lake drilling projects (Lake Van, Lake Ohrid). A visit of the LacCore facilities delivered valuable insights into state-of-the-art lacustrine core handling, analysis and storage.

Practical exercises at LacCore help the participants to internalize the acquired knowledge.

Schedules

IODP – Expedition Schedule http://www.iodp.org/expeditions/

	ESO Operations	Platform	Dates	Port of Origin
1	347 - Baltic Sea Paleoenvironment	MSP	Spring/Summer 2013	TBD
	USIO Operations *	**Platform**	**Dates**	**Port of Origin**
2	345 - Hess Deep Plutonic Crust	*JOIDES Resolution*	11 Dec. 2012–12 Feb. 2013	Puntarenas, Costa Rica
3	341 - Southern Alaska Margin Tetonics, Climate & Sedimentation	*JOIDES Resolution*	29 May–29 Jul. 2013	Victoria, Canada
4	346 - Asian Monsoon	*JOIDES Resolution*	29 Jul.–28 Sep. 2013	Valdez, U.S.A.
5	349 - South China Sea	*JOIDES Resolution*	28 Jan.–30 Mar.2014	Manila, Philippines
6	350 - Izu Bonin Mariana: Rearac	*JOIDES Resolution*	30 Mar.–30 May 2014	Okinawa, Japan
7	351 - Izu Bonin Mariana: Arc Origins	*JOIDES Resolution*	30 May–30 Jul. 2014	Yokohama, Japan
8	352 - Izu Bonin Mariana: Forearc	*JOIDES Resolution*	30 Jul.–29 Sep. 2014	Yokohama, Japan
	CDEX Operations *	**Platform**	**Dates**	**Port of Origin**
9	348 - NanTroSEIZE Plate Boundary Deep Riser	*Chikyu*	TBD	TBD

MSP=Mission-Specific Platforms   TBD=to be determined

* Sailing dates may change slightly. Staffing updates for all expeditions to be issued soon.

** CDEX schedule subject to final approval.

ICDP – Project Schedule http://www.icdp-online.org/projects/

	ICDP Projects	Drilling Dates	Location
1	GONAF	Sep. 2012–Jul. 2013	Istanbul, Turkey
2	Lake Ohrid	Apr. 2013–Jun. 2013	Macedonia, Albania
3	COSC	Jun. 2013–Sep. 2013	Jämtland, Sweden
4	Human Origins	Jun. 2013–Mar.2014	Kenya, Ethiopia